Université Fédérale
Toulouse Midi-Pyrénées

THÈSE

En vue de l'obtention du

DOCTORAT DE L'UNIVERSITÉ DE TOULOUSE

Délivré par :

Université Toulouse3 Paul Sabatier (UT3Paul Sabatier)

Présentée et soutenue par :
Nonkululeko Mantombi Nomalanga NGOLOYI
le mardi 15 décembre 2020

Titre :

Documentation du patrimoine de l'assemblage de fossiles du site de Kromdraai contenant des hominines (Afrique du Sud): techniques de numérisation 3D, analyse spatiale quantitative et estimation de volume.

École doctorale et discipline ou spécialité :
EDBSB: Anthropobiologie

Unité de recherche :
Centre d'Anthropobiologie et de Génomique de Toulouse

Directeur/trice(s) de Thèse :
Prof. José BRAGA
Dr. Jean DUMONCEL

Jury :

Prof. Melissa TERRAS (Rapporteure)
Prof. Manuel DOMÍNGUEZ-RODRIGO (Rapporteur)
Prof. Florence SEDÉS (Examinatrice)
Prof. Innocent PIKIRAYI (Examinateur)
Prof. José BRAGA (Directeur de thèse)
Dr. Jean DUMONCEL (Co-directeur de thèse)

ACKNOWLEDGEMENTS

First I acknowledge support of the French Ministry of Foreign Affairs, the Institut des Déserts et des Steppes (Paris) and the Institut Picot de Lapeyrouse (Toulouse) in financing the Kromdraai Research Project (KRP). I would like to further thank the "AESOP plus" programme of Erasmus Mundus (European Union), and Campus France through the French Embassy in South Africa for providing me with financial support.

I give the most heartfelt thanks to my supervisor **Prof. José Braga (**Computer-assisted Palaeoanthropology Team, UMR 5288 CNRS, Université de Toulouse III, Paul Sabatier; Evolutionary Studies Institute, University of the Witwatersrand) for your time and guidance. Thank you for always providing a different perspective, and for your patience and encouragement throughout this journey. I will fondly remember the passion with which described a successful excavation and the new specimens you recovered. Your support of my work with **Black Women In Science** has been paramount for my personal growth and the international visibility of the organisation.

To my co-supervisor **Dr. Jean Dumoncel (**Computer-assisted Palaeoanthropology Team, UMR 5288 CNRS, Université de Toulouse III, Paul Sabatier), thank you for your consistent kindness and willingness to share your time, knowledge and skills. Thank you for providing me with training in the technical aspects of this thesis and for always assisting me in finding practical solutions. I appreciate our moments of light-hearted conversation and laughter.

I extend my gratitude to **Dr. Jean-Baptiste Fourvel** (UMR 5608 TRACES) for your great contribution to this dataset and support; and **Dr. Benjamin Lans** (UMR 5608 TRACES, **Dr. Laurent Bruxelles** (UMR 5608 TRACES; INRAP) and **Raphaël Hautefort** for your vital input and readily providing me with guidance.

A special thank you to **Dr**. **Bernhard Zipfel** and **Prof**. **Francis Thackeray** (Evolutionary Studies Institute, University of the Witwatersrand) for your contributions. Thank you **Francis** for your enthusiasm to help and always sharing kind and encouraging words. To members of the **field staff,** I thank you. **Moleko Monyama**, your conversation and humour kept me going under the hot sun.

Special thanks go to **Prof**. **Florence Sèdes, Franck Jeveme Panta** and **Victoria Adeoye** (IRIT, Université de Toulouse III, Paul Sabatier); I value your support, time, assistance and contributions to this thesis.

To my dearest friends **Curswan**, **Delia**, **Gaby**, **Nokuphila**, **Ronel** and **Trang**, I appreciate you for holding space, offering me encouragement. To **Alice**, **Aurore**, **Carmina**, **Charles**, **Jose**, **Jordan**, **Kelly**, **Kévin**, **Liubomira**, **Raphael**, **Sharon**, **Youssef**, thank you for your friendship and playing a meaningful role in my integration in France.

To **Mathias**, your support is immeasurable. You have kept me motivated and been there through my best moments and the unimaginable. Thank you for being my mirror, balance, source of love, comfort and positivity. I give gratitude to your family, **Anne** and **Didier** for the their relentless love and support.

Thank you to my family for the support, especially **Buhle**, **Neo** and my **Dad** for your outpouring of love. To **Mom**, **Maureen** and **Ausi Ntswaki**, I cannot thank you enough. I give my deepest gratitude and love to you for holding space and providing me with unconditional love, comfort and safety.

Lastly, I give honour to the benevolent and ancient ones who walk beside me, guide me and remind me of my purpose. I honour the ancestors who laid the foundation for this work to exist.

Title

Heritage documentation from hominin-bearing fossil assemblage Kromdraai (South Africa): techniques for 3D digitization, quantitative spatial patterning and volume estimation.

ABSTRACT

This thesis explores the use of multi-scalar data to create a three-dimensional (3D) representation and, to generate a complete digital record of the early hominin-bearing fossil assemblage from the lithostratigraphic Unit P at Kromdraai in the *Cradle of Humankind* World Heritage Site (Gauteng Province, South Africa). The main purposes of this research were to record and illustrate in 3D the temporal and spatial progression of the excavations at Kromdraai since 2014, the discovery of its fossilized Plio-Pleistocene hominins, faunal assemblage and artefacts, and ultimately, to provide an archive documenting the archaeological heritage of Kromdraai. We provided a multi-scalar analysis of various aspects of the study site, with the application of modern, innovative methods such as multi-image land and aerial photogrammetry.

In alignment with the principles and guidelines for the management of archaeological heritage mandated by international agencies such as UNESCO, we also present a protocol for heritage documentation. We used 3D data capture technologies to record the Kromdraai site and the archaeological evidence discovered between 2014 and 2018 from its main excavation. This research presents an original technique developed for the quantification and visualization of the volume sediments removed

from the site during each excavation period. Volume estimations computed using 3D photogrammetry and digitization, provided a temporal and spatial context to the volume and location of material removed and, a visualization of the material. Furthermore, we implemented metadata modelling to demonstrate the use of 4D relational database management systems for the fusion, organisation and dissemination of the Kromdraai site dataset and the sharing of intellectual property.

We also introduce one of the first statistical approaches of 3D spatial patterning in Plio-Pleistocene early hominin-bearing assemblages in South Africa. Implementing classic statistical testing methods such as k-means and Density-Based Spatial Clustering and Application with Noise (DBSCAN) cluster computation in 3D, we investigated the spatial patterns of the fossil assemblage within Unit P, a sample of 810 individually catalogued specimens recovered between 2014 and 2018. The clustering of bovids, carnivores, hominins, and non-human primates revealed a non-uniform spatial distribution pattern of fossils in-situ.

This research presents valuable methods that can be applied at other hominin-bearing fossil sites within the *Cradle of Humankind* to document an archaeological excavation and to reconstruct of the site in 3D, to document heritage information, and to enhance the interpretation of the fossil assemblages using evidence-based assessment of spatial patterns within a hominin-bearing assemblage.

Table of Contents

List of figures

CHAPTER ONE: INTRODUCTION

CHAPTER TWO: Improving archaeological documentation and practices. A new protocol from the Plio-Pleistocene site of Kromdraai (Gauteng, South Africa).

CHAPTER THREE: A new method to evaluate 3D spatial patterns within early hominin-bearing sites. An example from Kromdraai (Gauteng Province, South Africa).

List of tables

CHAPTER ONE: INTRODUCTION

CHAPTER TWO: Improving archaeological documentation and practices. A new protocol from the Plio-Pleistocene site of Kromdraai (Gauteng, South Africa).

CHAPTER THREE: A new method to evaluate 3D spatial patterns within early hominin-bearing sites. An example from Kromdraai (Gauteng Province, South Africa).

List of plates

CHAPTER ONE: INTRODUCTION

Archaeology is the interpretation and understanding of cultural landscapes and past human behaviours through the recovery of fossil and material remains. These cultural landscapes are defined as the "interaction between cultural heritage and the natural environment" (Cocks et al., 2018:2). Heritage conservation is a precautionary measure implemented to preserve our fragile knowledge on past environments and human societies for future generations (Cocks et al., 2018). Heritage is an essential societal component that needs to be conserved for cultural and economic reasons (Yilmaz et al., 2008). Moreover, these landscapes are relevant in providing historical contexts of lands. Similarly, studying the heritage of these cultural landscapes is linked to the inherent desire amongst humans to find a sense of understanding with regards to their identity (Rössler, 2006; Cocks et al., 2018).

Documentary heritage according to the Memory of the World Programme (est. 1992, UNESCO) is the archiving and preservation of history in various formats ranging from books to digital files (Harvey, 2007). Heritage is documented for the purposes of information dissemination and the sharing of intellectual property reflective of the society being captured (Harvey, 2007). The UNESCO Charter on the Preservation of Digital Heritage defines digital heritage in Article 1, as "unique resources of human knowledge and expression" comprised of information relating to science, education and culture amongst other subjects (UNESCO, 2003, 2009; Pescarin, 2016). It entails the digitisation of existing data and information; or the innovative creation of diverse digitally formatted heritage resources such as databases, imagery, websites and texts (UNESCO, 2003, 2009; Pescarin, 2016). Article 2 of the charter emphasizes that the principle of digital heritage is public accessibility, particularly ensuring free and non-restrictive access for the purposes of

knowledge dissemination (UNESCO, 2003, 2009). Indeed, heritage digitisation globalizes information by removing the constraints of time, space and our perceived differences. In addition, it facilitates an educational exchange between individuals and the representation of information diversity across time and space (Article 9), an important long-term goal of this study (UNESCO, 2003, 2009). It is therefore important to ensure the permanency of heritage information and the consistency of heritage documentation. Articles 3, 4 and 5 of the charter proceed to highlight the need to guard against the threat of these digital resources being lost, article 5 particularly addresses digital continuity, which pertains to creating authentic and long-standing digital heritage materials by designing and implementing reliable techniques and procedures (UNESCO, 2003, 2009). Such digital materials require preservation to ensure their longevity for posterity. The charter further stipulates the importance of developing policies that prioritize digital heritage conservation (Article 6).

The CIPA Heritage Documentation (previously known as the 'International Committee for Heritage Documentation') is amongst the oldest International Scientific Committees (ISC, Patias, 2006). It was created for the purposes of fulfilling the growing needs of heritage documentation stated in the guidelines described above (Patias, 2006). Founded in 1968, the international organization is still actively operating to date and provides an international forum that strives to digitally document cultural heritage (D'Ayala and Smars, 2003, Patias, 2006, Patias and Santana, 2011; Dall'Astaa et al., 2016, CIPA, 2020). One of the five goals set by CIPA Heritage Documentation is to develop best practices and principles for the management and documentation of cultural heritage information (Quintero et al., 2017). Owing to the complexity of cultural heritage documentation, D'Ayala and

Smars (2003) list seven general guiding concepts that should be considered when informing best practices (Patias, 2007, Patias and Santana, 2011):

1. Objectivity: being free of bias when selecting which heritage to conserve and providing valid reasoning for the choice made. Objectivity also implies understanding that the chosen data acquisition method can cause a ripple effect on further actions in the site.
2. Values: conducting a thorough heritage recording so as to not lose any information that may be deemed important for the future.
3. Learning process: ensuring that new skills are developed whilst conducting heritage documentation.
4. Continuity: creating documentation that is useful and applicable in the future
5. Fabric: ensuring that documentation is integrated with other techniques.
6. Documentation sets: this pertains to the organisation of sets of data, such that it facilitates straightforward exchanges amongst specialists; e.g. categorizing data (text, images etc.) according to subject.
7. Redundancy: in the face of uncertainty, it is important to include additional information or different archives to supplement the documentation data in case of preservation failure or information loss.

In comparison to other continents, Africa lacks in international literature regarding heritage conservation frameworks, despite being rich and diverse in natural and cultural heritage; further reiterating the need for conservation by means of virtual digitization (Cocks et al., 2018).

In comparison to Europe and western continets, African history has largely been

overshadowed by the history of colonialism. Previously, cultural heritage such as African languages, customs and beliefs were disparaged and considered inferior (Cocks and Vetter, 2017). In South Africa for instance, colonialism and Apartheid were at the forefront of heritage documentation. In fact, cultural landscapes in Africa have been curated to suit what is considered a universally valuable or more palatable to the "elites" or western tourists and consumers (Lowenthal, 2005, Cocks and Vetter, 2017). In recent decades, research in South Africa has been dedicated to sharing the history of South African cultural landscapes (e.g. *Cradle of Humankind* Mapungubwe). Furthermore the involvement of local indigenous people strengthens the integrity of the documented heritage (Cocks and Vetter, 2017) and can have positive socio-economic impacts, which are discussed below in relation to the *Cradle of Humankind*. The use of 3D digital tools increases the value, integrity and redundancy of heritage data, and potentially increases the accessibility to heritage resource information by virtual means.

Of course, some limitations regarding the extent to which digital surveying methods can be applied in Africa exist. The main limitation is the cost of implementing such methods in some African countries where the financial resources to invest in equipment for heritage documentation are lacking. In the case of 3D visualizations of sites for example, laser scanning and drone photogrammetry may be cost-intensive. However, there exist low cost alternative methods for 3D digitization such as terrestrial photogrammetry (using a simple hand-held camera), and free post-processing softwares (e.g. Regard3D, MicMac).

The "*Cradle of Humankind*" represents a good example of a high potential UNESCO World Heritage Site (inscribed in 1999) in a developing country, that implements best practices for cultural heritage conservation at an international

standard (Magnussen and Visser, 2003).

Formally referred to as "Sterkfontein, Swartkrans, Kromdraai and Environs" (Hilton-Barber and Berger, 2002: 10), the region provides a wealth of information on hominin evolution and prehistoric human history. An amalgamation of major palaeoanthropological fossil hominin sites yielding fossils of australopithecines e.g. *Australopithecus africanus* (1-1 MYA; see 'Mrs Ples' - Broom, 1936, 1947; Berger, 1994; Lacruz et al., 2002 and enclosed references); Paranthropus e.g. *Paranthropus robustus* (2.0 – 1.0 MYA; see Broom, 1938; Braga et al., 2017, 2020 (in revision) and enclosed references); and early *Homo* (2.4 -1.8 MYA; see Brain, 1981, 1993; Braga and Thackeray, 2003 and enclosed references) amongst other hominin and faunal species (Figure 1), the *Cradle of Humankind* is a notable hub for human origins (Hilton-Barber and Berger, 2002). The World Heritage Site bridges the gap between the non-scientific understanding of cultural heritage and human history, and the scientific discovery and study of human origins, evolutions and innovations.

The cultural significance of the *Cradle of Humankind* has had a major influence in heritage tourism expansion within the region, and consequently impacting local economic development (Magnussen and Visser, 2003; Gustav and Rogerson, 2004, Rogerson, 2007; Rogerson and van der Merwe, 2016; Van der Merwe, 2016). Situated in one of the economically marginalised parts of Gauteng, the *Cradle of Humankind* is one of the key destinations in South Africa developed with the intention of job creation, skills development and sustainable tourism practises (Rogerson and van der Merwe, 2016). The National Heritage and Cultural Tourism Strategy of South Africa asserts the prioritisation of cultural heritage resource conservation, long-term sustainability and most importantly, raising awareness about the origins of humankind (Department of Tourism, 2012). For this reason the World

Heritage Site has been intentionally curated to be people-centred, educational, innovative and economically lucrative (Magnussen and Visser, 2003; Rogerson and van der Merwe, 2016). Official Visitor Centres for the *Cradle of Humankind* World Heritage Site, Maropeng and the Sterkfontein Caves are two prime examples of tourist experience infrastructure implemented for the promotion of cultural heritage conservation, innovative public education of scientific research and knowledge exchange (Naidu, 2008; Rogerson and van der Merwe, 2016).

Following the CIPA Heritage Documentation guidelines stipulated above, this thesis provides a synthesis of scientific techniques that have been recently applied at the Plio-Pleistocene fossil hominin site of Kromdraai (*Cradle of Humankind*, South Africa). This is in order to record the excavations within its lithostratigraphic Unit P (and to a lesser extent, Unit O) (Braga et al., 2020, in revision) and to inform best practices for heritage documentation. The research also presents innovative methods to observe, interpret and preserve archaeological sites due to the destructive nature of the excavation process (De Reu et al., 2013; Roosevelt et al., 2015). Additionally, it investigates the spatial patterning of excavated fossils and artifacts from Unit P in order to enhance our understanding of the taphonomic interpretations of accumulation agents and depositional processes of Unit P.

Previous spatial analytical studies in archaeology included the use of 2D topographical maps produced with Geographic Information System (GIS) mapping tools (Olson et al., 2013; Olson and Placchetti, 2015; Traviglia and Torsello, 2017). However, there has been a transition towards 3D digitization and visualisation, integrated with statistical packages for complex data analyses (Traviglia and Torsello, 2017; Buckland et al., 2018). Such 3D techniques are implemented in this study.

Background and rationale

Kromdraai (26°00’41” S, 27°44’60” E) is a hominin-bearing cave site located in the UNESCO World Heritage Site the “*Cradle of Humankind*” (inscribed in 1999) in the Gauteng province, South Africa (Braga et al., 2013). This Plio-Pleistocene palaeokarst site is truncated by surface erosion and sits on the south of the Bloubank stream. It is located to the east of the Sterkfontein Caves (~2 km’s) and within close proximity to Coopers and Swartkrans, which have also yielded hominins (Figure 1). Other localities within the *Cradle of Humankind* yielding hominin fossils include Coopers, Rising Star, Drimolen, Malapa, Gondolin and Gladysvale (Table 2). Outside of the province are the sites of Taung and Makapansgat from which the earliest known hominin specimens of *Australopithecus africanus* (Dart, 1925, 1957) were recovered. The *Cradle of Humankind* landscape is characterised by dolomitic cave rock forms, specifically the 2.6 – 2.8 Ga dolomitic limestone belonging to Malmani Subgroup, which forms part of the Transvaal Supergroup (Button, 1973; Eriksson and Truswell, 1974; Martini et al., 2003; Eriksson et al., 2006).

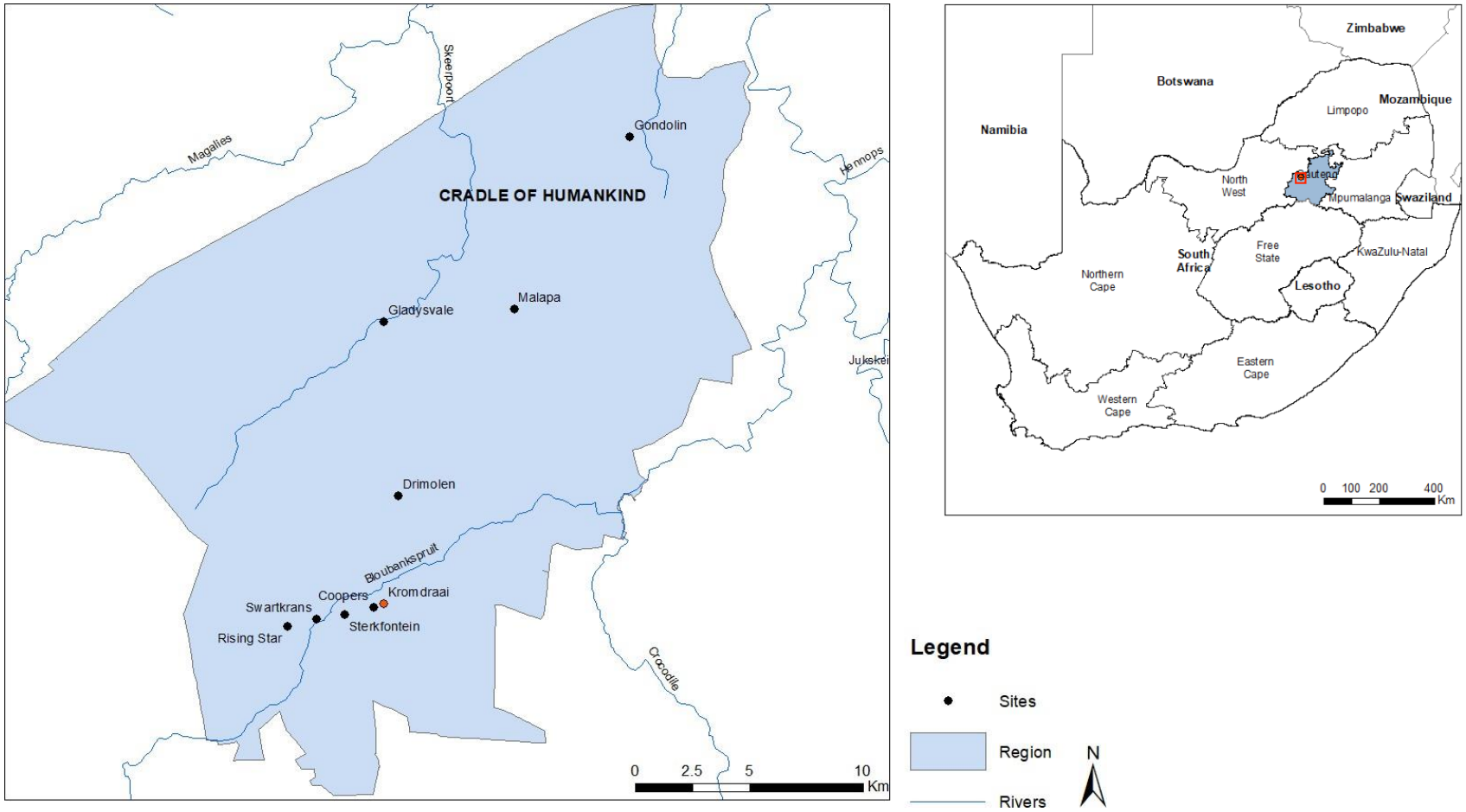

Figure 1. Map showing the location of Kromdraai within the *Cradle of Humankind* and the greater context of South Africa.

The context of Kromdraai

Braga et al. (2016a, b, 2017, 2020, in revision) describe four phases of archaeological research prior to 2014 that form the basis of Kromdraai excavations. Early excavations in Kromdraai conducted by Robert Broom (1938-1944) conceded the initial discovery of a partial skull and dentition of the holotype of *Paranthropus robustus*, TM 1517 (Broom, 1938). Broom's excavations were followed by excavations by Brain (1955-1956) during which the majority of the fossils were collected (Brain, 1981); Vrba (1977-1980), Thackeray (1993-2002) and most recently, the researchers from the Kromdraai Research Project (KRP) from April 2014 to present (Braga et al., 2017, 2020, in revision).

Brain (1958) classified two main fossil bearing localities, Kromdraai A (KA), and Kromdraai B (KB). Vrba (1981) further identified the separation of KB deposits by a septum of dolomite into KB East and KB West. KB yielded 6067 fossil remains between 1938 and 2002, 27 of which were craniodental and postcranial hominin specimens belonging to at least 17 individuals (Thackeray et al., 2001; Braga et al., 2013). Following the sites of Swartkrans and Drimolen, the third-largest sample of *P. robustus* in South Africa is allocated to this site. The current fifth phase of excavation at Kromdraai by the KRP focuses on the "loose fill" fossiliferous sediments, extending northwards of the dolomitic wall along the E-W trending trench previously excavated by Brain (1958, 1975) and Vrba (1981) (Braga et al., 2016a, 2017, 2020, in revision). Interpretations by both Brain (1975) and Vrba (1981) alluded to the futility of the area owing to the sterility of the first metre depth of surface soil (e.g. Braga and Thackeray, 2016; Braga et al., 2017, 2020, in revision). The development and extension of Kromdraai is discussed in more detail in several studies (e.g. Brain,

1958, 1975; Vrba, 1981; Braga et al., 2020, in revision), and the evolving stratigraphy is detailed in Brain (1958), Vrba (1981), Partridge (1982), Bruxelles et al. (2016).

A new nomenclature describing the distinct sedimentary deposits by "Unit" rather than "Member" has been proposed recently (Braga et al., 2020, in revision). This study focuses on Unit P previously named "Member 2" (see Vrba, 1981, Partridge, 1982 and Bruxelles et al., 2016) and considered as "nearly sterile" (Vrba, 1981). Between 2014 and 2018, the highly fossiliferous deposits of Unit P yielded bone tools, a minimum of two stone tools and over 3000 faunal fossils (Braga et al., 2017, 2020, in revision). The macro-mammal specimens include 35 carnivore fossils belonging to the felid, hyenid, canid, viverrid and mustelid taxa (Fourvel et al., 2016; Fourvel, 2018, Braga et al., 2020, in revision). Hominins were represented in 46 specimens detailed in Braga et al. (2020, in revision), 33 of which were craniodental belonging to 18 individuals (10 juvenile, 8 adult individuals), and 13 that were postcranial. Furthermore, Unit P has provided the first evidence of a simultaneous occurrence of *Paranthropus* and early *Homo* (Braga et al., 2020, in revision) at Kromdraai (after Swartkrans and Drimolen). Braga et al. (2020, in revision) report respective relative abundances of 89% and 11% of *Paranthropus* and *Homo*. The authors cited these values as comparable to relative abundances reported at Drimolen (84% and 16%) and Swartkrans (96% and 4%) (Moggi-Cecchi et al., 2010; Braga et al., 2020, in revision). It is implied that with further evidence, this interesting co-occurrence of *Paranthropus* and early *Homo* could provide important insights on taphonomy, especially carnivore involvement in bone accumulation (Braga et al., 2020, in revision).

Characterized by soft sediments (or rudites), Unit P overlies one of the oldest identified hominin-bearing sedimentary unit in the site thus far, Unit O (see Braga et

al., 2020, in revision). A distinct erosional unconformity layer at the upper limit of Unit O is indicative of a large temporal gap between the last deposition of Unit O and the onset of Unit P (Braga et al., 2020, in revision). Given that only the uppermost meter of Unit O is to be excavated, Braga et al. (2020, in revision) speculate the existence of at least one or more deposits below Unit O once the base is reached.

In a working hypothesis for Kromdraai, Braga and Thackeray (2016) observe that the recently realized (after 2014) sedimentary deposits of Unit P and Unit A, reveal an older unrealised temporal window of the co-occurring *P. robustus* and early *Homo* lineages in South Africa (Braga et al., 2017). To test this working hypothesis and further establish the chronological framework at Kromdraai, regular seasonal field studies are conducted. This entails research and analyses pertaining to the temporal depth, the definition of hominin and other faunal activities documented in the sedimentary units, and taphonomic interpretations. Although the study of early hominins and human evolution represents the crux of studies at Kromdraai, research activities are multi-disciplinary and encompass the study of the palaeoenvironmental, stratigraphic and taphonomic indicators (amongst others).

Taphonomic context of Kromdraai

Taphonomy analyses provide insight on the processes by which organisms decay and undergo fossilization. The complexity of sub-surface dolomitic cave systems such as those in the *Cradle of Humankind* requires the implementation of taphonomy to understand the formation of the fossil record. Fossil assemblages in caves provide the faunal and environmental history of a cave system, including insights on the complex physical (abiotic) and biological (biotic) agents of accumulation. These agents of

accumulation may have influenced the processes leading to the bone accumulation and preservation through a single event or several accumulations (concurrent or singular) over long periods of time. Such accumulation processes have implications on the structure of the assemblage, including the faunal diversity, the frequency and density of fossil elements within a space and representative of a time period.

Abiotic and biotic agents of accumulation

Abiotic taphonomic processes such as fluvial transportation, debris flow and gravity contribute to the posthumous, allochthonous allocation of fossil remains in cave systems (Adams et al., 2007). A familiar trait in the accumulation of deposits in the *Cradle of Humankind* is the formation of a talus cone underneath the cave roof opening (Brain, 1981; Hilton-Barber and Berger, 2002; Adams et al., 2007). Abiotic processes, particularly the dissolution of dolomite, form the talus cone which is comprised of faunal and floral remains, in-washed loose scree material and debris collected near the entrance of the cave (Brain, 1981; Hilton-Barber and Berger, 2002; Adams et al., 2007). Upon calcification, the cone transforms into "cave breccia" causing an expansion of the cave entrances (Hilton-Barber and Berger, 2002). As erosion proceeds, the cave becomes de-roofed, a common feature of the dolomitic landscape of the *Cradle of Humankind* (Hilton-Barber and Berger, 2002).

A subset of abiotic accumulation is natural animal death within the cave or from the effect of gravity by way of a death trap. A death trap denotes an unexpected fall through an inconspicuous vertical opening at the roof of a cave leading to an accidental death or the inability for mammals to exit a steep opening after entry (Brain, 1981, Vrba, 1981). A prominent example of death trap accumulation within the *Cradle of Humankind* is that of the australopithecine skeleton StW573 ("Little

Foot") recovered from Member 2 at Sterkfontein (Pickering et al., 2004; Clarke, 2007; Bruxelles et al., 2014). Other death trap scenario interpretations are proposed in Malapa for *Australopithecus sediba* (Dirks et al., 2010, Val et al., 2015), and in Kromdraai B East for the remains of *Paranthropus robustus* (Vrba, 1981; Vrba and Panagos, 1982). The possibility of natural accumulation by a death trap first suggested by Vrba (1981) for Units Q-R (previously Member 3) at Kromdraai is an important consideration in taphonomic studies of Unit P.

Cave environments serve a diverse range of purposes ranging from refuge (Brain, 1981; 1993; de Ruiter, 2001; Pickering, 2001a, 2001b; Carlson and Pickering, 2003; Pickering et al., 2004a, 2004b; 2004c; Val et al., 2015), feeding and a food caching (de Ruiter and Berger, 2000; Kuhn, 2005; Bountalis and Kuhn, 2014), latrine usage (Berger et al., 2009, Pineda et al., 2017) hibernation and roosting (van der Merwe, 1973, 1975; Kearney et al., 2017), thermoregulation (Barret et al., 2004; Pruetz, 2007) and natal dens for the rearing of young (Boydston et al., 2006; Bountalis and Kuhn, 2014; Kearney et al., 2017). For this reason, they are inhabited and frequented by range of animal species that can act as taphonomic agents. Biotic agents introduce faunal remains into the caves through actions of natural death, intentional accumulation and waste disposal. Such behaviours can provide the perspective of predator-prey interactions and/or scavenger behaviour (Brain, 1981; Carlson and Pickering, 2003). A plethora of studies in the *Cradle of Humankind* have addressed the role of a diverse range of biotic agents in taphonomic interpretations of cave deposit accumulations. This includes analysing behaviours of birds, rodents and carnivores amongst other biotic agents.

Birds

The “bird of prey hypothesis” (Hilton-Barber and Berger, 2002: 80) constitutes micromammal fossil accumulation by birds of prey inhabiting the cave region, primarily owl and eagle species (Brain, 1981; Avery, 2001; Val, 2016). Several studies at sites across the *Cradle of Humankind* reference avian accumulating agents e.g. Makapansgat (Levinson, 1982), Swartkrans and Sterkfontein (Avery, 2001) and Rising star (Val, 2016; Kruger and Badenhorst, 2018). The widely distributed barn owl (*Tyto alba*) is involved in the accumulation of microfauna at several Plio-Pleistocene sites in the *Cradle of Humankind* (Brain, 1981).

Physical evidence indicates that *T. alba* inhabit rock ledges, rock fissures and cave entrances to nest and roost (Avery, 2001; Reed, 2003, 2005; McCrae, 2009; Val, 2016; Kruger and Badenhorst, 2018). Pellets accumulated below the nesting site are often incorporated into “rodent breccia” in the cave (Levinson, 1982). Ecological evidence suggests that *T. alba* are opportunistic (Levinson, 1982) and have a wide range of prey in comparison to the other owl species (e.g. *Tyto capensis* or *Asio capensis*). *Tyto capensis* and *Asio capensis* have a preference for grassland or marsh environments to roost and nest, and have a narrow range of prey (Avery, 2001).

Nesting and roosting behaviours of raptors indicate that they prey and scavenge on lagomorphs and small mammals or their similar body size (Gifford-Gonzalez, 2018). In the context of the Plio-Pleistocene hominin fossil-bearing sites, eagles (and vultures) are acknowledged as contributors to the accumulation of microvertebrates, small and medium-sized fauna, e.g. non-hominin primates (Brain, 1981, 1985; Andrews, 1990; Hilton-Barber and Berger, 2002). Berger and Clarke (1995) attributed the two punctures in the skull of the australopithecine specimen the Taung child

(discovered by Dart in 1924) to an ancient African eagle comparable to the modern *Stephanoaetus coronatus* (crowned-hawk eagle; Berger and Clarke, 1995) or the *Aquila verreauxii* (black eagle; Hilton-Barber and Berger, 2002).

Rodents

Rodents have been associated with the accumulation of various assemblages in the *Cradle of Humankind*, and rodent behaviours are considered in many studies (Klein, 1975; Binford, 1981; Brain, 1981; Shipman and Rose, 1983; de Ruiter et al., 2008). Common rodent behaviours include bone modification (gnawing) and accumulation (scavenging) (Gifford-Gonzalez, 2018). Hughes (1961) and Brain (1981) both recognised bone-collecting behaviours of porcupines. Gnawing is a combative measure for mineral deficiencies amongst the *Hystrix africaeaustralis* (Cape porcupines) species (Gifford-Gonzalez, 2018). Additionally, porcupines and other rodent species gnaw on bones to reduce the size of their incisors that grow continually (Brain, 1981; Kibii, 2009; Gifford-Gonzalez, 2018). Although rodents are present in Unit P, the absence of taphonomic indicators (e.g. gnawing marks) suggests that they were not involved in the accumulation of the fossil assemblage (Fourvel et al., 2018).

Carnivores

Initial interpretations of African cave taphonomy pioneered by Dart (1949, 1957, 1962) who discovered the *Australopithecus africanis* (*prometheus*), purported cave accumulation to hominins (Riga et al., 2019). According to Dart (1957, 1962), taphonomic indicators such as bone damage, tool and fire use, and a disproportionate representation of faunal remains in the Makapansgat faunal assemblage, were suggestive of predatory and cannibalistic behaviours by australopithecines (Dart,

1957). However, subsequent studies (e.g. Skinner and van Aarde, 1981, 1991; Lam 1992) evidenced bone accumulation by carnivores, particularly hyena.

In order to understand the site formational processes of the Kromdraai fossil assemblage a multi-disciplinary approach has been adopted. Brain (1975) and Vrba (1981) proposed the initial taphonomic interpretations of KA and KB. According to Brain (1975), patterns of severe fragmentation in bone remains found within the decalcified breccia of KB revealed hominin food remains. Vrba (1981) attributed the extreme fragmentation of bones to disintegration due to the decalcification process and "subsequent trampling and overburden pressure on the weakened bone" (Vrba, 1981:1). Vrba (1981) alluded to the possibility of an autopod origin of Units Q-R ("Member 3") faunal assemblage and further attributed the accumulation of the deposits due to carnivore feeding behaviours inside the Kromdraai cave.

Many studies in the *Cradle of Humankind* have a proclivity for the carnivore accumulation theory (Brain, 1981). In the book *The Hunters or the Hunted? An Introduction to South African Cave Taphonomy* (Brain, 1981), Brain (1981) put forward the robust "carnivore-collecting hypothesis". In this book he focussed on the most prominent underground Plio-Pleistocene cave sites of Kromdraai, Sterkfontein and Swartkrans in this regard (Brain, 1981). The "carnivore-collecting hypothesis" by Brain (1981) refers mainly to the accumulation of hominin primates in carnivore lairs by large carnivores such as felids (e.g. *Panthera pardus* - leopards) and hyenids (Brain, 1981; 1993; de Ruiter, 2001; Pickering, 2001a, 2001b; Carlson and Pickering, 2003; Pickering et al., 2004a, 2004b; 2004c; Val et al., 2015; Fourvel et al., 2018).

Carnivore accumulation as a taphonomic interpretation is reflected in several hominin-bearing Plio-Pleistocene sites in the *Cradle of Humankind* (Table 1). A few examples of felid accumulation synonymous with those at Kromdraai are leopard

accumulations observed at Sterkfontein and Swartkrans (Brain, 1981; de Ruiter and Berger, 2000).

Table 1. Taphonomic accumulation agents hypothesised in hominin-bearing sites within the *Cradle of Humankind* (after Fourvel et al., 2018).

Site	Deposit	Accumulating agent	Reference
Kromdraai	A	Biotic - carnivore	Brain, 1973, 1981; Vrba, 1975
Kromdraai	B	Biotic - carnivore	Brain, 1981
Kromdraai	B East/Member 3	Abiotic - death trap/feeding	Vrba, 1981; Vrba and Panagos 1982
Kromdraai	Unit P	Biotic - carnivore	Fourvel et al., 2016, 2018
Swartkrans	Member 1	Biotic - carnivore	Brain, 1981, 1993; de Ruiter, 2001; Carlson and Pickering, 2003; Pickering et al., 2012, 2016
Swartkrans	Member 2	Biotic - carnivore	Brain, 1981, 1993; Carlson and Pickering, 2003; Pickering et al., 2016
Swartkrans	Member 3	Biotic - carnivore	Brain, 1981, 1993; Pickering et al., 2004b; Pickering et al., 2016
Swartkrans	Talus Cone Deposit	Biotic - carnivore	Pickering et al., 2016
Swartkrans	UNE	Biotic - carnivore	Pickering et al., 2016
Sterkfontein	Member 4	Biotic - carnivore	Brain 1981; Pickering et al., 2004b
Sterkfontein	Member 2	Abiotic - death trap/feeding	Pickering et al., 2004b; Clarke 2007; Bruxelles et al., 2014
Gondolin	GD 1	Abiotic - fluvial transportation	Adams et al., 2007
	GD 2	Biotic - carnivore	Menter et al., 1999; Adams et al., 2010; Grine et al., 2012
Malapa		Abiotic - death trap/feeding	Val et al., 2015
Gladysvale		Biotic - carnivore	Berger, 1993; Berger, 1994
Coopers		Biotic - carnivore	Steininger et al., 2008; de Ruiter et al., 2009; DeSilva et al., 2013

Drimolen Rising Star	Main Quarry	Biotic - carnivore	Gommery et al., 2002; O'Regan and Menter 2009; Moggi-Cecchi et al., 2010 Kruger et al., 2016

In the ongoing analyses at Kromdraai, preliminary results from Unit P suggested that the large presence of carnivores within the specific locality of the deposit has had taphonomic implications Fourvel et al. (2016, 2018). Fourvel et al. (2018) noted felids (leopards) as the main predator and potential accumulator at Kromdraai. Small canids such as the *Canis mesomelas* (black-backed jackal) and *Vulpes chama* (Cape fox), and hyenids (e.g. *Crocuta crocuta* (spotted hyena)) were considered secondary predators and potential accumulators (Fourvel et al., 2018). *Hyaena brunnea* (brown hyena) and *Hyaena hyaena* (striped hyaena) were categorised as secondary collectors (Fourvel et al., 2018).

To facilitate the further understanding the abovementioned abiotic and biotic agents of accumulation in future taphonomic studies, we will add the perspective of spatial patterning. Spatial patterning i.e. the structures derived from the locality and organisation of an object within a site, provides an informative perspective for taphonomic interpretation. Spatial distributions of fossil assemblages and the ensuing and the recognised patterns, can reveal relationships between the location of fossil and artefact remains relative to each other, physical site structures and surrounding site elements (Clarke, 1977; Wheatley & Gillings, 2013). These patterns also provide insight on the mechanisms of past depositional and post-depositional processes, the stratigraphic composition of the site, informing an aspect of the taphonomy (Reynolds, 2010).

The study of spatial patterning sets the precedent for future studies in taphonomy

and stratigraphy, particularly in the case that some units undergo post-depositional mixing.

As yet, research illustrating spatial distribution is evident in the *Cradle of Humankind* (e.g. Nigro et al., 2003; Rüther et al., 2014; Birkenfeld and Avery, 2015; Mokokwe, 2016; Stratford et al., 2016). However, few studies integrate 3D spatial pattern analysis to investigate the nature of spatial relationships between different fossil groups to support taphonomic interpretations (Nigro et al., 2003; Jennings and Hasiotis, 2006; Mallye, 2011). With the exception of Kruger (2017), 3D spatial and statistical analysis has not been applied in *The Cradle of Humankind* prior to this study (chapter 3).

In the on-going, taphonomic analyses of Unit P, spatial distribution trends viewed along with taphonomic indicators (see Fourvel et al., 2018) can provide insight on the accumulation process and activities of the deposit. This research assesses the fossil distribution of the Unit P faunal assemblage (including hominins), focussing on frequency and density of individual taxa groups and body parts within the space. Using statistical methods, in this study, we analyse the extent of heterogeneity or homogeneity in spatial patterning and the potential of these techniques to support the existing (e.g. Fourvel et al., 2016, 2018) and future taphonomic interpretations of Kromdraai.

GIS and Spatial analysis in Archaeological Sites

The Geographic Information System is a computer-based technology comprised of a combination of a database management system incorporating cartography and spatial analysis for visualisation and to support decision making (Gould and Herring,

2001; Verhagen, 2018; Awange and Kiema, 2019). There are a multitude of provisions within the technology catering to a number of different applications across disciplines. Geographic Information Systems are used to visualize, measure and analyse geographic objects, through various techniques the data is intentionally altered and relevant information is extracted, particularly information pertaining to the surrounding structures (such as social and environmental structures) and their relations to each other (Chrisman, 1999; Gould and Herring, 2001; Awange and Kiema, 2019).

Within the context of archaeology, GIS tools are applied to aid in the spatial organization and understanding of archaeological datasets and for multidimensional spatial database management (Chrisman, 1999; Stratford et al., 2016). Archaeological studies provide mapping information and specific spatial reference information defining the location of points and polygons within the context of the earth. Spatial data is derived from sources such as maps; Light Detection and Ranging (LIDAR), remote sensing visualisation technology for landscapes; and Global Positioning Systems (GPS) (Chase et al., 2017). In this research it was derived from point cloud data from geo-referenced photogrammetry and total station surveying. The increasing efficiency of these tools has led to better quality data and increased volumes of spatial data recorded (Marble, 1990; Chrisman, 1999; Gould and Herring, 2001; Verhagen, 2018).

Since its introduction there has been rapid progress in the development of GIS, and digitisation technology is now widely used by archaeologists worldwide for example in historical landscape archaeology (Wheatley and Gillings, 2013; Chase et al., 2017). This is because spatial information of objects (e.g. features, structure) forms a large and integral part of archaeological interpretation (Wheatley and Gillings, 2013).

GIS integration can be seen in the study of spatial pattern and density distributions, orientation patterns and site formation processes to examine taphonomic influences and site formation history, examples of this application exit worldwide e.g. Italy, Germany and Tanzania case studies detailed below (Boschian and Saccà, 2010; Benito-Calvo and de la Torre 2011, 2013; Böhner et al., 2015).

Archaeologists have been able to perform simulations about past environments for modern interpretation. This is achieved by using digital topographical data, information about the past environments and precise information regarding the artifacts (e.g. location, metadata).

Lastly, GIS can be integrated with 4D relational database tools for the management and further analysis of the dataset. Stratford et al. (2016) created a 3D GIS framework at Sterkfontein caves to be applied for spatial distribution analyses. In this research, a data model was created to inform an archaeological database to store the 3D data of Kromdraai.

Spatial Associations and Statistics

There is an uncertainty in inferring past dispersal patterns of an archaeological record based on present day observations. Spatial distribution maps are key tools for archaeological documentation and visualisation. However, there is a lack of reliability in making inferences from these maps that can be improved by adopting a spatial analytic approach and integrating this with knowledge of the taphonomy of the site. Previous spatial statistical tools used in archaeology were limited. However with the evolution of spatial analysis studies, a multi-variate statistical framework has been adopted. This has played an integral part in increasing the reliability and certainty of archaeological predictions and

inferences made about past human behaviours from spatial patterns (Domínguez-Rodrigo et al., 2017). An understanding of hominin-environment interactions is broadened with the application of spatial statistical tools (Domínguez-Rodrigo et al., 2017). Gopher et al. (2016) shares the same sentiments, emphasising that the use of mathematical-statistical methods for distribution analyses and understanding site formation processes are key elements of "effective" spatial analysis.

Few studies have introduced simple statistical tests to assess relations between fossil elements and the surrounding environment; these tests are being implemented to show "hotspots" or the density distribution of different elements within the site (e.g. Oron and Goren-Inbar, 2014; Gopher et al., 2016; Geiling et al., 2018). However, hotspot and density analyses are considered to be limiting and uninformative as they lack statistical significance (Oron and Goren-Inbar, 2014; Oron and Goren-Inbar, 2014). Geiling et al. (2018) add that although density indices are important, these merely form the basis of spatial analyses.

The significance of spatial patterning can be assessed using specific statistical tools such as Kernel density calculations or k-means clustering, the application of Density-Based Spatial Clustering and Application with Noise (DBSCAN). Furthermore, the degree of spatial randomness i.e. dispersed, random and clustered patterns can be tested in a number of ways such as, Chi-square tests, Moran's I global index tool and the Hopkins Statistic (Hopkins and Skellam, 1954) amongst others (Oron and Goren-Inbar, 2014; Geiling et al., 2018).

3D spatial analyses increase the potential to extract more information from the site data because all spatial orientations are taken into consideration. However, most spatial analysis studies implement GIS. The GIS framework is limiting in regard to its potential for 3D cluster or multi-variate analyses because of the 2D or 2.5D interface (Abdul-Rahman and Pilouk, 2007; Vavrek, 2011). A 3D point cloud, which contains

the horizontal, vertical and elevation (X, Y, Z) variables of points provides a more complete interpretation of spatial patterning. Archaeological studies therefore require an all-encompassing 3D framework that integrates quantitative tools and produces statistical outputs such as free statistical computing software, R 2.3.3 (https://cran.r-project.org) used in this research (Oron and Goren-Inbar, 2014; Carrer, 2017; Giusti et al., 2018).

Three-dimensional Digitisation and Photogrammetry

Archaeological studies have transitioned from conventional 2D surveying methods to 3D digitisation and visualisation to conserve heritage and archive data. The increasingly common practice of digitizing of excavation site in 3D, offers better solutions for site preservation and enables realistic site visualizations and more in-depth site analyses and interpretations (Olson and Placchetti, 2015; Zollhöfer et al., 2015; Greenop and Landorf, 2017; Hua et al., 2018;). Digitisation techniques have advanced during the last decade to preserve the visual integrity of cultural heritage sites (Yilmaz et al., 2008; Olson and Placchetti, 2015; Greenop and Landorf, 2017; Santos et al., 2017). Beyond preserving the visualisation of the site, with the integration of complementary techniques, 3D digitisation enables researchers to maximize site analysis potential and minimize data loss post-excavation.

Common 3D digitisation techniques implemented by archaeologists to record archaeological sites and their elements are laser scanning, lidar and photogrammetry (Rüther et al., 2009; Fonstad et al., 2013; McPherron, 2018). These useful techniques have mainly been applied for cultural heritage maintenance in archaeological sites (e.g. Barazzetti et al., 2011; Repola et al., 2018).

Several studies in studies of the *Cradle of Humankind* (Table 2) with the exception

of Coopers (*P. robustus*), Gondolin (*P. robustus*) implement 3D digitization techniques. There is no literature demonstrating the application of 3D spatial reconstruction at the significant hominin-bearing sites of Taung (*Au. Africanus*) and Makapansgat (*Au. Africanus*).

Table 2. Hominin-bearing sites in the *Cradle of Humankind* and studies implementing 3D analysis techniques.

Site	Hominin taxa	3D reconstruction, technique	Reference
Drimolen	*P. robustus*, early *Homo*	Computed tomography, terrestrial laser scanning, photogrammetry, total station theodolite	Edwards et al., 2017, Armstrong et al., 2018, Herries et al., 2018
Gladysvale	*Au. africanus*	Laser theodolite, GIS	Häusler et al., 2004, Schmid, & Berger, 2004
Kromdraai	*P. robustus*, early *Homo*	Laser scanning, microCT, terrestrial photogrammetry, UAV photogrammetry	Dumoncel et al., 2016, Ngoloyi et al., 2020, submitted
Malapa	*Au. sediba*	MicroCT, CT, synchrotron photogrammetry	Val et al., 2011, Val, 2014, Val et al., 2018
Rising Star	*Homo naledi*	Laser scanning, White-light source photogrammetry, UAV photogrammetry, Manual surveying	Kruger et al., 2016
Sterkfontein	*Au. Africanus, Australopithecus, Australopithecus "second species", P. robustus,* early *Homo, H. ergaster, H. , H.*	Laser scanning, 3D GIS	Subsol et al., 2015

	sapiens		
Swartkrans	*P. robustus*, early *Homo*, *H. sapiens*	Laser theodolite	Nigro et al., 2001, 2003

Close-range laser scanning involves the emission of a beam of light onto a specific object, this light is sensed by an optical detector which rapidly perceives the three dimensional pattern of that object by acquiring point cloud data by means of triangulation and time-of flight techniques, these can be further processed and reconstructed into 3D models (Pavlidis et al., 2007; Yastikli, 2007; Sturzenegger and Stead 2009).

Photogrammetry, that implements the structure from motion (SFM) approach has been applied as a mapping tool in archaeology to visualise objects, record their geometry, size, texture and other attributes in 3D; providing 3D vector and point cloud data for the generation of 3D surface models (Allen et al., 2004; Yastikli, 2007; Sturzenegger and Stead, 2009; Zollhöfer et al., 2015). It can be applied widely for a variety of purposes; for example site surface reconstructions (see Dumoncel et al., 2016; Kruger et al., 2016; Armstrong et al., 2018; Ngoloyi et al., 2020), in-situ fossil specimen and footprint imaging, 3D recording of ancient settlements and hominin assemblages (Bennett et al., 2013; Ashton et al., 2014; Remondino et al., 2010), analysis of prehistoric rock art panels allowed for a better analysis of the motifs (Carrero-Pazos et al., 2018). Comparing laser-scanning methods to terrestrial photogrammetry in the Drimolen Palaeocave System, Armstrong et al., (2018) demonstrated the applicability and usefulness of each method for site visualization. However, the authors concluded that photogrammetry was most effective in recording and visually demonstrating archaeological site transformation over time (Armstrong et al., 2018).

The multi-scalar 3D data record of Kromdraai, containing data surveys of the site and surrounding areas at varied spatial resolutions ranging from few microns to several km's, has been established since 2010 using micro-computed tomography (µCT), laser scanning techniques, photogrammetry (Table 3; Dumoncel et al., 2016).

Table 3. Parameters specified for 3D digitisation methods implemented at Kromdraai.

3D Digitisation Technique	Resolution (mm)	Accuracy	Object size (m)	Scale
UAS Photogrammetry	10	3 cm	100 - 1000	km
Terrestrial Laser Scanning	02-10	2 - 10 mm	10	m
Terrestrial Photogrammetry	0.1 - 1	cm - sub cm's	1	m - km's
Portal laser scanning	0.1	0.10 - 0.05 mm	1	m
Micro-CT	0.01		0.1	*c*m

Micro-computed tomography entailed the scanning of fossils, including artifacts enclosed in Breccia, at a high spatial resolution (a micron scale).

Laser scanning at Kromdraai was undertaken using two types of laser scanners namely the 360˚ Faro Focus 3D, which was used to digitise a large area of Kromdraai, having an accuracy between 2-10mm and; the Creaform Handyscan for the digitisation of in-situ features in the Kromdraai B excavation capturing specific objects and relationships for example, the contacts between Breccia and Flowstones within the site and, the true texture of the site with an accuracy of 0.05mm and a 0.1mm resolution. KRP researchers prior to my involvement in the team conducted all laser scanning.

Multi-image photogrammetry was also used to supply the 3D information of objects (Yastikli 2007). Multi-image photography achieves accurate close-range

photogrammetry owing to the fact that the method captures multiple images of a given area from various points of view in large overlaps, capturing its entirety at a regional and local scale (Yastikli 2007; Rüther et al., 2014). For 3D reconstruction of a regional area (several km's) surrounding Kromdraai, the "senseFly" eBee was used, producing time-stamped and georeferenced images (Dumoncel et al., 2016). Close range aerial photogrammetry was achieved with the DJI phantom drone, in addition to a hand-held camera for terrestrial photogrammetry (Dumoncel et al., 2016). For this particular research, multi-image photogrammetry using the DJI phantom drone and a hand-held camera was used to supply the 3D information of objects used to compute the 3D models and orthophoto's in chapters 2 and 3 respectively (Ngoloyi et al., 2020; Ngoloyi et al., 2020, submitted). Terrestrial photogrammetry was applied to visualise and compute overburden sediment volumes (chapter 2). Furthermore, orthophoto's produced from 3D point cloud data from drone photogrammetry were used to illustrate the in-situ localisation and spatial patterning of fossils (chapter 3, Ngoloyi et al., 2020). Drone photogrammetry is more expensive as it requires investment in drone equipment and the skills of a drone operator. This was conducted by R. Hautefort, the drone operator for the KRP over two one week long field visits in 2016 ad 2017. He also provided me with training for conducting close-range drone photogrammetry at a local scale (these images were not used in the thesis). Terrestrial photogrammetry was much more affordable as it only required a hand-held camera. I conducted terrestrial photogrammetry to capture the long-term transformation of the site under the training of L. Bruxelles twice in 2016 and 2017. Over the weeklong excavation photogrammetry was conducted on the final day at the end of the excavation. The remaining time in the filed was spent in the field assisting with the recovery of fossils. Long-term terrestrial photogrammetry was not used in this study.

Instead, short-term (2-day) photogrammetry conducted in 2020 by J. Braga was used in this research. I reconstructed all available photogrammetry images collected between 2014-2020; this data has been stored on a server for further applications.

Case Studies: Application of 3D photogrammetry and GIS in environmental and archaeological analysis worldwide

The application of GIS, 3D digitization and statistical techniques is vast and extensively implemented worldwide to extract a range of data. This section summarises studies demonstrating the diverse applications of these methods worldwide.

Photogrammetry, patterning, geostatistics and virtual simulations

Ashton et al (2014) applied multi-image photogrammetry methods to analyse ancient hominin footprints in Happisburgh (UK). Impacted by fluvial erosional processes at the site, the footprints were rapidly deteriorating and photogrammetry was an ideal recording method due to the limited amount of time for investigation (Ashton et al., 2014). Using photogrammetry the footprints were visualized in context to the surrounding environments and distinct features of the impressions were illustrated in 3D, for example, the depth of the foot hollows, spatial scale and dimensions (Ashton et al., 2014). The study also allowed for predictions to be made regarding human activity and settlement as well as analyses of the footprints to inform characteristics such as age and size, which was possible even after their complete destruction (Ashton et al., 2014).

The use of spatial analyses to determine distinct activity areas or the organisational pattern of archaeological sites is possible. Gopher et al. (2016) focused on the use of density analyses within a spatial framework to study lithic assemblages in Middle Pleistocene Qesem Cave in order to interpret the behaviours of an unknown hominin or Neanderthal population. The study of Qesem cave attempted to use the spatial patterning of lithic remains to infer the intensity of lithic activities and activity areas e.g. a fire-place or cooking area and density and frequency data measurements were used as indicators of past human behaviour and cave organisation (Gopher et al., 2016). Although the study showed the density of the assemblage across space, there was significant variability between the density and frequencies of the artefacts which was point of limitation to the study, this further reiterates the point that geostatistics need to be integrated in archaeological spatial patterning studies (Gopher et al., 2016). Correspondingly, Geiling et al. (2018) argued that although density indices are important, these merely form the basis of spatial analyses.

In the study of the Middle Paleolithic to the Bronze Age El Mirón Cave (Spain), density indices calculated for taphonomic groups were instead converted into polygons, positioned within the locality of the site and further analysed using GIS tools (Geiling et al., 2018). Profile plots and distribution maps created from the spatial distribution analyses within GIS, illustrated density variation in the archaeological assemblage of the cave (Geiling et al., 2018). Using the Moran's I global index tool the degree of randomness of the spatial patterns i.e. dispersed, random and clustered patterns, within each polygon was assessed – it was concluded that the vertical and horizontal distributions of the bone micro-fragments in the assemblage were not random, and they were indicative the different uses of space across the site and of past human activities, this was supported by taphonomic evidence.

Domínguez-Rodrigo et al. (2017) showed the usefulness of spatial analyses tools in spatial simulation and prediction models at David's Site (Bed I) in the Early Pleistocene site Olduvai Gorge, Tanzania. Statistical methods such as chi-square and Kolmogorov–Smirnov tests were used in the Olduvai site to test Complete Spatial Randomness (CSR) (Domínguez-Rodrigo et al., 2017). Log-linear methods such as linear regressions and polynomial regressions were used to understand the homogeneity of the point patterns displayed in the datasets and to indicate spatial trends (Domínguez-Rodrigo et al., 2017).

Although this is a fairly new concept in archaeology, the application of archaeological predictive modelling (APM) incorporating multivariate spatial pattern analysis tools is more common to interpret more recent, non-hominin archaeological site distributions and organisation. A recent study by Zhu et al. (2018) showed the use of APM studying the spatial patterning of historical trading and defense sites in China's Northern Silk Road (CNSR) and Great Wall regions – this shows the potential and applicability of these methods.

Another example of spatial simulation modelling is shown in the more recent Bronze Age site of Villaggio delle Macine in Italy, Achino and Barceló (2018) demonstrated the use of spatial interpolation techniques to predict the spatiality of intra-site activities. In this study, the consistent dispersal of bone fragments within a space was equated to intentional dispersal (i.e. specific disposal area) and a random spatial distribution indicated low intentionality in this regard; the study used information regarding the spatial dispersion of the archaeological materials to calculate the probability of intentional social behaviour (Achino & Barceló, 2018).

Changes in water levels at the lakeside site were factored in as depositional effects and therefore disturbances to the spatial pattern of the site, leading to a decreased fossil density and, a more homogenous and less distinct pattern of distribution (Achino & Barceló, 2018). The spatial process at the site was reconstructed through the interpolation different spatial theoretical or simulation models using geostatistical tools Kriging and the Gaussian model, this proved beneficial as dense sampling units for future analyses were well predicted (Achino & Barceló, 2018). In contrast to other sites, taphonomic and statistical evidence at the FLK Zinj and PTK I sites of Olduvai Gorge showed that post-depositional disturbances had no significant effect on the spatial associations of bone and lithic elements within the assemblages, indicating good preservation (Domínguez-Rodrigo & Cobo-Sánchez, 2017).

Domínguez-Rodrigo and Cobo-Sánchez (2017) found that the application of statistical spatial tools on archaeological assemblages at the FLK Zinj and PTK I sites could also indicate socio-economic organisation by hominins. As in David's Site, CSR tests were conducted at FLK Zinj and PTK I to test the homogeneity of the patterns and spatial randomness; the application of regression models enabled the simulation of clustering and scattering across the site (Domínguez-Rodrigo & Cobo-Sánchez, 2017). The spatial patterning and density distribution of the bones and lithic remains alluded to the existence of nuclear hominin families or social units responsible for food sharing and distribution, these families lived separately from the larger social group (Domínguez-Rodrigo & Cobo-Sánchez, 2017). Similar to the Domínguez-Rodrigo and Cobo-Sánchez (2017) study of hominins in Olduvai (FLK Zinj and PTK I), Spagnolo et al. (2018) showed the social and economic organization of the Oscurusciuto Rockshelter Neanderthal camp in their spatial distribution and spatial statistical analyses, using GIS and point pattern cluster analysis techniques.

Spatial distribution and taphonomy

In a study about the spatial patterning of the Middle Palaeolithic site Mousterian (Quneitra), Oron and Goren-Inbar (2014) used GIS to analyse, manage and visualise the bone and lithic artefact database. The results rendered were scatter maps displaying zones of high density which were found to be uninformative as they lacked statistical significance (Oron & Goren-Inbar, 2014). Determining the level of significance in the difference between the distribution patterns of specific categories of artefact types versus all other artefacts in the assemblage is challenging; to overcome this challenge, spatial patterning was determined by calculating the Kernel density of the points within each determined raster cell representing the surface of the site (Oron & Goren-Inbar, 2014). Furthermore, Chi-square tests were used to determine the non-randomness of the scattering and the difference between expected and observed densities (Oron & Goren-Inbar, 2014).These tests analysed the frequencies of specific variables against the larger dataset, for example, testing the significance of the frequency of hominin modified bones against the frequency all other bones within the dataset (Oron & Goren-Inbar, 2014).

Oron and Goren-Inbar (2014) acknowledge that the main challenges associated with using spatial analysis tools to understand human behaviour are taphonomy and time-span discrepancies. The archaeological assemblage/horizon is largely affected by taphonomy as this pertains to the effect of post-depositional processes on the burial and location of fossil items (Oron & Goren-Inbar, 2014). The length of the period represented by the assemblage and anthropogenic activity occurring within that time-frame also has implications on the spatial organisation patterns of archaeological sites. Therefore Oron and Goren-Inbar (2014) reiterate in the study of Mousterian that in order to fully interpret and understand the spatial organisation patterns of

prehistoric sites, site formation processes must be analysed. Giusti et al. (2018) echoed similar thoughts and implied that spatial associations of archaeological finds in the Middle Pleistocene site Marathousa are affected by taphonomy and are therefore unreliable if this aspect is not considered. Carrer (2017) adds that spatial and geostatistical (quantitative) analysis findings supplemented with ethnographic data is useful, this was the case for the archaeological interpretation of Val Maudagna (Italian western Alps). Using spatial point-pattern analyses the study provided insight on impact of past human behaviour on the taphonomy of the archaeological site further reaffirming the interdependence between taphonomy and spatial analyses (Carrer, 2017).

GIS test results of the Mousterian site corroborated previous taphonomic examinations that illustrated that water activity and changes in the waterline of the site had no bearing on the size sorting or the preservation of the artefacts (Oron & Goren-Inbar, 2014). Bone accumulations with bite marks concentrated in certain areas of the site supported taphonomic conclusions of animal activity and, the non-random scattering of lithic artefacts showed human activity (Oron & Goren-Inbar, 2014). Short episodes of human activity indicated by well-preserved bones and lithic items were determined for the site, and spatial patterning evidence showed hominins displaying a preference for particular areas within the site for specific activities for example, “carcass processing” (Oron & Goren-Inbar, 2014).

Giusti et al. (2018) study of Marathousa 1 focused on the use of geostatistics to understand site formation processes and their effect on the spatial patterning of faunal remains and lithic artefacts, in order to ultimately make inferences on hominin behaviours and their exploitation of animals, particularly elephants; this supported a

previous taphonomy study of the site showing distinctive evidence of mammal butchering (Giusti et al., 2018; Konidaris et al., 2018)(Oron & Goren-Inbar, 2014).

The geostatistical study incorporated fabric analyses which involved examining the orientation of the elongated sediments and archaeological finds (bones, artefacts) in order to determine site formation processes and understand taphonomy (Giusti et al., 2018). The in-situ linear, isotropic and planar orientation patterns were analysed, and used as indicators of the randomness of the fossil assemblage orientation (Giusti et al., 2018). Spatial point pattern analyses such as Kernel Density and Ripley's K-function were used to identify spatial trends and, were indicators of the spatial uniformity or randomness of distributions (caused by point processes such as mud-flows); 3D univariate and bivariate functions were used to determine the spatial associations between lithic artefacts and faunal remains (Giusti et al., 2018).

Results of the Marathousa 1 study showed the fossil assemblage to be autochonous and having maintained its initial attributes because of minor alterations by depositional processes however, due to a low spatio-temporal resolution of the study, inferences about past human behaviours within the site were not made. This is in agreement with a paper by Tourloukis et al. (2018) concluding that detailed hominin behavioural inferences were not possible from spatial distribution analyses of Marathousa 1 due to the local reworking of fossil finds at the site. It was however possible to identify activity areas such as tool maintenance regions and mammal exploitation regions based on spatial analyses and fossil evidence (Tourloukis et al., 2018).

Site orientation

Most previous studies agree that despite the involvement of biological agents, post-depositional processes have had little effect on the assemblages in Olduvai Gorge, Tanzania (Africa). On the contrary, with the recent introduction of GIS techniques to investigate orientation patterns and site formation processes in Olduvai Gorge, it was evident that environmental disturbances have played a role in the spatial patterning of the bone and stone tool assemblages (Benito-Calvo and de la Torre 2011, 2013). GIS and statistical analyses indicated an uncharacteristically clear pattern in the orientation of the specimens, presumably rendered by geological agents, erosional and fluvial processes; they also revealed the complexity of the site formation history. Similarly, with the application of GIS techniques on faunal assemblages at Middle Pleistocene site Castel di Guido (Italy), the orientation patterns of the distributions aided in distinguishing between fluvial or human agents of deposition (Boschian & Saccà, 2010).

On the contrary, a study conducted in Middle Pleistocene archaeological site, Spear Horizon (Germany), detailing the spatial distribution of bone, flint and wood remains rendered conflicting results (Böhner, Serangeli, & Richter, 2015). Results indicated that taphonomic processes had little effect on the distribution or orientation of the elements (Böhner et al., 2015). In fact, the orientation of the finds was observed to be completely random and taphonomic influences were small scale, mainly affecting the appearance of wooden artifacts (Böhner et al., 2015). The size and weight of remains was also found to have not significantly affected the dispersal and distribution of the fossils (Böhner et al., 2015). It must be noted that sediment composition, geological composition and geomorphology of sites influence the spatial distribution. These are aspects are an important consideration in interpreting spatial

patterning studies, in addition to observing spatial delimitations and the area of the excavated portions of the site.

GIS Applications in South Africa

The different applications of GIS in archaeology are not specific to the location, but rather adapted for the purpose. It is therefore common to find the same methods applied to various sites across the globe, some of the uses are detailed in case studies in this chapter.

Most uses of GIS tools in South Africa are centred on plotting settlement patterns and understanding environmental trends more than the spatiality of, and the relationships between, excavated artefacts such as fossils and tools. For example, Mokokwe (2016) visually represented the spatial distribution of fossil cercopithecoid postcrania based on their size class and age as well as their locality within the different members of the Sterkfontein cave using conventional methods. The author identified a lack of patterning in the spatial distribution of the assemblage owing to complex geological depositional processes characterised by phases of deposition, roof collapse and re-deposition (Mokokwe, 2016), the study was however limited to 2D analyses. Spatial arrangements within the archaeological site can also expose important relationships between site features, structures, and other elements (Clarke, 1977; Wheatley and Gillings, 2013).

GIS and 3D digitisation have also been applied to improve old datasets. The usefulness of GIS analyses for rediscovering, and interpreting low-resolution datasets lacking precise coordinates or point cloud data further demonstrated in the Wonderwerk Cave site (Birkenfeld et al., 2015). Similarly to the Sterkfontein study, Birkenfeld et al. (2015) were able to "back-plot" previous artifact archives missing geo-referenced data, and digitise the Wonderwerk Cave site in 3D. This GIS integration enabled the re-examination of relations and associations between different site elements, past and present, within a stratigraphic and

spatial context of the cave (Birkenfeld et al., 2015).

Metadata modelling and digital databases

Given the large data collection potential of archaeological sites, data storage is an important aspect for the documentation and preservation of archaeological findings. In addition, the reliance on stored data for the continuation of archaeological research is undeniable, particularly in relation to the redistribution and reuse of data for scientific collaboration amongst researchers. In order to efficiently implement 3D analysis techniques in future, a spatial data framework is required. Database Management System (DBMS) software packages enable the organisation of an interconnected data repository, and are equipped with a range of capabilities such as data modelling and querying.

While a relatively recent but rapidly developing concept, digital metadata modelling provides a structural description of the data by combining different metadata characteristics of an archaeological excavation in a single assemblage. A metadata modelling system encourages the fusion of long-term (past and present), comprehensive datasets and aids in the relay of information about multiple elements of the site within an organised, adaptable and accessible system. Additionally, automatic information retrieval, querying and cross-referencing of meaningful information is further enabled (Vlachidis et al., 2013).

Management and recent developments at Kromdraai

From 2014 – 2018, 4804 identifiable mammalian fossils were excavated from Units O and P, 43 of which were hominin specimens (Braga et al., 2020, in revision). To provide context to the site management and progression, the following presents a short summary of the textual documentation of the site, briefly detailing the progress of the excavation and noting some significant structural changes and observations over the periods of 2014- 2018, Plate 6 shows the excavation from the same perspective during the six successive stages of excavation:

December 2014

The period of April 2014 to December 2014 commenced with the northwards extension of the Brain and Vrba test pit (white) with the downward removal of continuous horizontal levels to the depth of 10-15 cm and exposure of 5 cm vertical thin sections (Plate 1).

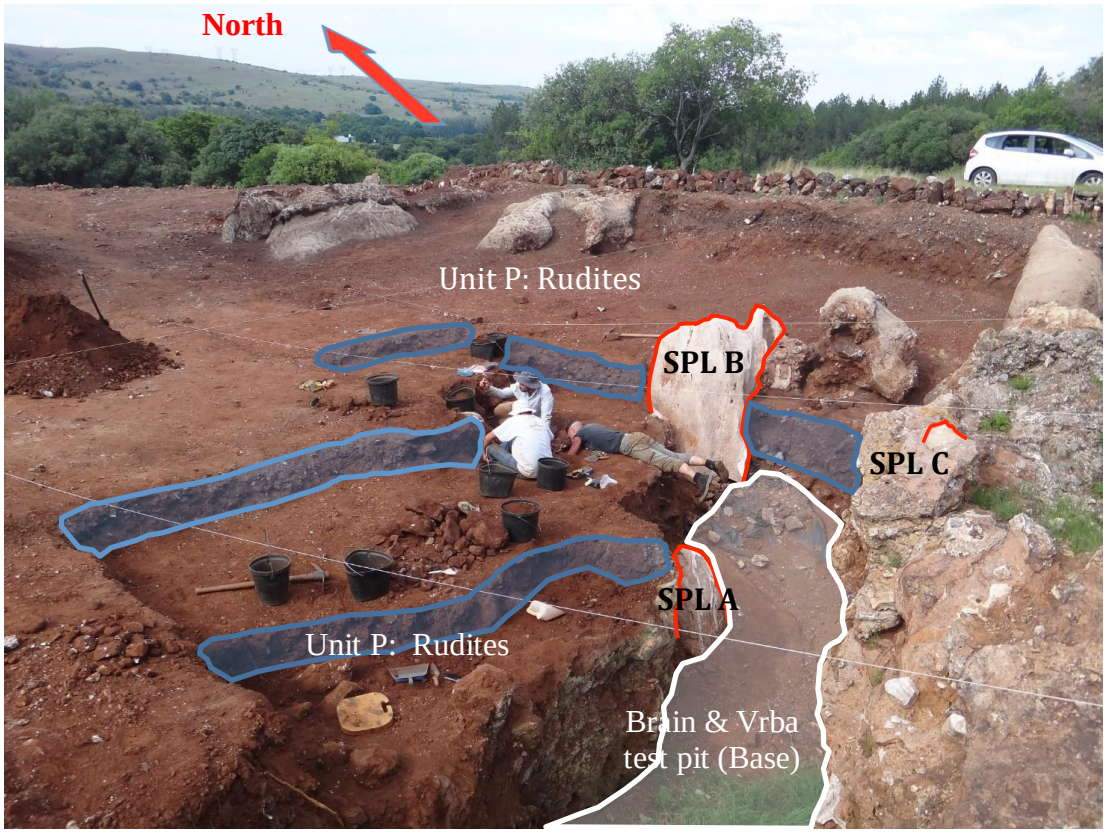

Plate 1. Stage 1 of Kromdraai excavation illustrating Unit P soft rudites, the base of Brain (1955 - 1956) and Vrba (1977 - 1980) test pit in white and three speleothems "speleothem A" (SPL A) at the base of Unit P and "speleothem B" (SPL B) at the top of the excavation and "speleothem C" (SPL C). Indicated in blue are successfully removed horizontal levels as the excavation extended northwards.

Consequently, two new speleothems were discovered (SPL A and SPL B) within Unit P, previously unconsidered by Brain (1981) and Vrba (1981). Another visible speleothem include "speleothem C" (SPL C) noted by Vrba (1981) as a stalagmite (Plate 1).

December 2015

The further excavation of Unit P in December 2015 revealed a large stalagmite of which SPL A is a component, and lead to a further northward extension as the removal of the continuous horizontal layers progressed (Plate 2). Indurated clastic

breccias formed part of the “Main Remnant”, a vertical mass that is a significant feature of the site.

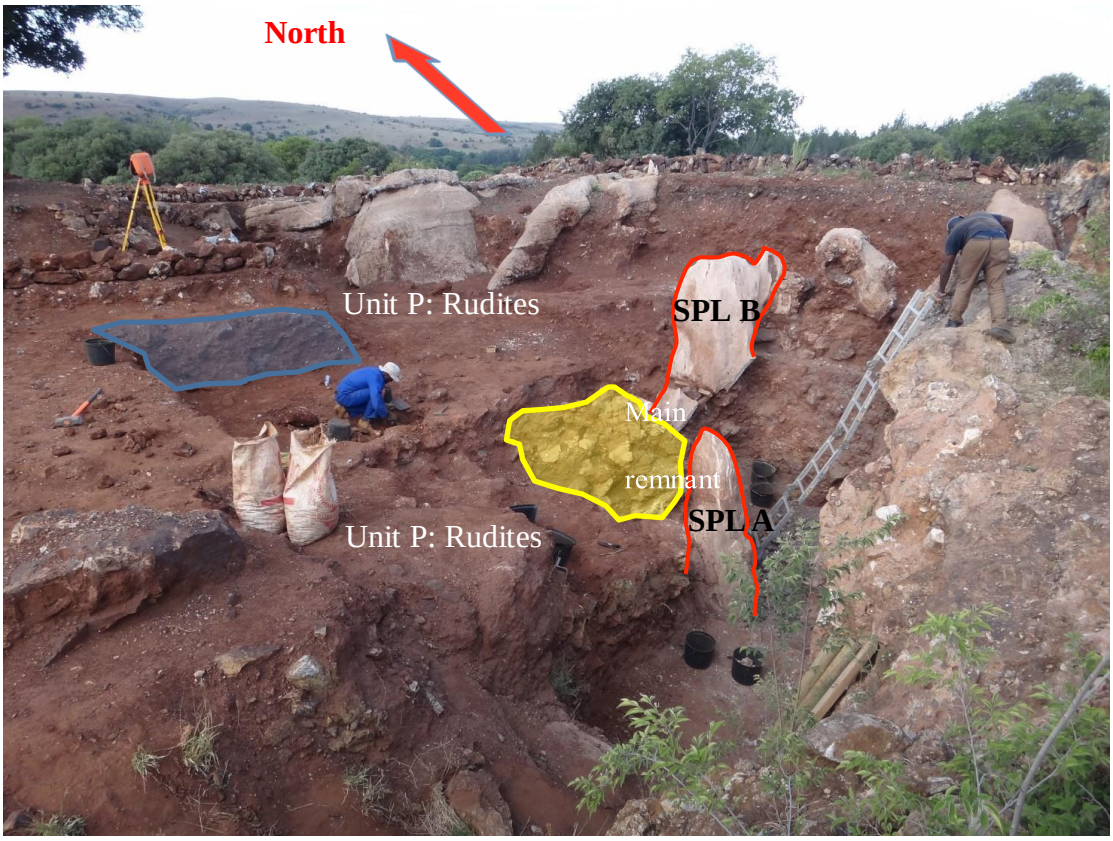

Plate 2. Stage 2 of Kromdraai excavation captured in December 2015. This image illustrates two speleothems “speleothem A” (SPL A) and “speleothem B” (SPL B) outlined in red. Two dolomitic roof pendants “dolomitic pendant A” (DP A) and “dolomitic pendant B” (DP B). The indurated breccias forming the “main remnant” positioned within soft rudites (indicated in yellow) are positioned near SPL A. Indicated in blue are successfully removed horizontal levels as the excavation extended northwards.

May 2016

In May, two dolomitic roof pendants (DP A, DP B) reminiscent of the previous ‘roof of the cavity’ and a one-meter wide gryke were exposed in the soft rudites with the downward progression in Unit P (Plate 3). Unit O was exposed within the “KW 9900 Test Pit” where the first vertical profile (1.5 m) in Unit P was shown.

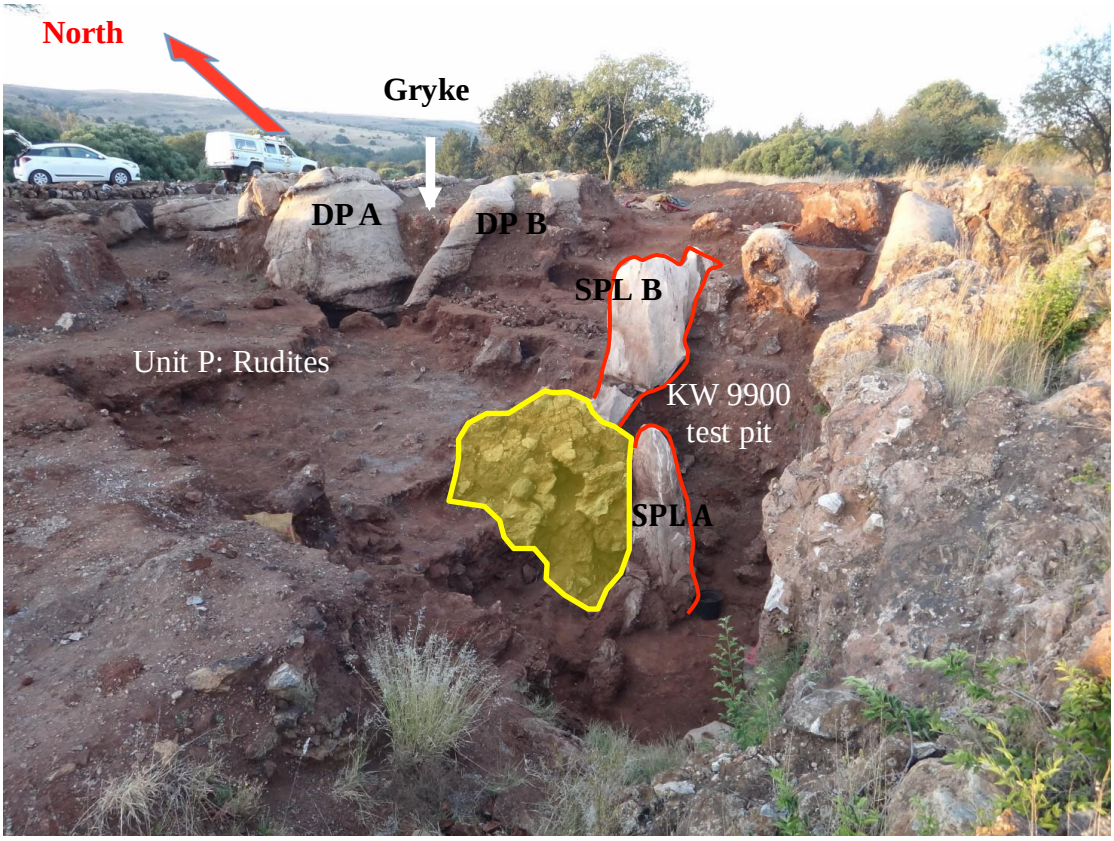

Plate 3. Stage 3 of Kromdraai excavation, May 2016. This image illustrates the Unit P rudites, the vertical profile of Unit P through the KW9900 test pit, showing the upper limit of Unit O at its base. Also visible are speleothems, "speleothem A" (SPL A) and "speleothem B" (SPL B). The indurated breccias forming the "main remnant" positioned within soft rudites (indicated in yellow) are positioned near SPL A. Two dolomitic roof pendants "dolomitic pendant A" (DP A) and "dolomitic pendant B" (DP B) within the soft rudites of Unit P. Exposed between the dolomitic roof pendants is a 1m wide gryke.

March and September 2017

As a precautionary measure to prevent a collapse into archaeological deposits, the previously discovered speleothem "SPL B" and dolomitic roof pendants "DP B" were removed in March (Plate 4). Subsequently, a mass of breccia aggregates coined "Chaos Block" were exposed (Plate 4). During the September excavation, the northward extension and advancement on the "KW 9900 Test Pit" continued,

enabling the study of sedimentary features found along a second 4 meter vertical profile in Unit P of which the base revealed the contact between Unit P and Unit O which for which spatial coordinates were recorded.

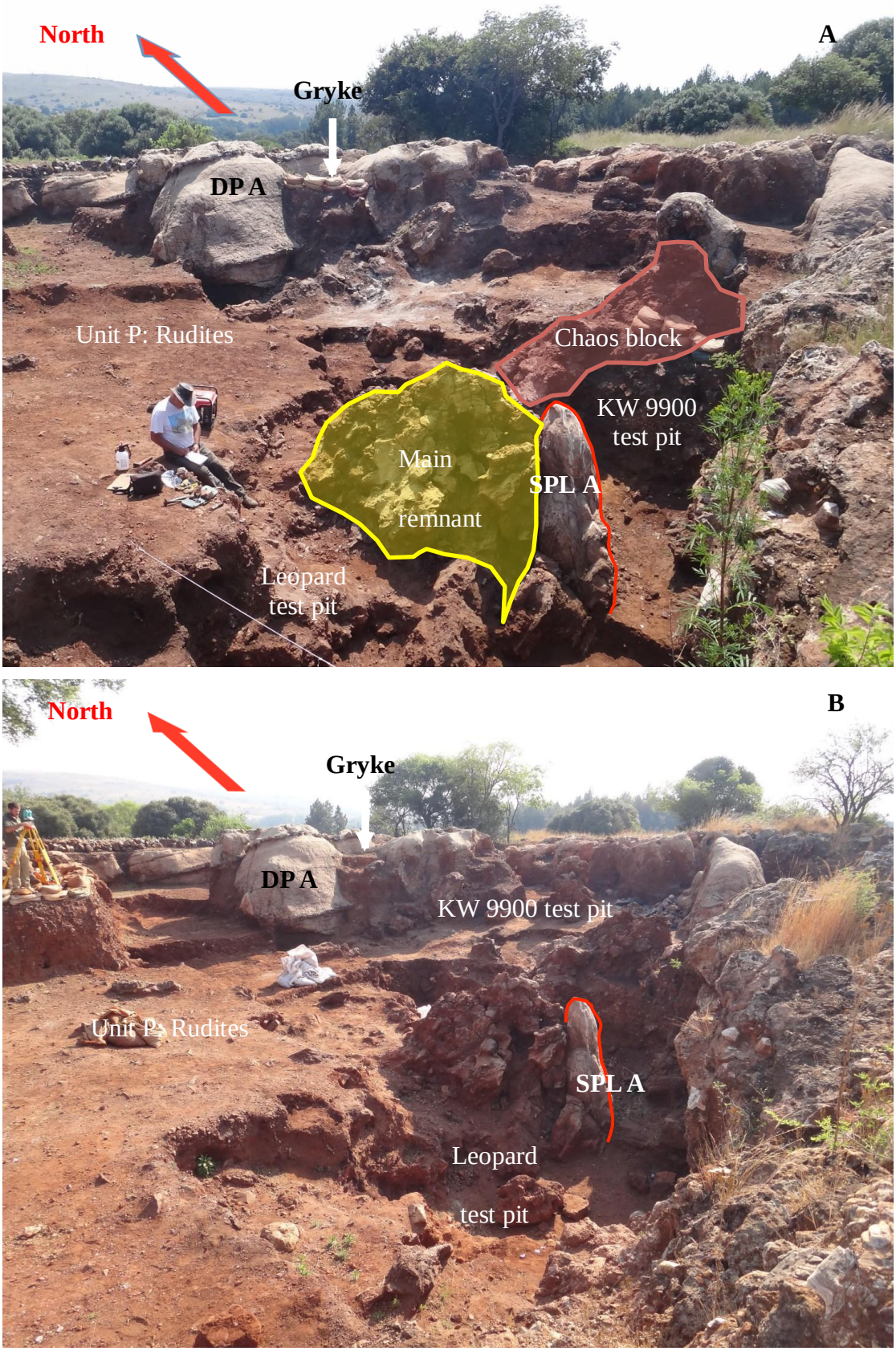

Plate 4. Stage 4 and 5 of Kromdraai excavation, March 2017 (A) and September 2017 (B) respectively. Images A and B show the absence of "dolomitic roof pendant B" (DP B).and "speleothem B" (SPL B) which have been removed, only "speleothem A"

(SPL A) and “dolomitic roof pendant A” (DP A) remain. Also shown are two vertical mass of indurated breccias namely the “main remnant” indicated in yellow and the “chaos block” in orange. The northwards extension and deepening of “KW 9900 Test Pit” are observed in images A and B, and the emergence of the “Leopard Test Pit” is visible in the foreground.

May 2018

Concluding excavations within Unit P, the limits of the 3 test pits were capped with sandbags along the edges in May (Plate 5). The 2018 phase of excavation was the onset of the excavation of Member O (Plate 5). A test pit was pursued and advanced eastwards, maintaining 1.5 meter vertical profiles as the excavation has progressed.

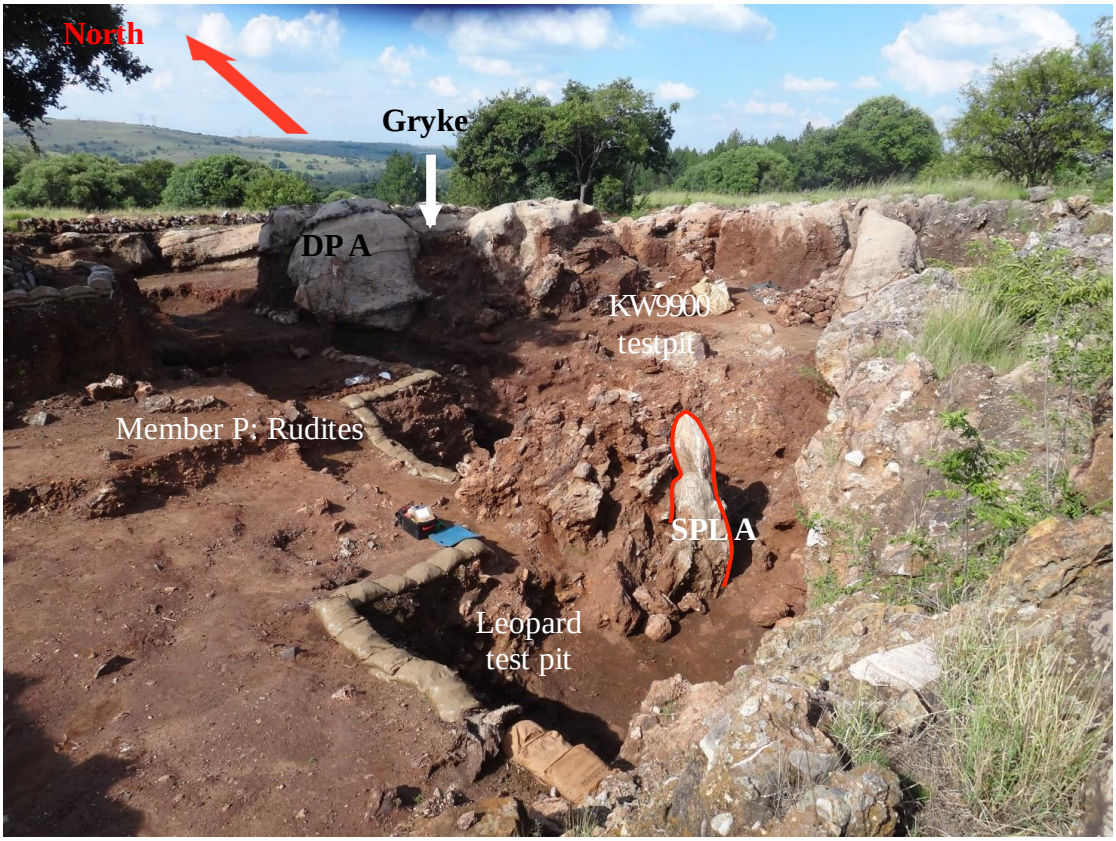

Plate 5. Stage six of Kromdraai excavation, May 2018, illustrating the leopard test pit in the foreground and the KW9900 test pit in the northwards extension of the site.

Also visible are “speleothem A” (SPL A) behind the leopard test pit and a “dolomitic roof pendant A” (DP A) and Gryke in the far north of the site.

Plate 6. South-western perspective showing the progression of the excavation over 6 successive stages between 2014 – 2018 of Unit P, Kromdraai.

Aims/objectives and thesis overview

Aim

This research investigates the spatial distribution patterns of fossils in Unit P using 3D digitisation techniques. The degree of reliability of spatial associations between the excavated fossils is important, it must therefore be supported by statistical evidence. This study therefore provides a unique perspective for the Kromdraai site by using a computer guided 3D spatial reconstruction that integrates statistical spatial analyses of 3D data. The results of this thesis are presented in the format of two manuscripts, the first submitted for publication (chapter 2) and the second published in the *Journal of Archaeological Science: Reports* (chapter 3). Each chapter addresses the thesis objectives, which are stipulated as follows:

Objectives

1.1. To integrate 3D digitization as a tool during the excavation to inform best field documentation practices, for spatial analysis and volume estimation.

1.2. To develop a sophisticated database for Kromdraai, enabling the fusion of 3D modelling and qualitative and quantitative data, for spatial analysis queries.

2. To create an authentic visualisation and assessment of spatial patterning of fossils in 3D using point cloud data.

3. To assess and interpret the spatial associations amongst and between discovered hominin and non-hominin fossils within the context of the cavity, in order to further discuss the taphonomy of Kromdraai.

Chapter one of this thesis contextualizes the research conducted and provided a rationale for the study. We introduced the framework of the research by defining the

specific aim and objectives for the study has also been provided. We presented a background of the study including a brief synopsis of 3D digitization and photogrammetry applications in hominin bearing open-roof cave systems of the *Cradle of Humankind* (Table 3). The research is contextualized within the framework of archaeological and cultural heritage documentation. An overview of the study site was also presented in chapter one, detailing the location of the site within the *Cradle of Humankind*.

Chapter two addresses the objective 1, which was two-fold. The first part of objective 1.1 was to develop a method that integrates 3D digitization as a tool during the excavation to inform best field documentation practices. In this study, we used terrestrial photogrammetry in order to model two successive stages of excavation in 3D, and to visualise and estimate the volume of over-burden sediments removed.

Given the digitization of the sub-volumes, we are able to allocate ex-situ fossils acquired by the wet-sieving mesh process post-excavation to a particular location and volume. This information can be used to supplement spatial patterning analysis and support more taphonomic insights (as mentioned in chapter 2).

Lastly, objective 1.2 introduces the application of 4D relational database systems for raw data archiving at Kromdraai. In this section of the chapter we present how metadata modelling was applied in this study as the initial step undertaken to facilitate in the management and organisation of vast and diverse datasets, including spatial information, and enhances archaeological spatial analysis.

Chapter three addresses the **second and third objectives** of the thesis and presents the first application a 3D approach towards spatial patterning analysis at

Kromdraai in the publication “A new method to evaluate 3D spatial patterns within early hominin-bearing sites. An example from Kromdraai (Gauteng Province, South Africa)” (Ngoloyi et al., 2020). Using k-means and dbscan clustering, the spatial patterning of the fossil assemblage was determined and visualized in 2D and 3D. Incorporating statistical techniques, the research supported the spatial trends revealed for the fossils recovered in-situ of Unit P - a rare approach to hominin fossil assemblages within the *Cradle of Humankind*.

CHAPTER TWO: Improving archaeological documentation and practices. A new protocol from the Plio-Pleistocene site of Kromdraai (Gauteng, South Africa).

Submitted manuscript: *Journal on Computing and Cultural Heritage*

Citation: Ngoloyi, N.M, Dumoncel, J., Zipfel, B., Thackeray, F., Adeoye, V., Panta, F.J., Sèdes, F., Braga, J. (2020, submitted). Improving archaeological documentation and practices. A new protocol from the Plio-Pleistocene site of Kromdraai (Gauteng, South Africa). *Journal on Computing and Cultural Heritage*.

Metadata modelling for the Kromdraai dataset was conducted in collaboration with the IRIT laboratory, as a masters research project by computer science student V. Adeoye. Adeoye worked under the supervision of F. Panta and F. Sèdes. I engaged in many discussions with the IRIT team to describe the metadata and also define the different relationships existing between taxa, skeletal region and tool elements in the model. I also discussed projected archaeological uses for this method, in order for the computer scientist to make an informed decision regarding the software to be used. I first initiated the idea of computing volume in 3D for ex-situ fossils using photogrammetry and VRMesh. Due to the limited usability of this software, J. Dumoncel and J. Braga suggested the use of segmentation in Avizo 8 following a similar process. J. Dumoncel developed and trained me in the method, which I then applied to both of the models that were used for volume estimation in this paper.

Improving archaeological documentation and practices. A new protocol from the Plio-Pleistocene site of Kromdraai (Gauteng, South Africa).

Nonkululeko Mantombi Ngoloyi*[a], Jean Dumoncel[a], Bernhard Zipfel[b], Francis Thackeray[b], Victoria Adeoye[c], Franck Jeveme Panta[c], Florence Sèdes[c], José Braga[ac]

[a]*Computer-assisted Palaeoanthropology Team, UMR 5288 CNRS-Université de Toulouse, Paul Sabatier, Toulouse, France*

[b]*Evolutionary Studies Institute, University of the Witwatersrand, PO WITS, Johannesburg, South Africa*

[c]*Evolutionary Studies Institute, University of the Witwatersrand, PO WITS, Johannesburg, South Africa*

*Corresponding Author

Email: mantombingoloyi@gmail.com

Abstract

The fragility of archaeological heritage necessitates the efficient documentation and preservation of heritage and the evolution of past societies. Following CIPA (International Committee of Architectural Photogrammetry) guidelines for archaeological heritage management mandated by UNESCO and similar international agencies that acknowledge the significance of cultural heritage documentation and best practices, we present a protocol for heritage documentation. This paper presents an original and unique volume reconstruction and estimation technique developed for the quantification and visualization of overburden volume sediments at Kromdraai. We implement 3D photogrammetry to estimate volumes and provide a temporal and spatial context to the volume of material removed. Close range photogrammetry provides an inclusive approach for volume estimation in archaeology. In order to ensure accuracy, we provided a comparative analysis of the results of the volume measurements using different software. Furthermore, we introduce a metadata modelling to show the potential use of 4D relational database management systems for the fusion, organisation and dissemination of the Kromdraai site dataset and the sharing of intellectual property. Our results demonstrated the usefulness of photogrammetry and present a successful new method for volume estimation.

Keywords: Kromdraai; volume estimation; archaeological documentation; database management; photogrammetry

Introduction

Archaeological heritage represents a fragile and non-renewable documentation of past human societies that evolved and interacted with their changing environments. It is therefore essential to minimize its destruction during excavation, to enhance its documentation and reconstruction, whereby the necessary archaeological information is better recorded and more efficiently organized towards achieving preservation and a dissemination strategy for the benefit of present and future generations. Cultural heritage documentation is now a global priority (Dall'Astaa et al., 2016). Acknowledging the significance of cultural heritage documentation, a number of international organizations and committees (e.g. the International Council on Monuments and Sites or ICOMOS, the International Committee for the Management of Archaeological Heritage or ICAHM) are connected to international agencies such as UNESCO (Dall'Astaa et al., 2016). They have mandates to define principles and guidelines relating to the various processes involved in the study, protection, preservation and management of archaeological heritage, from excavation to information dissemination and the sharing of intellectual property (Dall'Astaa et al., 2016).

Archaeological data, documentation, and best practices

The UNESCO Charter on the Preservation of Digital Heritage defines digital heritage as "unique resources of human knowledge and expression" comprised of information relating to science, education and culture amongst other subjects (http://portal.unesco.org/), and it need not be repeated here. However, in dealing with the scientific investigation of an archaeological site, we briefly give some background information to introduce the present study, which focuses on methods for the

innovative creation of digitally formatted integrated databases and imagery. Our aim is to enhance the fullest possible palaeontological, archaeological, sedimentary and geochemical evidence to be documented, preserved and shared in order to minimize any loss during the excavation, as well as to improve the continuous, dynamic process of multi-proxy data gathering as a primary resource database made available to the scientific community. More specifically, we focus on digital methods carried out on the Kromdraai palaeontological site (26°00'41''S, 27°44'60''E) (Gauteng, South Africa), a palaeokarst situated along the southern flank of the Bloubank River (Figure 2) where important early hominins have been discovered during recent excavations (Braga et al., 2013, 2017, 2020 in revision). The Kromdraai site is listed within the UNESCO World Heritage Site referred to as the '*Cradle of Humankind*' (Gauteng Province, South Africa).

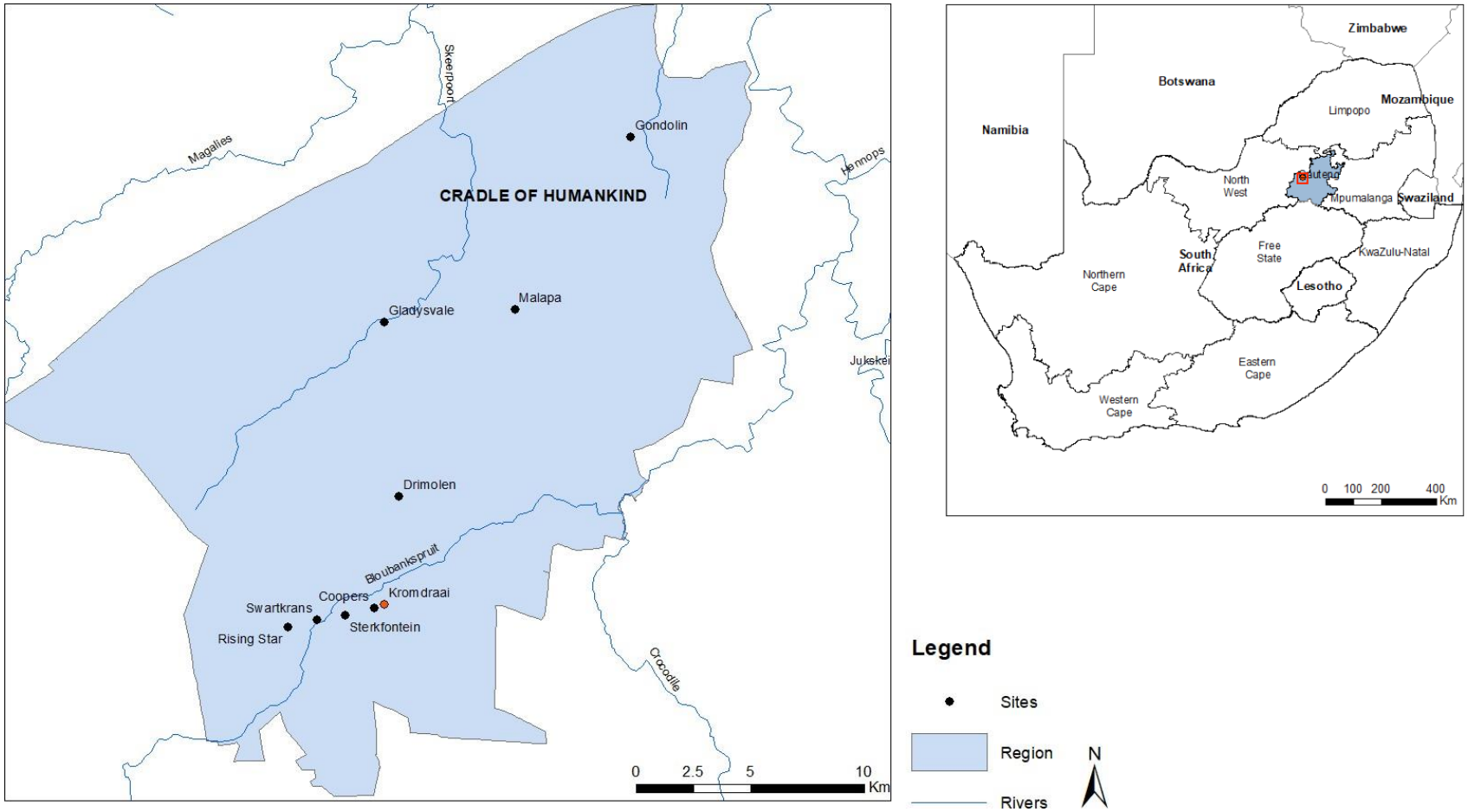

Figure 1. Map showing the location of Kromdraai within the *Cradle of Humankind* and the greater context of South Africa.

The CIPA (one of the oldest international scientific committees of ICOMOS) has played monumental roles in the development of guidelines and best practices of heritage documentation and the publication of the applications of specific digital documentation practices (CIPA, 2020, Quintero et al., 2017). Four of the most common impositions in these guidelines for efficient heritage documentation are: (i) accruing multi-scalar, detailed recordings of information about the site (including textual records); (ii) creating digital records such as dated images or 3D recordings; (iii) developing a rational 4D data management system to enable future information dissemination; (iv) presenting an understandable and accessible means of information communication through visualization (Patias, 2006, Patias and Santana, 2011).

Other considerations to take into account include the cost-effectiveness, applicability and flexibility of the methods employed (Dall'Astaa et al., 2016). Owing to the complexity of heritage documentation however, D'Ayala and Smars (2003) list general guiding concepts that should be considered when informing best practices (Patias, 2006, Patias and Santana, 2011). Among them, we list here the following guiding concepts: (i) ensure that we do not remove any archaeological information that may be deemed important for the future; (ii) ensure that new skills are developed whilst creating a documentation that is useful, integrated with other techniques and will be applicable in the future; (iii) organize the data such that it facilitates straightforward exchanges amongst specialists.

Aims

Following the guidelines stipulated above, this paper presents a new protocol that uses three-dimensional (3D) data capture technologies to record as much of the Kromdraai site and its contained archaeological evidence as possible, before, during

and post-excavation. More specifically, we use the ‘grave-to-cradle’ concept (Greenop and Landorf, 2017) whereby an authentic visual memory of the site is preserved digitally for further data extraction, analyses and interpretation despite the physical deterioration of archaeological sites, and significant data loss caused by the destructive nature of the excavation processes – therefore maximizing the overall research potential of the site post-excavation. Indeed, maps, drawings or photographs do not suffice to produce a 3D representation of the periodic and successive phases of excavation at any given archaeological site.

At Kromdraai, the advanced digitisation of the site was introduced during the renewal of excavations at the site (Braga et al., 2016a, 2017) by way of a transition from traditional methods towards the implementation of various methods of 3D data collection, processing and visualisation (Dumoncel et al., 2016, Ngoloyi et al., 2020). The combined use of a total station (or theodolite), short and long range 3D scanning (using structured light technology and laser, respectively), photogrammetry (either terrestrial or using unmanned aerial vehicles) and micro-computed X-ray tomography (micro-CT) allowed for the in situ collection and the 3D visualization of important palaeontological and archaeological discoveries at Kromdraai (Dumoncel et al., 2016, Ngoloyi et al., 2020). The 3D visualization of key stratigraphic, taphonomic, and more generally geological features allowed for the reconstruction of paleoenvironments and the accumulation process of the deposits.

Even though significant fossils and artefacts are discovered in situ near the surface level at Kromdraai (Braga et al., 2020, in revision), with the possibility of concealment within removed sediments and aggregates, some fossils are not immediately visible in-situ to the naked eye. Therefore, through the wet-sieving process, some fossils are accessioned post excavation. This procedure is commonly

used in most archaeological excavations. The sieved fossil finds can always be relocated within the excavation because the overburden sediments are related to either a grid system (usually metric) or a horizontal and vertical mapping system (using GPS and a Total Station) before being sieved. However, the exact post-excavation repositioning and 3D representation, and the quantification of the volumes of overburden sediments removed daily by each excavator are most often neglected or ignored. Here, we argue that if otherwise integrated in a visual, 3D point cloud database of the site, the volume and repositioning of overburden sediments removed daily could provide important information. Indeed, the quantification of the exact positions and relative proportions of the volume of sediments and fossils removed daily within a space (area) and over time (consecutive excavations) may represent useful indicators for future expectations. In this regard, here we present for the first time a new digital recording protocol that is carried out continuously (i.e., on a daily basis) during excavations at Kromdraai.

We then demonstrate the use of a metadata modelling system that will encourage the fusion of long-term (past and present) and comprehensive datasets. This will aid in the relay of information about palaeontological, archaeological, sedimentological and geochemical elements of the Kromdraai site within an organised, adaptable and accessible system. This article discusses the step-by-step application of photogrammetry in the documentation of overburden sediments, the metadata modelling system and its positive impact on archaeological work, the Kromdraai site being taken as a case in point.

Materials and Methods

As a case study to assess the quality and adequacy of information gathered, here we focus the analyses on two relatively small areas of interest investigated by two different experimented excavators (J. Braga and Moleko Monyama) over a two-day period in January 2020. Therefore, two separate and relatively small volumes of overburden sediments were collected and wet sieved during this excavation. On this occasion, no fossil or bone flake was discovered in situ or after sieving, we will therefore rather only report on the methods applied to acquire volume data and not the fossil assemblage. I defined a workflow to virtually generate, align and segment volumes of overburden sediments (Figure 2).

Three-dimensional (3D) modelling and measurements

I used photogrammetry in association with the user-friendly and low-cost Agisoft Photoscan software to generate the 3D information of objects and surface areas at the local scale. Since I added manually established ground control points (GCPs, Figure 3), measured by a total station in the field and using the original grid system adopted by Elisabeth Vrba (1981) for the Kromdraai datum benchmarks, I could compare the 3D models to their real-world dimensions and therefore assess their accuracy. The advantage of the combined use of 3D photogrammetric models and GCPs was the possibility to obtain direct and accurate measurements from 3D models without necessarily visiting the excavation. The workflow of the whole process is described as follows:

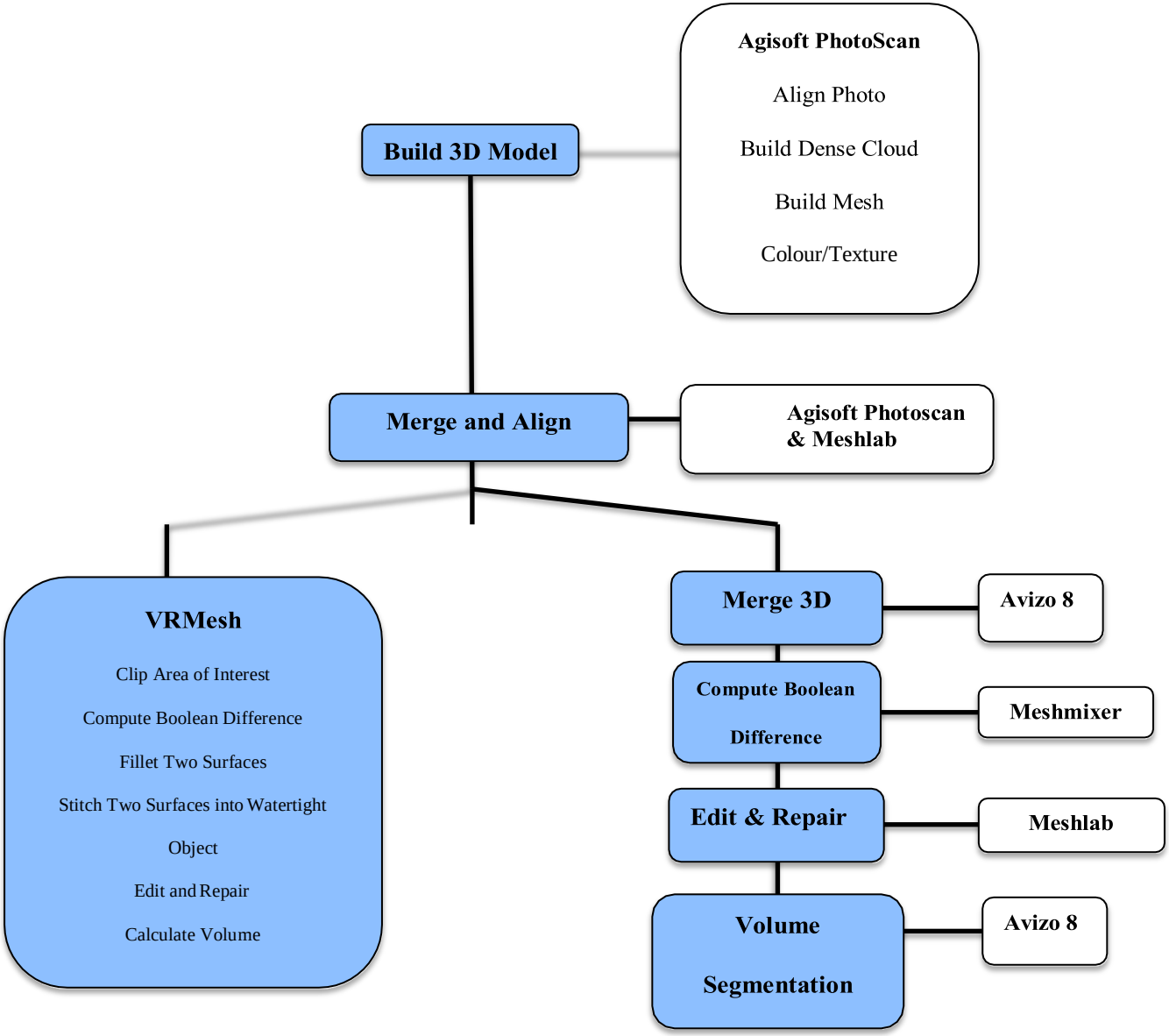

Figure 2. Workflow process for 3D model generation, alignment and segmentation to compute the volume.

Ground control points and photogrammetry data acquisition

The series of geo-referenced GCP's (in decimal degrees) were spread across the excavation of the Kromdraai site (Figure 3, Table 1). The GCP coordinates were established by previous researchers; and measured using a Leica TCRP 120 Total Station (with accuracy to 3mm) and the geographic coordinate reference system WGS84/ UTM Zone 35S (used in the southern hemisphere, between 24°E and 30°E) by B. Lans of the KRP.

Table 1. Ground Control Point coordinates

Name	X	Y	Z
GCP 1	575071.418	7122849.822	1475.529
GCP 2	575060.025	7122862.292	1474.724
GCP 3	575048.677	7122854.083	1475.03
GCP 4	575051.287	7122845.274	1474.791
GCP 5	575062.471	7122846.238	1475.896
GCP 6	575059.762	7122848.797	1472.717
GCP 7	575059.603	7122852.319	1472.314
KROM_DAT1	575059.505	7122843.968	1475.453
KROM_DAT5	575046.307	7122847.066	1474.793

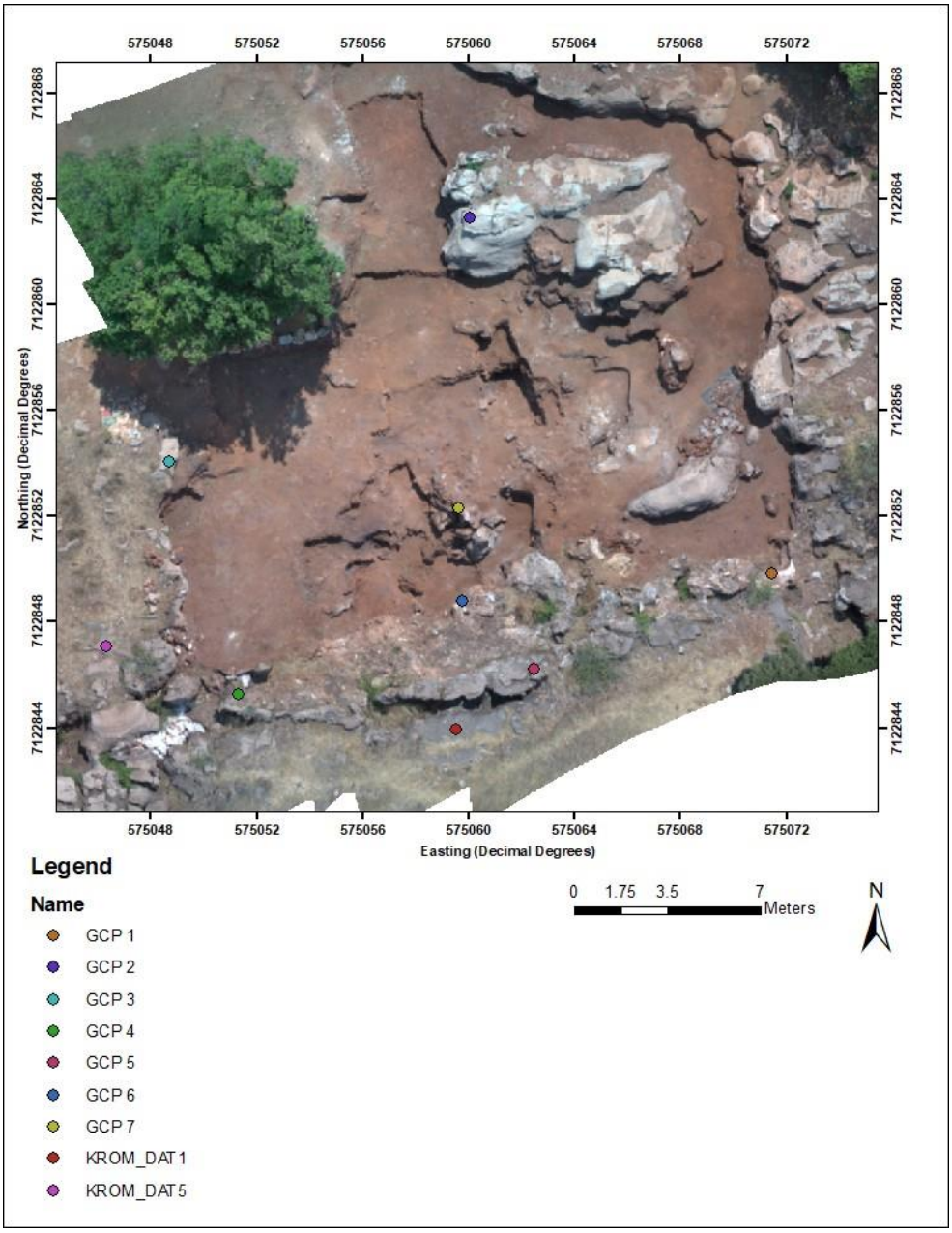

Figure 3. Permanent ground control points (GCPs) used to correctly georeference the 3D models.

Here, I focus on only part of the excavation. In order to obtain the highest resolution and quality, the terrestrial photogrammetric process was based on overlapping digital photographs taken by a hand-held camera from various angles and positions at a set focal length (f = 4). These photographs taken by J. Braga covered two relatively small areas excavated over a one-day period in January 2020 (Table 2). For larger more regional areas, the use of drone imagery would be required. Since photographing the excavations was weather permitting and largely dependent on the light conditions, photogrammetry was performed in the early morning to avoid a cast of shadows in the images. In the laboratory (post-excavation) generated a 3D model of the two areas of interest before excavation (early Day 1). I then generated another 3D model of the two areas of interest after excavation (early Day 2). The computation of 3D non geo-referenced dense point cloud was then reconstructed from the photographs using the Agisoft Photoscan workflow (Figure 2), as detailed in Dumoncel et al. (2016). The GCPs were then applied to geo-reference the point cloud in Photoscan and to perform spatial alignments (Figure 3). The 3D models were then exported in PLY file format into MeshLab and further aligned using the iterative closest point algorithm (Figure 3), ensuring the production of high-resolution 3D meshes that were compatible in the softwares subsequently used to visualize and manipulate the data.

Table 2. Photogrammetry parameters for 3D models representing the site before and after excavations, and for the merged and aligned model combining the two.

Date	Number of photos	Camera	Terrestrial/Drone	Focal length (mm)	Number of faces: vertices (millions)	Dimensions (m)
15.01.2020 (Before)	90	Sony DSC TX-10	Terrestrial	4	0.4/0.2	12 x 16
16.01.2020 (After)	301	Sony DSC TX-10	Terrestrial	4	0.3/0.1	9 x 11
Merged	391	Sony DSC TX-10	Terrestrial	4	0.7/0.4	12 x 16

Segmentation and volume measurements

Volume computation was achieved using three softwares, Avizo 8, Meshmixer and Meshlab, each having a specific function. Known all-encompassing softwares (e.g. VRMesh, AutoCAD Civil 3D) developed for the calculation of volumes between scans are expensive. To maintain cost efficiency, the approach applied in this study used freely available Meshmixer and Meshlab. Avizo 8, though not free, was readily available for this study in 3D digitisation laboratory. There are several alternative open-source 3D segmentation tools available (see Virzì et al., 2019).

To quantitatively record the transformation of the site post excavation, the two volumes of overburden sediments (here referred to as Volume 1 and Volume 2) were

computed by combining photogrammetry and segmentation techniques. For each area of interest, we merged the geo-referenced photogrammetric models generated successively before and after the excavation in order to compare the 3D meshes and to measure the volume occupying the space in-between the models. In order to fill the negative space in-between the two models (before and after excavation), we appended and merged the 3D photogrammetry model (merged) to a solid cube using the Avizo 8 software. For each area of interest, the Boolean difference (subtraction) operation was performed using the Meshmixer software. Before this step, each 3D mesh was cleaned and repaired in Meshlab. This entailed the filling of holes and the reduction of the number of faces, vertices and edges. To fill in the void between the two surfaces representing the area before and after excavation, we aligned and appended a solid cube to the exact excavation area in the 3D model in Avizo 8. The merged model and cube were cropped to size in Meshmixer in preparation for segmentation (Figure A, supplementary materials).

Figure 4 shows the two volumes removed from the area of interest within the site as they were positioned between the two layers representing the progress of the excavation. Each layer of the negative space was then segmented using Avizo 8 in order to visualize the two volumes of overburden sediments (Figure 4 (c); Figure B, supplementary materials) and to measure their volumes (m^3). This also resulted in the precise visualization of the removed volumes shown in Figure 4 (a, b). A 360° perspective of this figure is provided in the supplementary materials (Figure C). A more detailed demonstration of the volume estimation process is included in the supplementary materials (Appendix C).

No statistical tests we done to confirm the accuracy of this approaches. Ideally, a comparative analysis between the real-life volumes versus the computed volume

measurements would aid in assessing the accuracy of the photogrammetric approach. This will be implemented in future studies.

Instead, in order to confirm the accuracy of our results and to demonstrate the capability and potential of Avizo 8 for archaeological applications, I compared volume estimations rendered in Avizo 8 to those achieved by the all-inclusive software VRMesh for the same meshes (Table 3). Following the same workflow as above to build, merge and align the 3D models in Agisoft Photoscan and Meshlab, we then imported the 3D mesh of the merged models into VRMesh and calculated the estimated volume in one step.

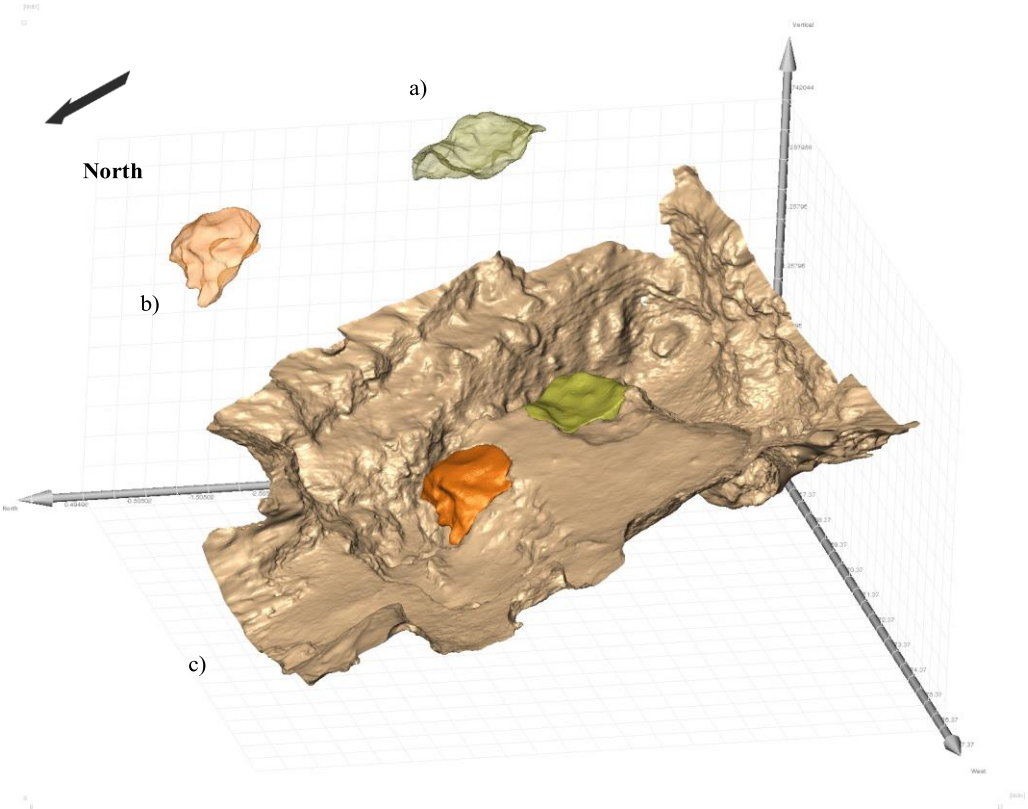

Figure 4. Visual representations of Volume 1 (a) and Volume 2 (b) removed during the excavation within the context of site (c).

Table 3. Volume estimations for "Volume 1" and "Volume 2" between 15 – 16 January 2020 and mesh material statistics in Avizo versus VR Mesh.

Software	Avizo	VR Mesh	Avizo	VR Mesh
Material	Volume 1	Volume 1	Volume 2	Volume 2
Volume ($m^{3)}$	**0.688865**	**0.682691**	**0.702942**	**0.695259**
Area (m^2)		**7.254173**		**5.726358**
Local Co-ordinates				
Center X	2.278911	2.35	3.025502	3.085
Center Y	6.027451	6.028	4.13153	4.182
Center Z	1470.93201	1470.95	1471.93567	1471.915

Figure 2 shows the workflow for the complete processing of two 3D surface layers for volume estimation. The first step in VRMesh requires that the area of interest be manually clipped for the 3D mesh. The shortcoming of this approach is that inaccuracies that may arise regarding the precision of the size and extent of the delineated area of interest because it is performed manually and subject to human error. Thereafter, within the same software the two separate models are 'filleted' to create a single 'watertight' object, edited and repaired, and the volume is calculated.

Database Management System/Metadata Modelling – Archaeological Data library

As explained above, no archaeological discoveries were made during the one-day excavation conducted to present this case study. However, for each of the two small-

excavated volumes presented here, we collected one sample of overburden for further sedimentological and geochemical analyses. Therefore, here we present the metadata and data modelling performed at the site of Kromdraai in association with the 3D recording of (i) the archaeological discoveries (already detailed in Dumoncel et al., 2016 and Ngoloyi et al., 2020) and (ii) the overburden (detailed in the present study).

Victoria Adeoye developed the database with Oracle Spatial; this is database management system optimized for storing and querying data related to geographically referenced objects. It provides special operators, functions, and indexes to perform spatial queries. The database was developed using Oracle SQL developer due to its ability to enhance user flexibility, and the possibility to add new metadata (e.g. sedimentary and geochemical data) and to be used for prediction purposes in the future. Additionally, the modelled database allows for further implementation of different tools, software packages and various applications that could aid in the visual representation and analysis of data, for example Geographic Information Systems (GIS).

A generic data model is presented here (Figure 5). It was designed using metadata from a limited sample of the complete Kromdraai fossil assemblage. Indeed, we created a database documenting 850 fossils and artefacts (elements) excavated within Unit P between 2014 -2018. Each specimen was named and identified by its unique fossil ID number. The metadata used to differentiate each element were: (i) taxa categorized into four select groups (bovids, carnivores, hominins and non-human primates); (ii) age (non-adult, young adult, old adult); (iii) size class (small, medium, large); (iv) skeletal region (i.e., the general part of the body to which the fossil belongs), (v) tools which can vary from bone to stone (for more details regarding metadata (i) to (iv), see Fourvel et al., 2018; Braga et al., 2020, in revision).

Logical database structures such as tables, columns, primary keys (PK), foreign keys (FK), and the relationships between tables denoted by annotated lines showing the direction of the associations were defined. Referential integrity rules including foreign keys, triggers and set constraints were defined while setting up the tables and columns in the database. To ensure that data and metadata were correctly represented in accordance to the set out business rules, column attributes such as data types were also specified.

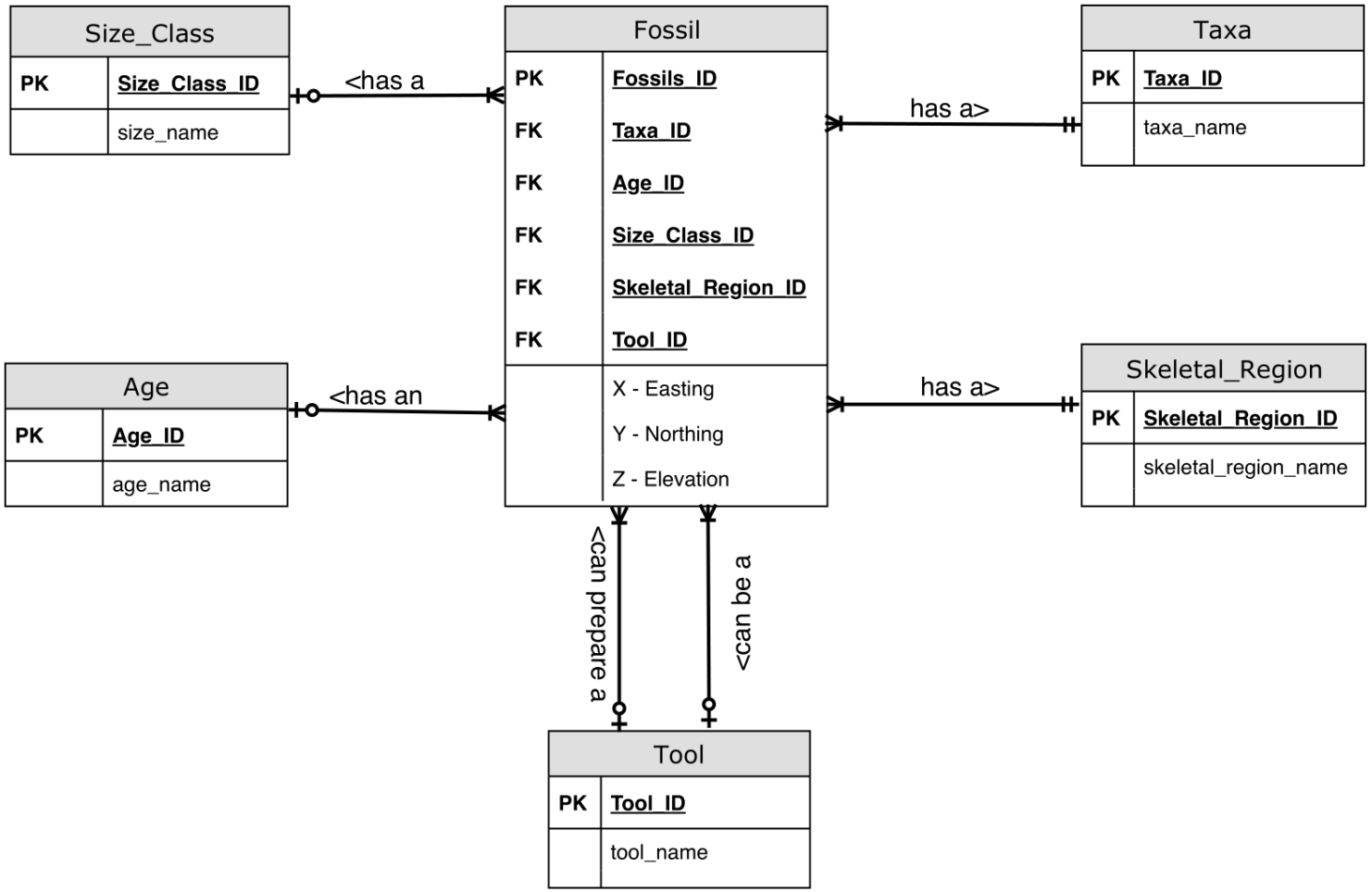

Figure 5. Data model schema showing metadata of the complete Kromdraai database for Unit P, excavated from 2014 – 2018.

Results and Discussion

The focus of this study was on (i) the development of a methodology for 3D modelling of all the excavation steps, to document its process as a scientific research tool and (ii) the storage of the meta-data generated from this process together with the original dataset in a proper database. We could generate an exploded 3D model whose disjointed pieces represent sub-volumes of overburden sediments excavated over a short period of time (depending on the concentration of fossils and artefacts, usually on a daily basis) (Figure 4, supplementary materials). Such a model allows us to keep a visual memory of the successive stages of the excavations at the site of Kromdraai that is now digitally preserved with great detail for further data extraction, analyses and interpretation despite its excavation. Moreover, the metadata model built using the Oracle SQL developer is flexible in that new metadata can be attached as the dataset expands. This is particularly important in the archaeological context because the database is constantly changing as the excavation progresses. Furthermore, contrary to traditional 'simple data' databases typically used in archaeology, this database manages complex datasets and it may be queried and implemented within software such as GIS for further analyses. The data model created can be applied to the current dataset and adapted to accommodate future datasets as the excavation continues, and more information is collected that needs to be stored. For example, in addition to the metadata categories (taxa, age, size-class, skeletal region, tool) defined for the Kromdraai dataset (Figure 5), more metadata e.g. species, family, genus, and fossil names, can be easily added as they are identified. A digital database has the potential to archive and catalogue all information regarding the fossil assemblage

excavated in a site, and the easy accessibility of the database facilitates an exchange of data and information between members of research teams within one system.

The three main guidelines for efficient archaeological documentation found in varying documentation agreements (Patias, 2006, Patias and Santana, 2011) were applied to the Kromdraai site as follows: (i) multi-scalar, detailed recordings of information about the site over a wide range of subjects, documented in various forms of literature including journal articles (e.g. Braga and Thackeray, 2016; Braga et al., 2017, 2020 submitted; Fourvel et al., 2018; Ngoloyi et al., 2020); (ii) digital records such as dated images acquired from different techniques (see above; Dumoncel et al., 2016) and multi-scalar 3D model reconstructions of the site and surrounding areas at varied spatial resolutions, ranging from several kilometres to a few microns, representing different periods of excavation. ; (iii) a metadata schema (Figure 5) that represents the structure of the Kromdraai database. This 4D relational database management system was created to enable information dissemination between the Kromdraai Research Project (KRP) team and participating researchers. We acknowledge that there is a need to provide access to archaeological information and communicate this by visual (and interactive) means. Currently, the 3D visualisation of the site is mostly restricted to 2D presentation in publications. The 3D model and database of the Kromdraai site will be used to communicate our results to either an academic or a wider public audience, and/or to give virtual access to documented data. A future component of the research would be facilitating information dissemination, and the education of the public. This would entail the application of the modelled database in the development of publically accessible website interfaces, 3D animation and games, virtual reality, science, tourism and other interactive scientific communication efforts.

In the present study, we developed a new volume reconstruction and estimation technique that allowed us to quantify and visualize the volumes of overburden sediments. Importantly, we ensure the traceability of the spatial provenance and quantity of each sub-volume of sediments and samples taken daily from the site by each excavator. Therefore, we are able to attach a temporal and spatial context to the volume material, and at a later stage, assign fossils to the sediment object. Table 3 shows that the volume measurements, rounded off to the second decimal place, were similar at 0.69 m^3 and 0.68 m^3 for Volume 1, and 0.70 m^3 for Volume 2 (Figure 4 (a, b)) in both the Avizo 8 and VRMesh. By comparing the measured volumes using both software applications, we were able to demonstrate the accuracy of automated algorithms in each software. The benefit of VRMesh is that unlike other methods, all processes for volume computation are completed within one software. It is however a shortcoming that trimming the 3D meshes to isolate the location of interest is manual and instinctive, which increases the risk of human error for volume measurements.

Our method shows the applicability of a more convenient and precise measurement for the precise position and volume of overburden sediments taken by each excavation over very short periods of time. In addition to the use of tools such as Geographic Information Systems (GIS) to visualize the precise spatial distribution of fossils within the site and analyses spatial patterns (Ngoloyi et al., 2020), we now add to our documentation protocol, the computation and calculation of the volume of the overburden sediments. We are now able to account for sieved fossil finds within the context of the site (spatial) and for a specified duration of time (temporal). In comparison to comprehensive photogrammetric methods, classical methods are typically laborious, non-autonomous (requiring at least two people), time consuming and in some cases cost-intensive (Yakar and Yilmaz, 2008, Yakar et al., 2010).

Provided that known GCP's have already been allocated, despite the complexity of the site, terrestrial and drone photogrammetry can be performed independently on-site, and volume computation from the 3D point clouds can be processed post-excavation off-site to an authentic accuracy, significantly decreasing operational costs (Yakar and Yilmaz, 2008).

The pilot project developed at Kromdraai demonstrates a potential for interactions between the archaeologists working at the site (i.e., in the field), their collaborators working in their laboratory (with no direct access to the site), visualization and data to improve interpretations. As we continue with this study, we will apply this method to previous 3D photogrammetry models from different periods of excavation to quantify the variation in the site and support the textual (historical) account of the site with the progression of the excavation over time. We will corroborate documented accounts of the site pre and post excavation for past excavation missions (2014-2018) with digitized 3D models and volume computations, visualizing the transformation of the site and providing a quantitative estimate of the amount of sediment removed. When applied to other sites, we also hope that our protocol will encourage the archaeologists and researchers to reanalyse their original dataset of descriptions, drawings and sections.

CHAPTER THREE: A new method to evaluate 3D spatial patterns within early hominin-bearing sites. An example from Kromdraai (Gauteng Province, South Africa).

Published: *Journal of Archaeological Science: Reports*

Citation: Ngoloyi, N. M., Dumoncel, J., Thackeray, J. F., Braga, J. (2020). A new method to evaluate 3D spatial patterns within early hominin-bearing sites. An example from Kromdraai (Gauteng Province, South Africa). *Journal of Archaeological Science: Reports*, *32*, 102376.

A user-guidline detailing the R Scripts and fucntions adapted and used to conduct the research is available in the Appendix C (supplementary materials). The R scripts for k-means and DBSCAN clustering were sourced from several websites (specified in supplementary materials). Engineer, Jean Dumoncel assisted in developing the tools such that they were applicable for 3D spatial analysis. I conducted further analyses using these scripts and interpreted the results. J Braga in the interpretation of the spatial patterning results and J. Thackeray (one of the KRP project coordinators) participated in reviewing the final manuscript.

Journal of Archaeological Science: Reports 32 (2020) 102376

Contents lists available at ScienceDirect

Journal of Archaeological Science: Reports

journal homepage: www.elsevier.com/locate/jasrep

A new method to evaluate 3D spatial patterns within early hominin-bearing sites. An example from Kromdraai (Gauteng Province, South Africa)

Nonkululeko Mantombi Ngoloyi[a,□], Jean Dumoncel[b], John Francis Thackeray[c], José Braga[b,c]

[a] Anthropologie Moléculaire et Imagerie de Synthèse, Université de Toulouse, Paul Sabatier, Toulouse, France
[b] Computer-assisted Palaeoanthropology Team, UMR 5288 CNRS-Université de Toulouse, Paul Sabatier, Toulouse, France
[c] Evolutionary Studies Institute, University of the Witwatersrand, PO WITS, Johannesburg, South Africa

ARTICLEINFO

Keywords:
Kromdraai
3D spatial patterning
Statistical testing
Cluster analysis
Spatial heterogeneity

ABSTRACT

Despite its potential to unravel past behaviors, statistical testing of spatial patterns within early hominin-bearing fossil assemblages has generally been overlooked. For instance, previous investigations of spatial patterning within sites from the *Cradle of Humankind* World Heritage area (Gauteng Province, South Africa) (with notable exceptions of studies at Rising Star) have relied primarily on visual interpretations of fossil-plotted point clouds against photographs or stretched drawings of stratigraphic interpretations. The main purpose of this study is to describe a new method to evaluate 3D spatial patterns within early hominin-bearing fossil assemblages in general and, secondly, to apply this method to the fossils recently recovered from the unroofed cave system of Kromdraai for a tentative interpretation. We therefore undertake one of the first statistical approaches of 3D spatial patterning in Plio-Pleistocene early hominin-bearing assemblages in South Africa. We identify four clusters in the Kromdraai dataset that correspond mainly to the oldest yet known hominin-bearing lithostratigraphic unit from this site - Unit P - that has recently yielded a rich Plio-Pleistocene fauna. This spatial patterning reveals a non-uniform distribution of fossils within Unit P. As yet it is too preliminary to interpret the statistically grounded spatial patterning described in this study of the Kromdraai. However, we recommend the application of our proposed approach to deposits at other sites in the *Cradle of Humankind* for a more evidence-based assessment of spatial patterns within hominin-bearing assemblages in this region.

1. Introduction

Integrated studies of fossil hominin-bearing assemblages aim to reconstruct the interactions between biological, ecological and behavioural factors during the course of human evolution. When the precise location and organisation of fossils within an archaeological unit reveals spatial patterning, the description and discussion of particular arrangements in space are improved and may therefore provide insights into past behaviours (Clarke, 1977; Wheatley and Gillings, 2013). Geographic Information System (GIS) tools have been largely applied to the study of archaeological sites in order to facilitate interpretations of spatial distribution patterns of fossils recovered in situ and represented by their three dimensional (3D) coordinates (e.g., Kintigh and Ammerman,1982). Spatial patterns also provide insights on the detailed depositional and post-depositional processes within a site, as well as other geological aspects that may inform taphonomic processes (e.g., Schneider et al., 2020, in revision).

Geographic Information Systems and 2D or 3D visualisation techniques have been used to describe inter and intra-site formation processes, and interpret their influence on the localisation of fossils in relation to stratigraphy and/or orientation. Such methods have been applied to Plio-Pleistocene hominin localities from Olduvai Gorge in Tanzania (e.g., Benito-Calvo and de la Torre, 2011; de la Torre and Benito-Calvo, 2013; Diez-Martín et al., 2014; Domínguez-Rodrigo and Cobo-Sánchez, 2017; de la Torre and Wehr, 2018) and sites such as Sterkfontein and Swartkrans (e.g., Nigro et al., 2001; Nigro et al., 2003; Mokokwe, 2016) within the UNESCO World Heritage Site referred to as the "*Cradle of Humankind*" (Gauteng Province, South Africa). However, these traditional qualitative approaches rely, to some extent, on visual interpretations of the 2D or 3D spatial patterns (e.g., Kintigh and Ammerman, 1982) of point distributions within archaeological sites, and are therefore not necessarily replicable. Indeed, the shortcoming of visual interpretations of GIS data is that they lack statistical significance. Thus, archaeologists have developed a preference towards

*Corresponding author.
E-mailaddresses: nonkululeko.ngoloyi@univ-tlse3.fr (N.M. Ngoloyi), jean.dumoncel@univ-tlse3.fr (J. Dumoncel), Francis.Thackeray@wits.ac.za (J.F. Thackeray), jose.braga@univ-tlse3.fr (J. Braga).

https://doi.org/10.1016/j.jasrep.2020.102376
Received 11 November 2019; Received in revised form 10 April 2020; Accepted 17 April 2020
Available online 08 June 2020
2352-409X/

more quantitative techniques that provide a more objective scrutiny of large datasets, and present complex spatial patterns and statistically significant outputs (Kintigh and Ammerman, 1982). These approaches combine the use of GIS mapping tools and statistical packages for data analyses (Nigro et al., 2001; Traviglia and Torsello, 2017; Buckland et al., 2018).

An array of statistical methods can be used to investigate spatial patterns. However, they are often limited to 2D or 2.5D within the GIS structure (Nigro et al., 2001; Nigro et al., 2003; Abdul-Rahman and Pilouk, 2007; Vavrek, 2011). Though valid and useful, these GIS approaches are limited because they do not manage and investigate 3D data completely (Nigro et al., 2001; Katsianis, 2012). Nearest neighbour analysis (NNA) for instance, presents a common challenge for spatial analysis because it does not consider the contextual information regarding a dataset. As emphasized by Kintigh and Ammerman (1982), the single statistical output of NNA that summarises the spatial pattern of a site does not factor-in its environment or other factors that may be crucial for subsequent archaeological interpretations. Cluster analysis is another commonly used approach to describe groupings among spatial data and to visually depict them in archaeological sites (Domínguez-Rodrigo and Cobo-Sánchez, 2017; Mendez-Quintas et al., 2019). Clusters can be defined as the propensity for data points to group together around their centroid; the clusters are areas with relatively high densities of points as compared to those of surrounding areas. The points located outside of a given cluster will typically denote noise (Ester et al., 1996). Spatial randomness will define the extent to which point patterns exhibit clustering (i.e., a complex, irregular or heterogeneous patterning) or alternatively homogeneous patterning (Shu et al., 2019). Important studies have used cluster analysis and implemented density-based approaches (e.g., "hotspot analysis"; Ester et al., 1996) to assess the relationships between fossils and the surrounding environment. They have provided scatter maps, visually displaying zones of high or low densities of different elements within a site (e.g., Werdelin and Lewis, 2013; Oron and Goren-Inbar, 2014; Birkenfeld et al., 2015; Domínguez-Rodrigo and Cobo-Sánchez, 2017; Wright et al., 2017; Wills et al., 2018; Mendez-Quintas et al., 2019). For instance, the "density based unsupervised spatial clustering algorithm" (Ester et al., 1996; Gaonkar and Sawant, 2013) mirrors "human intuitive clustering". It is considered to accurately identify clusters in datasets exceeding several thousands of objects, widespread outliers being easily recognised (Ester et al., 1996; Makantasis et al., 2016). In another example, Kruger (2017) used a "two-step cluster analysis method" to investigate spatial associations within the Dinaledi Chamber fossil assemblage in the Rising Star cave system (Gauteng, South Africa) in 3D. However, further statistical probing can potentially provide more information regarding the significance of spatial patterns from this site, as well as from other Plio-Pleistocene hominin-bearing assemblages within the *Cradle of Humankind*. To do so, the use of k-means for cluster analysis and the analyses of intra- and inter-site spatial patterns deserves particular attention. This approach has been long-standing within archaeology (Kintigh and Ammerman, 1982; Simek, 1984; Enloe et al., 1994; McAndrews et al., 1997; Vaquero, 1999; Lemke, 2013; Baxter, 2015; Mendez-Quintas et al., 2019). However, few studies have specifically used k-means for more evidence-based analyses of 3D spatial patterns at archaeological sites (Koetje, 1994; Anderson and Burke, 2008).

In the present study, we attempt to circumvent this lack of statistical testing of significance with the use of k-means clustering (Forgy, 1965; MacQueen, 1967). To do so, we investigate in 3D the spatial patterning of fossils recently recovered from the hominin-bearing site of Kromdraai (26°00′41″ S, 27°44′60″ E) located in the *Cradle of Humankind* (Braga et al. 2017, 2020, submitted). We focus our analyses on a stratigraphically seriated assemblage of 810 identified faunal remains (including hominins) attributed to a family and a size class, and recovered in situ from both soft and solid sediments of Unit P (between 2014 and 2018), which records one of the earliest phases of sedimentation at this site (Braga et al. 2020, submitted). We assess the randomness, or uniformity of the distribution of fossils from Unit P, by analysing their 3D coordinates collected by a total station. We also further evaluate the effect of potential factors of bias on clustering sensitivity. These factors include non-representative sampling (in the context of the recording method and excavation protocol), bone fragmentation and stratigraphic provenience. To do so we will discuss our results in the light of sedimentological, taphonomic and other contextual information already detailed by Fourvel et al. (2018), Schneider et al (2020, in revision) and Braga et al. (2020, submitted) and not repeated here. Moreover, we add a smaller sample of 40 identified faunal remains (excluding hominins) also discovered in-situ from soft sediments at Kromdraai (in 2016 and 2017) in close proximity to Unit P, though they clearly belong to a stratigraphically much younger and not yet defined Unit.

2. Materials

2.1. General context

The work that Broom initiated in 1938 at the "Kromdraai B" (KB) locality was the first in a series of four phases of field research activities at this site before 2014 that have been detailed by Braga et al. (2017). In this study, we investigate the 3D spatial patterning of data obtained during the ongoing phase of excavations and research at Kromdraai that was initiated in April 2014 (Braga et al., 2017, 2020, submitted). The fossil assemblage investigated here was recovered from an area previously regarded by Brain (1975) and Vrba (1981) as containing only "loose fill" unfossiliferous sediments, which were considered to be excluded from further investigation (Braga et al., 2020, submitted). The taxonomic attributions of the faunal and hominin samples recovered since 2014, as well as their stratigraphic and taphonomic contexts are detailed in separate papers (Fourvel et al., 2018; Schneider et al., 2020, in revision; Braga et al., 2020, submitted). Here, we nevertheless briefly present the contextual information needed to discuss our results.

2.2. Stratigraphy and sedimentological characteristics

The interpretation of the highly complex stratigraphy of Kromdraai (Bruxelles et al., 2016) and the relationships between the different deposits will inevitably alter as excavation continues. Therefore, in recognition of this complexity, a new nomenclature for the Kromdraai deposits has been proposed in Schneider et al. (2020, in revision). In this new system, the term "Unit" replaces "Member" to name the distinct sedimentary deposits from Kromdraai. Moreover, letters designate the currently known units. Unit O was not recognized in the stratigraphic interpretation proposed by Bruxelles et al. (2016) and represents the oldest fossiliferous sedimentary unit known thus far from Kromdraai. New fossiliferous units that might be recognized in the future will be slotted before Unit O if appropriate. Unit P, which is the focus of the present study, was previously named "Member 2" by Vrba (1981), Partridge (1982) and Bruxelles et al. (2016). This nomenclature was used in other papers such as, Braga et al. (2017) and Fourvel et al. (2018). In the present study and in all subsequent papers, "Unit P" will replace "Member 2". Unit O is older than the overlying Unit P. The younger "Member 3" described by Vrba (1981) and Partridge (1982) corresponds to both Unit Q and its overlying Unit R (here noted "Units Q-R"). No fossil discoveries from Units O, Q and R are presented or discussed in this paper. However, we only add to the sample of 810 specimens from Unit P (here called "Unit P sample"), a smaller sample of 40 specimens recovered from a distinct and discordantly overlying new stratigraphic Unit (Fig. 1B). When compared to Unit P, this new Unit corresponds to a much later phase of sedimentation when the cave was deroofed and it will be detailed in a separate paper. Here, we solely add that the new Unit is stratigraphically younger than Units Q-R. As explained above, the small sample recovered thus far from this Unit is used in the present study and referred to as a "test sample" in order to

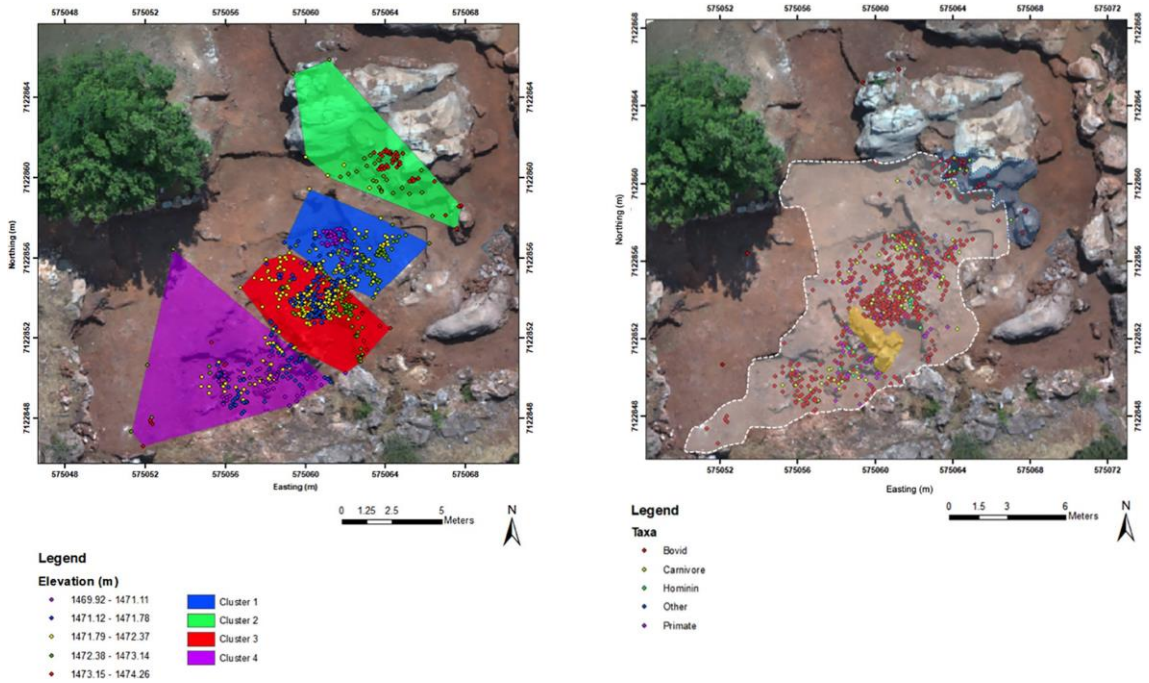

Fig. 1. 2D perspective of 3D k-means clustering (A, left), colour differentiated by elevation and the in situ taxa (B, right) distribution of the fossil assemblage projected onto a 2D orthophotography of Kromdraai. In figure B, Unit P is delineated in white and the "Main Remnant" is indicated in orange within Unit P. The area where the "test sample" was recovered is delineated in blue and does not correspond to Unit P. The four elements falling outside the area delineated as Unit P probably belong to this Unit. Deeper excavations will allow us to confirm this.

discuss further the sensitivity of our clustering results on the stratigraphic provenience. Indeed, the "test sample" (Fig. 1B) has been recovered and recorded in situ at the north-east corner of the on-going excavation during mitigation strategies/risk actions that included the removal of one very large dolomite block.

Unit P, is a 2 m (minimum) thick fossiliferous deposit consisting mainly of soft sediments (or rudites). Unit P and Unit O are separated by an erosional unconformity in the form of a 10 cm thick chert pebble conglomerate belonging to Unit O. Moreover, Unit P is also separated from Unit Q by a distinct unconformity layer. It is important to add here that cross contaminations between Unit P and its overlaid (Unit O) and overlying (Unit Q) deposits are extremely unlikely because of the distinct demarcations (i.e., clear unconformities) between these sediments. The contacts between Unit P, the overlaid Unit O and the overlying Unit Q are illustrated in Schneider et al. (2020, in revision) and Braga et al. (2020, submitted). Moreover, the separation between the "Unit P sample" and the "test sample" investigated here is illustrated in Fig. 1B and represented within cluster 2. Since the vast majority of the sample investigated here (95%) derives from Unit P, we briefly describe below the main features of this Unit, more specifically in terms of its various states of induration. The other sedimentological characteristics and features of Unit P are detailed in Schneider et al. (2020, in revision).

The vast majority of the volume yet excavated within Unit P is represented by gravel and rudite. Schneider et al. (2020, in revision) noted that firstly, except for carbonate cements that are absent in gravel deposits, the petrographic composition of the rudite and gravel is very similar; and secondly, the rudite was decalcified to gravel, with both deposits corresponding to one single lithostratigraphic unit. Moreover, Schneider et al. (2020, in revision) could not find evidence for extensive erosion of Unit P with the formation of voids subsequently infilled by more recent sediments. They therefore excluded the possibility that Unit P represented a mixture of older residual material with younger fossils. In comparison to the surrounding gravel deposits, two small areas showed varying states of induration and were detailed in Schneider et al. (2020, in revision). These two areas of limited extension are delineated in Fig. 1. First, the rudite from the "Main Remnant" displays a lower amount of matrix with numerous speleothem fragments concentrated at its top. However, similar sedimentation processes were observed during the deposition of the rudite from the "Main Remnant" (before cementation) and other Unit P sediments (Schneider et al., 2020, in revision). Second, the "Block Chaos" deposits are poorly consolidated and therefore remain friable. Because of the scattering of its clast orientations and the partial cementation of its deposits, the "Block Chaos" was interpreted as a block chaos that accumulated underneath a vertical shaft of limited extent. However, simultaneously, during most of the time of the formation of Unit P, clastic talus cone deposits were distributed both vertically and laterally towards the North, mainly by continuous autochtonous and allochtonous clastic influxes that represent the vast majority of the deposits investigated here.

2.3. Excavation method

During the 2014–2018 period, the in situ excavation method consisted of successive 1-to-2 m wide and 1-to-4 m long rectangular and contiguous test pits distributed uniformly across a surface area of 20 m × 20 m. Our skilled field assistants used hand tools to excavate soft and variably consolidated sediments from the "Block Chaos" in a staggered series of vertical faces of *circa* 5 cm in height, at successive depths. This methodology did not involve a grid layout but instead the use of a horizontal and vertical mapping system using GPS and a Total Station (with an accuracy of 3 mm) to systematically record the

position of each hominin or non-hominin specimen discovered in situ with no size threshold. In other words, each element excavated in situ (i.e., found prior to sieving) was plotted as one single point (projected according to the WGS84/ UTM Zone 35S coordinate system) regardless of its size or shape (see below). In order to avoid the possibility of bias during in situ discoveries, the identifications of all of the elements were made by JB Fourvel and/or J Braga. When an element was considered significant, we also produced its in situ high-resolution photogrammetric model. When a feature was encountered lying partly in one section or profile within a test pit, it was left and not fully exposed. When necessary, the feature was protected using field jacketing until the excavation advanced to the next test pit to be brought into full view. The successive test pits were designed to: (i) expose, record and sample sedimentary deposits, (ii) collect the associated fossil material, (iii) investigate the depositional processes in situ, and (iv) obtain stratigraphic sequences. In order to ensure crew safety, we limited the depth of each test pit to a maximum depth of 150 cm. Therefore, when we needed to reach deeper deposits with a new test pit, we first excavated and lowered the immediate neighboring areas (to a maximal width of 1-to-2 m) in order to maintain each vertical profile to a maximal height of 150 cm. This methodology was useful to obtain single and relatively long (to a maximum of 4 m) vertical (to a maximum of 150 cm) sedimentary perpendicular profiles along both West-to-East and North-to-South transect lines at regular intervals. These profiles formed the baseline for future stratigraphic interpretations. Since we excavated a series of contiguous exploratory test pits, we could; first, investigate the contacts between the sedimentary units and assess their horizontal extent; second, ensure that our sampling documentation was spatially consistent (i.e. the same resolution was employed across the excavated area), with the exception of the "Main Remnant" which was not excavated. However, there was a possibility of bias in the sampling during excavation. Indeed, our study represents only a partial view of the assemblage, given that it represents fossils found in situ only, not those discovered through the screening process. We used hand screens of 3 and 0.5 mm to systematically check the excavated soil (we systematically collected 10% of the dry residues on the lower screen). Finally, we used water screening (with a 0.5 mm mesh) to check the remaining 90% of the dry residues on the lower screen. The elements discovered in sieves were not plotted but were allocated to "volumes of interest" instead. A follow up to this study would include assigning sieve finds to a quantified volume of soil removed through excavation. The methodology presented here was applied to the soft and consolidated sediments and provided excellent recovery without damaging or destroying very fragile fossil bones and teeth (including hominins). For instance, our methodology allowed us to recover a high proportion of juvenile hominin bones and teeth in situ, as well as one hominin middle ear ossicle (KW 9900). Since the methodology described here was systematic, we consider that the fossil assemblage investigated in this study constitutes a representative sample of the deposits from Unit P as yet excavated (delineated in Fig. 1B), with a limited spatial bias in the documentation.

2.4. Fossil assemblage

The specific metadata considered in this study were the taxa and skeletal region categories. Fossils were categorised into five groups, namely bovids, carnivores, hominins, primates, and "other" which denoted fossils of taxa not belonging to the four aforementioned primary groups. The identified element reflected skeletal region and skeletal elements documented in this study included the cranium, isolated teeth; components of the appendicular skeleton including the girdles (pelvic and pectoral), the spinal column, thoracic cage, tusk and horn elements, and lower and upper limbs. In the event of an uncertainty in the identification of upper or lower limbs, fossils have been assigned to the general category of "limb".

2.5. Taphonomy: Bone fragmentation, skeletal parts and size classes

Unit P has a fossil assemblage of high taxanomic diversity, yielding fossils within 8 orders and 16 families. A high diversity is especially noted for herbivores and carnivores, and amongst hominins *Paranthropus* sp. has been of particular importance to the site (Fourvel et al., 2018) but it is not the only hominin taxon represented within Unit P (Braga et al. 2020 submitted). The representation of carnivores in Unit P in comparison to Plio-Pleistocene sites with hominin-bearing deposits within the Cradle of Humankind is slightly comparable. However, distinctive features of the Unit P that differiente the deposit from similar in age deposits (e.g. "Swartkrans Member 1 and Drimolen Main Quarry") include the high species richness demonstrated in carnivores, Fourvel et al. (2018) identified 18 genera and 22 species within the fossil assemblage, some of which emerged in the younger deposits of Unit P for the first time. Most of the information on the taphonomy, the high species richness (Fourvel et al. (2018) and hominin abundance (Braga et al. 2020, submitted) of the assemblage recovered from Unit P thus far is not repeated here.

From a taphonomic point of view, all the faunal (including hominin) remains from Unit P and from the "test sample" are very fragmented but well preserved. Therefore, even if the percentage of bone survival of the faunal assemblage is very low (Fourvel et al. 2018), the fossils rarely suffered sufficient post-depositional damage to alter their representation. Braga et al. (2020, submitted) noted that for some specimens, several fragments were discovered and plotted separately but were in very close proximity during the excavation. In some instances, these fragments could be subsequently refitted to reconstruct more complete elements.

To evaluate the possibility of a biased distribution in terms of fragmentation, the percentage of "Isolated Teeth" (the smallest fossil size class) occurring within each cluster will be assessed. Most of the assemblage was assigned to the bovid group (n = 647) and amongst the skeletal regions limbs. This category encompasses most of the dataset, comprising a total of 432 fossils. Bovid size classes were recognised, as defined by Brain (1981). Given the degree of fragmentation of the fossils and the large predominance of small–sized and medium-sized bovids, carnivores and primates, all the elements plotted in this study (including tusks) were of limited size and could be reasonably plotted with a single point.

3. Methods

All statistical analyses were performed in RStudio (Team, 2015)

Table 1
Synthesis of R packages used, authors and the application.

Package	Author/s	Application Details
rgl	Adler and Murdoch (2012)	Interactive 3D visualisation
clustertend	YiLan and RuTong (2015)	Cluster tendency evaluation, implementation of Hopkins statistic clustering index
dbscan	Hahsler and Piekenbrock (2017)	DBSCAN cluster computation
fpc	Hennig and Imports (2015)	Modification of DBSCAN algorithm for eps determination and DBSCAN computation
factoextra	Kassambara and Mundt (2017)	Silhouette analysis of clusters
gplots	Warnes et al. (2016)	Venn diagram computation for common cluster memberships

(Table 1, see database repository [dataset]).

3.1. Measuring clustering Tendency.

We first applied k-means clustering to the complete dataset. Whenever possible we then investigated separately sub-datasets representing each taxon and skeletal region categories. Some of these sub-datasets studied were not represented with the same or similar number of specimens; despite this fact, these individual sub-datasets had no influence on the final results as we focussed on the analysis of the dataset as a whole. The Density-Based Spatial Clustering and Application with Noise (DBSCAN) clustering algorithm was implemented to corroborate the spatial pattering of clusters determined by the k-means methods. However, further inspection was conducted using the clusters derived from k-means.

The Hopkins Statistic (Hopkins and Skellam, 1954) was used to measure the likelihood that the sample dataset renders a uniform spatial distribution, and the statistical index "H" was calculated for individual groups belonging to both the taxa and skeletal region categories. Uniform and non-uniform distributions represented no meaningful clusters (null hypothesis) and meaningful clusters (alternative hypothesis) respectively. Low clusterability was denoted by a calculated H value below 0.5 and close to 0, whereas values closer to 1 demonstrated non-uniform data with statistically significant clusters.

3.2. K-means Clustering.

We then implemented spatial k-means clustering, an unsupervised method (Forgy, 1965; MacQueen, 1967; Hartigan and Wong, 1979; Lloyd, 1982) used to divide the dataset into meaningful clusters based on the 3D spatial matrix. This method provides meaningful clusters for samples sizes exceeding a minimum of 500 points. The number of clusters to divide the dataset was calculated using the elbow method (Bholowalia and Kumar, 2014). “Optimal k”, the nearly optimal clustering value required for k-means clustering, was determined using the “within cluster sum of errors” (WCSS) calculation in the elbow method (Bholowalia and Kumar, 2014). Indeed, other clustering methods used for spatial data in 3D such as the two-step approach (e.g., Kruger, 2017) automate the determination of the number of clusters. In this case, “optimal k” was user-specified in the computation of k-means. K-means cluster analysis was used to search for similarity in the 3D point cloud matrix, and the k-means algorithm measured the distances between coordinate points, minimising the distance in order to find the optimal number of clusters. After partitioning the dataset into clusters, we calculated the squared distance from any data point to the centroid of its cluster. The frequency of elements contained within each cluster and the category to which they are assigned was also determined for the complete dataset, and k-means clusters were displayed in 2D and 3D plots and described according to Universal Transverse Mercator (UTM) coordinate system. 3D point data were automatically transformed in *factoextra* (Kassambara and Mundt, 2017) using a PCA, and a new dimension was created, allowing for efficient visualisation of the 3D clusters in 2D.

3.3. Density-Based spatial clustering and application with noise (DBSCAN).

This approach was developed by Ester et al. (1996) and was applied for purposes of identifying regions (or “hotspots”) where the spatial distribution of objects points was densely packed around a central point (Gaonkar and Sawant, 2013; Rahmah and Sitanggang, 2016). Two user-specified parameters (*MinPts* and epsilon, *eps*) were determined (Gaonkar and Sawant, 2013; Rahmah and Sitanggang, 2016). The *eps* value representing the radius extending from the central point of a cluster (Hennig and Imports, 2015) was calculated by transforming Euclidean coordinates into a distance matrix, which was then used to determine the average k nearest-neighbours, i.e. the average distances between two-points (Rahmah and Sitanggang, 2016). The *MinPts* (k) parameter indicates the minimum number of points to create a cluster. Here, this number was specified to three, due to the small size of the dataset. A small *MinPts* value is best suited for smaller datasets (Gaonkar and Sawant, 2013). The k-distance curve was plotted where the optimal eps value was indicated by the maximum point or sharpest bend of the curve (Rahmah and Sitanggang, 2016).

The model specified the *MinPts* and *eps* parameters, resulting in a 2D and 3D map of the density clusters. Finally, to confirm the efficacy of using the simple k-means clustering method for 3D spatial clustering, we compared visually the 2D and 3D clustering representation determined from both methods, based on the correspondence of the clusters. The overlap of objects occurring within the same spatial region was evaluated using Venn diagrams.

DBSCAN (Ester et al., 1996) was implemented as a supplementary step to ensure the validity of the 3D clusters generated by k-means preceding statistical validation of the spatial patterning. This method was therefore applied only to the complete dataset and not to individual taxa or skeletal regions. Although DBSCAN specifies the analysis of spatial data, the algorithm is best suited for larger datasets (several 1000 s). Since the dataset in this study represents a smaller sample of a larger database, statistical analyses of the 3D clusters were completed using the results of k-means clustering.

3.4. Clustering Validation

The Silhouette Statistic (Rousseeuw, 1987; Kaufman and Rousseeuw, 2009) was applied to validate the k-means clustering of the dataset. This method calculates the similarity of each point within each cluster relative to surrounding clusters, estimating the average distance. Silhouette plots illustrated the size of each cluster, the number of features in each cluster and the silhouette width for each cluster (S_i ranged between −1, indicating an incorrect assignment of clusters, and 1, suggesting that features were well allocated to their cluster).

4. Results

4.1. Fossils assigned to each taxon and represented within each skeletal region

The quantity of fossils assigned to each taxon category is skewed in favor of bovids (647 specimens) that represent most of the dataset and are widely distributed across the site (Fig. 1B), followed by carnivores (109 specimens), primates (63 specimens) and hominins (25 specimens). The “Other” category is the least represented with only 6 fossil specimens, comprising Proboscidea and unidentifiable taxa. Regarding the skeletal region to which the fossils were assigned, the most prominent body parts within the dataset were limbs, of which the majority were unidentified (432 specimens); the remaining were attributed to lower (167 specimens) and upper limbs (136 specimens). Isolated teeth and cranial fragments were found in relatively high quantities within the dataset at 122 and 91 specimens respectively, followed by spinal column (82 specimens) and horn fragments (52 specimens) whilst thoracic cage (24 specimens), pelvic (22 specimens) and pectoral (19 specimens) girdles, and tusk fragments (5 specimens) were amongst the least represented.

4.2. Optimal numbers of clusters for each taxon and skeletal region

Calculated using the elbow method, the ideal number of clusters (k) for the complete sample dataset was 4. Considering individual taxa separately, bovids, the largest group, produced the largest number of optimal clusters with 4, successively followed by carnivores (k = 3), hominins (k = 2) and primates (k = 2). Larger skeletal body part groups (≥82 specimens) were clustered into three clusters whilst the remaining had only two.

Table 2
Hopkins Statistic clustering index values (H) for the complete dataset categorised according to taxa and skeletal region.

Category	Name	No. of specimens	Randomly Simulated (H)	Hopkins Statistic (H)
Complete Taxa		850	0.5053796	0.9087083
	Bovid	647	0.5018342	0.9069146
	Carnivore	109	0.5134197	0.8073848
	Hominin	25	0.5519830	0.8301601
	Primate	63	0.5198199	0.8350589
	Other	6	–	0.7835098
Skeletal Region	Isolated Teeth	122	0.5024097	0.8201467
	Cranium	91	0.5130276	0.8024741
	Lower Limb	167	0.5312510	0.8344276
	Upper Limb	136	0.4518458	0.8113151
	Thoracic Cage	24	0.4502317	0.6881538
	Pelvic Grid	22	0.5560473	0.7233677
	Pectoral Girdle	19	0.4449972	0.6218314
	Spinal Column	82	0.4954356	0.8951292
	Horn	52	0.4986627	0.7809656
	Tusk	5	0.2813364	0.4787301
	Limb	129	0.4949066	0.8519713

4.3. Hopkins Statistic values categorized according to taxa and skeletal region

In consistency with expectations, the randomly simulated dataset resulted in Hopkins's Statistic (H) values within close range of 0.5 for the complete dataset and all individual groups (Table 2). A non-uniform distribution was demonstrated for the complete dataset with H = 0.91, signifying the occurrence of meaningful clusters across the site. Noticeable clusterability was observed for all individual taxa, each showing Hopkins index values above H = 0.80 (Table 2). We observed a greater variation in the clusterability of body parts for the complete dataset. The majority of the individually identified skeletal regions showed an H value close to or above 0.80 (isolated teeth, cranium, limbs, spinal column) (Table 2). The least represented body parts (e.g. tusk fragments and pelvic girdles) showed H values closer to 0.5, indicating their uniformity and low clusterability (Table 2).

4.4. K-means Clustering

The k-means clustering for the complete dataset is illustrated in 2D (Fig. 1A) and 3D (Fig. 2). Moreover, a video is provided to show the full perspective of the 3D clustering (supplementary materials). A stacked bar plot (Fig. 3) illustrates the size of each k-means cluster for the complete dataset, depicting the respective proportions of cluster elements according to taxa. The prominent occurrence of bovids in the complete dataset is consistent for all clusters. However, cluster 3 contains the highest frequency overall, dominated by bovids (309 specimens) followed by carnivores (41 specimens), non-human primates (24 specimens) and the largest group of hominins (11 specimens) (Table 3). The respective proportions of different skeletal regions within each cluster are also detailed in Table 3. The most prominent occurrences in the largest cluster (cluster 3) were limbs, isolated teeth and cranium, and the smallest sized fossils ('isolated teeth') were distributed across all clusters occurring in the highest quantities within the smallest cluster (cluster 2) at (27.4%) and the largest cluster (cluster 3) at 16.8% (Table 4). Importantly, Cluster 2 contains elements from Unit P (Fig. 1A, indicated between elevations 1468.92 and 1473.14 m) and the 40 elements from the "test sample" (Fig. 1A, B, indicated between elevations 1473.15 and 1474.26 m).

4.5. DBSCAN clustering

DBSCAN clustering for the complete dataset also produced four clusters and 23 outliers (Fig. 4). A video showing a view of all perspectives of this figure is provided in the supplementary materials. In a similar way to k-means clustering, two large clusters encompass most of the dataset. By visual inspection, it is observed that there was a correlation between the localities of clusters within the XYZ spatial plane (despite the random auto-generated numbering). Venn diagrams illustrate the most significant overlaps in clusters described above, showing the number of common fossils within the union of coinciding clusters (Fig. 5). A densely packed DBSCAN cluster 1 (596 specimens) corresponds with k-means clusters 1 and 3 (612 specimens combined) (Fig. 5A). K-means cluster 4 corresponds with and both DBSCAN clusters 2 and 5 which overlap by 158 and 4 specimens respectively (Fig. 5B). K-means cluster 2 (11 specimens) completely encompasses DBSCAN clusters 3 (11 specimens) and 4 (specimens) (Fig. 5C).This demonstrates the usefulness of simple k-means clustering for identifying major clusters in a small dataset (greater than 500 and less than 1000 points).

4.6. Silhouette widths.

We measured the silhouette widths obtained for each k-means cluster (a value of 1 indicates that fossils are well classified into their clusters) (Table 5), and each object per k-means cluster was portrayed in a silhouette plot (Fig. 6). For the complete dataset, we observed an average silhouette width (S_i) of 0.42, suggesting that objects were reasonably classified but most objects possibly fell between 2 clusters (Table 5). Cluster 2 shows the best classification (S_i = 0.54), followed by cluster 4 (S_i = 0.47) (Table 5). The silhouette width of cluster 4 indicates a reasonably clustered structure despite the poor classification of some of its objects seen at the boundary of cluster 2 (Fig. 6). Silhouette widths of the largest clusters (1 and 3) were both much below 0.5 and therefore showed a relatively inaccurate classification (Table 5). In Fig. 6, clusters 1 and 3 also showed a gradual decreasing gradient (as compared to clusters 2 and 4 which decrease more sharply) with cluster 1 showing negative S_i values at the cluster 3 boundary, indicating poorly classified fossil specimens.

When we considered the k-means clustering of individual taxa separately, the best-classified clusters were obtained for carnivores and hominins. Hominins showed the highest average silhouette widths of 0.64 indicating reasonable cluster allocation. Bovids showed the least efficient clustering (S_i = 0.43). The best-classified fossil group according to skeletal region is the tusk category with an average S_i of 0.65. This is the smallest group. Followed by the larger spinal column group with an average S_i of 0.63, lower limbs (S_i = 0.55), unidentified limbs (S_i = 0.54) and teeth (S_i = 0.54), all indicating reasonable cluster structures. Most of the skeletal parts have S_i values closer to 0.5 indicating that most objects could fall between two clusters. Thoracic cage fossils have a very low S_i value of only 0.41.

5. Discussion

The purpose of spatial analyses in archaeology is primarily to offer significant interpretations of point spatial distribution patterns within sites. Until recently the most common form of spatial analysis was the visual inspection of profiles and maps showing plotted point clouds. Several studies of Plio-Pleistocene fossil sites in the *Cradle of Humankind* have however incorporated GIS and/or 3D digitisation techniques to convey the visual spatial patterning of fossils (e.g., Nigro et al., 2001; Nigro et al., 2003; Mokokwe, 2016; Stratford et al., 2016). Similar 2D/3D visualisation techniques using GIS have been applied to understand inter and intra-site accumulation processes and their influence on the localisation of fossils in relation to stratigraphy at the Plio-Pleistocene hominin site of Olduvai Gorge, Tanzania (e.g., Benito-Calvo and de la

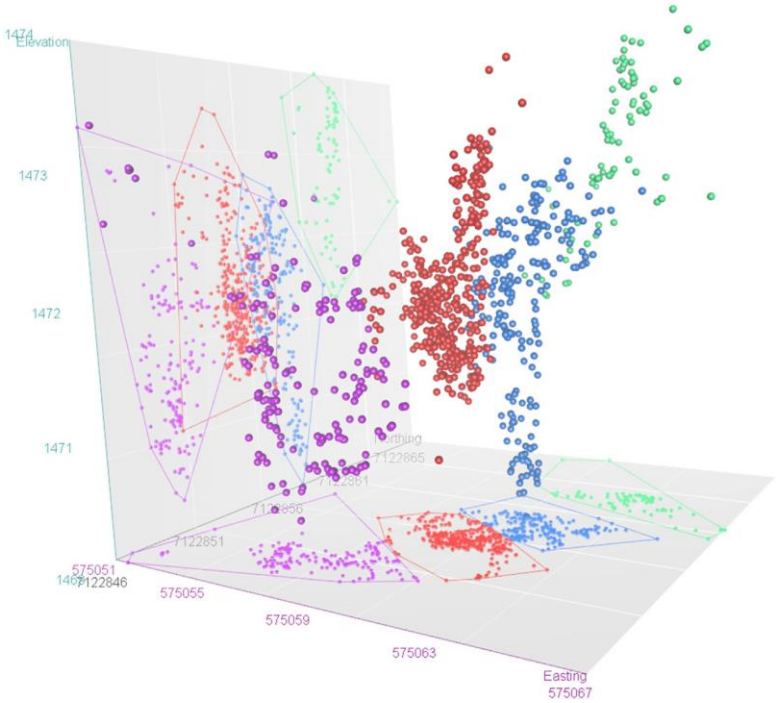

Fig. 2. 3D k-means clustering, clusters are differentiated by colour: 1 (Blue), 2 (Green), 3 (Red), 4 (Purple).

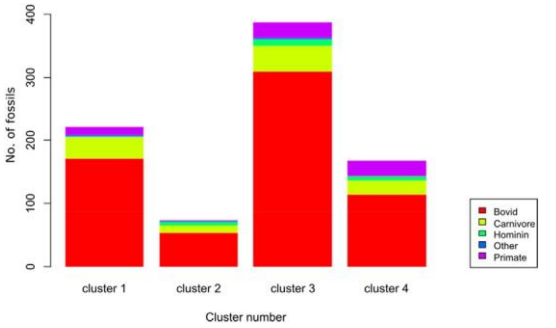

Fig. 3. Stacked bar plot illustrating frequency of occurrences within the k-means cluster 1–4 of the complete dataset, differentiated by taxa.

Torre, 2011; de la Torre and Benito-Calvo, 2013; Diez-Martín et al., 2014; Domínguez-Rodrigo and Cobo-Sánchez, 2017; de la Torre and Wehr, 2018). However, as already emphasized here, the results of these studies rely primarily on visual interpretation with a general lack of statistical significance.

A few studies have used more sophisticated statistical approaches methods to investigate the spatial distribution patterns of fossils recovered in situ within Plio-Pleistocene sites. Within the *Cradle of Humankind*, Kruger (2017) used the "two-step cluster analysis method" to investigate the spatial associations within the Dinaledi Chamber in the Rising Star Cave fossil assemblage from the Mid-Pleistocene. However, to the best of our knowledge, no studies have focused on the 3D spatial patterning and quantitative statistical significance of Pliocene or Pleistocene hominin-bearing fossil assemblages. As also emphasized here, the use of k-means for cluster analysis of spatial patterns within fossil assemblages may provide new insights into past

Table 3
Total cluster frequency in k-means clusters 1–4 for the complete dataset and the distribution of Taxa and Skeletal Regions within each cluster.

		Cluster Frequency			
		1	2	3	4
Total Frequency		222	73	387	168
Taxa	Bovid	171	53	309	114
	Carnivore	34	12	41	22
	Hominin	1	6	11	7
	Primate	13	1	24	25
	Other	3	1	2	0
Skeletal Region	Cranium	33	5	40	13
	Horn	20	6	21	5
	Isolated Teeth	18	20	65	19
	Limb	38	12	52	28
	Lower Limb	36	12	71	48
	Pectoral Girdle	6	3	4	6
	Pelvic Grid	7	1	9	5
	Spinal Column	12	3	58	9
	Thoracic Cage	9	2	11	2
	Tusk	3	–	2	–
	Upper Limb	40	9	54	33

Table 4
Percentage of Isolated Teeth calculated from k-means clustering within clusters 1–4.

Cluster	No. Isolated Teeth	Cluster Total	Isolated Teeth (%)
1	18	222	8.1
2	20	73	27.4
3	65	387	16.8
4	19	168	11.3

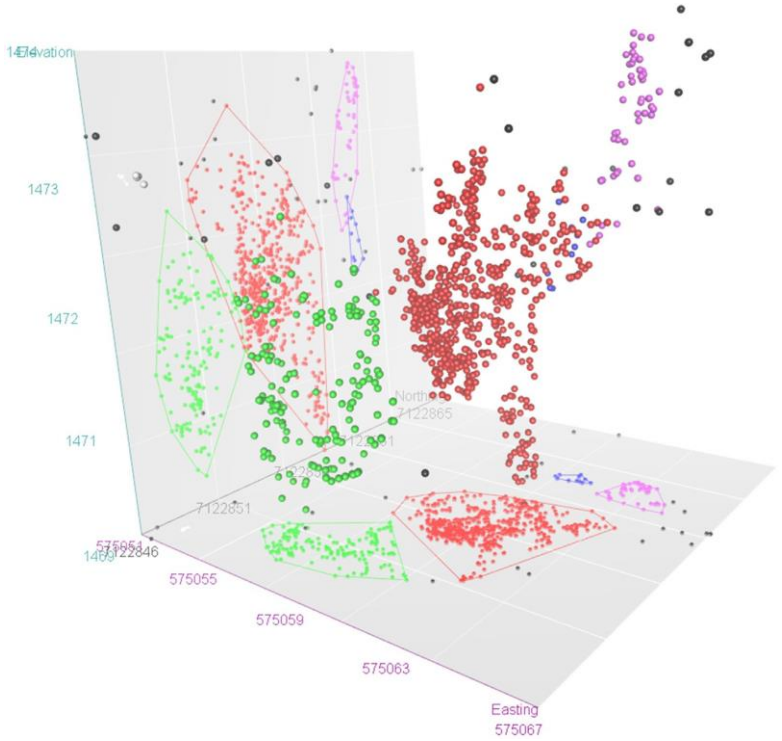

Fig. 4. 3D DBSCAN clustering, clusters differentiated by colour: 1 (Red), 2 (Green), 3 (Blue), 4 (Purple), 5 (Grey) and outliers in black.

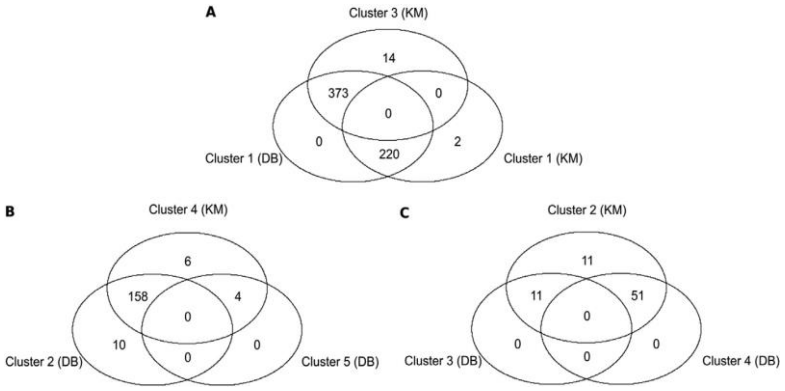

Fig. 5. Venn diagrams illustrating the intersection of data points occurring in clusters 1–4 from 3D k-means clustering and clusters 1–5 from 3D DBSCAN clustering.

behaviours. As yet, few studies have used k-means for 3D spatial patterning analysis in archaeological sites (Koetje, 1994; Anderson and Burke, 2008). The main aim of our study has been to fill this research gap in an attempt to use statistical testing of significance, in order to detect a potential non-homogeneous arrangement in space of fossils within Unit P at Kromdraai. In particular, we have aimed to test whether the assemblage from Unit P at Kromdraai was associated with a natural death trap, a hominin opportunistic scavenger or hunter, or a carnivore lair. Fourvel et al. (2018) considered that carnivores clearly had an important involvement in the accumulation of Unit P. They reported 6% of tooth marks and digestion marks within Unit P, a relatively high frequency when compared to other fossil carnivore lairs from the surrounding areas (Fourvel et al., 2018 and references therein). They also reported that most of the hominin postcranial bones from Unit P (e.g. the KW 8182 patella) have undergone carnivore damage. Vrba (1981) interpreted the assemblage from Unit Q, the next youngest sedimentary unit that overlies Unit P. She concluded that Unit Q likely accumulated not only as a result of carnivore feeding behaviors, but also as a deathtrap. Here, we cannot exclude the possibility of a deathtrap scenario, associated with the accumulation of at least some remains within Unit P. Neither can we exclude the possibility of alternating hominin-carnivore occupations.

We have applied a new method to evaluate 3D spatial patterns within the early hominin-bearing site of Kromdraai, but our results are

Table 5
Cluster size and average silhouette widths (S_i) from k-means clustering of the complete dataset and from k-means clustering of individual taxa and skeletal region.

	Cluster	Size	Sil.width (S_i)	Avg.sil.width (S_i)
Complete Dataset				
	1	222	0.35	0.42
	2	73	0.47	
	3	387	0.42	
	4	168	0.56	
Taxa				
Bovid	1	110	0,49	0,43
	2	318	0,43	
	3	53	0,55	
	4	166	0,36	
Carnivore	1	73	0,51	0,56
	2	23	0,69	
	3	13	0,64	
Hominin	1	18	0,60	0,64
	2	7	0,72	
Primate	1	29	0,65	0,5
	2	34	0,37	
Skeletal Region				
Isolated Teeth	1	22	0,44	0.54
	2	79	0,56	
	3	21	0,61	
Cranium	1	13	0,48	0.42
	2	30	0,33	
	3	48	0,45	
Lower Limb	1	15	0,58	0.55
	2	103	0,55	
	3	49	0,55	
Upper Limb	1	33	0,57	0.46
	2	59	0,47	
	3	44	0,35	
Limb	1	80	0,57	0.54
	2	21	0,4	
	3	29	0,56	
Thoracic Cage	1	13	0,49	0.45
	2	11	0,39	
Pelvic Grid	1	16	0,47	0.46
	2	6	0,43	
Pectoral Girdle	1	9	0,48	0.5
	2	10	0,52	
Spinal Column	1	6	0,43	0.63
	2	9	0,41	
	3	67	0,68	
Horn	1	3	0,60	0.42
	2	20	0,32	
	3	29	0,46	
Tusk	1	2	0,89	0.65
	2	3	0,49	

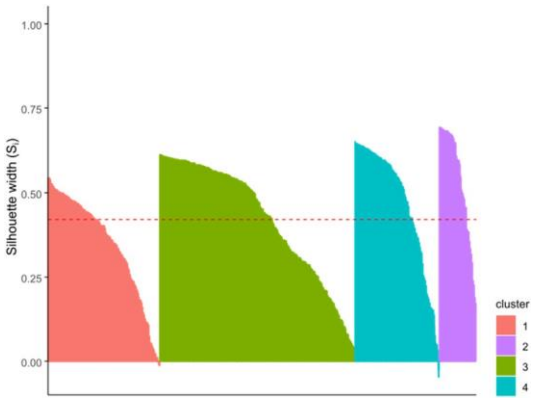

Fig. 6. Silhouette plot for k-means clustering of the complete dataset.

only tentative and should be considered as a point of departure until more data are collected and more tests are done. The present study has been oriented towards methodology, employing k-means for the study of 3D spatial patterning analysis in an archaeological context. Once all the potential factors of bias on clustering sensitivity have been analysed, the tentative results presented below may be further discussed.

We identify four meaningful clusters for the complete dataset (Figs. 1, 2, 3 and supplementary materials) that suggest a non-uniform distribution of the fossils across the site. It is important to emphasize here again that the area delineated in Fig. 1B has been systematically excavated in the same way at all locations (see above). Only the "Main Remnant" (also delineated in Fig. 1B) was not systematically excavated, even though a few elements recovered in situ from this area were also plotted. Three areas between adjacent clusters (i.e., between clusters 1 and 2, clusters 1 and 3, cluster 3 and 4) are worth discussing in more detail here. First, we observe an area with no elements located between the adjacent clusters 1 and 2. This absence of identified elements is not caused by the absence of excavations in this area but only by the absence of elements identified in situ during the excavations. Second, in the area between the two adjacent and largest clusters 1 and 3, the border elements are very densely spaced and were discovered at similar elevations and within types of soft sediments. However, the "Silhouette Statistic" demonstrates that clusters 1 and 3 show a relatively inaccurate classification of fossils. The inaccuracy of fossil classification within these clusters suggests that most fossils fall on or within proximity to the decision boundaries between clusters. The higher frequency of fossils within these clusters increases the propensity of the fossils to be distributed across a larger spatial area, and therefore interact with neighbouring clusters. Third and, interestingly enough, cluster 3 encompasses the "Main remnant", i.e., contains elements recovered from both eastern and western edges of this area of consolidated sediments that has not been explored as yet. In other words, some elements recovered from the western edge of the "Main Remnant" belong to cluster 3. They were discovered in closer proximity to fossils classified within cluster 4. Another result is important to discuss here in order to evaluate the effect of stratigraphic provenience on clustering. Indeed, cluster 2 contains elements from Unit P and the "test sample", i.e. outliers representing another stratigraphic unit. This result indicates that clustering should be applied to elements securely tied to stratigraphic units. We observed that the fossils were reasonably classified within cluster 2 and, to a lesser extent, cluster 4. This implies that fossils within the smaller clusters are more secluded from neighbouring clusters and could therefore be more accurately discriminated from other clusters.

With further a inspection of the fossil locations, specific specimen characteristics, taphonomic indicators and site processes, as well as insight on the consolidation of fossils belonging to specific individuals across space, can be provided. Importantly, when we consider the k-means clustering of individual taxa separately, the best-classified clusters were obtained for carnivores and hominins. Hominins indicated reasonable cluster allocation while bovids showed the least efficient clustering. Therefore, the hominins recovered within Unit P do not show a homogeneous spatial patterning. Instead, a heterogeneous patterning is reflected. Further investigations and refinements of our database will help us to better understand the significance of the tentative results presented here.

6. Conclusions

The particular clusters observed within Unit P are not intended here to be interpreted as "activity areas". We consider that clusters observed here only provide additional evidence that should be discussed in combination with taphonomic indicators already assessed by Fourvel et al. (2018). The clusters identified here within Unit P can be simply interpreted as areas of higher density of points compared to those of surrounding areas within the same deposit. Inter alia, they may

correspond perhaps to particular abiotic accumulation processes such as, for instance, distinct entrances and/or distinct phases of accumulation within Unit P.

Spatial analysis has the potential to provide insights into past behaviors because it can potentially explain the correlation between particular categories of objects such as carnivore and hominin remains. Our results do not as yet provide enough evidence to identify alternating hominin carnivore occupations within Unit P at Kromdraai, and to address questions related to hominin behaviours, such as those presented by Brain (1981). However, here we demonstrate that several clusters of fossils can be revealed visually within Unit P (Figs. 1 and 2). More data available in the near future will help to interpret further the first evidence for 3D spatial patterning within Unit P. We also hope that our approach combining different methods (including statistics) will be applied to deposits in other sedimentary formations and sites from the *Cradle of Humankind* World Heritage Site and, thus will be a useful contribution to the study of human evolution in South Africa.

CRediT authorship contribution statement

Nonkululeko Mantombi Nomalanga Ngoloyi: Conceptualization, Investigation, Formal analysis, Methodology, Visualization, Writing - original draft. Jean Dumoncel: Investigation, Methodology, Software, Validation. John Francis Thackeray: Investigation, Writing - review & editing. José Braga: Conceptualization, Investigation, Supervision, Writing - review & editing, Project administration.

Acknowledgements

This work has been supported by the French Ministry of Foreign Affairs, the Institut des Déserts et des Steppes (Paris), the Institut Picot de Lapeyrouse (Toulouse), the “AESOP plus” programme is a part of Erasmus Mundus; European Union, and Campus France through the French Embassy in South Africa. We thank the Cradle Management Authority, the South African Heritage Resources Agency and Mr. Riaan Lotz for their continuous support. We warmly acknowledge Dr. Jean-Baptiste Fourvel and Dr. Benjamin Lans for efficient assistance during the fieldwork and for having provided information about GIS.

Appendix A. Supplementary data

Supplementary data to this article can be found online at https://doi.org/10.1016/j.jasrep.2020.102376.

References

Abdul-Rahman, A., Pilouk, M., 2007. Spatial data modelling for 3D GIS. Springer Science & Business Media.

Adler, D., & Murdoch, D. (2012). rgl: 3D visualization device system (OpenGL). R package version 0.92. 880. In.

Anderson, K.L., Burke, A., 2008. Refining the definition of cultural levels at Karabi Tamchin: a quantitative approach to vertical intra-site spatial analysis. J. Archaeol. Sci. 35 (8), 2274–2285. https://doi.org/10.1016/j.jas.2008.02.011.

Baxter, M. (2015). Spatial k-means clustering in archaeology–variations on a theme. Academia (Accessed February 17, 2017). https://www.academia.edu/18142974/Spatial_k-means_clustering_in_archaeology–variationsonatheme.

Benito-Calvo, A., de la Torre, I., 2011. Analysis of orientation patterns in Olduvai Bed I assemblages using GIS techniques: implications for site formation processes. J. Hum. Evol. 61 (1), 50–60. https://doi.org/10.1016/j.jhevol.2011.02.011.

Bholowalia, P., Kumar, A., 2014. EBK-means: A clustering technique based on elbow method and k-means in WSN. International J. Comput. Appl. 105 (9).

Birkenfeld, M., Avery, M.D., Horwitz, L.K., 2015. GIS virtual reconstructions of the temporal and spatial relations of fossil deposits at Wonderwerk Cave (South Africa). African Archaeol. Rev. 32 (4), 857–876. https://doi.org/10.1007/s10437-015-9209-4.

Braga, J., Thackeray, J.F., Bruxelles, L., Dumoncel, J., Fourvel, J.-B., 2017. Stretching the time span of hominin evolution at Kromdraai (Gauteng, South Africa): Recent discoveries. C.R. Palevol 16 (1), 58–70. https://doi.org/10.1016/j.crpv.2016.03.003.

Braga, J., Fourvel, J.-B., Ngoloyi, M., Zipfel, B., Bruxelles, L., Schneider, J.-L., Zimmer, V., Steininger, C., Patel, A.B., de Beer, F., Hoffman, J., Thackeray, J.F., Grine, F. (2020, submitted). Paranthropus and Homo associated with a pre-2 Ma faunal assemblage at Kromdraai. Quaternary Science Reviews.

Brain, C.K. (1975). An interpretation of the bone assemblage from the Kromdraai australopithecine site, South Africa. In: Tuttle, R.H. (Ed.), Palaeontology, Morphology and Palaeoecology, 225–243.

Brain, C.K., 1981. The hunters or the hunted?: an introduction to African cave taphonomy. University of Chicago Press.

Bruxelles, L., Maire, R., Couzens, R., Thackeray, F., Braga, J., 2016. A revised stratigraphy of Kromdraai. In: Braga, J., Thackeray, J.F. (Eds.), Kromdraai, a Birthplace of Paranthropus in the Cradle of Humankind. SunMedia Metro, Johannesburg, pp. 31–47.

Buckland, P. I., Nyqvist, R., Alexander, B., Palsson, G., & Eriksson, S. (2018). The Swedish Transport Administration's Toolbox and its Potential in Archaeological and Cultural Heritage Survey: Including a brief review of remote sensing, prospection and geodata analysis methods for archaeology and cultural heritage. In: Umeå universitet.

Clarke, D.L., 1977. Spatial information in archaeology. Spat. Archaeol. 1, 32.

de la Torre, I., Benito-Calvo, A., 2013. Application of GIS methods to retrieve orientation patterns from imagery; a case study from Beds I and II, Olduvai Gorge (Tanzania). J. Archaeol. Sci. 40 (5), 2446–2457. https://doi.org/10.1016/j.jas.2013.01.004.

de la Torre, I., Wehr, K., 2018. Site formation processes of the early Acheulean assemblage at EF-HR (Olduvai Gorge, Tanzania). J. Hum. Evol. 120, 298–328. https://doi.org/10.1016/j.jhevol.2017.07.002.

Diez-Martín, F., Sánchez-Yustos, P., Uribelarrea, D., Domínguez-Rodrigo, M., Fraile-Márquez, C., Obregón, R.-A., et al., 2014. New archaeological and geological research at SHK main site (Bed II, Olduvai Gorge, Tanzania). Quat. Int. 322, 107–128. https://doi.org/10.1016/j.quaint.2013.11.004.

Domínguez-Rodrigo, M., Cobo-Sánchez, L., 2017. A spatial analysis of stone tools and fossil bones at FLK Zinj 22 and PTK I (Bed I, Olduvai Gorge, Tanzania) and its bearing on the social organization of early humans. Palaeogeogr. Palaeoclimatol. Palaeoecol. 488, 21–34. https://doi.org/10.1016/j.palaeo.2017.04.010.

Enloe, J.G., David, F., Hare, T.S., 1994. Patterns of faunal processing at Section 27 of Pincevent: the use of spatial analysis and ethnoarchaeological data in the interpretation of archaeological site structure. J. Anthropol. Archaeol. 13 (2), 105–124. https://doi.org/10.1006/jaar.1994.1007.

Ester, M., Kriegel, H.-P., Sander, J., & Xu, X. (1996). A density-based algorithm for discovering clusters in large spatial databases with noise. Paper presented at the Kdd.

Forgy, E.W., 1965. Cluster analysis of multivariate data: efficiency versus interpretability of classifications. Biometrics 21, 768–769.

Fourvel, J.-B., Thackeray, J.F., Brink, J.S., O'regan, H., Braga, J., 2018. Taphonomic interpretations of a new Plio-Pleistocene hominin-bearing assemblage at Kromdraai (Gauteng, South Africa). Quat. Sci. Rev. 190, 81–97. https://doi.org/10.1016/j.quascirev.2018.04.018.

Gaonkar, M.N., Sawant, K., 2013. AutoEpsDBSCAN: DBSCAN with Eps automatic for large dataset. Int. J. Adv. Comput Theory Eng. 2 (2), 11–16.

Hahsler, M., & Piekenbrock, M. (2017). dbscan: Density Based Clustering of Applications with Noise (DBSCAN) and Related Algorithms. R package version, 1.1-1.

Hartigan, J.A., Wong, M.A., 1979. Algorithm AS 136: A k-means clustering algorithm. J. Roy. Stat. Soc.: Ser. C (Appl. Stat.) 28 (1), 100–108. https://doi.org/10.2307/2346830.

Hennig, C., & Imports, M. (2015). Package 'fpc'. URL: http://cran.r-project.org/web/packages/fpc/fpc.pdf (available 08.07. 2017).

Hopkins, B., Skellam, J.G., 1954. A new method for determining the type of distribution of plant individuals. Ann. Bot. 18 (2), 213–227. https://doi.org/10.1093/oxfordjournals.aob.a083391.

Kassambara, A., & Mundt, F. (2017). Package 'factoextra'. Extract and visualize the results of multivariate data analyses, 76.

Katsianis, M., 2012. Conceptual and Practical Issues in the Use of GIS for Archaeological Excavations. *Thinking Beyond the Tool: Archaeological Computing and the Interpretive Process*. BAR Int. Ser. 2344, 51–71.

Kaufman, L., & Rousseeuw, P. J. (2009). Finding groups in data: an introduction to cluster analysis (Vol. 344): John Wiley & Sons.

Kintigh, K.W., Ammerman, A.J., 1982. Heuristic approaches to spatial analysis in archaeology. Am. Antiq. 47 (1), 31–63. https://doi.org/10.2307/280052.

Koetje, T.A., 1994. Intrasite spatial structure in the European Upper Paleolithic: Evidence and patterning from the SW of France. J. Anthropol. Archaeol. 13 (2), 161–169. https://doi.org/10.1006/jaar.1994.1011.

Kruger, A. (2017). Site formation processes at Rising Star: taphonomy and 3D spatial analyses of the Homo naledi assemblage.

Lemke, A.K., 2013. Cutmark systematics: analyzing morphometrics and spatial patterning at Palangana. J. Anthropol. Archaeol. 32 (1), 16–27. https://doi.org/10.1016/j.jaa.2012.08.001.

Lloyd, S., 1982. Least squares quantization in PCM. IEEE Trans. Inf. Theory 28 (2), 129–137. https://doi.org/10.1109/TIT.1982.1056489.

MacQueen, J. (1967). Some methods for classification and analysis of multivariate observations. Paper presented at the Proceedings of the fifth Berkeley symposium on mathematical statistics and probability.

Makantasis, K., Doulamis, A., Doulamis, N., Loannides, M., 2016. In the wild image retrieval and clustering for 3D cultural heritage landmarks reconstruction. Multimedia Tool Appl. 75 (7), 3593–3629. https://doi.org/10.1007/s11042-014-2191-z.

McAndrews, T.L., Albarracin-Jordan, J., Bermann, M., 1997. Regional settlement patterns in the Tiwanaku Valley of Bolivia. J. Field Archaeol. 24 (1), 67–83. https://doi.org/10.1179/jfa.1997.24.1.67.

Mendez-Quintas, E., Panera, J., Altamura, F., Di Bianco, L., Melis, R.T., Piarulli, F., et al., 2019. Gombore II (Melka Kunture, Ethiopia): A new approach to formation processes and spatial patterns of an Early Pleistocene Acheulean site. J. Archaeol. Sci. 108, 104975. https://doi.org/10.1016/j.jas.2019.104975.

Mokokwe, D. W. (2016). Taxonomy, taphonomy and spatial distribution of the

cercopithecoid postcranial fossils from Sterkfontein caves.
Nigro, J.D., Limp, W., Kvamme, K., De Ruiter, D., Berger, L., 2001. The creation and potential applications of a 3-dimensional GIS for the early hominin site of Swartkrans. University of Arkansas, Fayetteville, South Africa.
Nigro, J.D., Ungar, P.S., de Ruiter, D.J., Berger, L.R., 2003. Developing a geographic information system (GIS) for mapping and analysing fossil deposits at Swartkrans, Gauteng Province, South Africa. J. Archaeol. Sci. 30 (3), 317–324. https://doi.org/10.1006/jasc.2002.0839.
Oron, M., Goren-Inbar, N., 2014. Mousterian intra-site spatial patterning at Quneitra, Golan Heights. Quat. Int. 331, 186–202. https://doi.org/10.1016/j.quaint.2013.04.013.
Partridge, T.C. (1982). Some preliminary observations on the stratigraphy and sedimentology of the Kromdraai B hominid site. In: Coetzee, J.A.N.,Van Zinderen Bakker, E.M. (Eds.), Palaeoecology of Africa and the Surrounding Islands, Vol. 15. CRC Press, Taylor & Francis Group, New York, pp. 3–12.
Rahmah, N., & Sitanggang, I. S. (2016). Determination of optimal epsilon (eps) value on dbscan algorithm to clustering data on peatland hotspots in sumatra. Paper presented at the IOP Conference Series: Earth and Environmental Science. doi: 10.1088/1755-1315/31/1/012012.
Rousseeuw, P.J., 1987. Silhouettes: a graphical aid to the interpretation and validation of cluster analysis. J. Comput. Appl. Math. 20, 53–65. https://doi.org/10.1016/0377-0427(87)90125-7.
Schneider, J.-L., Lans, B., Le Bourdonnec, F.-X., Cornuault, A., Thackeray, J. F., & Braga, J. (2020, in revision). From macroscopic fabric to depositional dynamics of a cave talus cone: Unit P of the Plio-Pleistocene hominin-bearing Kromdraai site (Gauteng, South Africa). Sedimentary Geology.
Shu, H., Pei, T., Song, C., Ma, T., Du, Y., Fan, Z., et al., 2019. Quantifying the spatial heterogeneity of points. Int. J. Geograph. Informat. Scie. 33 (7), 1355–1376. https://doi.org/10.1080/13658816.2019.1577432.
Simek, J.F., 1984. A K-means Approach to the Analysis of Spatial Structures in Upper Paleolithic Habitation Sites Le Flageolet I and Pincevent Section 36. BAR. International Series(205).
Stratford, D., Merlo, S., Brown, S., 2016. The development of a new geospatial framework for the palaeoanthropological site of the Sterkfontein Caves, Cradle of Humankind, Gauteng, South Africa. J. Field Archaeol. 41 (2), 211–221. https://doi.org/10.1080/00934690.2016.1157679.
Team, R. (2015). RStudio: integrated development for R. RStudio, Inc., Boston, MA URL http://www.rstudio.com, 42, 14.
Traviglia, A., Torsello, A., 2017. Landscape pattern detection in archaeological remote sensing. Geosciences 7 (4), 128. https://doi.org/10.3390/geosciences7040128.
Vaquero, M., 1999. Intrasite spatial organization of lithic production in the Middle Palaeolithic: the evidence of the Abric Romaní (Capellades, Spain). Antiquity 73 (281), 493–504. https://doi.org/10.1017/S0003598X00065054.
Vavrek, M.J., 2011. Fossil: palaeoecological and palaeogeographical analysis tools. Palaeontol. Electronica 14 (1), 16.
Vrba, E., 1981. The Kromdraai australopithecine site revisited in 1980; recent investigations and results. Ann. Transv. Museum 33 (3), 17–60.
Warnes, M. G. R., Bolker, B., Bonebakker, L., & Gentleman, R. (2016). Package 'gplots'. Various R Programming Tools for Plotting Data.
Werdelin, L., Lewis, M.E., 2013. Temporal change in functional richness and evenness in the eastern African Plio-Pleistocene carnivoran guild. PLoS ONE 8 (3), e57944. https://doi.org/10.1371/journal.pone.0057944.
Wheatley, D., & Gillings, M. (2013). Spatial technology and archaeology: the archaeological applications of GIS: CRC Press. doi:10.1201/b12806.
Wills, S., Choiniere, J.N., Barrett, P.M., 2018. Predictive modelling of fossil-bearing locality distributions in the Elliot Formation (Upper Triassic-Lower Jurassic), South Africa, using a combined multivariate and spatial statistical analyses of present-day environmental data. Palaeogeogr. Palaeoclimatol. Palaeoecol. 489, 186–197. https://doi.org/10.1016/j.palaeo.2017.10.009.
Wright, D.K., Thompson, J.C., Schilt, F., Cohen, A.S., Choi, J.-H., Mercader, J., et al., 2017. Approaches to Middle Stone Age landscape archaeology in tropical Africa. J. Archaeol. Sci. 77, 64–77. https://doi.org/10.1016/j.jas.2016.01.014.
YiLan, L., & RuTong, Z. (2015). clustertend: Check the Clustering Tendency. R package version, 1.

CHAPTER FOUR: General Discussion and Conclusions

Discussion

This chapter provides a synthesis of the results rendered from this research. Firstly, we address the application of photogrammetry for the visualisation and quantification of overburden volume sediments at Kromdraai (Chapter 2). In the same chapter we address the application of metadata modelling for the creation of 4D relational databases in archaeology. Secondly, we discuss the results of the published study evaluating the 3D spatial patterns of the Unit P fossil assemblage at Kromdraai (chapter 3).

3D photogrammetry, volume estimation and metadata modelling

In addressing the first objective of the study, we focussed on the use of photogrammetry as a 3D digitization and quantitative tool in chapter 2. Aerial photogrammetry was first used to develop a 3D model reconstruction of Unit P from point cloud data coordinates in order to develop the orthomosaic maps used to illustrate the 2D fossil spatial patterns in chapter 3. However, chapter 2 detailed how the cost-effective terrestrial photogrammetry method was applied to reconstruct the site in 3D and therefore visually track the progress of the excavation over 2 days. The overlaid 3D models developed for the area of interest pre and post excavation enabled the in-situ visualisation of the area excavated by means of negative space computation, and facilitated its spatial traceability and volume estimation. Using a combination of Avizo 8, Meshlab and Meshmixer software the developed volume

estimation method enabled the visualisation of the two sub-volumes of overburden sediments removed from the site (over a short-term excavation period) in-situ and separately in the form of disjointed pieces. In comparing volume estimations computed within the Avizo 8 software versus the VRMesh software, the results demonstrated the efficiency and accuracy of this method, as the volume estimations were highly comparable. In fact, the volume 1 measurement was off by only $0.01m^2$, and volume 2 was exactly the same using both software. In a study comparing volume calculations from classical geodetic methods to the photogrammetric method, Yakar and Yilmaz (2008) demonstrated an average higher accuracy (12.83%), cost-effectiveness (32.33%) and time efficiency (21.89%) in the modern method (Samad et al., 2012, Yakar et al., 2010). Similarly, against laser scanning, Tucci et al. (2019) demonstrated the high accuracy and "perfect" adequacy of volume computations of stockpile surfaces based on UAV photogrammetry. The success of the pilot method implemented in chapter 2 illustrated long-term potential for further applications of 3D modeling within the site, particularly in regard to the allocation of displaced fossils recovered through the ex-situ wet sieving process.

3D k-means clustering and spatial patterning

In Chapter 3, we demonstrated that, in comparison to studies on other Plio-Pleistocene fossil sites in the *Cradle of Humankind* using 3D digitization techniques and GIS technology (e.g. Nigro et al., 2001; Nigro et al., 2003; Mokokwe, 2016; Stratford et al., 2016), spatial analyses integrated with statistical studies such as cluster analysis and the use of statistical validation tools contribute significantly to the identification of point spatial distribution patterns within Unit P at Kromdraai. These

non-uniform spatial patterns can then be analysed simultaneously, with a more detailed analysis of taphonomic indicators for future interpretations.

K-means analysis identified four main clusters for the complete dataset from Unit P, suggestive of a non-uniform spatial distribution. However, this analysis represented only a partial view of the assemblage, given that it represented fossils found in situ only. Therefore, the incorporation of the fossils discovered through the screening process (chapter 2) could be beneficial in order to perform further analyses on a more complete dataset.

The results showed that the very densely packed clusters 1 and 3, overlapped along the borders at similar elevations. This suggested that the discrepancy between the two clusters was not clearly distinguished. This was expected given the high frequency of fossils within the small space. Furthermore, the "Silhouette Statistic" which indicated an inaccuracy in the fossil classification supported this observation. This is plausible given that the stratigraphy of the site suggests that these clusters occurred in the same layer of soft sediments with no major structural boundaries separating the area. Although the "Main remnant" clearly distinguished between the eastern and western edges of Unit P, cluster 3 contained fossils from both sides. This too was very likely considering that it was the largest cluster (387 fossils), and possible inaccuracies in the classification of the fossils as indicated by the silhouette analysis. In contrast, the clustering of the smallest cluster (cluster 4) was shown to be more accurate. Similarly, the observed clustering results for the smallest taxa group (hominins) was more efficient than that of the largest (bovids). These observations confirmed that frequency did indeed have an impact of the clustering efficacy of the fossil assemblage. Furthermore, the lack of statistical significance shown in the largest clusters results demonstrates the purely exploratory nature of the k-means clustering

tool.

The purpose of this research was to provide a technical methodology that can be implemented to provide an additional perspective on site taphonomy thereby revealing more clues about the formation processes of Unit P. Indeed, there are studies integrating spatial analysis for taphonomic interpretations in 2D (e.g. Gallotti et al., 2011; Oron and Goren-Inbar, 2014). However, as demonstrated in this study, 3D analyses provide an additional perspective that improves on the visualisation of complex spatial patterns and density distributions. With the addition of 3D topology, our analyses in R considered elevation (z-coordinate) as a spatial coordinate, whereas most GIS packages integrate z-values as attributes (Gallotti et al., 2011).

The results do not show the statistical significance of spatial patterning k-means, but show that spatial analyses have the potential to support taphonomic interpretations by revealing patterns in the arrangement that can be either homogenous or heterogeneous. In regards to the implementation of spatial analysis in taphonomy, the first point of focus could be to compare spatial patterning results to taphonomic interpretations.

According to Fourvel (2018), Kromdraai Unit P (Member 2) represents a carnivore lair. Focussing on carnivores, it would be noteworthy to consider specific predator-prey interactions from a spatial perspective. For instance, spatial analyses could be used for assessing the association between the locality of these fossils and the taphonomic interpretations of skeletal part distributions, bone fragmentation and bone modification. In agreement with observations by Fourvel et al. (2018), our results show bovids occurring mainly in clusters 1 and 3 dominate the Unit P accumulation. These clusters are highly represented by limb bones (Table 3). Taphonomic interpretations show that appendicular bones of bovids dominated the skeletal

representation of bovids in Unit P, a common characteristic of carnivore dens (Fourvel et al., 2018). Furthermore, a high frequency (6%) of tooth-marks indicative of carnivore damage was observed for the Unit P sample (see Fourvel et al., 2016, 2018). Fourvel et al. (2018) report carnivore damage on the majority of postcranial bones of hominins from Unit P (e.g. the KW 8182 patella) suggestive of a partial accumulation of hominin bones by carnivores. Within Unit P, clusters 1 and 3 combined also represented the majority of non-hominin primate remains in the sample, another characteristic of carnivore lairs (Brain, 1981; Fourvel et al., 2018).

Although all fossils in clusters 1, 3 and 4 represent the Unit P assemblages, perhaps further spatial patterning analyses (in conjunction with taphonomic indicators) could reveal information regarding the deposition of different zones within the unit. This leads one to a few questions to gain perspective in future studies; does spatial patterning reveal specific zones of activity? What does this high density of fossils in one area say about taphonomy or depositional processes? Another question to ask would be, does spatial pattern analysis discriminate between different stratigraphic units?

These questions may be answered upon further taphonomic inspection (e.g. fragmentation, bone damage) of the specific fossils represented within these clusters. Given the specific locality of clusters 1 and 3, which have a high density of carnivore and bovid fossils, perhaps a hypothesis for future studies could be that non-uniform spatial patterning within the same unit indicates intra-site zones of biotic accumulation. Another hypothesis could be that a non-uniform distribution is reflective of distinct phases of accumulation caused by abiotic processes. As revealed in the study (chapter 3, Figure 1B), cluster analysis distinguished the 40 outliers from cluster 2 that were attributed to the “test sample” (indicated in blue) representing a

new unit. This demonstrated the potential for clustering to distinguish clusters within a single deposit and possibly between distinct stratigraphic units.

Alternatively, a uniform spatial arrangement of fossils is reflective of a single depositional process or size sorting through some abiotic process (e.g. fluvial transportation). Of course, there is much more to consider in this respect e.g. sediment type, site processes, stratigraphy, fossil size and other taphonomic indicators. The addition of ex-situ fossils within these specific localities as suggested in chapter 2, will provide much more information regarding taxa and skeletal types within the different clusters or zones of accumulation, and the taphonomic implications thereof.

A comparative analysis of spatial patterning and taphonomic indicators between different units could possibly inform faunal behaviours during different phases of deposition. To make substantial taphonomic inferences, these results must be viewed simultaneously with taphonomic indicators.

Conclusions and future research prospects

In this thesis I have acknowledged that through physical deterioration by way of the destructive excavation process of excavation, significant data loss occurs at archaeological sites. I therefore recognized the need for an authentic visual memory of the site that can be manipulated for further analyses, data extraction, and data interpretation and archiving. Additionally, I noted the importance of integrating innovative digital techniques for cultural heritage preservation and knowledge dissemination. In reviewing the guidelines for best practices and principles in heritage documentation and specific digital documentation practices (chapter 1) stipulated by CIPA and detailed in D'Ayala and Smars (2003), this study cohered to the guiding

concepts of “values”, “learning process”, “continuity”, “fabric” “documentation sets” and “redundancy”.

The new protocol of survey excavation detailed in chapter 2 will be employed in future excavations. Focusing on small sections within the site, more precise short-term (2 day) excavations will be undertaken to visualize and estimate overburden sediments volumes (enclosed within) using photogrammetry and 3D digitization. This new method will contribute to a better recording of the evolution of the site for heritage documentation. Additionally, the metadata model can also be used to create an archaeological database for Kromdraai to facilitate data archiving and other applications, such applications include spatiotemporal querying and prediction (Keßler and Farmer, 2015).

Both chapters 2 and 3 prioritized the preservation of data for future analyses and applications. Chapter 2 especially focused on preserving information regarding the volume of over-burden sediments to provide a temporal and spatial context for the future allocation of ex-situ fossil finds through the sieving process and their integration in spatial analyses. Additionally, the presented method for 3D volume estimation was innovative and has not been applied in this regard within the *Cradle of Humankind* or other archaeological sites. This is therefore a valuable method that can be applied in other archaeological sites to develop the spatial patterning of fossil assemblages in relation to the stratigraphy of the deposit.

Chapter 3 aimed to use the k-means is an exploratory (not a confirmatory tool) to reveal in the distribution patterns of the fossils in Kromdraai. By integrating point cloud data generated from 3D photogrammetry, and the precise fossil locations from total station coordinates, 3D spatial analysis were performed on the dataset in order to reveal the spatial patterning of the fossil assemblage of Unit P which can be further

used to assess potential taphonomic and depositional agents on the site. In addition, an assessment of the interrelations of fossil elements relative to the spatial context of the cavity and the associations or trends between various fossil groupings was conducted.

The results rendered in this study are considered positively as they efficiently assessed the frequency and density of the defined sub-groups in the fossil assemblage. Furthermore they have demonstrated the potential of spatial patterning analysis to help support taphonomic interpretations. To ensure "continuity" and "redundancy" (D'Ayala and Smars, 2003; CIPA, 2020) of this research, more studies that support and amplify it must be conducted. In fact, methods more suited to assessing heterogeneous datasets such as k-mediods or k-medians can be implemented in future. Furthermore, instead of the Hopkins statistical test, the application of second order tests (e.g. K, G, F, PCF functions) and testing the 3D spatial Poisson process will be considered to document clustering and extract more information.

For future studies at Kromdraai, considering the spatial patterning of specific taxa groups simultaneously for example hominins and carnivores (to the species level) would provide further insight on the hominin-carnivore relationship. Further probing into these results along with taphonomy and stratigraphy of the site could reveal details on the distinct phases of deposition and possible faunal behaviours. Another interesting observation would be the proximity of the hominin or carnivore fossils to the cave entrance and the taphonomic implications. An interesting consideration for future studies in order to minimize any clustering bias would be the fossil size and fragmentation. It would also be interesting to analyse possible abiotic processes that may have had implications on the precise location of the fossils in order to rule out any non-vertebrate depositional agent. Additional tools to implement in 3D could be spatial simulation tools (e.g. kriging and the Gaussian model) and prediction models

(e.g. archaeological predictive modelling (APM) and regression models) (Achino and Barceló, 2018; Domínguez-Rodrigo et al., 2017; Zhu et al., 2018).

Importantly, it would be beneficial to integrate the complete 3D representation of Unit P into a publically accessible virtual environment or 3D animation and games (non-scientific communication) in order to innovatively disseminate information about Kromdraai for academic, entertainment or tourism purposes.

REFERENCES

Abdul-Rahman, A., Pilouk, M. (2007). Spatial data modelling for 3D GIS: Springer Science & Business Media.

Achino, K. F., Barceló, J. A. (2018). Spatial Prediction: Reconstructing the "Spatiality" of Social Activities at the Intra-Site Scale. *Journal of Archaeological Method and Theory*, 1-23.

Adams, J. W., Herries, A. I., Kuykendall, K. L., Conroy, G. C. (2007). Taphonomy of a South African cave: geological and hydrological influences on the GD 1 fossil assemblage at Gondolin, a Plio-Pleistocene paleocave system in the Northwest Province, South Africa. *Quaternary Science Reviews, 26*(19-21), 2526-2543.

Adams, J.W., Herries, A.I.R., Hemingway, J., Kegley, A.D., Kgasi, L., Hopley, P., Reade, H., Potze, S., Thackeray, J.F. (2010). Initial fossil discoveries from Hoogland, a new Pliocene primate-bearing karstic system in Gauteng Province, South Africa. *Journal of Human Evolution, 59* (6), 685.

Adams, J.W., Herries, A.I.R., Kuykendall, K.L., Conroy, G.C. (2007) Taphonomy of a South African cave: geological and hydrological influences on the GD 1 fossil assemblage at Gondolin, a Plio-Pleistocene paleocave system in the Northwest Province, South Africa, *Quaternary Science Reviews, 26,* 2526-2543.

Adler, D., Murdoch, D. (2012). rgl: 3D visualization device system (OpenGL). R package version 0.92.

Allen, P., Feiner, S., Troccoli, A., Benko, H., Ishak, E., Smith, B. (2004). Seeing into the past: Creating a 3D modeling pipeline for archaeological visualization. In Proceedings. 2nd International Symposium on 3D Data Processing, Visualization and Transmission (pp. 751-758). IEEE.

Anderson, K. L., Burke, A. (2008). Refining the definition of cultural levels at Karabi Tamchin: a quantitative approach to vertical intra-site spatial analysis. *Journal of Archaeological Science, 35*(8), 2274-2285. https://doi.org/10.1016/j.jas.2008.02.011

Andrews, P. (1990). *Owls, Caves, and Fossils: Predation, Preservation, and Accumulation of Small Mammal Bones in Caves, with An Analysis of the Pleistocene Cave Faunas from Westbury-sub-Mendip, Somerset, UK [M]. Chicago: University of Chicago Press, 1990.*

Armstrong, B. J., Blackwood, A. F., Penzo-Kajewski, P., Menter, C. G., Herries, A. I. (2018). Terrestrial laser scanning and photogrammetry techniques for documenting fossil-bearing palaeokarst with an example from the Drimolen Palaeocave System, South Africa. *Archaeological Prospection*, *25*(1), 45-58.

Ashton, N., Lewis, S.G., De Groote, I., Duffy, S.M., Bates, M., Bates, R., Hoare, P., Lewis, M., Parfitt, S.A., Peglar, S., Williams, C. (2014). Hominin footprints from early Pleistocene deposits at Happisburgh, UK. *PLoS One*, *9*(2), e88329.

Awange, J., & Kiema, J. (2019). Fundamentals of GIS. In *Environmental Geoinformatics* (pp. 203-212). Springer, Cham.

Barazzetti, L., Binda, L., Scaioni, M., Taranto, P. (2011). Photogrammetric survey of complex geometries with low-cost software: Application to the 'G1′ temple in Myson, Vietnam. *Journal of Cultural Heritage, 12*(3), pp.253-262.

Barrett, L., Gaynor, D., Rendall, D., Mitchell, D., Henzi, S.P. (2004). Habitual cave use and thermoregulation in chacma baboons (*Papiohamadrysursinus)*. *Journal of Human Evolution, 46*, 215-222.

Baxter, M. (2015). Spatial k-means clustering in archaeology–variations on a theme. *Academia (Accessed February 17, 2017). https://www.academia.edu/18142974/Spatial_kmeans_clustering_in_archaeology–variationsonatheme*.

Benito-Calvo, A., de la Torre, I. (2011). Analysis of orientation patterns in Olduvai Bed I assemblages using GIS techniques: implications for site formation processes. *Journal of Human Evolution, 61*(1), 50-60. https://doi.org/10.1016/j.jhevol.2011.02.011

Bennett, M.R., Falkingham, P., Morse, S.A., Bates, K., Crompton, R.H. (2013). Preserving the impossible: conservation of soft-sediment hominin footprint sites and strategies for three-dimensional digital data capture. *PLoS One, 8*(4), e60755.

Berger, L. R. (1993). A preliminary estimate of the age of the Gladysvale australopithecine site. *Palaeontologia Africana, 30*, 51-55.

Berger, P. V. (1994). New discoveries at the early hominid site of Gladysvale, South Africa. *South African Journal of Science, 90*(4), 223-226.

Berger, L. R., Clarke, R. J. (1995). Eagle involvement in accumulation of the Taung child fauna. *Journal of Human Evolution, 29*(3), 275-299.

Berger, L. R., Pickering, R., Kuhn, B., Backwell, L., Hancox, P. J., Kramers, J. D., Boshoff, P. (2009). A Mid-Pleistocene in situ fossil brown hyaena (Parahyaena brunnea) latrine from Gladysvale Cave, South Africa. *Palaeogeography, Palaeoclimatology, Palaeoecology*, *279*(3-4), 131-136.

Bholowalia, P., Kumar, A. (2014). EBK-means: A clustering technique based on elbow method and k-means in WSN. *International Journal of Computer Applications, 105*(9), 17-24.

Binford, L. R. (1981). *Bones: ancient men and modern myths*. Academic press.

Birkenfeld, M., Avery, M. D., Horwitz, L. K. (2015). GIS virtual reconstructions of the temporal and spatial relations of fossil deposits at Wonderwerk Cave (South Africa). *African Archaeological Review, 32*(4), 857-876. https://doi.org/10.1007/s10437-015-9209-4

Böhner, U., Serangeli, J., Richter, P. (2015). The Spear Horizon: First spatial analysis of the Schöningen site 13 II-4. *Journal of human evolution*, *89*, 202-213.

Boschian, G., Saccà, D. (2010). Ambiguities in human and elephant interactions? Stories of bones, sand and water from Castel di Guido (Italy). *Quaternary International*, 214(1-2), 3-16.

Bountalis, A. C., Kuhn, B. F. (2014). Cave usage by multiple taphonomic agents: issues towards interpreting the fossil bearing cave deposits in South Africa. *American Journal of Zoological Research*, *2*(4), 55-61.

Boydston, E. E., Kapheim, K. M., Holekamp, K. E. (2006). Patterns of den occupation by the spotted hyaena (Crocuta crocuta). *African Journal of Ecology*, *44*(1), 77-86.

Braga, J., Thackeray, J. F. (2003). Early Homo at Kromdraai B: probabilistic and morphological analysis of the lower dentition. *Comptes Rendus Palevol*, *2*(4), 269-279.

Braga, J., Thackeray, J.F., Dumoncel, J., Descouens, D., Bruxelles, L., Loubes, J.M., Kahn, J.L., Stampanoni, M., Bam, L., Hoffman, J., de Beer, F., Spoor, F. (2013). A new partial temporal bone of a juvenile hominin from the site of Kromdraai B (South Africa). *Journal of Human Evolution*, 65, 447-456.

Braga, J., Fourvel, Thackeray, J. F. (2016). Kromdraai: A preliminary hypothetical evolutionary scenario. In: Braga, J., Thackeray, J.F. (Eds.), *Kromdraai: a Birthplace of Paranthropus in the Cradle of Humankind*, pp. 107-109. Sun Media Metro, Johannesburg.

Braga, J., Fourvel, J.B., Lans, B., Bruxelles, L., Thackeray, J.F., 2016a. Evolutionary, chrono-cultural and palaeoenvironmental backgrounds to the Kromdraai site: a regional perspective. In: Braga, J., Thackeray, J.F. (Eds.), *Kromdraai, a Birthplace of Paranthropus in the Cradle of Humankind*, pp. 1-16. Sun Media Metro, Johannesburg.

Braga, J., Dumoncel, J., Duployer, B., Tenailleau, C., de Beer, F., Thackeray, J.F., 2016b. The Kromdraai hominins revisited with an updated portrayal of differences between *Australopithecus africanus* and *Paranthropus robustus*. In: Braga, J., Thackeray, J.F. (Eds.), *Kromdraai, a Birthplace of Paranthropus in the Cradle of Humankind*, pp. 49-68. Sun Media Metro, Johannesburg.

Braga, J., Thackeray, J. F., Bruxelles, L., Dumoncel, J., Fourvel, J.-B. (2017). Stretching the time span of hominin evolution at Kromdraai (Gauteng, South Africa): Recent discoveries. *Comptes Rendus Palevol, 16*(1), 58-70. https://doi.org/10.1016/j.crpv.2016.03.003

Braga, J., Fourvel, J.-B., Ngoloyi, M., Zipfel, B., Bruxelles, L., Schneider, J.-L., Zimmer, V., Steininger, C., Patel, A.B., de Beer, F., Hoffman, J., Thackeray, J.F., Grine, F. (2020, in revision). Paranthropus and Homo associated with a pre-2 Ma faunal assemblage at Kromdraai. *Quaternary Science Reviews*.

Brain, C.K. (1958) *The Transvaal Ape-Man-Bearing Cave Deposits*, Transvaal Museum Memoirs, no.11.

Brain, C.K. (1975). An interpretation of the bone assemblage from the Kromdraai australopithecine site, South Africa. In: Tuttle, R.H. (Ed.), *Palaeontology, Morphology and Palaeoecology*, 225–243.

Brain, C. K. (1981). *The hunters or the hunted?: an introduction to African cave taphonomy*: University of Chicago Press.

Brain, C.K. (1993) *Swartkrans, A Cave's Chronicle of Early Man*. Brain, C.K. (ed.) Transvaal Museum Monograph No.8: Pretoria.

Broom, R. (1936) New fossil anthropoid skull from South Africa, *Nature*, 138, 486-488.

Broom, R. (1938) The Pleistocene Anthropoid Apes of South Africa, *Nature*, 142, 377-379.

Broom, R. (1947) Discovery of a new skull of the South African ape-man, *Plesianthropus*, *Nature*, 159, 672.

Bruxelles, L., Clarke, R. J., Maire, R., Ortega, R., & Stratford, D. (2014). Stratigraphic analysis of the Sterkfontein StW 573 Australopithecus skeleton and implications for its age. *Journal of human evolution*, *70*, 36-48.

Bruxelles, L., Maire, R., Couzens, R., Thackeray, F., Brain, J. (2016). A revised stratigraphy of Kromdraai. In: Braga, J., Thackeray, J.F. (Eds.), *Kromdraai, a Birthplace of Paranthropus in the Cradle of Humankind*, pp. 31-47. Sun Media Metro, Johannesburg.

Buckland, P. I., Nyqvist, R., Alexander, B., Palsson, G., Eriksson, S. (2018). *The Swedish Transport Administration's Toolbox and its Potential in Archaeological and Cultural Heritage Survey: Including a brief review of remote sensing, prospection and geodata analysis methods for archaeology and cultural heritage*. Report produced for the Swedish Transport Authority (Trafikverket) by the Environmental Archaeology Lab, Umeå University.

Button, A. (1973). The stratigraphic history of the Malmani dolomite in the eastern and north-eastern Transvaal. *South African Journal of Geology*, *76*(3), 229-247.

Carlson, K.J., Pickering, T.R. (2003) Intrinsic qualities of primate bones as predictors of skeletal element representation in modern and fossil carnivore feeding assemblages, *Journal of Human Evolution*, 44, 431-450.

Carrer, F. (2017). Interpreting intra-site spatial patterns in seasonal contexts: an ethnoarchaeological case study from the western Alps. *Journal of Archaeological Method and Theory*, 24(2), 303-327.

Carrero-Pazos, M., Vilas-Estévez, B., Vázquez-Martínez, A. (2018). Digital imaging techniques for recording and analysing prehistoric rock art panels in Galicia (NW Iberia). *Digital applications in archaeology and cultural heritage*, *8*, 35-45.

Chase, A. S., Chase, D. Z., & Chase, A. F. (2017). LiDAR for archaeological research and the study of historical landscapes. In *Sensing the Past* (pp. 89-100). Springer, Cham.

Chrisman, N. R. (1999). What does 'GIS'mean?. *Transactions in GIS*, *3*(2), 175-186.

CIPA Heritage Documentation. 2020. What is CIPA. [ONLINE] Available at: https://www.cipaheritagedocumentation.org/. [Accessed 27 March 2020].

Clarke, D. L. (1977). Spatial information in archaeology. *Spatial archaeology*, *1*, 32.

Clarke, R.J. (2007) Taphonomy of Sterkfontein *Australopithecus* skeletons, In: Pickering, T.R., Schick, K., Toth, N. (eds.) *Breathing Life into Fossils: Taphonomic Studies in Honor of C.K. (Bob) Brain*, pp. 199-205. Bloomington (Indiana): Stone Age Institute Press.

Cocks, M., Vetter, S., Wiersum, K.F. (2017). From universal to local: perspectives on cultural landscape heritage in South Africa. *International Journal of Heritage Studies*, *24*(1), 35-52.

D'Ayala, D., Smars, P. (2003). Minimum requirement for metric use of non-metric photographic documentation, University of Bath Report. Access: https://smars.yuntech.edu.tw/papers/eh_report.pdf

Dall'Astaa, E., Bruno, N., Bigliardi, G., Zerbi, A., Roncella, R. 2016. Photogrammetric techniques for promotion of archaeological heritage: the

archaeological museum of Parma (Italy). *International Archives of the Photogrammetry, Remote Sensing Spatial Information Sciences*, *41*, 243-250.

Dart, R. A., Salmons, A. (1925). *Australopithecus africanus*: the man-ape of South Africa. *A Century of Nature: Twenty-One Discoveries that Changed Science and the World*, 10-20.

Dart, R.A. (1949) Innominate fragments of *Australopithecus Prometheus*, American Journal of Physical Anthropology, *7*(3), 301-334.

Dart, R. (1957). The Osteodontokeratic culture of Australopithecus Promethius: Discussion. *Transvaal Museum Memoirs*, *10*(1), 87-101.

Dart, R. A. (1962). The gradual appraisal of Australopithecus. In G. Kurth (Ed.), *Evolution und Hominisation*, pp. 141–156. Stuttgart, Germany: Gustav Fischer Verlag.

de la Torre, I., Benito-Calvo, A. (2013). Application of GIS methods to retrieve orientation patterns from imagery; a case study from Beds I and II, Olduvai Gorge (Tanzania). *Journal of Archaeological Science*, *40*(5), 2446-2457. https://doi.org/10.1016/j.jas.2013.01.004

de la Torre, I., Wehr, K. (2018). Site formation processes of the early Acheulean assemblage at EF-HR (Olduvai Gorge, Tanzania). *Journal of Human Evolution*, *120*, 298-328. https://doi.org/10.1016/j.jhevol.2017.07.002

De Reu, J., Plets, G., Verhoeven, G., De Smedt, P., Bats, M., Cherretté, B., De Maeyer, W., Deconynck, J., Herremans, D., Laloo, P., Van Meirvenne, M. (2013). Towards a three-dimensional cost-effective registration of the archaeological heritage. *Journal of archaeological science*, *40*(2), 1108-1121.

de Ruiter, D.J., Berger, L.R. (2000) Leopards as taphonomic agents in dolomitic caves - implications for bone accumulation in the hominid-bearing deposits of South Africa. *Journal of Archaeological Science*, *27*, 665-684.

de Ruiter, D.J. (2001) A Methodological Analysis of the Relative Abundance of Hominids and Other Macromammals from the Site of Swartkrans, South Africa, Ph.D. thesis, University of the Witwatersrand, Johannesburg.

de Ruiter, D.J., Sponheimer, M., Lee-Thorpe, J. (2008) Indications of habitat association of *Australopithecus robustus* in the Cradle of Humankind, South Africa, *Journal of Human Evolution*, *55*, 1015-1030.

de Ruiter, D.J., Pickering, R., Steininger, C.M., Kramers, J.D., Hancox, P.J., Churchill, S.E., Berger, L.R., Backwell, L. (2009). New australopithecus robustus fossils and associated U-Pb dates from Cooper's cave (Gauteng, South Africa). *Journal of Human Evolution*, *56*(5), 497-513.

Department of Tourism (2012) National Heritage and Cultural Tourism Strategy. Pretoria: Government Printer.

DeSilva, J. M., Steininger, C. M., Patel, B. A. (2013). Cercopithecoid primate postcranial fossils from Cooper's D, South Africa. *Geobios*, *46*(5), 381-394.

Diez-Martín, F., Sánchez-Yustos, P., Uribelarrea, D., Domínguez-Rodrigo, M., Fraile-Márquez, C., Obregón, R.A., Díaz-Muñoz, I., Mabulla, A., Baquedano, E., Pérez-González, A., Bunn, H.T., (2014). New archaeological and geological research at SHK main site (Bed II, Olduvai Gorge, Tanzania). *Quaternary international*, *322*, 107-128.

Dirks, P.H.G.M., Kibii, J.M., Kuhn, B.F., Steininger, C., Churchill, S.E., Kramers, J.D., Pickering, R., Farber, D.L., Mériaux, A.-S., Herries, A.I.R., King, G.C.P., Berger, L.R. (2010) Geological setting and age of *Australopithecus sediba* from Southern Africa. *Science*, *328*, 205-208.

Domínguez-Rodrigo, M., Cobo-Sánchez, L. (2017). A spatial analysis of stone tools and fossil bones at FLK Zinj 22 and PTK I (Bed I, Olduvai Gorge, Tanzania) and its bearing on the social organization of early humans. *Palaeogeography, Palaeoclimatology, Palaeoecology, 488*, 21-34. https://doi.org/10.1016/j.palaeo.2017.04.010

Domínguez-Rodrigo, M., Cobo-Sánchez, L., Uribelarrea, D., Arriaza, M.C., Yravedra, J., Gidna, A., Organista, E., Sistiaga, A., Martín-Perea, D., Baquedano, E. and Aramendi, J., 2017. Spatial simulation and modelling of the early Pleistocene site of DS (Bed I, Olduvai Gorge, Tanzania): a powerful tool for predicting potential archaeological information from unexcavated areas. *Boreas, 46*(4), pp.805-815.

Dumoncel, J., Lans, B., Braga, J., Subsol, G., Jessel, J-P., Thackeray, JF., Moreno, B., Plate, N., de Beer, F., Ngoloyi, N. (2016). A computer-guided 3D multiscale reconstruction of the Kromdraai site. In: Braga, J., Thackeray, J.F. (Eds.), *Kromdraai, a Birthplace of Paranthropus in the Cradle of Humankind*, pp. 19-28. SunMedia Metro, Johannesburg.

Edwards, T., Grono, E., Herries, A.I., Brink, F.J., Troitzsch, U., Senden, T., Turner, M., Barron, A., Prossor, L., Denham, T. (2017). Visualising scales of process: Multi-scalar geoarchaeological investigations of microstratigraphy and

diagenesis at hominin bearing sites in South African karst. *Journal of Archaeological Science, 83*, pp.1-11.

Enloe, J. G., David, F., Hare, T. S. (1994). Patterns of faunal processing at Section 27 of Pincevent: the use of spatial analysis and ethnoarchaeological data in the interpretation of archaeological site structure. *Journal of Anthropological Archaeology*, *13*(2), 105-124. https://doi.org/10.1006/jaar.1994.1007

Eriksson, J. F. (1974). Stratotypes from the Malmani subgroup north-west of Johannesburg, South Africa. *South African Journal of Geology*, *77*(3), 211-222.

Eriksson, P. G., Altermann, W., Hartzer, F. J. (2006). The Transvaal Supergroup and its precursors. *The Geology of South Africa*, 237-260.

Ester, M., Kriegel, H.P., Sander, J., Xu, X. (1996). A density-based algorithm for discovering clusters in large spatial databases with noise. In *Kdd-96 Proceedings, 96*(34), 226-231.

Fonstad, M. A., Dietrich, J. T., Courville, B. C., Jensen, J. L., Carbonneau, P. E. (2013). Topographic structure from motion: a new development in photogrammetric measurement. *Earth Surface Processes and Landforms*, *38*(4), 421-430.

Forgy, E. W. (1965). Cluster analysis of multivariate data: efficiency versus interpretability of classifications. *Biometrics, 21*, 768-769.

Fourvel, J.B., Brink, J., O'Regan, H., Beaudet, A., Pavia, M. (2016). Some preliminary interpretations of the oldest faunal assemblage from Kromdraai.

In: Braga, J., Thackeray, J.F. (Eds.), *Kromdraai, a Birthplace of Paranthropus in the Cradle of Humankind*, pp. 71-106. Sun Media Metro, Johannesburg.

Fourvel, J.-B., Thackeray, J. F., Brink, J. S., O'Regan, H., Braga, J. (2018). Taphonomic interpretations of a new Plio-Pleistocene hominin-bearing assemblage at Kromdraai (Gauteng, South Africa). *Quaternary Science Reviews, 190*, 81-97. https://doi.org/10.1016/j.quascirev.2018.04.018

Gaonkar, M. N., Sawant, K. (2013). AutoEpsDBSCAN: DBSCAN with Eps automatic for large dataset. *International Journal on Advanced Computer Theory and Engineering, 2*(2), 11-16.

Geiling, J. M., Marín-Arroyo, A. B., Straus, L. G., González Morales, M. R. (2018). Deciphering archaeological palimpsests with bone micro-fragments from the Lower Magdalenian of El Mirón cave (Cantabria, Spain). *Historical Biology*, *30*(6), 730-742.

Gifford-Gonzalez, D. (2018). *An introduction to zooarchaeology*. Springer.

Giusti, D., Tourloukis, V., Konidaris, G., Thompson, N., Karkanas, P., Panagopoulou, E., Harvati, K. (2018). Beyond maps: patterns of formation processes at the Middle Pleistocene open-air site of Marathousa 1, Megalopolis Basin, Greece. *Quaternary International*, *497*, 137-153.

Gommery, D., Sénut, B., Keyser, A. (2002). Description of a fragmentary basin of Paranthropus robustus from the Plio-Pleistocene site of Drimolen (South Africa). *Geobios* , *35* (2), 265-281.

Gopher, A., Parush, Y., Assaf, E., Barkai, R. (2016). Spatial aspects as seen from a density analysis of lithics at Middle Pleistocene Qesem Cave: Preliminary

results and observations. *Quaternary International*, 398, 103-117. doi:https://doi.org/10.1016/j.quaint.2015.09.078

Gould, M., Herring, J. R. (2001). Redefining GIS. In *Proceedings of the 4th AGILE Conference on Geographic Information Science. Brno* Czech Republic, April 19-21, 2001.

Greenop, K., Landorf, C. J. H. E. (2017). Grave-to-cradle: a paradigm shift for heritage conservation and interpretation in the era of 3D laser scanning. *Historic Environment*, *29*(1), 44.

Grine, F. E., Jacobs, R. L., Reed, K. E., Plavcan, J. M. (2012). The enigmatic molar from Gondolin, South Africa: implications for Paranthropus paleobiology. *Journal of human evolution*, *63*(4), 597-609.

Hahsler, M., Piekenbrock, M. (2017). dbscan: Density Based Clustering of Applications with Noise (DBSCAN) and Related Algorithms. *R package version*, 1.1-1.

Hartigan, J. A., Wong, M. A. (1979). Algorithm AS 136: A k-means clustering algorithm. *Journal of the Royal Statistical Society. Series C (Applied Statistics)*, *28*(1), 100-108. https://doi.org/10.2307/2346830

Harvey, D. R. (2007). UNESCO's Memory of the World Programme. *Library Trends*, *56*(1s), 259-274.

Häusler, M., Isler, K., Schmid, P., Berger, L. (2004). 3-D digital mapping of the early hominid site of Gladysvale cave, South Africa. *Human evolution*, *19*(1), 45-52.

Hennig, C., Imports, M. (2015). Package 'fpc'. *URL: http://cran.r-project.org/web/packages/fpc/fpc.pdf (available 08.07. 2017)*.

Herries, A.I., Murszewski, A., Pickering, R., Mallett, T., Joannes-Boyau, R., Armstrong, B., Adams, J.W., Baker, S., Blackwood, A.F., Penzo-Kajewski, P. and Kappen, P. (2018). Geoarchaeological and 3D visualisation approaches for contextualising in-situ fossil bearing palaeokarst in South Africa: a case study from the∼ 2.61 Ma Drimolen Makondo. *Quaternary International*, *483*, 90-110.

Hilton-Barber, B., Berger, L. (2002). The Official Field Guide to the Cradle of Humankind. Struik Publishers, Cape Town.

Hopkins, B., Skellam, J. G. (1954). A new method for determining the type of distribution of plant individuals. *Annals of Botany, 18*(2), 213-227. https://doi.org/10.1093/oxfordjournals.aob.a083391

Hua, L., Chen, C., Fang, H., Wang, X. (2018). 3D documentation on Chinese Hakka Tulou and Internet-based virtual experience for cultural tourism: A case study of Yongding County, Fujian. *Journal of Cultural Heritage*, *29*, 173-179.

Hughes, A. R. (1961). Further notes on the habits of hyaenas and bone gathering by porcupines. *Zoological Society of South Africa News Bulletin*, *3*(1), 35–37.

Jennings, D. S., Hasiotis, S. T. (2006). Taphonomic analysis of a dinosaur feeding site using geographic information systems (GIS), Morrison Formation, southern Bighorn Basin, Wyoming, USA. *Palaios*, *21*(5), 480-492.

Kassambara, A., Mundt, F. (2017). Package 'factoextra'. *Extract and visualize the results of multivariate data analyses*, *76*.

Katsianis, M. (2012). Conceptual and Practical Issues in the Use of GIS for Archaeological Excavations. *Thinking Beyond the Tool: Archaeological Computing and the Interpretive Process. BAR International Series, 2344*, 51-71.

Kaufman, L., Rousseeuw, P. J. (2009). *Finding groups in data: an introduction to cluster analysis* (Vol. 344): John Wiley and Sons.

Kearney, T. C., Keith, M., Seamark, E. C. (2017). New records of bat species using Gatkop Cave in the maternal season. *Mammalia*, *81*(1), 41-48.

Keßler, C., Farmer, C. J. (2015). Querying and integrating spatial–temporal information on the web of data via time geography. *Journal of Web Semantics, 35*, 25-34.

Kibii, J. M. (2009) Taphonomic aspects of African porcupines (*Hystrix cristata*) in the Kenyan Highlands, *Journal of Taphonomy*, *7*(1), 21-27.

Kintigh, K. W., Ammerman, A. J. (1982). Heuristic approaches to spatial analysis in archaeology. *American Antiquity*, *47*(1), 31-63. https://doi.org/10.2307/280052

Klein, R. G. (1975). Paleoanthropological implications of the nonarcheological bone assemblage from Swartklip I, south-western Cape Province, South Africa. *Quaternary Research*, *5*(2), 275-288.

Koetje, T. A. (1994). Intrasite spatial structure in the European Upper Paleolithic: Evidence and patterning from the SW of France. *Journal of Anthropological Archaeology*, *13*(2), 161-169. https://doi.org/10.1006/jaar.1994.1011

Kruger, A., Randolph-Quinney, P., Elliott, M. (2016). Multimodal spatial mapping and visualisation of Dinaledi Chamber and Rising Star Cave. *South African journal of science*, *112*(5-6), 1-11.

Kruger, A. (2017). *Site formation processes at Rising Star: Taphonomy and 3D spatial analyses of the Homo naledi assemblage* (Doctoral dissertation).

Kruger, A., Badenhorst, S. (2018). Remains of a barn owl (Tyto alba) from the Dinaledi Chamber, Rising Star Cave, South Africa. *South African Journal of Science*, *114*(11-12), 1-5.

Kuhn, B. (2005). The faunal assemblages and taphonomic signatures of five striped hyaena (Hyaena hyaena syriaca) dens in the desert of eastern Jordan. *Levant*, *37*(1), 221-234.

Lacruz, R.S., Brink, J.S., Hancox, P.J., Skinner, A.R., Herries, A., Schmid, P., Berger, L.R. (2002). Palaeontology and geological context of a middle Pleistocene faunal assemblage from Gladysvale Cave, South Africa. *Palaeontologia Africana*, *38,* 99–114.

Lam, Y.M. (1992) Variability in the behaviour of spotted hyaenas as taphonomic agents. *Journal of Archaeological Science*, *19*(4), 389-406.

Lemke, A. K. (2013). Cutmark systematics: analyzing morphometrics and spatial patterning at Palangana. *Journal of Anthropological Archaeology*, *32*(1), 16-27. https://doi.org/10.1016/j.jaa.2012.08.001

Levinson, M. (1982). Taphonomy of microvertebrates-from owl pellets to cave breccia. *Annals of the Transvaal Museum*, *33*(6), 115-121.

Lloyd, S. (1982). Least squares quantization in PCM. *IEEE transactions on information theory, 28*(2), 129-137. https://doi.org/10.1109/TIT.1981056489

MacQueen, J. (1967). *Some methods for classification and analysis of multivariate observations.* Paper presented at the Proceedings of the fifth Berkeley symposium on mathematical statistics and probability.

Magnussen, A., Visser, G. (2003). Developing a World Heritage Site: the cradle of humankind. *Africa Insight*, *33*(1/2), 78-86.

Makantasis, K., Doulamis, A., Doulamis, N., Loannides, M. (2016). In the wild image retrieval and clustering for 3D cultural heritage landmarks reconstruction. *Multimedia Tools and Applications, 75*(7), 3593-3629. https://doi.org/10.1007/s11042-014-2191-z

Mallye, J.B. (2011). Badger (Meles meles) remains within caves as an analytical tool to test the integrity of stratified sites: The contribution of Unikoté cave (Pyrénées-Atlantiques, France). *Journal of Taphonomy, 9*(1): 15-36.

Martini, J. E., Wipplinger, P. E., Moen, H. F., Keyser, A. (2003). Contribution to the speleology of sterkfontein cave, Gauteng Province, South Africa. *International Journal of Speleology*, *32*(1), 4.

McAndrews, T. L., Albarracin-Jordan, J., Bermann, M. (1997). Regional settlement patterns in the Tiwanaku Valley of Bolivia. *Journal of Field Archaeology*, *24*(1), 67-83. https://doi.org/10.1179/jfa.1997.24.1.67

McCrae, C. (2009). A comparative study of Late Holocene and Plio-Pleistocene-aged micromammalian owl accumulations from South Africa. *Palaeontologia Africana*, *44*, 190-191.

McPherron, S.P. (2018). Additional statistical and graphical methods for analyzing site formation processes using artifact orientations. *PloS one*, *13*(1), p.e0190195.

Mendez-Quintas, E., Panera, J., Altamura, F., Di Bianco, L., Melis, R.T., Piarulli, F., Ruta, G., Mussi, M. (2019). Gombore II (Melka Kunture, Ethiopia): A new approach to formation processes and spatial patterns of an Early Pleistocene Acheulean site. *Journal of Archaeological Science*, *108*, 104975.

Menter, C. G., Kuykendall, K. L., Keyser, A. W., Conroy, G. C. (1999). First record of hominid teeth from the Plio-Pleistocene site of Gondolin, South Africa. *Journal of Human Evolution*, *37*(2), 299-307.

Moggi-Cecchi, J., Menter, C., Boccone, S., Keyser, A. (2010). Early hominin dental remains from the Plio-Pleistocene site of Drimolen, South Africa. *Journal of Human Evolution*, *58*(5), 374-405.

Mokokwe, D. W. (2016). *Taxonomy, taphonomy and spatial distribution of the cercopithecoid postcranial fossils from Sterkfontein caves* (Doctoral dissertation).

Naidu, M. (2008). Creating an African tourist experience at the cradle of humankind world heritage site. *Historia*, *53*(2), 182-207.

Ngoloyi, N. M., Dumoncel, J., Thackeray, J. F., Braga, J. (2020). A new method to evaluate 3D spatial patterns within early hominin-bearing sites. An example from Kromdraai (Gauteng Province, South Africa). *Journal of Archaeological Science: Reports*, *32*, 102376.

Nigro, J. D., Limp, W., Kvamme, K., De Ruiter, D., Berger, L. (2001). *The creation and potential applications of a 3-dimensional GIS for the early hominin site of Swartkrans, South Africa* (Doctoral dissertation, University of Arkansas, Fayetteville).

Nigro, J. D., Ungar, P. S., de Ruiter, D. J., Berger, L. R. (2003). Developing a geographic information system (GIS) for mapping and analysing fossil deposits at Swartkrans, Gauteng Province, South Africa. *Journal of Archaeological Science, 30*(3), 317-324. https://doi.org/10.1006/jasc.2002.0839

O'Regan, H. J., Menter, C. G. (2009). Carnivora from the Plio-Pleistocene hominin site of Drimolen, Gauteng, South Africa. *Geobios, 42*(3), 329-350.

Olson, B. R., Placchetti, R. A., Quartermaine, J., Killebrew, A. E. (2013). The Tel Akko Total Archaeology Project (Akko, Israel): Assessing the suitability of multi-scale 3D field recording in archaeology. *Journal of Field Archaeology, 38*(3), 244-262.

Olson, B. R., Placchetti, R. A. (2015). A discussion of the analytical benefits of image based modeling in archaeology. *Visions of substance: 3D imaging in Mediterranean archaeology*, 17-25.

Oron, M., Goren-Inbar, N. (2014). Mousterian intra-site spatial patterning at Quneitra, Golan Heights. *Quaternary international, 331*, 186-202. https://doi.org/10.1016/j.quaint.2013.04.013

Partridge, T.C. (1982). Some preliminary observations on the stratigraphy and sedimentology of the Kromdraai B hominid site. In: Coetzee, J.A.N.,Van

Zinderen Bakker, E.M. (Eds.), Palaeoecology of Africa and the Surrounding Islands, Vol. 15, pp. 3–12. CRC Press, Taylor and Francis Group, New York.

Patias, P. (2006). Cultural heritage documentation. International Summer School Digital Recording and 3D Modeling, Aghios Nikolaos, Creta, Grecia, Abril, 24-29.

Patias, P., Santana, M. (2011). Introduction to heritage documentation. In: Stylianidis, E., Patias, P., Quintero, M. S., International Committee of Architectural Photogrammetry International Council on Monuments Sites International Society for Photogrammetry Remote Sensing (Eds.), CIPA Heritage Documentation: Best Practices and Applications: Series 1, 2007 and 2009: XXI International Symposium-CIPA 2007, Athens, XXII International Symposium-CIPA 2009, Kyoto: CIPA, 9-13.

Pavlidis, G., Koutsoudis, A., Arnaoutoglou, F., Tsioukas, V., Chamzas, C. 2007. Methods for 3D digitization of cultural heritage. *Journal of Cultural Heritage, 8*(1)**,** 93-98.

Pescarin, S. (2016). Digital heritage into practice. *SCIRES-IT-SCIentific RESearch and Information Technology*, *6*(1), 1-4.

Pickering, T.R. (2001a) Taphonomy of the Swartkrans hominid post-crania and its bearing on issues of meat-eating and fire management, In: Stanford, C.B., Bunn, H.T. (eds.) *Meat-Eating and Human Evolution*, pp.31-51. Oxford University Press: Oxford.

Pickering, T.R. (2001b) Carnivore voiding; a taphonomic process with the potential for the deposition of forensic evidence. *Journal of Forensic Science*, 46, 406-411.

Pickering, T.R. Clarke, R.J., Heaton, J.L. (2004a) The context of Stw 573, an early hominid skull and skeleton from Sterkfontein Member 2: taphonomy and paleoenvironment. *Journal of Human Evolution*, vol.46, pp.279-297.

Pickering, T.R., Clarke, R.J., Moggi-Cecchi, J. (2004b) The role of carnivores in the accumulation of the Sterkfontein Member 4 hominid assemblage: a taphonomic reassessment of the complete hominid fossil sample (1936-1999). *American Journal of Physical Anthropology*, *125*, 1-15.

Pickering, T.R., Domínguez -Rodrigo, M., Egeland, C.P., Brain, C.K. (2004c) Beyond leopards: tooth marks and the contribution of multiple carnivore taxa to the accumulation of the Swartkrans Member 3 fossil assemblage. *Journal of Human Evolution*, *46*, 595-604.

Pickering, T. R., Heaton, J. L., Clarke, R. J., Sutton, M. B., Brain, C. K., Kuman, K. (2012). New hominid fossils from Member 1 of the Swartkrans formation, South Africa. *Journal of human evolution*, *62*(5), 618-628.

Pickering, T. R., Heaton, J. L., Sutton, M. B., Clarke, R. J., Kuman, K., Senjem, J. H., Brain, C. K. (2016). New early Pleistocene hominin teeth from the Swartkrans formation, South Africa. *Journal of human evolution*, *100*, 1-15.

Pineda, A., Saladié, P., Expósito, I., Rodríguez-Hidalgo, A., Cáceres, I., Huguet, R., Rosas, A., López-Polín, L., Estalrrich, A., García-Tabernero, A. and Vallverdú, J. (2017). Characterizing hyena coprolites from two latrines of the Iberian Peninsula during the Early Pleistocene: Gran Dolina (Sierra de Atapuerca, Burgos) and la Mina (Barranc de la Boella, Tarragona). *Palaeogeography, Palaeoclimatology, Palaeoecology*, *480*, 1-17.

Pruetz, J. D. (2007). Evidence of cave use by savanna chimpanzees (Pan troglodytes verus) at Fongoli, Senegal: implications for thermoregulatory behavior. *Primates*, *48*(4), 316-319.

Quintero, M. S., Georgopoulos, A., Stylianidis, E., Lerma, J. L., Remondino, F. (2017). CIPA's mission: Digitally documenting cultural heritage. *APT Bulletin: The Journal of Preservation Technology*, *48*(4), 51-54.

Rahmah, N., Sitanggang, I. S. (2016). *Determination of optimal epsilon (eps) value on dbscan algorithm to clustering data on peatland hotspots in sumatra.* Paper presented at the IOP Conference Series: Earth and Environmental Science. https://doi.org/10.1088/1755-1315/31/1/012012

Reed, D. N. (2003). *Micromammal paleoecology: past and present relationships between African small mammals and their habitats* (Doctoral dissertation, State University of New York at Stony Brook).

Reed, D. N. (2005). Taphonomic implications of roosting behavior and trophic habits in two species of African owl. *Journal of Archaeological Science*, *32*(11), 1669-1676.

Remondino, F., Rizzi, A., Girardi, S., Petti, F. M., Avanzini, M. (2010). 3D Ichnology—recovering digital 3D models of dinosaur footprints. *The Photogrammetric Record*, *25*(131), 266-282.

Repola, L., Scotto di Carlo, N., Signoretti, D., & Leidwanger, J. (2018). Virtual simulation of a late antique shipwreck at Marzamemi, Sicily: Integrated processes for 3D documentation, analysis and representation of underwater archaeological data. *Archaeological Prospection*, *25*(2), 99-109.

Reynolds, S. C. (2010). Where the wild things were: spatial and temporal distribution of carnivores in the cradle of humankind (Gauteng, South Africa) in relation to the accumulation of mammalian and hominin assemblages. *Journal of Taphonomy*, *8*(2-3), 233-257.

Riga, A., Mori, T., Pickering, T. R., Moggi‐Cecchi, J., Menter, C. G. (2019). Ages‐at‐death distribution of the early Pleistocene hominin fossil assemblage from Drimolen (South Africa). *American journal of physical anthropology*, *168*(3), 632-636.

Rogerson 1, C. M. (2007). Reviewing Africa in the global tourism economy. *Development Southern Africa*, *24*(3), 361-379.

Rogerson, C. M., Van der Merwe, C. D. (2016). Heritage tourism in the global South: Development impacts of the cradle of humankind world heritage site, South Africa. *Local Economy*, *31*(1-2), 234-248.

Roosevelt, C. H., Cobb, P., Moss, E., Olson, B. R., Ünlüsoy, S. (2015). Excavation is destruction digitization: advances in archaeological practice. *Journal of Field Archaeology*, *40*(3), 325-346.

Rössler, M. (2006). World heritage cultural landscapes: a UNESCO flagship programme 1992–2006. *Landscape Research*, *31*(4), 333-353.

Rousseeuw, P. J. (1987). Silhouettes: a graphical aid to the interpretation and validation of cluster analysis. *Journal of computational and applied mathematics, 20*, 53-65. https://doi.org/10.1016/0377-0427(87)90125-7.

Rüther, H., Chazan, M., Schroeder, R., Neeser, R., Held, C., Walker, S.J., Matmon, A., Horwitz, L.K. (2009). Laser scanning for conservation and research of

African cultural heritage sites: the case study of Wonderwerk Cave, South Africa. *Journal of Archaeological Science, 36* (9), 1847-1856.

Rüther, H., Smit, J., Kamamba, D. (2014). A Comparison of Close-Range Photogrammetry to Terrestrial Laser Scanning for Heritage Documentation. *South African Journal of Geomatics*, 1(2), 149-162.

Samad, A.M., Asri, N. A., Ahmad, A. (2012). The use of digital image for volume determination using digital close range photogrammetric method. In *2012 IEEE 8th International Colloquium on Signal Processing and its Applications* (pp. 321-324). IEEE.

Santos, P., Ritz, M., Fuhrmann, C., Fellner, D. (2017). 3D mass digitization: a milestone for archeological documentation. *Virtual Archaeology Review*, *8*(16), 1-11.

Shipman, P., Rose, J. (1983). Early hominid hunting, butchering, and carcass-processing behaviors: approaches to the fossil record. *Journal of anthropological Archaeology*, *2*(1), 57-98.

Shu, H., Pei, T., Song, C., Ma, T., Du, Y., Fan, Z., Guo, S., 2019. Quantifying the spatial heterogeneity of points. *International Journal of Geographical Information Science*, *33*(7), pp.1355-1376.

Simek, J. F. (1984). A K-means Approach to the Analysis of Spatial Structures in Upper Paleolithic Habitation Sites Le Flageolet I and Pincevent Section 36. *BAR. International Series*, 205.

Skinner, J. D., Van Aarde, R. J. (1981). The distribution and ecology of the brown hyaena Hyaena brunnea and spotted hyaena Crocuta in the central Namib Desert. *Madoqua*, *12*(4), 231-239.

Skinner, J. D., Van Aarde, R. J. (1991). Bone collecting by brown hyaenas Hyaena brunnea in the central Namib Desert, Namibia. *Journal of Archaeological Science*, *18*(5), 513-523.

Steininger, C., Berger, L. R., Kuhn, B. F. (2008). A partial skull of Paranthropus robustus from Cooper's Cave, South Africa. *South African Journal of Science*, *104*(3-4), 143-146.

Stratford, D., Merlo, S., Brown, S. (2016). The development of a new geospatial framework for the palaeoanthropological site of the Sterkfontein Caves, *Cradle of Humankind*, Gauteng, South Africa. *Journal of Field Archaeology*, *41*(2), 211-221. https://doi.org/10.1080/00934690.2016.1157679

Sturzenegger, M., Stead, D. (2009). Close-range terrestrial digital photogrammetry and terrestrial laser scanning for discontinuity characterization on rock cuts. *Engineering Geology*, *106*(3–4), 163-182. doi:http://dx.doi.org/10.1016/j.enggeo.2009.03.004

Subsol, G., Moreno, B., Jessel, J., Braga, J., Bruxelles, L., Thackeray, F., Clarke, R. (2015). In situ 3D digitization of the 'Little Foot'Australopithecus skeleton from Sterkfontein. *Paleoanthropology*, 44-53.

Team, R. (2015). RStudio: integrated development for R. *RStudio, Inc., Boston, MA URL http://www.rstudio.com*, *42*, 14.

Thackeray, J.F., de Ruiter, D.J., Berger, L.R., van der Merwe, N.J. (2001). Hominid fossils from Kromdraai: a revised list of specimens discovered since 1938. *Annals of the Transvaal Museum, 38,* 43-56

Traviglia, A., Torsello, A. (2017). Landscape pattern detection in archaeological remote sensing. *Geosciences*, *7*(4), 128.

Tucci, G., Gebbia, A., Conti, A., Fiorini, L., Lubello, C. (2019). Monitoring and Computation of the Volumes of Stockpiles of Bulk Material by Means of UAV Photogrammetric Surveying. *Remote Sensing*, *11*(12), 1471.

Val, A., Carlson, K. J., Steininger, C., Kibii, J. M., Churms, C., Kuhn, B. F., Berger, L. R. (2011). 3D techniques and fossil identification: An elephant shrew hemi-mandible from the Malapa site. *South African Journal of Science*, *107*(11-12), 01-05.

Val, A. M. S. (2014). *A 3D approach to understand the taphonomy of the early hominins from the Plio-Pleistocene cave site of Malapa* (Doctoral dissertation).

Val, A., Dirks, P. H., Backwell, L. R., d'Errico, F., Berger, L. R. (2015). Taphonomic analysis of the faunal assemblage associated with the hominins (*Australopithecus sediba*) from the Early Pleistocene cave deposits of Malapa, South Africa. *PloS one*, *10*(6), e0126904.

Val, A. (2016). Deliberate body disposal by hominins in the Dinaledi Chamber, Cradle of Humankind, South Africa. *J Hum Evol*, *96*, 145-148.

Val, A., Backwell, L. R., Dirks, P. H., d'Errico, F., Berger, L. R. (2018). Reconstruction of the burial position of two hominin skeletons

(Australopithecus sediba) from the early Pleistocene Malapa cave site, South Africa. *Geoarchaeology*, *33*(3), 291-306.

Van der Merwe, M. (1973). Aspects of social behaviour in the Natal clinging bat *Miniopterus schreibersi natalensis* (A. Smith, 1834). *Mammalia*, *37*, 379–389.

Van der Merwe, M. (1975). Preliminary study on the annual movements of the Natal Clinging bat. *South African Journal of. Science, 71*, 237–241.

Van der Merwe, C. D. (2016). Tourist guides' perceptions of cultural heritage tourism in South Africa. *Bulletin of Geography. Socio-economic Series*, *34*(34), 117-130.

Vaquero, M. (1999). Intrasite spatial organization of lithic production in the Middle Palaeolithic: the evidence of the Abric Romaní (Capellades, Spain). *Antiquity*, *73*(281), 493-504. https://doi.org/10.1017/S0003598X00065054

Vavrek, M. J. (2011). Fossil: palaeoecological and palaeogeographical analysis tools. *Palaeontologia Electronica*, *14*(1), 16.

Verhagen, P. (2018). Spatial analysis in archaeology: moving into new territories. In *Digital Geoarchaeology* (pp. 11-25). Springer, Cham.

Virzì, A., Muller, C. O., Marret, J. B., Mille, E., Berteloot, L., Grévent, D., ... & Bloch, I. (2020). Comprehensive review of 3D segmentation software tools for MRI usable for pelvic surgery planning. *Journal of Digital Imaging*, *33*(1), 99-110.

Vlachidis, A., Binding, C., May, K., Tudhope, D. (2013). Automatic metadata generation in an archaeological digital library: Semantic annotation of grey

literature. In *Computational linguistics* (pp. 187-202). Springer, Berlin, Heidelberg.

Vrba, E. (1981). The Kromdraai australopithecine site revisited in 1980; recent investigations and results. *Annals of the Transvaal Museum, 33*(3), 17-60.

Vrba E., Panagos DC. (1982). New perspectives on taphonomy, palaeoecology and chronology of the Kromdraai apeman In: JA Coetzee and EM van Zinderen Bakker (eds). Palaeoecology of Africa and the surrounding islands. Volume 15. 13-26.

Warnes, M. G. R., Bolker, B., Bonebakker, L., Gentleman, R. (2016). Package 'gplots'. *Various R Programming Tools for Plotting Data*.

Werdelin, L., Lewis, M. E. (2013). Temporal change in functional richness and evenness in the eastern African Plio-Pleistocene carnivoran guild. *PLoS One, 8*(3), e57944. https://doi.org/10.1371/journal.pone.0057944

Wheatley, D., Gillings, M. (2013). *Spatial technology and archaeology: the archaeological applications of GIS*: CRC Press. https://doi.org/10.1201/b12806

Wills, S., Choiniere, J. N., Barrett, P. M. (2018). Predictive modelling of fossil-bearing locality distributions in the Elliot Formation (Upper Triassic–Lower Jurassic), South Africa, using a combined multivariate and spatial statistical analyses of present-day environmental data. *Palaeogeography, Palaeoclimatology, Palaeoecology, 489*, 186-197. https://doi.org/10.1016/j.palaeo.2017.10.009

Wright, D. K., Thompson, J. C., Schilt, F., Cohen, A. S., Choi, J.-H., Mercader, J., Nightingale, S., Miller, C.E., Mentzer, S.M., Walde, D., Welling, M. (2017). Approaches to Middle Stone Age landscape archaeology in tropical Africa. *Journal of Archaeological Science, 77*, 64-77. https://doi.org/10.1016/j.jas.2016.01.014

Yakar, M., Yilmaz, H. M. (2008). Using in volume computing of digital close range photogrammetry. *The International Archives of the Photogrammetry, Remote Sensing and Spatial Information Sciences*. *37* (Part B3b), 119 -124.

Yakar, M., Yilmaz, H. M., Mutluoglu, O. (2010). Close range photogrammetry and robotic total station in volume calculation. *International Journal of Physical Sciences*, *5*(2), 86-96.

Yastikli, N. (2007). Documentation of cultural heritage using digital photogrammetry and laser scanning. *Journal of Cultural Heritage*, *8*(4), 423-427. doi:http://dx.doi.org/10.1016/j.culher.2007.06.003

YiLan, L., RuTong, Z. (2015). clustertend: Check the Clustering Tendency. *R package version*, *1*.

Yilmaz, H. M., Yakar, M., Yildiz, F. (2008). Documentation of historical caravansaries by digital close range photogrammetry. *Automation in Construction*, *17*(4), 489-498.

Zhu, X., Chen, F., Guo, H. (2018). A Spatial Pattern Analysis of Frontier Passes in China's Northern Silk Road Region Using a Scale Optimization BLR Archaeological Predictive Model. *Heritage, 1*(1), 15-32.

Zollhöfer, M., Siegl, C., Vetter, M., Dreyer, B., Stamminger, M., Aybek, S., Bauer, F. (2015). Low-Cost Real-Time 3D Reconstruction of Large-Scale Excavation Sites. *Journal on Computing and Cultural Heritage (JOCCH)*, *9*(1), 2.

APPENDICES

Appendix A: Supporting materials for Chapter Two.

Supplementary Figures

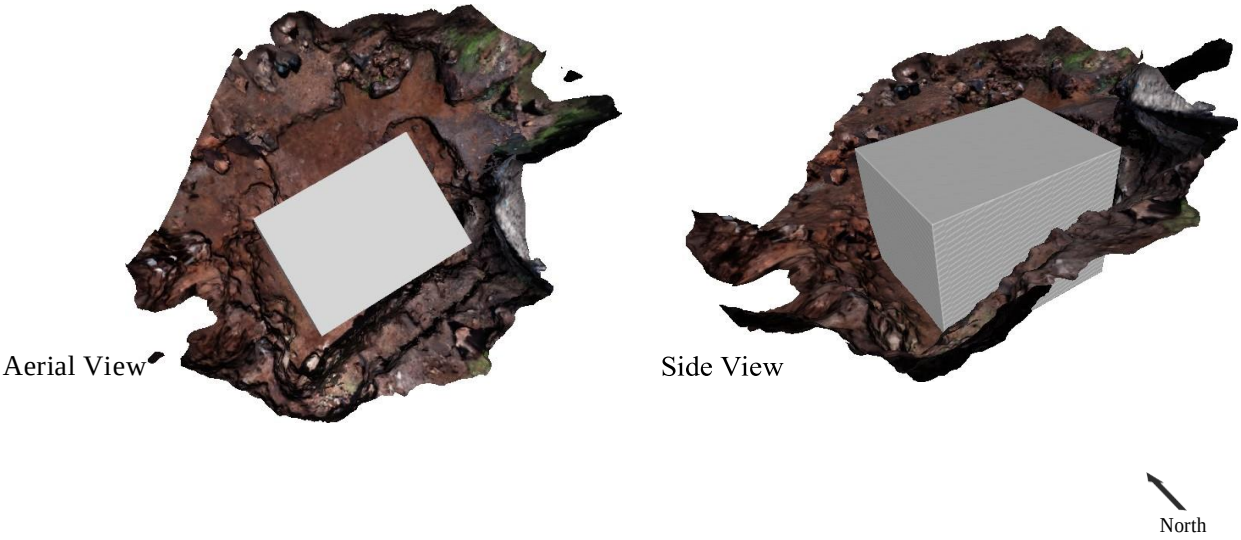

Figure A. 3D cube alignment filling the negative space of the merged 3D models representing the “before” and “after” excavation.

A

B

C

Figure B. Volume computation performed in Avizo 8. The merged 3D models with the volume contained pre-excavation (A), the in-situ visualisation of the volume removed (B), the section post-excavation (C).

3D Videos and Caption

Supplementary File – click **here** to view 3D model in data repository.

Figure C. 3D movie showing a visual representation of the overburden soils. Volumes 1 (green) and 2(orange) removed during the excavation within the context of site.

Appendix B: Supporting materials for Chapter Three.

Publication

Please click here to access the publication.

Raw Dataset

Table A. Raw dataset used showing individual fossil name (KW_ID), XYZ coordinates and fossil assignment to taxa and skeletal region.

KW_ID	X	Y	Z	Taxa	Skeletal Region
KW_10006	575060.66	7122855.405	1471.686	Bovid	Cranium
KW_10007	575062.461	7122856.484	1471.875	Bovid	Upper Limb
KW_10008	575062.535	7122856.308	1471.684	Bovid	Upper Limb
KW_10009	575061.686	7122856.348	1471.922	Bovid	Thoracic Cage
KW_10010	575061.654	7122856.267	1471.877	Bovid	Spinal Column
KW_10011	575062.486	7122856.35	1471.714	Bovid	Upper Limb
KW_10013	575058.06	7122850.742	1470.69	Primate	Lower Limb
KW_10014	575057.732	7122850.459	1470.617	Carnivore	Lower Limb
KW_10015	575058.082	7122850.254	1470.652	Primate	Upper Limb
KW_10016	575058.411	7122849.489	1470.726	Bovid	Lower Limb
KW_10017	575060.751	7122855.743	1471.708	Bovid	Upper Limb
KW_10018	575061.159	7122856.187	1471.683	Bovid	Upper Limb

KW_10019	575061.564	7122856.567	1471.68	Bovid	Cranium
KW_10020	575061.382	7122856.301	1471.651	Bovid	Upper Limb
KW_10022	575060.674	7122854.984	1471.52	Bovid	Lower Limb
KW_10023	575060.689	7122854.757	1471.431	Bovid	Lower Limb
KW_10024	575060.65	7122854.521	1471.483	Bovid	Cranium
KW_10025	575060.517	7122854.857	1471.458	Bovid	Lower Limb
KW_10026	575059.882	7122853.935	1471.568	Carnivore	Isolated Teeth
KW_10028	575061.274	7122853.972	1471.603	Carnivore	Lower Limb
KW_10053	575060.524	7122857.136	1471.925	Bovid	Pectoral Girdle
KW_10054	575060.398	7122856.608	1471.743	Bovid	Tusk
KW_10055	575060.523	7122857.294	1471.834	Bovid	Lower Limb
KW_10056	575059.871	7122849.226	1470.793	Bovid	Upper Limb
KW_10057	575059.616	7122849.118	1470.772	Bovid	Lower Limb
KW_10058	575059.573	7122848.852	1470.775	Bovid	Lower Limb
KW_10059	575060.483	7122855.638	1471.773	Bovid	Isolated Teeth
KW_10061	575060.457	7122856.965	1471.714	Bovid	Thoracic Cage
KW_10062	575059.833	7122849.54	1470.789	Bovid	Upper Limb
KW_10063	575059.93	7122849.366	1470.798	Bovid	Isolated Teeth
KW_10064	575059.01	7122849.085	1470.698	Bovid	Limb
KW_10065	575059.219	7122848.626	1470.778	Primate	Isolated Teeth
KW_10066	575059.981	7122855.456	1471.868	Bovid	Isolated Teeth
KW_10069	575061.217	7122853.521	1471.712	Bovid	Upper Limb
KW_10070	575060.657	7122853.889	1471.537	Bovid	Horn
KW_10071	575060.485	7122854.189	1471.552	Bovid	Horn
KW_10072	575060.252	7122855.702	1471.794	Bovid	Upper Limb
KW_10073	575060.788	7122853.587	1471.644	Bovid	Spinal Column
KW_10074	575060.634	7122853.298	1471.649	Bovid	Lower Limb
KW_10075	575059.081	7122854.16	1471.945	Bovid	Horn
KW_10076	575060.558	7122855.692	1471.254	Bovid	Lower Limb
KW_10077	575060.713	7122856.09	1471.426	Bovid	Pectoral Girdle
KW_10088	575061.14	7122860.125	1471.994	Carnivore	Isolated Teeth
KW_10099	575058.128	7122855.277	1472.243	Bovid	Tusk
KW_10101	575057.814	7122854.926	1472.168	Bovid	Upper Limb
KW_10102	575058.19	7122855.007	1472.108	Carnivore	Isolated Teeth
KW_10103	575059.494	7122854.968	1471.673	Bovid	Spinal Column

KW_10104	575061.764	7122855.639	1470.932	Bovid	Limb
KW_10106	575061.927	7122855.679	1471.103	Bovid	Upper Limb
KW_10107	575058.15	7122855.38	1472.157	Bovid	Tusk
KW_10108	575058.15	7122855.38	1472.157	Bovid	Upper Limb
KW_10110	575058.764	7122855.009	1471.731	Primate	Isolated Teeth
KW_10111	575058.329	7122854.886	1471.819	Primate	Isolated Teeth
KW_10113	575058.693	7122854.987	1471.751	Bovid	Isolated Teeth
KW_10114	575058.533	7122854.903	1471.85	Bovid	Isolated Teeth
KW_10115	575061.8	7122855.716	1470.86	Bovid	Limb
KW_10116	575061.75	7122855.58	1471.081	Bovid	Limb
KW_10117	575059.759	7122853.141	1472.046	Carnivore	Cranium
KW_10118	575059.712	7122853.219	1472.097	Bovid	Spinal Column
KW_10119	575062.374	7122855.527	1471.57	Bovid	Spinal Column
KW_10121	575061.838	7122856.731	1471.348	Primate	Upper Limb
KW_10122	575056.772	7122854.504	1471.931	Bovid	Isolated Teeth
KW_10123	575058.82	7122855.171	1471.758	Bovid	Tusk
KW_10124	575062.873	7122852.518	1472.98	Primate	Upper Limb
KW_10125	575058.732	7122855.565	1471.851	Primate	Upper Limb
KW_10126	575057.459	7122854.988	1471.97	Bovid	Thoracic Cage
KW_10127	575061.927	7122860.61	1472.17	Bovid	Lower Limb
KW_10131	575061.479	7122856.727	1471.079	Bovid	Horn
KW_10132	575061.488	7122857.158	1471.574	Bovid	Upper Limb
KW_10133	575058.969	7122855.393	1471.816	Bovid	Isolated Teeth
KW_10134	575062.922	7122851.889	1473.16	Bovid	Lower Limb
KW_10135	575056.158	7122849.539	1471.36	Bovid	Limb
KW_10136	575056.138	7122849.949	1471.556	Carnivore	Isolated Teeth
KW_10137	575056.663	7122849.37	1471.158	Carnivore	Isolated Teeth
KW_10138	575062.024	7122857.36	1471.602	Bovid	Limb
KW_10139	575058.06	7122855.914	1472.136	Bovid	Cranium
KW_10141	575059.064	7122855.925	1472.182	Carnivore	Isolated Teeth
KW_10142	575058.796	7122855.792	1472.139	Bovid	Spinal Column
KW_10143	575059	7122856.02	1472.108	Bovid	Spinal Column
KW_10145	575058.728	7122856.02	1471.947	Bovid	Spinal

					Column
KW_10146	575059.203	7122856.235	1471.852	Bovid	Lower Limb
KW_10147	575062.022	7122856.962	1471.287	Bovid	Upper Limb
KW_10149	575061.481	7122857.163	1470.951	Bovid	Limb
KW_10160_1	575062.248	7122860.497	1472.36	Hominin	Isolated Teeth
KW_10160_2	575062.309	7122860.125	1472.265	Hominin	Isolated Teeth
KW_10160_3	575062.043	7122860.199	1471.956	Hominin	Isolated Teeth
KW_10160_4	575061.897	7122860.836	1471.95	Hominin	Isolated Teeth
KW_10160_5	575061.205	7122860.356	1471.838	Hominin	Isolated Teeth
KW_10160_6	575061.304	7122859.977	1471.863	Hominin	Isolated Teeth
KW_10161	575061.337	7122857.295	1470.802	Bovid	Horn
KW_10165	575061.106	7122857.202	1470.959	Carnivore	Upper Limb
KW_10167_1	575061.042	7122857.251	1470.812	Carnivore	Pectoral Girdle
KW_10167_2	575061.042	7122857.251	1470.812	Carnivore	Upper Limb
KW_10167_3	575061.042	7122857.251	1470.812	Carnivore	Upper Limb
KW_10167_4	575061.042	7122857.251	1470.812	Carnivore	Upper Limb
KW_10168	575060.504	7122856.986	1471.336	Bovid	Upper Limb
KW_10182	575062.54	7122856.054	1471.424	Bovid	Upper Limb
KW_10183	575062.182	7122856.333	1471.026	Bovid	Horn
KW_10184	575062.169	7122856.33	1470.97	Bovid	Cranium
KW_10185	575062.335	7122856.696	1471.232	Bovid	Pelvic Grid
KW_10188	575062.71	7122856.102	1471.532	Bovid	Lower Limb
KW_10189	575062.444	7122856.18	1470.986	Carnivore	Cranium
KW_10190	575056.838	7122848.238	1471.354	Bovid	Upper Limb
KW_10191	575056.835	7122848.864	1471.271	Bovid	Upper Limb
KW_10192	575056.501	7122848.646	1471.314	Bovid	Upper Limb
KW_10193	575057.007	7122848.793	1471.278	Bovid	Pelvic Grid
KW_10194	575056.448	7122848.669	1471.301	Bovid	Limb
KW_10195	575056.371	7122848.848	1471.328	Bovid	Lower Limb
KW_10196	575057.089	7122848.803	1471.282	Bovid	Upper Limb
KW_10197	575055.612	7122850.651	1471.476	Bovid	Spinal Column
KW_10199	575055.721	7122850.062	1471.671	Carnivore	Lower Limb
KW_10200	575055.838	7122850.293	1471.26	Bovid	Upper Limb
KW_10203	575062.058	7122856.348	1470.599	Bovid	Lower Limb
KW_10204	575059.386	7122865.189	1472.872	Bovid	Isolated Teeth

KW_10206	575061.219	7122865.885	1472.864	Bovid	Limb
KW_10207	575062.13	7122856.187	1470.445	Bovid	Horn
KW_10208	575057.035	7122848.818	1471.279	Carnivore	Isolated Teeth
KW_10210	575061.859	7122856.464	1470.607	Bovid	Limb
KW_10212	575061.878	7122856.886	1470.67	Carnivore	Upper Limb
KW_10213	575056.945	7122848.359	1471.145	Bovid	Spinal Column
KW_10214	575055.905	7122848.776	1471.579	Bovid	Thoracic Cage
KW_10215	575056.295	7122848.512	1471.561	Bovid	Upper Limb
KW_10379	575063.75	7122852.618	1473.792	Primate	Lower Limb
KW_10380	575062.116	7122856.826	1470.8	Carnivore	Upper Limb
KW_10381	575061.812	7122856.938	1470.555	Carnivore	Upper Limb
KW_10382	575061.56	7122856.722	1470.506	Carnivore	Pelvic Grid
KW_10383	575061.611	7122856.884	1470.508	Carnivore	Cranium
KW_10384	575064.242	7122852.484	1473.438	Carnivore	Isolated Teeth
KW_10386	575056.197	7122849.912	1470.845	Bovid	Lower Limb
KW_10387	575056.051	7122850.134	1470.897	Carnivore	Upper Limb
KW_10390	575055.992	7122849.745	1471.123	Bovid	Lower Limb
KW_10391	575055.923	7122850.101	1470.951	Bovid	Upper Limb
KW_10393	575055.905	7122849.701	1471.23	Bovid	Cranium
KW_10394	575061.791	7122855.974	1470.307	Bovid	Lower Limb
KW_10396	575060.853	7122856.732	1470.846	Bovid	Upper Limb
KW_10398	575061.686	7122856.961	1470.43	Carnivore	Upper Limb
KW_10399	575061.64	7122856.932	1470.445	Bovid	Horn
KW_10400	575061.514	7122856.872	1470.449	Carnivore	Thoracic Cage
KW_10402	575061.364	7122856.697	1470.464	Carnivore	Upper Limb
KW_10403	575061.071	7122856.623	1470.626	Bovid	Horn
KW_10405	575055.797	7122850.187	1470.962	Bovid	Cranium
KW_10407	575055.681	7122849.845	1471.091	Bovid	Lower Limb
KW_10408	575055.848	7122849.618	1471.221	Bovid	Lower Limb
KW_10409	575061.095	7122857.061	1470.766	Bovid	Limb
KW_10410	575061.177	7122857.051	1470.777	Bovid	Cranium
KW_10411	575055.654	7122850.081	1470.985	Bovid	Pectoral Girdle
KW_10412	575055.777	7122850.238	1470.964	Bovid	Lower Limb
KW_10413	575055.642	7122850.106	1471.128	Bovid	Lower Limb
KW_10414	575055.747	7122850.212	1471.134	Bovid	Lower Limb
KW_10417	575061.277	7122857.077	1470.601	Bovid	Lower Limb
KW_10418	575055.902	7122848.7	1470.961	Bovid	Upper Limb
KW_10419	575056.085	7122848.903	1470.816	Carnivore	Isolated Teeth
KW_10420	575056.107	7122849.059	1470.785	Bovid	Upper Limb

KW_10421	575056.226	7122849.115	1470.739	Bovid	Lower Limb
KW_10422	575055.651	7122850.229	1471.112	Bovid	Lower Limb
KW_10423	575061.22	7122856.652	1470.422	Carnivore	Lower Limb
KW_10424	575060.896	7122857.331	1470.695	Carnivore	Upper Limb
KW_10425	575061.705	7122857.47	1470.543	Bovid	Horn
KW_10426	575061.99	7122857.14	1470.419	Bovid	Lower Limb
KW_10428	575058.25	7122852.873	1471.323	Carnivore	Isolated Teeth
KW_10431	575061.915	7122857.071	1470.281	Carnivore	Lower Limb
KW_10432	575061.918	7122857.192	1470.341	Bovid	Lower Limb
KW_10433	575061.568	7122857.025	1470.302	Bovid	Upper Limb
KW_10434	575061.994	7122856.944	1470.249	Bovid	Upper Limb
KW_10436	575061.786	7122857.418	1470.301	Bovid	Upper Limb
KW_10437	575061.586	7122857.44	1470.302	Bovid	Upper Limb
KW_10438	575059.269	7122856.492	1471.664	Carnivore	Isolated Teeth
KW_10439	575061.384	7122856.994	1470.288	Carnivore	Spinal Column
KW_10440	575060.725	7122857.058	1470.735	Bovid	Cranium
KW_10441	575058.977	7122856.77	1471.527	Bovid	Horn
KW_10442	575061.105	7122856.747	1470.354	Carnivore	Spinal Column
KW_10443	575061.15	7122856.61	1470.349	Carnivore	Pelvic Grid
KW_10444	575062.638	7122853.021	1472.777	Bovid	Limb
KW_10445	575055.864	7122849.074	1470.738	Bovid	Lower Limb
KW_10446	575061.112	7122857.302	1470.108	Bovid	Lower Limb
KW_10447	575061.279	7122857.309	1470.123	Bovid	Lower Limb
KW_10449	575059.663	7122856.848	1471.628	Bovid	Cranium
KW_10507	575059.847	7122853.796	1471.58	Carnivore	Spinal Column
KW_10508	575062.314	7122853.47	1472.652	Carnivore	Cranium
KW_10509	575062.363	7122853.175	1472.719	Bovid	Isolated Teeth
KW_10512	575061.72	7122853.092	1472.368	Bovid	Upper Limb
KW_10513	575061.904	7122853.241	1472.388	Bovid	Lower Limb
KW_10514	575061.578	7122853.157	1472.249	Primate	Isolated Teeth
KW_10515	575060.51	7122850.035	1471.072	Bovid	Isolated Teeth
KW_10516	575062.524	7122855.164	1471.522	Bovid	Limb
KW_10520	575056.727	7122850.044	1470.21	Bovid	Limb
KW_10521	575061.124	7122849.969	1471.248	Bovid	Isolated Teeth
KW_10523	575056.947	7122849.91	1470.472	Bovid	Limb
KW_10524	575060.992	7122850.033	1471.239	Bovid	Isolated Teeth

KW_10525	575060.455	7122852.749	1471.639	Bovid	Thoracic Cage
KW_10526	575062.525	7122852.142	1472.597	Primate	Upper Limb
KW_10527	575062.54	7122852.104	1472.589	Primate	Limb
KW_10528	575063.52	7122854.234	1472.247	Bovid	Spinal Column
KW_10529	575062.607	7122852.104	1472.633	Primate	Upper Limb
KW_10532	575060.82	7122853.038	1471.429	Bovid	Cranium
KW_10534	575060.848	7122852.739	1471.465	Bovid	Lower Limb
KW_10535	575061.278	7122849.814	1471.426	Bovid	Isolated Teeth
KW_10536	575060.798	7122852.807	1471.359	Bovid	Cranium
KW_10537	575061.77	7122854.022	1471.979	Bovid	Spinal Column
KW_10540	575060.468	7122853.115	1471.505	Bovid	Lower Limb
KW_10541	575060.71	7122853.274	1471.501	Carnivore	Upper Limb
KW_10543_A	575060.547	7122853.205	1471.445	Carnivore	Limb
KW_10543_B	575060.547	7122853.205	1471.445	Carnivore	Spinal Column
KW_10544	575062.176	7122852.953	1472.333	Bovid	Lower Limb
KW_10546	575060.735	7122853.505	1471.528	Carnivore	Upper Limb
KW_10548	575060.618	7122853.69	1471.443	Bovid	Upper Limb
KW_10549	575060.758	7122853.624	1471.476	Bovid	Limb
KW_10550	575060.866	7122853.763	1471.533	Carnivore	Cranium
KW_10552	575061.047	7122853.806	1471.493	Bovid	Spinal Column
KW_10553	575062.633	7122851.091	1472.649	Bovid	Lower Limb
KW_10554	575061.486	7122857.022	1469.921	Bovid	Cranium
KW_10555	575060.758	7122853.747	1471.489	Bovid	Lower Limb
KW_10556	575060.685	7122853.055	1471.357	Bovid	Cranium
KW_10558	575060.677	7122853.163	1471.353	Bovid	Isolated Teeth
KW_10563	575059.344	7122854.938	1471.241	Bovid	Lower Limb
KW_10564	575059.36	7122855.162	1471.293	Bovid	Pelvic Grid
KW_10566	575062.798	7122851.46	1472.772	Bovid	Upper Limb
KW_10567	575062.656	7122852.316	1472.571	Primate	Lower Limb
KW_10568	575064.535	7122860.87	1473.386	Bovid	Lower Limb
KW_10569	575062.713	7122850.968	1472.882	Bovid	Lower Limb
KW_10570	575060.298	7122853.273	1471.202	Bovid	Pectoral Girdle
KW_10571	575058.679	7122855.167	1471.358	Bovid	Isolated Teeth
KW_10572	575061.019	7122853.806	1471.438	Bovid	Lower Limb
KW_10573	575061.077	7122853.943	1471.447	Bovid	Upper Limb
KW_10575	575060.68	7122853.822	1471.308	Bovid	Limb

KW_10576	575060.87	7122853.034	1471.247	Bovid	Limb
KW_10579	575058.764	7122854.453	1471.507	Bovid	Upper Limb
KW_10580	575062.758	7122851.022	1472.911	Bovid	Cranium
KW_10581	575062.749	7122850.999	1472.995	Bovid	Lower Limb
KW_10582	575060.95	7122852.991	1471.335	Bovid	Cranium
KW_10583	575061.266	7122853.852	1471.533	Bovid	Upper Limb
KW_10585	575060.906	7122854.766	1471.521	Bovid	Spinal Column
KW_10586	575058.065	7122855.71	1471.577	Bovid	Pelvic Grid
KW_10588	575061.36	7122854.055	1471.531	Bovid	Limb
KW_10590	575061.092	7122853.674	1471.496	Bovid	Lower Limb
KW_10591	575061.124	7122854.182	1471.446	Bovid	Cranium
KW_10622	575058.553	7122854.234	1471.795	Bovid	Thoracic Cage
KW_10623	575056.057	7122850.724	1470.756	Bovid	Limb
KW_10624	575055.736	7122850.424	1471.089	Carnivore	Cranium
KW_10625	575056.001	7122850.114	1470.496	Bovid	Limb
KW_10626	575060.967	7122854.212	1471.453	Bovid	Spinal Column
KW_10627	575060.809	7122853.855	1471.444	Bovid	Upper Limb
KW_10628	575060.853	7122853.808	1471.468	Bovid	Upper Limb
KW_10629	575062.704	7122850.833	1472.899	Bovid	Isolated Teeth
KW_10631	575059.448	7122855.939	1471.817	Bovid	Horn
KW_10632	575062.855	7122851.159	1472.911	Bovid	Limb
KW_10633	575062.864	7122851.205	1472.964	Bovid	Lower Limb
KW_10634	575055.978	7122850.284	1470.41	Primate	Isolated Teeth
KW_10635	575062.778	7122850.857	1473.087	Bovid	Upper Limb
KW_10636	575061.487	7122854.167	1471.541	Carnivore	Spinal Column
KW_10637	575060.839	7122853.718	1471.377	Bovid	Isolated Teeth
KW_10638	575061.373	7122854.012	1471.491	Carnivore	Cranium
KW_10642	575060.888	7122853.706	1471.382	Bovid	Thoracic Cage
KW_10643	575061.008	7122854.396	1471.38	Bovid	Limb
KW_10644	575061.175	7122854.272	1471.304	Bovid	Limb
KW_10645	575061.223	7122854.22	1471.311	Bovid	Cranium
KW_10646	575061.323	7122854.297	1471.356	Bovid	Limb
KW_10647	575061.275	7122854.119	1471.306	Bovid	Limb
KW_10648	575060.766	7122854.153	1471.216	Carnivore	Lower Limb
KW_10651	575061.137	7122854.114	1471.21	Bovid	Horn
KW_10652	575061.31	7122854.182	1471.249	Bovid	Lower Limb
KW_10656	575061.397	7122854.313	1471.294	Bovid	Limb
KW_10657	575061.259	7122853.999	1471.223	Bovid	Limb

KW_10658	575060.289	7122854.542	1471.36	Bovid	Limb
KW_10659	575060.213	7122854.522	1471.343	Bovid	Lower Limb
KW_10660	575060.402	7122854.672	1471.374	Bovid	Limb
KW_10662	575061.266	7122854.083	1471.257	Bovid	Cranium
KW_10663	575060.48	7122855.682	1471.327	Bovid	Limb
KW_10664	575063.075	7122851.419	1473.202	Bovid	Cranium
KW_10665	575060.732	7122853.538	1471.183	Bovid	Isolated Teeth
KW_10667	575060.095	7122854.505	1471.249	Bovid	Spinal Column
KW_10668	575055.855	7122849.686	1470.497	Bovid	Horn
KW_10669	575055.956	7122849.65	1470.303	Bovid	Lower Limb
KW_10670	575060.602	7122854.974	1471.208	Bovid	Horn
KW_10671	575060.622	7122855.079	1471.266	Bovid	Spinal Column
KW_10678	575060.118	7122855.721	1471.01	Bovid	Limb
KW_10679	575060.011	7122855.651	1471.051	Carnivore	Pelvic Grid
KW_10680	575059.825	7122855.72	1471.059	Bovid	Horn
KW_6420	575062.339	7122852.576	1473.143	Hominin	Cranium
KW_7613	575062.124	7122853.799	1473.244	Carnivore	Cranium
KW_7614	575062.067	7122853.904	1473.171	Bovid	Lower Limb
KW_7615	575062.065	7122854.138	1473.076	Bovid	Limb
KW_7616	575061.932	7122854.356	1473.071	Bovid	Limb
KW_7617	575061.965	7122854.428	1473.074	Carnivore	Spinal Column
KW_7618	575061.695	7122854.484	1472.941	Bovid	Lower Limb
KW_7619	575061.786	7122854.828	1473.023	Bovid	Limb
KW_7620	575059.205	7122850.496	1472.096	Bovid	Cranium
KW_7621	575058.889	7122850.428	1472.274	Bovid	Cranium
KW_7623	575058.742	7122851.444	1472.355	Bovid	Lower Limb
KW_7625	575062.157	7122853.831	1473.184	Bovid	Lower Limb
KW_7626	575062.242	7122854.08	1473.15	Bovid	Horn
KW_7628	575061.99	7122854.664	1473.176	Bovid	Upper Limb
KW_7629	575059.147	7122849.99	1470.691	Carnivore	Cranium
KW_7630	575062.002	7122850.258	1470.843	Bovid	Upper Limb
KW_7631	575058.571	7122851.599	1472.34	Bovid	Lower Limb
KW_7632	575058.743	7122851.143	1470.754	Bovid	Limb
KW_7633	575060.212	7122855.55	1472.769	Bovid	Horn
KW_7634	575060.894	7122855.294	1472.69	Bovid	Lower Limb
KW_7635	575061.034	7122855.167	1472.645	Bovid	Lower Limb
KW_7636	575062.799	7122855.56	1472.924	Bovid	Upper Limb
KW_7637	575062.038	7122853.706	1472.995	Bovid	Lower Limb
KW_7638	575058.468	7122849.933	1472.049	Bovid	Lower Limb
KW_7639	575058.265	7122849.878	1472.017	Bovid	Limb
KW_764	575060.164	7122855.766	1472.698	Bovid	Horn

KW_7640	575057.754	7122849.966	1472.171	Bovid	Lower Limb
KW_7641	575057.713	7122849.93	1472.172	Bovid	Pectoral Girdle
KW_7642	575057.749	7122849.849	1472.147	Bovid	Lower Limb
KW_7643	575058.544	7122851.644	1472.313	Bovid	Lower Limb
KW_7646	575058.233	7122850.701	1472.017	Bovid	Pectoral Girdle
KW_7655	575063.685	7122854.745	1472.859	Bovid	Cranium
KW_7656	575063.732	7122854.839	1472.854	Bovid	Limb
KW_7657	575058.139	7122850.015	1471.953	Bovid	Cranium
KW_7658	575058.264	7122850.13	1471.974	Bovid	Limb
KW_7659	575061.656	7122856.197	1472.868	Bovid	Isolated Teeth
KW_7660	575063.737	7122856.383	1472.95	Bovid	Pelvic Grid
KW_7661	575063.972	7122856.274	1473.036	Bovid	Limb
KW_7662	575061.092	7122854.908	1472.581	Bovid	Cranium
KW_7664	575059.145	7122850.578	1472.011	Bovid	Upper Limb
KW_7666	575059.566	7122850.781	1471.638	Primate	Isolated Teeth
KW_7667	575060.593	7122855.276	1472.326	Bovid	Limb
KW_7669	575061.201	7122854.95	1472.654	Bovid	Upper Limb
KW_7670	575063.746	7122856.43	1472.902	Bovid	Tusk
KW_7671	575063.619	7122856.321	1472.902	Bovid	Horn
KW_7672	575059.189	7122850.895	1471.434	Bovid	Horn
KW_7932	575060.207	7122856.328	1472.384	Carnivore	Cranium
KW_7934	575059.723	7122850.885	1471.447	Primate	Limb
KW_7935	575058.673	7122850.281	1471.446	Carnivore	Upper Limb
KW_7936	575058.289	7122850.697	1471.966	Bovid	Limb
KW_8100	575059.512	7122851.529	1472.088	Hominin	Isolated Teeth
KW_8110	575059.516	7122851.528	1472.086	Hominin	Upper Limb
KW_8117	575059.448	7122851.521	1471.919	Primate	Isolated Teeth
KW_8118	575059.769	7122851.013	1471.543	Primate	Cranium
KW_8119	575059.874	7122850.979	1471.519	Primate	Limb
KW_8120A	575058.87	7122851.215	1471.968	Hominin	Lower Limb
KW_8120B	575058.867	7122851.321	1471.962	Hominin	Lower Limb
KW_8120C	575058.575	7122851.595	1472.083	Hominin	Pelvic Grid
KW_8120D	575058.646	7122851.524	1471.987	Hominin	Pelvic Grid
KW_8121	575059.764	7122850.952	1471.395	Primate	Limb
KW_8122	575058.934	7122851.159	1471.648	Bovid	Horn
KW_8123	575060.677	7122853.718	1472.282	Bovid	Horn
KW_8124	575060.432	7122853.909	1472.205	Bovid	Limb
KW_8125	575060.354	7122853.512	1472.233	Bovid	Isolated Teeth
KW_8126	575060.188	7122853.635	1472.221	Bovid	Lower Limb

KW_8127	575061.419	7122853.542	1472.884	Bovid	Spinal Column
KW_8128	575059.534	7122856.622	1472.527	Bovid	Cranium
KW_8129	575057.91	7122850.873	1471.867	Bovid	Pectoral Girdle
KW_8130	575059.347	7122851.041	1471.455	Bovid	Limb
KW_8163	575059.283	7122851.658	1471.769	Primate	Lower Limb
KW_8175	575059.555	7122853.76	1472.3	Bovid	Upper Limb
KW_8176	575059.858	7122853.362	1472.384	Bovid	Lower Limb
KW_8177	575059.93	7122853.426	1472.293	Bovid	Spinal Column
KW_8178	575059.839	7122853.511	1472.251	Bovid	Spinal Column
KW_8197	575059.405	7122853.261	1472.546	Bovid	Upper Limb
KW_8198	575059.517	7122853.145	1472.447	Bovid	Thoracic Cage
KW_8199	575059.954	7122853.193	1472.245	Bovid	Cranium
KW_8200	575060.517	7122853.357	1472.268	Bovid	Limb
KW_8221	575060.251	7122853.039	1472.203	Bovid	Lower Limb
KW_8222	575060.001	7122853.295	1472.183	Bovid	Lower Limb
KW_8223	575060.124	7122853.29	1472.171	Bovid	Spinal Column
KW_8224	575060.047	7122853.209	1472.213	Bovid	Lower Limb
KW_8225	575059.063	7122854.522	1472.393	Primate	Isolated Teeth
KW_8226	575058.879	7122854.488	1472.364	Bovid	Limb
KW_8227	575059.198	7122854.497	1472.269	Other	Tusk
KW_8228	575059.224	7122854.859	1472.46	Other	Tusk
KW_8229	575058.835	7122854.556	1472.466	Bovid	Limb
KW_8230	575058.892	7122854.531	1472.426	Bovid	Upper Limb
KW_8248	575058.638	7122855.479	1472.269	Carnivore	Cranium
KW_8285	575056.933	7122849.429	1472.321	Bovid	Upper Limb
KW_8286	575058.361	7122851.61	1471.494	Primate	Upper Limb
KW_8287	575058.496	7122851.696	1471.591	Bovid	Lower Limb
KW_8288	575059.728	7122849.665	1471.137	Primate	Upper Limb
KW_8289	575058.344	7122851.354	1471.378	Primate	Lower Limb
KW_8290	575058.676	7122851.268	1471.354	Primate	Lower Limb
KW_8292	575057.239	7122849.698	1472.828	Carnivore	Spinal Column
KW_8293	575056.001	7122850.648	1473.245	Bovid	Spinal Column
KW_8295	575059.204	7122850.606	1471.333	Primate	Spinal Column
KW_8296	575059.066	7122850.266	1471.242	Carnivore	Coprolite
KW_8297	575059.301	7122850.07	1471.306	Primate	Upper Limb
KW_8299	575059.523	7122849.896	1471.337	Carnivore	Upper Limb

KW_8300	575058.879	7122850.089	1471.283	Hominin	Upper Limb
KW_8301	575059.07	7122850.579	1471.342	Hominin	Cranium
KW_8302	575058.186	7122850.438	1471.311	Hominin	Upper Limb
KW_8417	575061.77	7122860.036	1472.682	Other	Pectoral Girdle
KW_8418	575067.006	7122858.138	1473.613	Carnivore	Lower Limb
KW_8419	575062.582	7122860.301	1472.514	Bovid	Horn
KW_8420	575062.178	7122860.19	1472.442	Bovid	Horn
KW_8421	575060.23	7122850.268	1471.237	Primate	Isolated Teeth
KW_8422	575060.099	7122850.169	1470.986	Primate	Spinal Column
KW_8423	575060.091	7122849.985	1471.035	Primate	Lower Limb
KW_8424	575060.797	7122849.683	1471.108	Bovid	Isolated Teeth
KW_8425	575060.23	7122859.458	1471.989	Bovid	Cranium
KW_8426	575060.03	7122861.033	1472.025	Bovid	Isolated Teeth
KW_8561	575067.781	7122858.555	1472.676	Bovid	Limb
KW_8562	575066.453	7122859.824	1474.26	Bovid	Limb
KW_8564	575065.652	7122859.971	1473.627	Bovid	Limb
KW_8565	575065.356	7122859.82	1473.575	Bovid	Thoracic Cage
KW_8567	575065.47	7122859.896	1473.487	Bovid	Limb
KW_8568	575065.364	7122859.976	1473.437	Bovid	Lower Limb
KW_8569	575065.422	7122859.868	1473.506	Bovid	Lower Limb
KW_8570	575065.21	7122859.801	1473.455	Bovid	Limb
KW_8571	575067.802	7122858.616	1473.889	Bovid	Cranium
KW_8572	575067.684	7122858.563	1473.866	Bovid	Cranium
KW_8573	575067.578	7122857.479	1473.974	Bovid	Upper Limb
KW_8594	575058.235	7122851.78	1472.005	Primate	Thoracic Cage
KW_8595	575058.111	7122851.72	1471.972	Bovid	Isolated Teeth
KW_8596	575058.014	7122852.033	1471.934	Bovid	Lower Limb
KW_8602	575058.293	7122852.143	1471.936	Primate	Cranium
KW_8603	575058.41	7122851.779	1471.941	Bovid	Cranium
KW_8612	575065.82	7122860.383	1472.87	Bovid	Thoracic Cage
KW_8614	575058.715	7122852.329	1472.057	Primate	Upper Limb
KW_8616_L1	575058.308	7122849.82	1470.964	Carnivore	Lower Limb
KW_8616_L2	575058.151	7122849.42	1470.984	Carnivore	Lower Limb
KW_8616_L3	575058.103	7122849.691	1470.957	Carnivore	Lower Limb
KW_8616_	575057.896	7122849.863	1470.902	Carnivore	Lower Limb

L4					
KW_8616_ L5	575057.596	7122850.005	1470.656	Carnivore	Upper Limb
KW_8616_ L6	575057.615	7122850.406	1470.692	Carnivore	Limb
KW_8616_ L7	575056.952	7122849.975	1470.499	Carnivore	Lower Limb
KW_8617	575058.564	7122849.862	1471.063	Bovid	Limb
KW_8618	575058.557	7122849.98	1471.006	Bovid	Upper Limb
KW_8619	575058.042	7122849.793	1470.93	Bovid	Lower Limb
KW_8620	575057.497	7122849.693	1472.362	Bovid	Lower Limb
KW_8621	575064.418	7122859.244	1472.966	Bovid	Horn
KW_8622	575064.86	7122859.478	1473.04	Bovid	Spinal Column
KW_8623	575065.199	7122859.174	1472.925	Bovid	Lower Limb
KW_8624	575058.578	7122850.087	1470.945	Bovid	Lower Limb
KW_8625	575061.433	7122855.259	1472.49	Bovid	Limb
KW_8626	575056.808	7122849.274	1472.106	Bovid	Upper Limb
KW_8627	575056.947	7122850.305	1471.975	Bovid	Upper Limb
KW_8630_ A	575061.791	7122853.811	1472.761	Hominin	Isolated Teeth
KW_8630_ B	575061.815	7122853.983	1472.82	Hominin	Isolated Teeth
KW_8630_ C	575061.871	7122854.071	1472.798	Hominin	Isolated Teeth
KW_8631	575058.306	7122852.182	1471.408	Bovid	Upper Limb
KW_8632	575060.261	7122852.648	1471.92	Bovid	Isolated Teeth
KW_8633	575060.183	7122852.744	1472.112	Bovid	Limb
KW_8634	575058.504	7122852.529	1471.908	Bovid	Upper Limb
KW_8635	575058.41	7122852.463	1471.839	Bovid	Limb
KW_8636	575058.379	7122852.329	1471.749	Bovid	Cranium
KW_8637	575057.139	7122849.303	1471.479	Bovid	Limb
KW_8638A	575058.634	7122850.177	1470.929	Primate	Lower Limb
KW_8638B	575058.605	7122850.141	1470.93	Primate	Lower Limb
KW_8639	575058.523	7122850.022	1470.948	Primate	Upper Limb
KW_8996	575063.697	7122859.524	1472.895	Bovid	Limb
KW_8997	575063.828	7122859.386	1472.902	Bovid	Limb
KW_8998	575063.817	7122859.294	1472.897	Bovid	Limb
KW_9000	575061.852	7122853.636	1472.616	Hominin	Cranium
KW_9001	575063.929	7122860.058	1472.921	Carnivore	Cranium
KW_9002	575063.959	7122860.434	1473.232	Bovid	Pectoral Girdle
KW_9003	575063.81	7122860.411	1473.241	Bovid	Lower Limb
KW_9004	575063.781	7122860.565	1473.288	Bovid	Horn
KW_9005	575063.865	7122860.582	1473.293	Carnivore	Upper Limb

KW_9006	575064.087	7122860.613	1473.573	Carnivore	Upper Limb
KW_9007	575058.241	7122851.094	1471.04	Bovid	Lower Limb
KW_9008	575061.543	7122853.565	1472.551	Carnivore	Isolated Teeth
KW_9009	575061.584	7122853.968	1472.412	Carnivore	Isolated Teeth
KW_9010	575061.507	7122853.416	1472.51	Primate	Upper Limb
KW_9013	575063.555	7122859.825	1472.486	Bovid	Horn
KW_9014	575063.429	7122859.867	1472.394	Bovid	Cranium
KW_9015	575061.475	7122853.253	1472.513	Bovid	Upper Limb
KW_9016	575061.633	7122853.246	1472.59	Bovid	Cranium
KW_9017	575061.443	7122853.267	1472.456	Bovid	Spinal Column
KW_9018	575061.277	7122852.979	1472.328	Bovid	Limb
KW_9019	575061.181	7122852.969	1472.33	Bovid	Isolated Teeth
KW_9020	575061.175	7122853.179	1472.319	Bovid	Lower Limb
KW_9021	575061.238	7122853.368	1472.263	Bovid	Isolated Teeth
KW_9023	575061.406	7122853.426	1472.31	Bovid	Spinal Column
KW_9024	575061.314	7122853.35	1472.262	Bovid	Spinal Column
KW_9025	575061.234	7122853.369	1472.257	Bovid	Upper Limb
KW_9026	575061.151	7122853.24	1472.214	Bovid	Lower Limb
KW_9028	575064.09	7122859.895	1472.502	Carnivore	Isolated Teeth
KW_9029	575064.164	7122860.523	1473.213	Bovid	Isolated Teeth
KW_9030	575061.419	7122854.627	1472.444	Bovid	Isolated Teeth
KW_9031	575055.216	7122850.58	1472.41	Bovid	Cranium
KW_9032	575055.245	7122850.247	1472.407	Bovid	Limb
KW_9033	575061.596	7122854.458	1472.629	Bovid	Lower Limb
KW_9035	575061.631	7122854.312	1472.55	Bovid	Isolated Teeth
KW_9323	575056.913	7122848.941	1472.211	Bovid	Limb
KW_9324	575062.464	7122856.852	1472.46	Bovid	Lower Limb
KW_9325	575062.847	7122856.97	1472.506	Bovid	Thoracic Cage
KW_9326	575064.36	7122857.627	1472.437	Bovid	Horn
KW_9328	575055.904	7122849.6	1472.033	Carnivore	Upper Limb
KW_9329	575055.972	7122849.324	1472.001	Bovid	Spinal Column
KW_9330	575056.544	7122849.557	1471.931	Bovid	Pelvic Grid
KW_9331	575055.692	7122850.797	1472.226	Bovid	Limb
KW_9333	575063.048	7122857.075	1472.592	Bovid	Upper Limb

KW_9334	575054.837	7122850.084	1472	Bovid	Lower Limb
KW_9335	575056.029	7122849.757	1472.015	Bovid	Upper Limb
KW_9336	575055.216	7122849.599	1472.098	Carnivore	Upper Limb
KW_9337	575055.213	7122849.272	1472.083	Bovid	Upper Limb
KW_9338	575054.806	7122849.578	1472.093	Bovid	Lower Limb
KW_9418	575053.418	7122856.417	1472.902	Bovid	Lower Limb
KW_9419	575055.308	7122851.795	1473.259	Bovid	Pectoral Girdle
KW_9420	575052.39	7122847.722	1473.202	Bovid	Lower Limb
KW_9421	575052.344	7122848.035	1473.119	Bovid	Horn
KW_9421B	575052.3	7122847.806	1473.183	Bovid	Horn
KW_9422	575052.274	7122847.884	1473.192	Bovid	Lower Limb
KW_9423	575051.899	7122846.625	1473.553	Bovid	Limb
KW_9424	575057.976	7122848.825	1471.414	Primate	Spinal Column
KW_9425_A	575061.992	7122853.603	1472.736	Carnivore	Isolated Teeth
KW_9425_B	575061.992	7122853.603	1472.736	Carnivore	Isolated Teeth
KW_9426	575062.029	7122853.437	1472.877	Bovid	Limb
KW_9427	575061.983	7122853.331	1472.903	Bovid	Upper Limb
KW_9428	575062.244	7122853.601	1473.109	Carnivore	Limb
KW_9429	575062.244	7122853.601	1473.109	Bovid	Isolated Teeth
KW_9431	575062.208	7122853.595	1473.034	Bovid	Limb
KW_9432	575062.057	7122853.34	1472.874	Bovid	Lower Limb
KW_9433	575062.077	7122853.53	1472.8	Bovid	Lower Limb
KW_9434	575062.205	7122853.64	1472.884	Primate	Upper Limb
KW_9435	575062.318	7122853.637	1473.053	Bovid	Limb
KW_9437	575062.182	7122853.481	1472.881	Bovid	Isolated Teeth
KW_9439	575062.15	7122853.217	1472.949	Bovid	Lower Limb
KW_9440	575062.234	7122853.279	1473.013	Bovid	Limb
KW_9441	575062.273	7122853.114	1472.935	Bovid	Upper Limb
KW_9442	575061.878	7122855.932	1472.576	Bovid	Isolated Teeth
KW_9443	575062.012	7122856.211	1472.426	Carnivore	Isolated Teeth
KW_9444	575062.204	7122853.574	1472.9	Bovid	Lower Limb
KW_9445	575062.849	7122853.275	1473.744	Carnivore	Pelvic Grid
KW_9446	575064.71	7122857.068	1472.612	Bovid	Limb
KW_9447	575064.581	7122856.848	1472.601	Bovid	Limb
KW_9448	575064.418	7122856.816	1472.74	Bovid	Cranium
KW_9449	575062.444	7122853.593	1473.192	Bovid	Lower Limb
KW_9450	575062.087	7122855.518	1472.58	Bovid	Lower Limb
KW_9451	575062.275	7122855.626	1472.56	Carnivore	Upper Limb

KW_9453	575064.326	7122856.443	1472.541	Carnivore	Isolated Teeth
KW_9454	575062.414	7122855.85	1472.669	Bovid	Isolated Teeth
KW_9455	575061.94	7122855.205	1472.527	Bovid	Isolated Teeth
KW_9456	575062.847	7122853.235	1473.276	Bovid	Isolated Teeth
KW_9457	575062.531	7122853.558	1473.027	Bovid	Lower Limb
KW_9460	575060.072	7122852.749	1472.067	Bovid	Upper Limb
KW_9461	575062.96	7122855.899	1472.865	Bovid	Horn
KW_9462	575062.892	7122855.93	1472.769	Bovid	Pectoral Girdle
KW_9463	575062.899	7122855.923	1472.777	Bovid	Cranium
KW_9463_B	575062.911	7122856.018	1472.752	Bovid	Cranium
KW_9463_C	575062.936	7122856.061	1472.75	Bovid	Cranium
KW_9463_D	575062.925	7122856.026	1472.751	Bovid	Cranium
KW_9463_E	575062.902	7122856.124	1472.702	Bovid	Cranium
KW_9463_F	575062.813	7122856.13	1472.646	Bovid	Cranium
KW_9463_G	575062.913	7122856.038	1472.738	Bovid	Cranium
KW_9463_H	575062.886	7122855.773	1472.716	Bovid	Cranium
KW_9463_I	575062.897	7122856.031	1472.719	Bovid	Cranium
KW_9465	575063.998	7122856.696	1472.562	Bovid	Limb
KW_9466	575062.951	7122855.978	1472.771	Bovid	Limb
KW_9467	575063.931	7122856.413	1472.468	Bovid	Isolated Teeth
KW_9468	575063.162	7122855.817	1472.733	Bovid	Thoracic Cage
KW_9469	575064.013	7122856.039	1472.615	Bovid	Lower Limb
KW_9470	575062.095	7122854.912	1472.583	Bovid	Cranium
KW_9472	575064.179	7122855.895	1472.83	Bovid	Limb
KW_9473	575063.56	7122856.145	1472.69	Bovid	Spinal Column
KW_9475	575056.929	7122849.933	1471.481	Bovid	Limb
KW_9564	575056.76	7122849.883	1471.47	Bovid	Limb
KW_9565	575057.173	7122850.68	1471.273	Bovid	Upper Limb
KW_9566	575063.319	7122855.19	1472.543	Bovid	Lower Limb
KW_9567	575063.104	7122855.184	1472.555	Primate	Lower Limb
KW_9568	575063.614	7122854.933	1472.525	Bovid	Limb
KW_9569	575065.014	7122857.145	1472.613	Bovid	Lower Limb

KW_9570	575063.415	7122855.05	1472.532	Carnivore	Isolated Teeth
KW_9571	575063.412	7122854.856	1472.548	Carnivore	Cranium
KW_9571_B	575063.31	7122854.683	1472.438	Carnivore	Isolated Teeth
KW_9573	575062.525	7122854.601	1472.473	Bovid	Isolated Teeth
KW_9574	575062.364	7122854.527	1472.475	Bovid	Spinal Column
KW_9575	575062.116	7122854.392	1472.498	Bovid	Isolated Teeth
KW_9576	575061.828	7122854.234	1472.341	Bovid	Isolated Teeth
KW_9577	575062.167	7122854.514	1472.281	Bovid	Limb
KW_9578	575062.182	7122854.811	1472.265	Bovid	Limb
KW_9579	575062.533	7122854.623	1472.298	Bovid	Spinal Column
KW_9580	575062.327	7122854.911	1472.289	Bovid	Horn
KW_9582	575057.249	7122850.024	1470.662	Bovid	Limb
KW_9583	575062.458	7122855.003	1472.323	Carnivore	Upper Limb
KW_9584	575062.78	7122855.608	1472.429	Bovid	Limb
KW_9585	575062.78	7122855.608	1472.429	Bovid	Limb
KW_9586	575060.239	7122852.988	1472.049	Bovid	Limb
KW_9587	575061.029	7122853.129	1472.136	Bovid	Horn
KW_9588	575061.088	7122853.068	1472.124	Bovid	Upper Limb
KW_9590	575063.135	7122855.333	1472.395	Bovid	Upper Limb
KW_9591	575063.309	7122855.644	1472.528	Bovid	Thoracic Cage
KW_9592	575061.589	7122855.296	1472.262	Other	Tusk
KW_9593	575064.419	7122860.84	1474.131	Bovid	Isolated Teeth
KW_9595	575061.188	7122853.168	1472.143	Bovid	Upper Limb
KW_9596	575061.153	7122853.134	1472.084	Bovid	Limb
KW_9597	575060.116	7122854.108	1472.064	Bovid	Spinal Column
KW_9598	575060.13	7122852.987	1472.02	Carnivore	Isolated Teeth
KW_9600_A	575062.914	7122855.446	1472.393	Primate	Cranium
KW_9600_B	575063.266	7122855.284	1472.494	Primate	Cranium
KW_9601	575064.384	7122860.875	1474.029	Bovid	Isolated Teeth
KW_9602	575064.721	7122860.776	1474.09	Bovid	Isolated Teeth
KW_9603	575063.491	7122855.187	1472.196	Carnivore	Lower Limb
KW_9604	575061.688	7122855.641	1472.007	Bovid	Isolated

					Teeth
KW_9605	575060.256	7122854.301	1471.963	Bovid	Spinal Column
KW_9606	575060.2	7122854.185	1472.016	Bovid	Thoracic Cage
KW_9607	575058.525	7122852.572	1471.774	Primate	Upper Limb
KW_9608	575063.939	7122861.282	1473.96	Bovid	Limb
KW_9609	575058.688	7122853.931	1472.167	Bovid	Isolated Teeth
KW_9610	575061.066	7122854.273	1472.212	Hominin	Isolated Teeth
KW_9611	575060.45	7122853.272	1471.996	Bovid	Horn
KW_9612	575061.113	7122853.437	1471.923	Bovid	Limb
KW_9613	575060.58	7122853.276	1472.013	Primate	Cranium
KW_9614	575060.55	7122853.304	1472.008	Bovid	Pelvic Grid
KW_9615	575064.271	7122861.294	1473.941	Primate	Lower Limb
KW_9616	575060.449	7122853.816	1472.138	Bovid	Upper Limb
KW_9617	575061.033	7122853.484	1471.936	Bovid	Lower Limb
KW_9618	575057.866	7122853.565	1472.038	Bovid	Pelvic Grid
KW_9619	575060.359	7122853.201	1471.931	Primate	Cranium
KW_9621	575060.276	7122853.582	1472.051	Bovid	Isolated Teeth
KW_9622	575060.443	7122853.046	1471.9	Carnivore	Limb
KW_9624	575060.385	7122853.393	1471.895	Bovid	Cranium
KW_9625_A	575060.317	7122853.187	1471.906	Primate	Isolated Teeth
KW_9625_B	575060.317	7122853.187	1471.906	Primate	Isolated Teeth
KW_9626	575059.968	7122853.634	1472.036	Bovid	Horn
KW_9627	575062.107	7122854.818	1472.28	Bovid	Limb
KW_9628	575062.035	7122854.746	1472.228	Bovid	Thoracic Cage
KW_9630	575061.99	7122854.624	1472.249	Bovid	Lower Limb
KW_9631	575058.659	7122853.557	1472.08	Bovid	Horn
KW_9632	575059.887	7122853.08	1471.944	Bovid	Spinal Column
KW_9634	575064.241	7122861.196	1473.912	Bovid	Limb
KW_9635	575064.232	7122861.17	1473.972	Bovid	Spinal Column
KW_9636	575064.249	7122861.274	1473.925	Bovid	Isolated Teeth
KW_9637	575062.205	7122854.906	1472.26	Bovid	Lower Limb
KW_9638	575062.21	7122854.91	1472.221	Carnivore	Lower Limb
KW_9639	575060.291	7122853.676	1471.909	Bovid	Upper Limb
KW_9641	575060.219	7122853.696	1471.948	Bovid	Pectoral Girdle
KW_9643	575059.945	7122853.737	1471.932	Bovid	Upper Limb

KW_9644	575061.216	7122854.084	1472.134	Carnivore	Cranium
KW_9646	575058.77	7122854.117	1471.876	Bovid	Thoracic Cage
KW_9647	575060.274	7122853.882	1472.052	Bovid	Spinal Column
KW_9648	575062.276	7122855.08	1472.06	Bovid	Limb
KW_9649	575064.701	7122860.65	1473.905	Bovid	Pelvic Grid
KW_9650	575064.383	7122860.736	1473.722	Carnivore	Upper Limb
KW_9651	575064.072	7122861.254	1473.876	Bovid	Isolated Teeth
KW_9652	575064.172	7122861.234	1473.881	Bovid	Isolated Teeth
KW_9653	575060.832	7122855.515	1471.982	Primate	Limb
KW_9654	575059.915	7122853.059	1471.938	Bovid	Thoracic Cage
KW_9655	575062.142	7122854.876	1472.097	Bovid	Limb
KW_9656	575060.587	7122853.165	1471.74	Bovid	Lower Limb
KW_9657	575060.315	7122853.675	1471.991	Bovid	Lower Limb
KW_9659	575061.468	7122854.38	1472.206	Bovid	Upper Limb
KW_9660	575062.329	7122854.988	1472.123	Primate	Upper Limb
KW_9661	575064.692	7122860.658	1473.817	Carnivore	Isolated Teeth
KW_9662	575059.932	7122853.077	1471.961	Primate	Isolated Teeth
KW_9663	575060.276	7122853.753	1471.937	Bovid	Upper Limb
KW_9664	575061.757	7122854.818	1472.039	Bovid	Lower Limb
KW_9665	575064.034	7122861.395	1473.878	Bovid	Lower Limb
KW_9666	575059.999	7122853.798	1471.941	Bovid	Upper Limb
KW_9667	575060.25	7122852.962	1471.725	Bovid	Cranium
KW_9668	575060.156	7122853.922	1471.926	Bovid	Spinal Column
KW_9670	575060.468	7122853.699	1471.973	Carnivore	Lower Limb
KW_9671	575061.65	7122854.361	1472.089	Carnivore	Lower Limb
KW_9672	575061.639	7122854.589	1472.056	Bovid	Limb
KW_9673	575062.245	7122854.66	1472.05	Primate	Isolated Teeth
KW_9674	575064.094	7122861.314	1473.772	Carnivore	Lower Limb
KW_9675	575064.733	7122860.674	1473.761	Carnivore	Isolated Teeth
KW_9676	575060.542	7122853.432	1471.87	Bovid	Lower Limb
KW_9677	575062.324	7122854.777	1471.99	Primate	Cranium
KW_9678	575061.068	7122853.604	1471.976	Bovid	Isolated Teeth
KW_9679	575059.72	7122853.858	1471.969	Bovid	Isolated Teeth
KW_9680	575059.788	7122853.827	1471.97	Bovid	Pelvic Grid
KW_9681_	575059.815	7122854.085	1472.011	Bovid	Cranium

A					
KW_9681_B	575059.815	7122854.085	1472.011	Bovid	Cranium
KW_9682	575059.87	7122854.081	1472.001	Bovid	Pelvic Grid
KW_9683	575060.41	7122853.11	1471.835	Bovid	Spinal Column
KW_9686	575059.669	7122853.81	1471.983	Bovid	Spinal Column
KW_9687	575061.338	7122854.632	1472.04	Bovid	Isolated Teeth
KW_9688	575062.354	7122854.989	1471.985	Bovid	Upper Limb
KW_9689	575062.304	7122854.913	1472.007	Bovid	Pectoral Girdle
KW_9690	575062.619	7122855.836	1472.049	Bovid	Horn
KW_9691	575060.878	7122853.592	1472.036	Bovid	Isolated Teeth
KW_9692	575061.519	7122854.806	1472.253	Bovid	Upper Limb
KW_9693	575063.426	7122854.008	1472.581	Bovid	Isolated Teeth
KW_9694	575058.306	7122852.785	1471.632	Bovid	Limb
KW_9695	575059.828	7122854.046	1471.942	Bovid	Cranium
KW_9696	575059.647	7122853.908	1471.925	Bovid	Lower Limb
KW_9697	575059.69	7122853.704	1471.92	Bovid	Spinal Column
KW_9698	575060.145	7122853.143	1471.873	Bovid	Spinal Column
KW_9699	575061.023	7122853.678	1471.882	Bovid	Isolated Teeth
KW_9702	575061.174	7122853.777	1472.148	Bovid	Isolated Teeth
KW_9703	575063.641	7122854.462	1472.753	Bovid	Limb
KW_9704	575059.815	7122854.029	1471.776	Bovid	Upper Limb
KW_9705	575056.532	7122848.685	1471.676	Bovid	Isolated Teeth
KW_9706	575063.427	7122855.676	1472.44	Bovid	Limb
KW_9707	575059.864	7122853.853	1471.788	Bovid	Spinal Column
KW_9708	575056.603	7122849.012	1471.758	Bovid	Isolated Teeth
KW_9711	575060.753	7122853.489	1471.999	Bovid	Isolated Teeth
KW_9712	575060.522	7122853.762	1471.835	Bovid	Limb
KW_9713	575060.989	7122853.797	1471.873	Bovid	Limb
KW_9714	575061.067	7122854.025	1471.891	Bovid	Limb
KW_9715	575061.205	7122853.928	1471.872	Bovid	Isolated Teeth
KW_9716	575061.245	7122854.203	1471.964	Carnivore	Spinal

					Column
KW_9717	575059.842	7122853.623	1471.825	Carnivore	Spinal Column
KW_9718	575059.652	7122853.719	1471.84	Bovid	Lower Limb
KW_9719	575059.818	7122853.963	1471.821	Bovid	Limb
KW_9720	575059.933	7122853.973	1471.803	Bovid	Lower Limb
KW_9721	575059.68	7122853.97	1471.886	Bovid	Isolated Teeth
KW_9722	575060.227	7122853.177	1471.708	Bovid	Horn
KW_9723	575060.177	7122853.168	1471.715	Bovid	Upper Limb
KW_9724	575060.277	7122853.227	1471.708	Primate	Isolated Teeth
KW_9725	575059.66	7122853.993	1471.927	Bovid	Spinal Column
KW_9726	575059.61	7122853.772	1472.014	Bovid	Cranium
KW_9727	575062.145	7122854.806	1471.643	Primate	Lower Limb
KW_9728	575061.356	7122853.705	1472.002	Carnivore	Isolated Teeth
KW_9729	575059.49	7122853.937	1471.921	Bovid	Cranium
KW_9730	575063.838	7122861.062	1473.705	Bovid	Pectoral Girdle
KW_9731	575060.382	7122854.254	1471.98	Bovid	Spinal Column
KW_9732	575063.228	7122859.498	1472.325	Bovid	Cranium
KW_9733	575063.028	7122855.805	1471.985	Bovid	Limb
KW_9734_A	575061.71	7122855.462	1471.788	Bovid	Lower Limb
KW_9734_B	575061.644	7122855.334	1471.756	Bovid	Lower Limb
KW_9735	575061.549	7122855.42	1472.079	Bovid	Limb
KW_9736	575061.793	7122855.311	1471.892	Bovid	Lower Limb
KW_9737	575056.932	7122848.794	1471.662	Bovid	Limb
KW_9738	575056.292	7122848.629	1471.69	Bovid	Isolated Teeth
KW_9739	575056.482	7122848.966	1471.695	Bovid	Isolated Teeth
KW_9740	575056.595	7122849.031	1471.679	Bovid	Pectoral Girdle
KW_9741	575056.668	7122849.175	1471.669	Bovid	Lower Limb
KW_9743	575061.881	7122855.38	1471.785	Bovid	Spinal Column
KW_9744	575060.339	7122854.344	1471.986	Bovid	Spinal Column
KW_9745	575061.936	7122854.877	1471.819	Bovid	Isolated Teeth
KW_9746	575060.519	7122853.049	1471.698	Bovid	Lower Limb
KW_9747	575060.509	7122853.034	1471.722	Bovid	Lower Limb

KW_9749	575059.727	7122854.077	1471.633	Bovid	Lower Limb
KW_9750	575059.618	7122854.145	1471.804	Bovid	Cranium
KW_9751	575059.768	7122854.213	1471.769	Bovid	Spinal Column
KW_9752	575059.942	7122854.228	1471.866	Bovid	Spinal Column
KW_9753	575059.439	7122853.965	1471.77	Bovid	Spinal Column
KW_9754	575059.36	7122853.722	1471.795	Bovid	Spinal Column
KW_9755	575059.275	7122853.902	1471.74	Bovid	Upper Limb
KW_9756	575059.276	7122853.785	1471.734	Bovid	Upper Limb
KW_9757	575060.129	7122853.973	1471.782	Bovid	Isolated Teeth
KW_9762	575062.156	7122855.005	1471.656	Bovid	Cranium
KW_9763	575062.128	7122854.982	1471.615	Bovid	Lower Limb
KW_9765	575062.281	7122854.88	1471.655	Bovid	Cranium
KW_9766	575062.134	7122854.899	1471.657	Bovid	Horn
KW_9767	575062.152	7122855.049	1471.646	Bovid	Thoracic Cage
KW_9771	575063.405	7122854.832	1472.226	Bovid	Pelvic Grid
KW_9772	575064.879	7122861.194	1474.082	Carnivore	Limb
KW_9780	575060.905	7122854.729	1472.036	Bovid	Lower Limb
KW_9781	575062.085	7122855.42	1471.629	Bovid	Lower Limb
KW_9783	575060.492	7122854.272	1471.801	Bovid	Thoracic Cage
KW_9784	575060.678	7122855.559	1472.011	Bovid	Limb
KW_9785	575060.708	7122855.688	1472.061	Bovid	Lower Limb
KW_9786	575060.758	7122855.538	1471.846	Carnivore	Lower Limb
KW_9787	575061.175	7122853.329	1472.107	Bovid	Isolated Teeth
KW_9788	575060.6	7122853.263	1471.721	Bovid	Spinal Column
KW_9789	575060.92	7122853.137	1471.639	Bovid	Cranium
KW_9790	575059.803	7122854.056	1471.693	Bovid	Spinal Column
KW_9804	575060.683	7122853.196	1471.756	Bovid	Lower Limb
KW_9807	575059.576	7122853.55	1471.887	Bovid	Spinal Column
KW_9808	575059.849	7122853.683	1471.894	Bovid	Cranium
KW_9809	575059.737	7122853.781	1471.871	Bovid	Spinal Column
KW_9810	575059.688	7122853.551	1471.844	Bovid	Spinal Column
KW_9811	575059.814	7122853.612	1471.882	Bovid	Spinal Column
KW_9812	575060.296	7122854.647	1472.108	Bovid	Limb

KW_9813	575060.088	7122854.367	1472.108	Bovid	Isolated Teeth
KW_9815	575061.509	7122854.388	1471.885	Bovid	Upper Limb
KW_9817	575062.645	7122854.898	1472.091	Bovid	Limb
KW_9818	575064.551	7122861.242	1473.807	Bovid	Lower Limb
KW_9819	575064.581	7122860.973	1473.543	Bovid	Upper Limb
KW_9820	575064.63	7122861.143	1473.778	Bovid	Lower Limb
KW_9821	575061.639	7122854.912	1471.63	Bovid	Spinal Column
KW_9822	575061.609	7122854.86	1471.533	Bovid	Pelvic Grid
KW_9826	575061.572	7122854.609	1471.531	Bovid	Horn
KW_9827	575061.291	7122856.133	1472.134	Bovid	Lower Limb
KW_9828	575060.733	7122855.477	1471.892	Bovid	Cranium
KW_9829	575060.928	7122855.086	1471.711	Bovid	Lower Limb
KW_9830	575062.909	7122855.57	1471.629	Bovid	Upper Limb
KW_9831	575062.744	7122855.346	1471.572	Bovid	Limb
KW_9832	575063.745	7122860.85	1472.947	Bovid	Spinal Column
KW_9833	575063.655	7122860.898	1472.924	Bovid	Upper Limb
KW_9835	575060.681	7122853.327	1471.634	Bovid	Spinal Column
KW_9836	575060.682	7122853.233	1471.583	Bovid	Upper Limb
KW_9838	575060.433	7122853.082	1471.585	Bovid	Limb
KW_9839	575060.668	7122853.194	1471.587	Bovid	Spinal Column
KW_9840	575060.46	7122853.359	1471.656	Carnivore	Spinal Column
KW_9841	575060.665	7122853.245	1471.587	Bovid	Limb
KW_9842	575060.812	7122853.308	1471.593	Bovid	Pectoral Girdle
KW_9843	575060.736	7122853.366	1471.61	Bovid	Cranium
KW_9844	575060.554	7122853.132	1471.636	Bovid	Limb
KW_9845	575060.719	7122853.294	1471.608	Bovid	Spinal Column
KW_9846	575059.442	7122853.592	1471.573	Carnivore	Spinal Column
KW_9847	575059.821	7122853.681	1471.553	Bovid	Horn
KW_9848	575060.331	7122853.595	1471.681	Bovid	Lower Limb
KW_9849	575060.402	7122853.745	1471.694	Bovid	Lower Limb
KW_9850	575061.314	7122854.801	1471.741	Hominin	Cranium
KW_9851	575060.445	7122853.846	1471.672	Bovid	Limb
KW_9852	575060.446	7122854.159	1471.662	Carnivore	Spinal Column
KW_9853	575060.373	7122853.996	1471.667	Bovid	Cranium
KW_9854	575060.544	7122853.974	1471.591	Bovid	Lower Limb
KW_9855	575059.55	7122853.735	1471.562	Bovid	Limb

KW_9856	575059.891	7122854.027	1471.572	Carnivore	Isolated Teeth
KW_9857	575059.83	7122853.836	1471.511	Carnivore	Isolated Teeth
KW_9858	575061.572	7122854.737	1471.437	Bovid	Spinal Column
KW_9859	575061.409	7122854.594	1471.619	Carnivore	Upper Limb
KW_9860	575061.421	7122854.766	1471.531	Bovid	Pectoral Girdle
KW_9861	575064.6	7122860.996	1473.57	Carnivore	Upper Limb
KW_9862	575064.624	7122861.044	1473.734	Bovid	Horn
KW_9863	575064.412	7122861.091	1473.445	Bovid	Isolated Teeth
KW_9865	575060.562	7122854.172	1471.621	Bovid	Lower Limb
KW_9866	575060.087	7122853.007	1471.917	Bovid	Lower Limb
KW_9867	575062.172	7122854.651	1471.723	Bovid	Horn
KW_9868	575060.108	7122853.087	1471.626	Bovid	Limb
KW_9869	575060.413	7122853.664	1471.676	Bovid	Lower Limb
KW_9870	575060.516	7122853.564	1471.703	Bovid	Thoracic Cage
KW_9871	575060.444	7122853.573	1471.629	Bovid	Upper Limb
KW_9873	575061.841	7122856.889	1472.158	Carnivore	Pectoral Girdle
KW_9874	575060.531	7122856.418	1472.082	Bovid	Limb
KW_9875	575062.68	7122857.193	1472.172	Bovid	Lower Limb
KW_9900	575060.392	7122854.858	1471.753	Hominin	Cranium
KW_9900_BIS	575060.54	7122855.457	1471.801	Hominin	Cranium
KW_9923	575062.482	7122857.427	1472.203	Bovid	Isolated Teeth
KW_9924	575063.095	7122857.33	1472.23	Other	Tusk
KW_9943	575063.21	7122856.451	1472.116	Primate	Cranium
KW_9944	575062.619	7122856.461	1472.091	Other	Tusk
KW_9946	575063.772	7122856.6	1472.361	Bovid	Limb
KW_9948	575064.084	7122856.11	1472.564	Bovid	Upper Limb
KW_9949	575064.013	7122856.04	1472.577	Bovid	Pelvic Grid
KW_9950	575063.804	7122856.21	1472.537	Hominin	Lower Limb
KW_9951	575063.585	7122856.155	1472.483	Bovid	Upper Limb
KW_9953	575063.884	7122856.59	1472.16	Bovid	Spinal Column
KW_9954	575063.72	7122856.088	1472.394	Bovid	Spinal Column
KW_9955	575063.916	7122856.131	1472.432	Bovid	Horn
KW_9957	575063.988	7122857.094	1472.283	Carnivore	Lower Limb
KW_9958	575063.764	7122857.963	1472.173	Bovid	Limb
KW_9959	575064.119	7122856.811	1472.184	Bovid	Lower Limb
KW_9960	575064.138	7122856.668	1472.175	Primate	Cranium

KW_9961	575063.931	7122856.676	1472.159	Bovid	Limb
KW_9962	575064.122	7122857.019	1472.239	Bovid	Upper Limb
KW_9963	575064.371	7122857.048	1472.256	Bovid	Horn
KW_9964	575052.12	7122850.67	1472.544	Bovid	Pelvic Grid
KW_9965	575051.308	7122847.361	1472.756	Bovid	Spinal Column
KW_9966	575066.194	7122856.742	1472.752	Bovid	Upper Limb
KW_9967	575066.37	7122858.076	1472.683	Bovid	Upper Limb
KW_9968	575065.844	7122859.252	1472.659	Bovid	Upper Limb
KW_9972	575060.752	7122853.861	1471.726	Bovid	Limb
KW_9973	575060.528	7122853.432	1471.588	Bovid	Lower Limb
KW_9977	575060.607	7122854.431	1471.764	Primate	Upper Limb
KW_9978	575060.485	7122854.231	1471.61	Bovid	Lower Limb
KW_9979	575060.922	7122853.418	1471.747	Bovid	Lower Limb
KW_9981	575060.971	7122853.599	1471.76	Bovid	Spinal Column
KW_9982	575060.971	7122853.599	1471.76	Bovid	Isolated Teeth
KW_9983	575063.192	7122855.912	1472.022	Primate	Cranium
KW_9984	575061.071	7122854.402	1471.728	Bovid	Spinal Column
KW_9985	575061.083	7122854.396	1471.736	Bovid	Upper Limb
KW_9986	575061.185	7122854.331	1471.831	Bovid	Lower Limb
KW_9987	575061.494	7122854.08	1472.208	Bovid	Limb
KW_9988	575061.425	7122853.894	1472.133	Bovid	Pelvic Grid
KW_9989	575061.285	7122854.479	1471.679	Bovid	Lower Limb
KW_9992	575060.748	7122855.492	1471.829	Primate	Isolated Teeth
KW_9993	575062.615	7122856.219	1471.821	Bovid	Thoracic Cage
KW_9994	575060.093	7122855.36	1471.891	Bovid	Limb
KW_9995	575060.894	7122855.826	1471.978	Bovid	Horn
KW_9996	575058.005	7122849.352	1470.75	Primate	Limb
KW_9997	575060.686	7122855.096	1471.639	Bovid	Thoracic Cage
KW_9999	575059.097	7122854.606	1471.895	Bovid	Spinal Column

3D Videos and Captions

Supplementary Files – click **here** to view 3D models in data repository.

Figure 2. Movie showing a rotating plot of the 3D k-means clustering from multiple perspectives. Clusters: 1 (Blue), 2 (Green), 3 (Red) and 4 (Purple).

Figure 4. Movie showing a rotating plot of the 3D DBSCAN clustering from multiple perspectives. Clusters: 1 (Red), 2 (Green), 3 (Blue), 4 (Purple), 5 (Grey) and outliers in black.

Appendix C: Supporting materials for methodology –a user-guideline.

USER GUIDELINE

POST-PROCESSING TOOLS AND METHODS

2020

FOR

3D spatial pattern analysis and volume estimation at Kromdraai

PREPARED BY

NONKULULEKO NGOLOYI

JEAN DUMONCEL

JOSE BRAGA

Summary

The provided raw data presents the methods applied for 3D visual representation using photogrammetry, 3D spatial patterning, and over-burden sediment volume estimations in 3D. These methods have contributed to the 3D digital documentation of Unit P, Kromdraai Plio-Pleistocene site in the *Cradle of Humankind*, South Africa.

For more information on the results of the methods consult chapters 2 and 3 of the following thesis:

"Heritage documentation from hominin-bearing fossil assemblage Kromdraai (South Africa): techniques for 3D digitization, quantitative spatial patterning and volume estimation" by Ngoloyi, N.

Chapter Two: Improving archaeological documentation and practices. A new protocol from the Plio-Pleistocene site of Kromdraai (Gauteng, South Africa).

Chapter Three: A new method to evaluate 3D spatial patterns within early hominin-bearing sites. An example from Kromdraai (Gauteng Province, South Africa).

Contents

Included are R-codes, functions and methods required for the following:

3D Visualisation using Photogrammetry

K-Means 2D and 3D clustering in RStudio

DBSCAN 2D and 3D clustering in RStudio

Volume estimation of overburden soils

Part 1

3D visual modelling using photogrammetry

Data collection

Multi-Image Photogrammetry

Data for this research was acquired using multi-image photogrammetry (Table 1.1), this is a tool used to supply the 3D information of objects (e.g. texture characteristics) at both local and regional scales (Yastikli 2007). Multi-image photography is the preferred method to achieve accurate close-range photogrammetry owing to the large overlaps (up to 100%) of a given area, capturing its entirety from multiple points of view (Rüther *et al.* 2014).

Close- Range Terrestrial and Drone Photogrammetry

Terrestrial photogrammetry involves the reconstruction of a 3D point cloud using a series of manually acquired overlapping photographs of an area on interest from multiple points of view using any type of digital camera at a set focal length. Using the Structure-From-Motion method the dense cloud points from the scene are reconstructed into a 3D model (Rüther *et al.* 2014). To acquire drone imagery two types of drones namely the "senseFly" eBee and the DJI phantom drones were used, using the Canon IXUS 127 HS and DJI FC350 cameras respectively. For the aerial 3D reconstruction of the site and regional area (several km's) UAV photogrammetry with the "senseFly" eBee drone was used, allowing for a series of overlapping georeferenced photographs from various viewpoints to be acquired. The DJI drone provided a concise non-georeferenced 3D reconstruction of the site from an aerial viewpoint following the same process as the "senseFly" eBee drone.

Post-Processing

The computation of photographic data can be achieved with the fully automated software Agisoft Photoscan which utilizes image algorithms and bundle adjustments to produce a 3D

model of dense clouds (Rüther *et al.* 2014). The advantages of Photoscan include its cost-effectiveness, its user-friendliness and the ability for the software to produce files formats (e.g. ply) compatible with many 3D visualization and manipulation software. 3D model generation is achieved using defined workflow processes in Photoscan through batch processing or manually.

Software: Agisoft Photoscan

File format: JPEG, PLY

Batch Processing

Table 1. Batch process settings showing the parameters of the workflow process for 3D photogrammetry in Photoscan before and after adding GCP points.

Workflow Process	**Parameters**
Batch Process 1	
Add Photo's	
Align Photo's	Accuracy: Medium Pair selection: Reference (Drone) or Disabled
Build Dense Cloud	Quality: Medium Depth filtering: Moderate
Allocate GCP's and georeference model	
Batch Process 2	
Align Photo	Accuracy: High Pair selection: Generic
Optimise alignment	Default settings
Build Dense Cloud	Quality: High Depth Filtering: Moderate
Build Mesh	Face Count: Medium

Texture	Texture size: 8192 x 8192 pixels
Build DEM	Default settings
Build Orthomosaic	Default settings

Manual Processing

Add photos

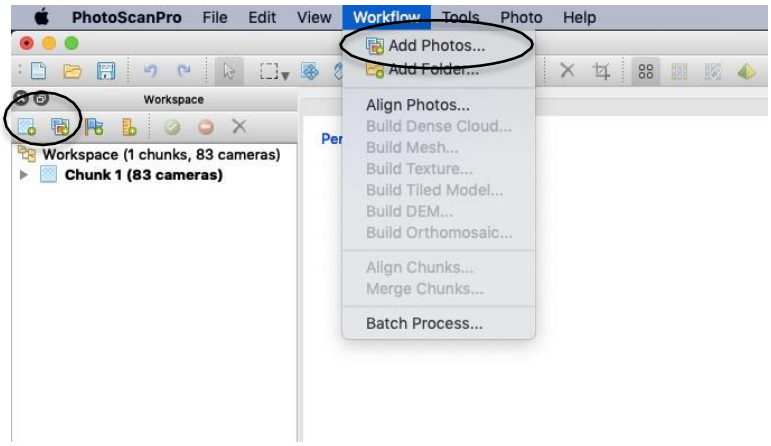

Align photos

Build dense cloud

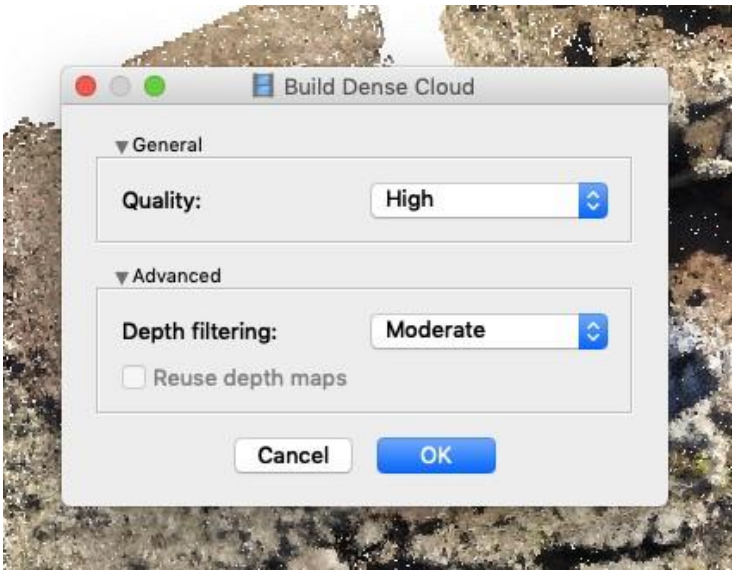

Build mesh

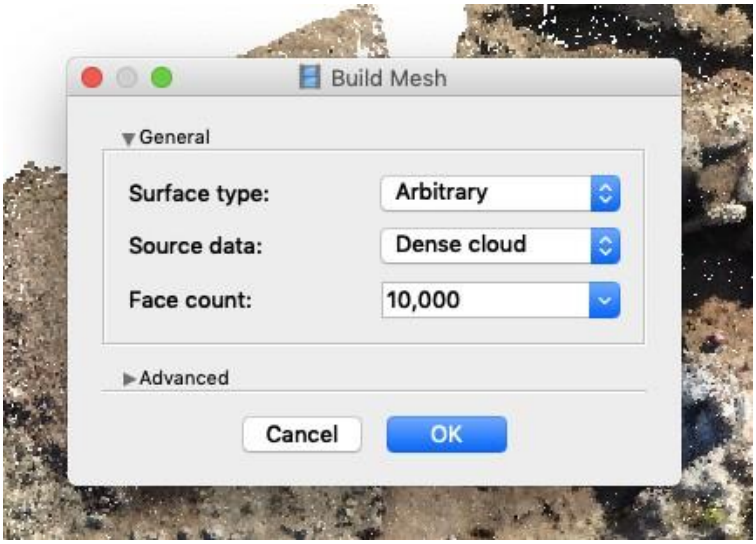

Build texture

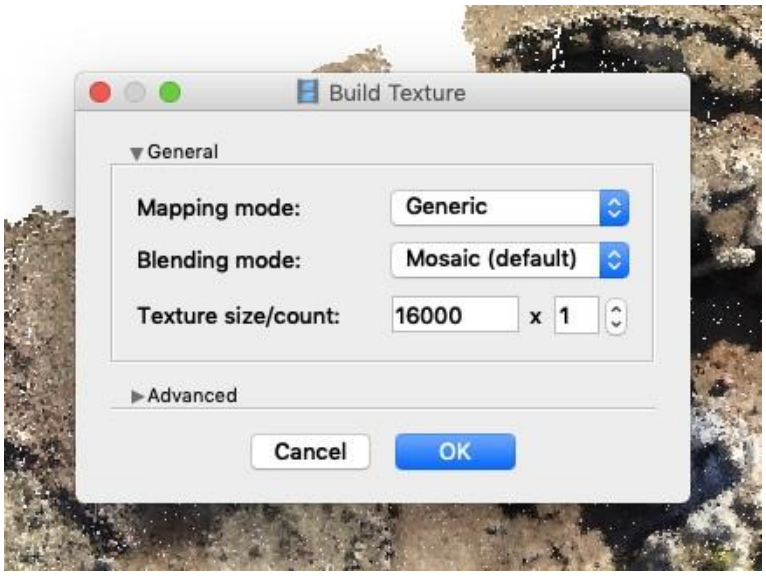

Build DEM

Adjust 3D model and set the projection plane to “Current View” > OK.

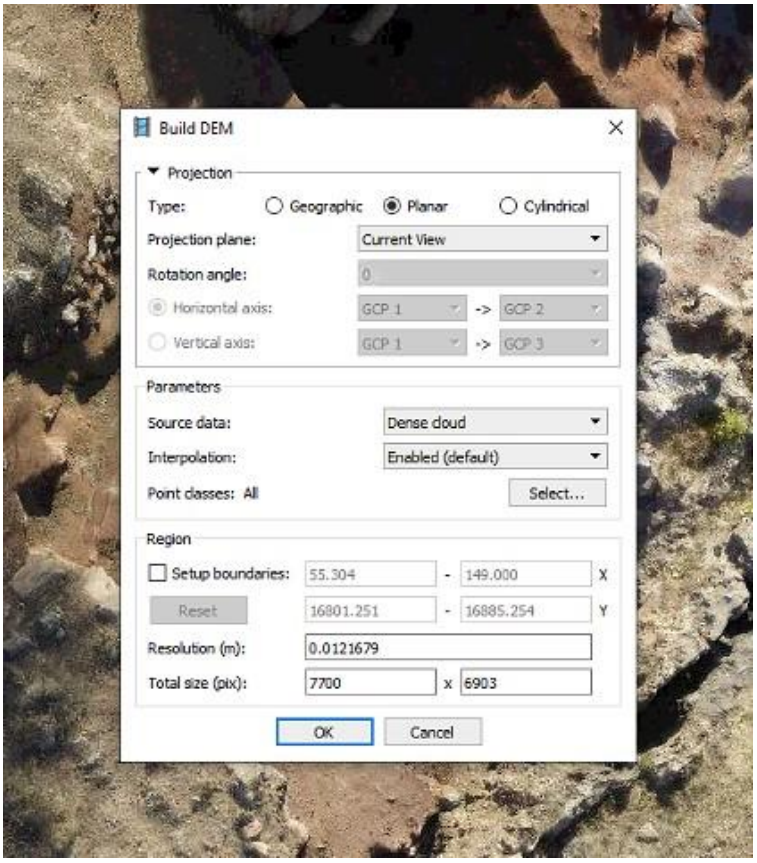

Export DEM

File > Export > Export DEM > Export “TIF/BIL/XYZ” > Export

Set the coordinate system accordingly

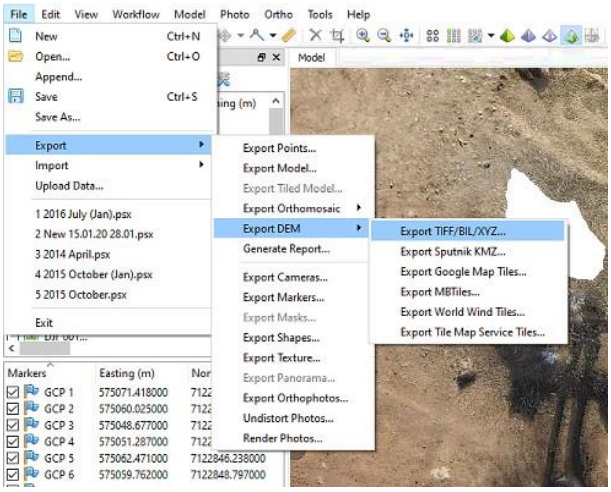

Build Orthomosaic

- Adjust 3D model and set the projection plane to “Current View” > OK.

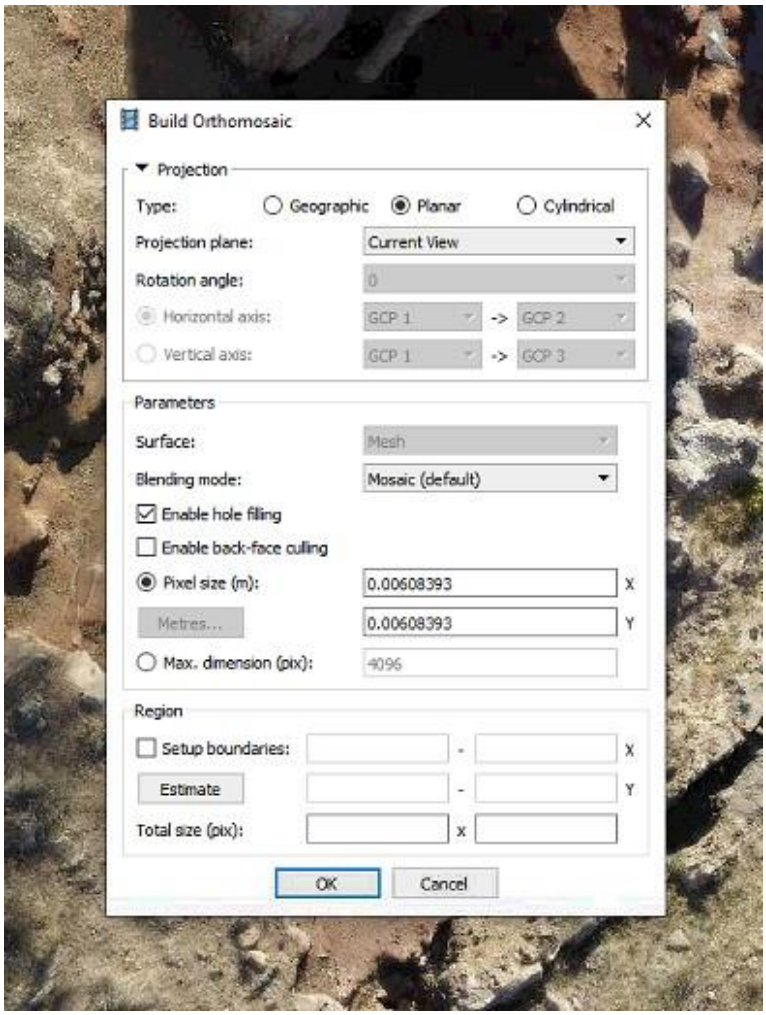

Export orthomosaic

- Set the coordinate system accordingly.
- File > Export > Export orthomosaic > Export “JPG/TIFF/PNG”

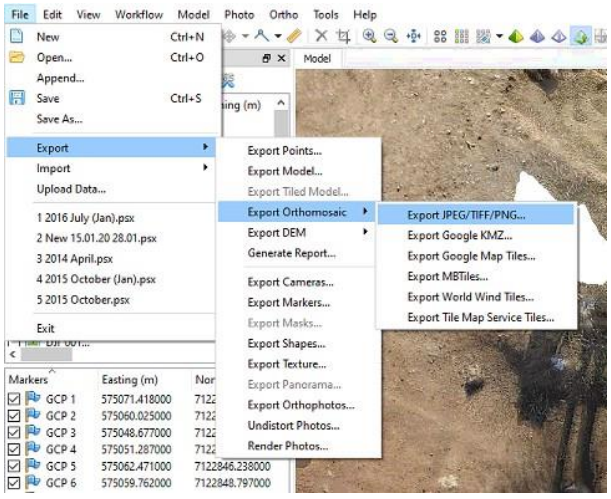

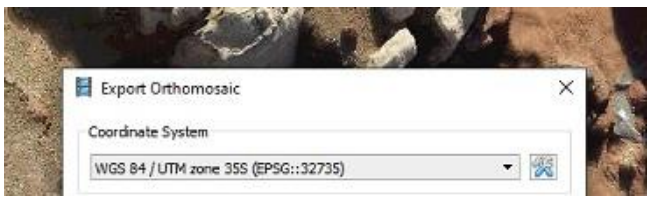

Part 2

Over-burden sediment volume estimations in 3D

Applied in: "Improving archaeological documentation and practices. A new protocol from the Plio-Pleistocene site of Kromdraai (Gauteng, South Africa)".

The section details the steps followed to estimate over-burden sediment volumes at the Kromdraai excavation. Over-burden sediments contain fossil finds recovered ex-situ, through the wet-sieving process.

The complete process described below combines known methods applied in 3D reconstructions, but it is the first to be applied for the purpose of volume estimation of a physical archaeological site.

It is advised that all photogrammetry images be conducted in the early morning to avoid a shadow cast in the images.

The time spent on the site is largely dependent on the length of the excavation. It is not necessary to be on-site for the entirety of the excavation to collect photogrammetry images. However, for volume estimation, photogrammetry must be conducted prior to the commencement of digging on the first day of excavation, and at the end of the excavation on the final day.

For volume estimation at a local scale only close-range terrestrial photogrammetry is required, this is a cost-efficient approach using only a hand-held camera. Drone imagery is only necessary for large, regional scale excavations in order to achieve an aerial view.

Software: Agisoft Photoscan, Avizo 8, MeshLab, Meshmixer

Open-source alternatives to Agisoft Photoscan: Regard3D and MicMac

Read more about alternatives to Avizo 8 here:

https://perso.telecom-paristech.fr/bloch/papers/JDigitalImaging-Alessio-2019.pdf

File format: JPEG, PLY

1. Compute 3D photogrammetry models (see part 1 of this guideline) representing the site before and after excavation.
For the purposes of this demonstration, “before” and “after” are labeled “2020.01.15” and “2020.01.16” respectively.

Merging and aligning 3D models

Software: Agisoft photoscan.

Alignment:

open 2020.01.15

append 2020.01.16

check that both models have the same number of ground control points in the same order.

“Workflow”-> “Align Chunks”. For Method, choose “Marker based”

The aligned model can then be saved as a ply.

Avizo Part 1 - Aligning cube to 3D models

- Import 3D model before excavation > surface view
- Import 3D model after excavation
- Import cube (ply) > surface view

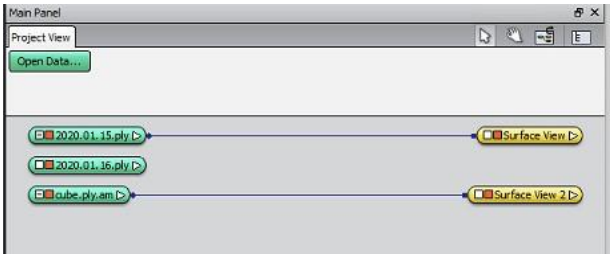

- Align ply cube to the 3D models
- Select cube > align principle axis > go

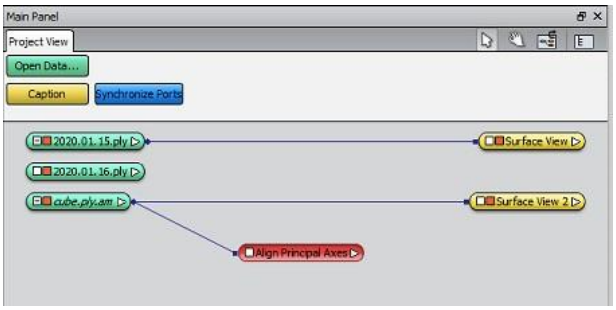

Align the cube and 3D surfaces

- Select cube > align surfaces > connect to 3D model before excavation.

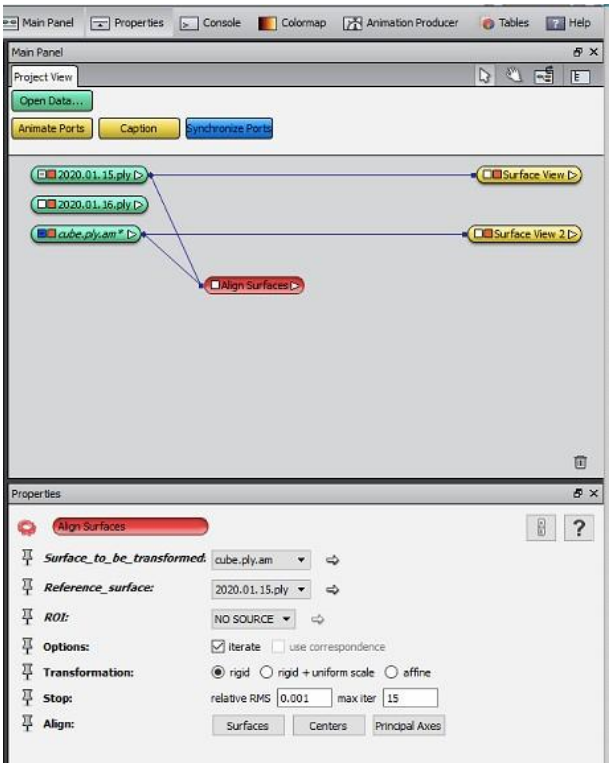

- In the properties box select the “manipulator” and adjust the cube accordingly around the excavation area. Ensure that both models are covered. Delete aligned surfaces tab.

Apply Transformation

- Manipulator > TransformBox > Apply Transformation > Proceed

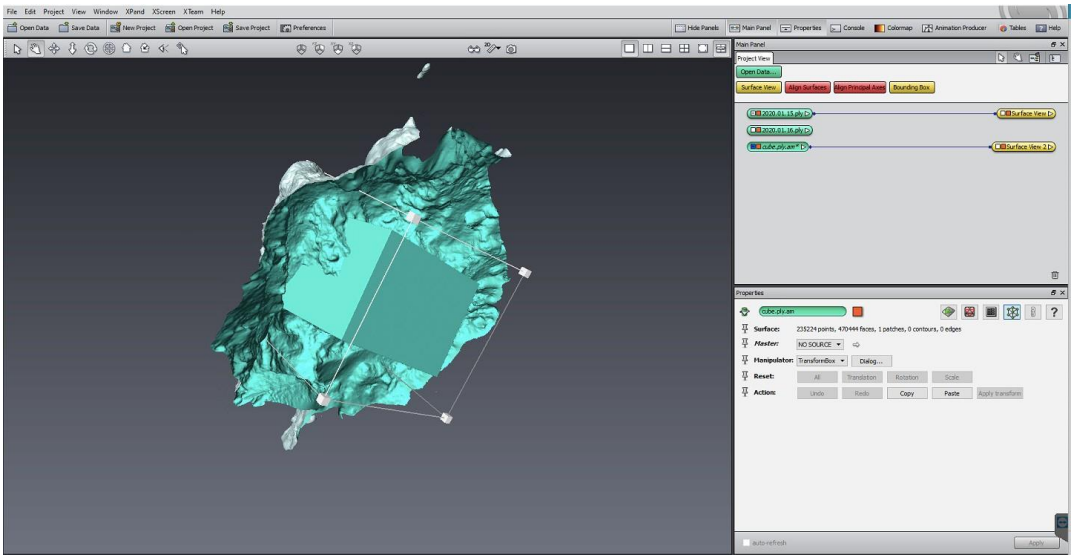

- Save (standford ply) and rename the aligned cube > exit Avizo

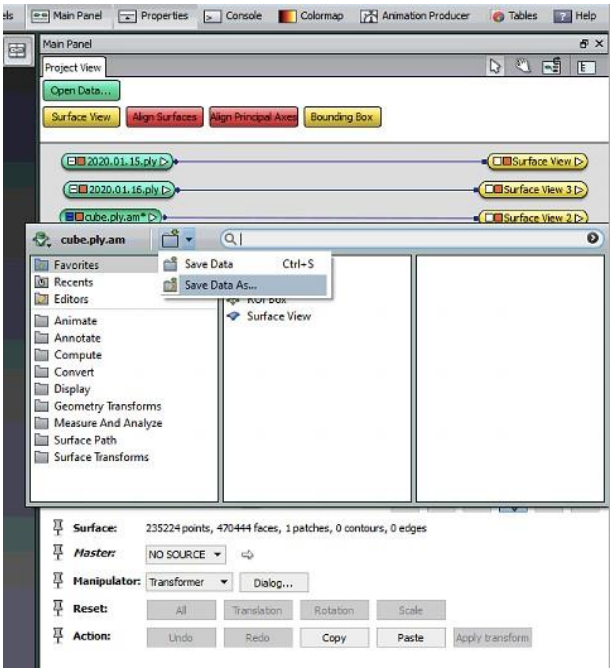

Meshmixer

- Import cube object Meshmixer
- Import “before excavation” 3D model > Append > Select “No” to shift the position of the objects

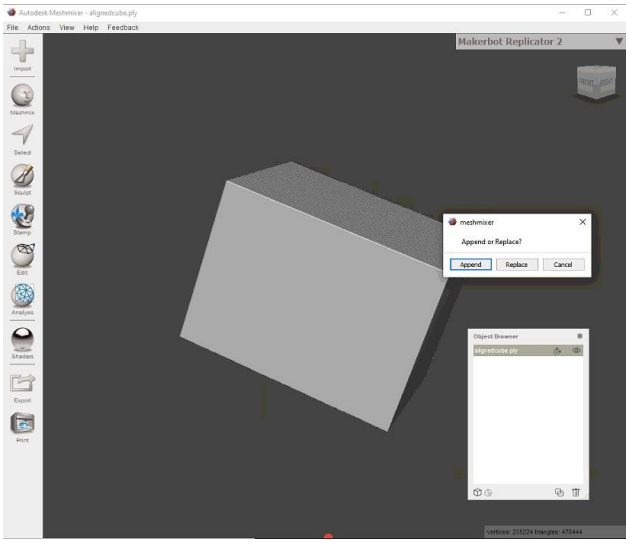

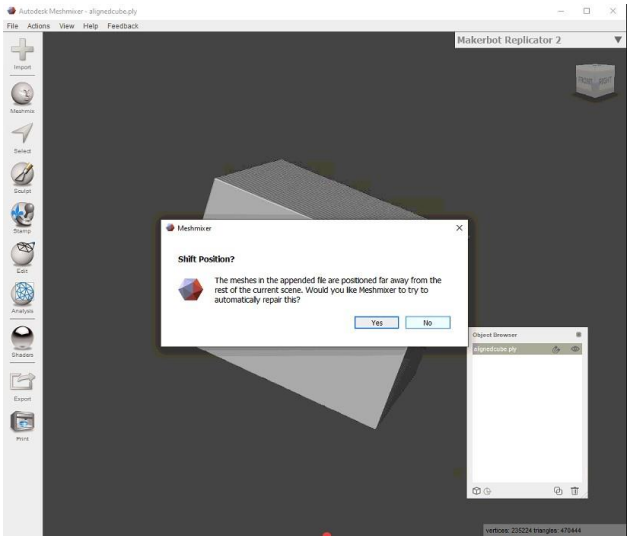

- Shift select aligned cube (first) and 3D model > Select “Boolean difference”

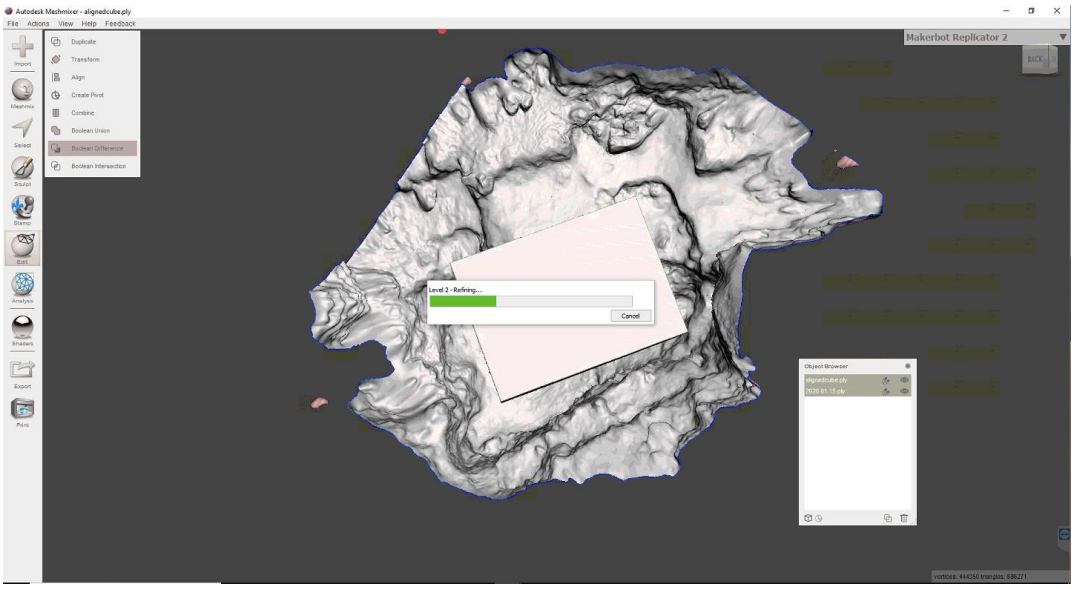

- Difference panel > select “Auto reduce result”
- Advanced panel > adjust “merge border rings” to “1”
- Difference panel > set solution mode to “max quality” > accept

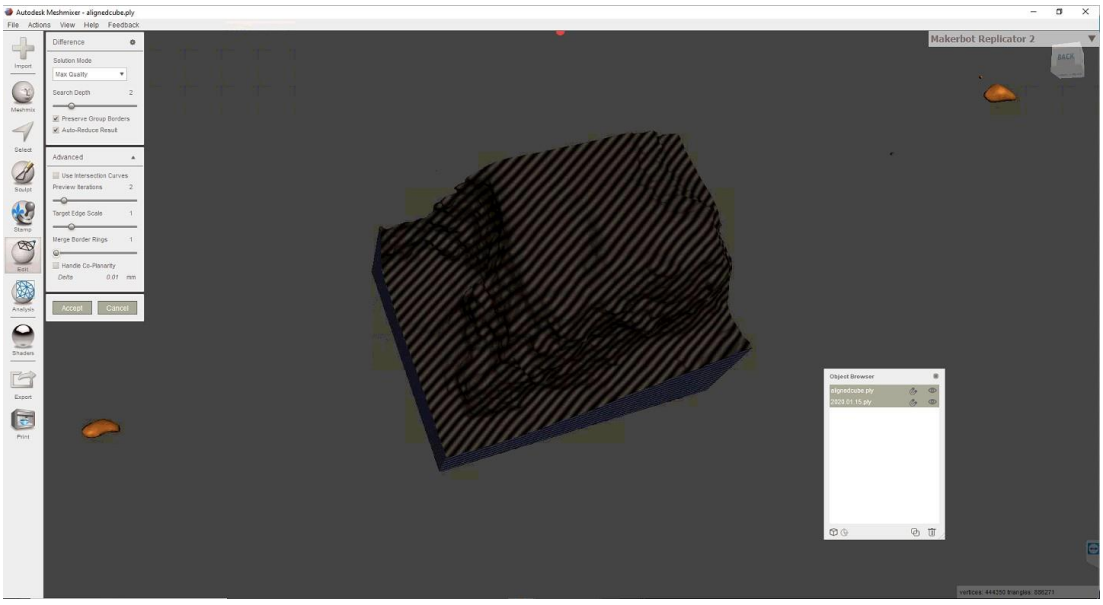

- Export the aligned 3D object > save.

MeshLab

Cleaning and Repairing

- Import 3D object into MeshLab.
- Filters > Cleaning and Repairing > remove unreferenced vertices
- Filters > Cleaning and Repairing > remove isolated pieces (wrt Face Num.) > enter minimum conn. comp size: 2500 > apply > close

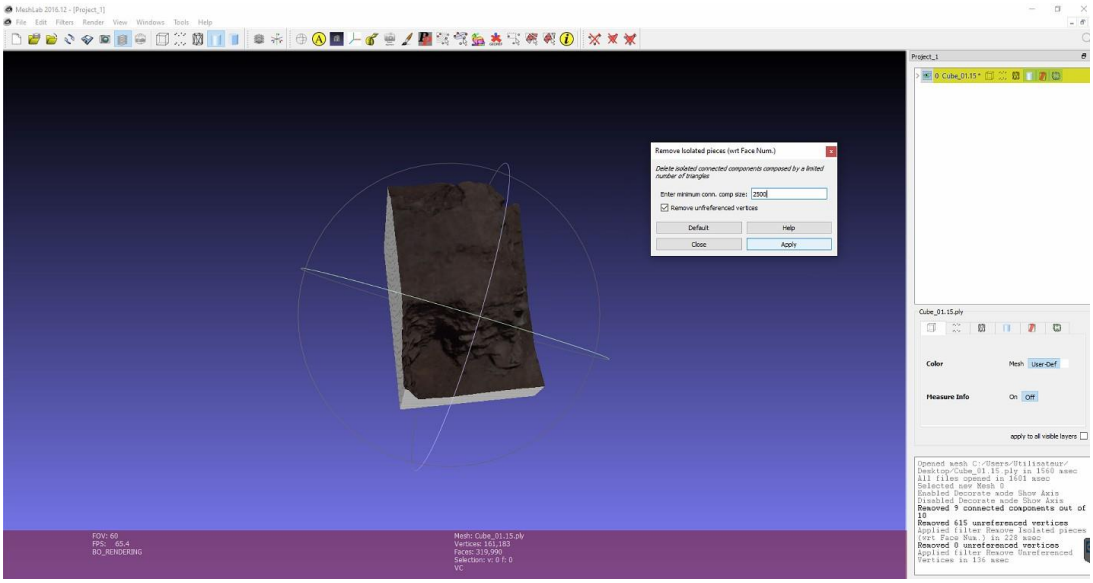

- Filters > Cleaning and Repairing > Merge close vertices > apply

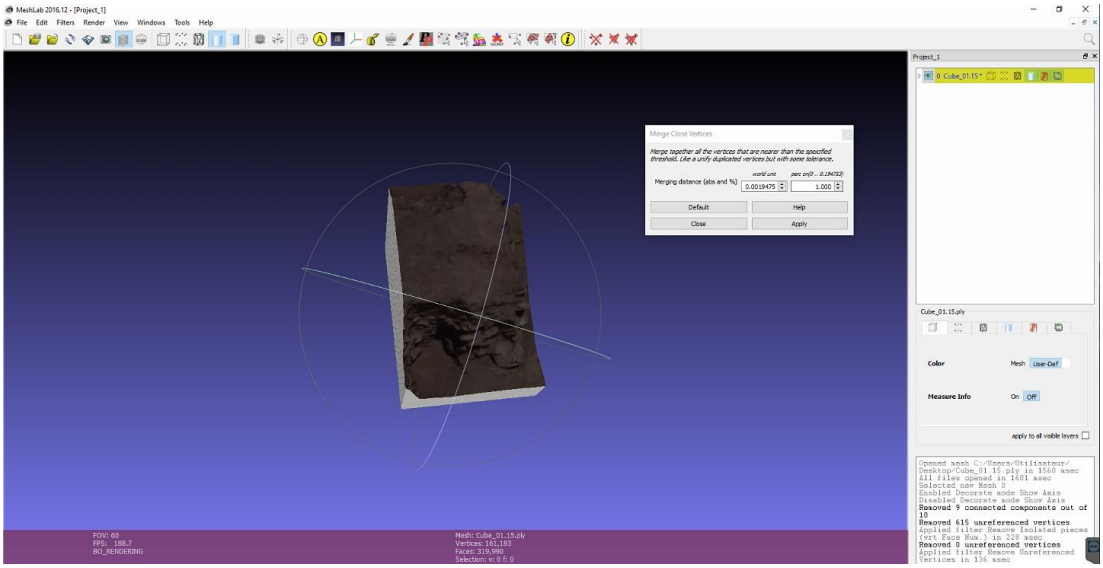

Remeshing, Simplification and Reconstruction > close holes > apply > close

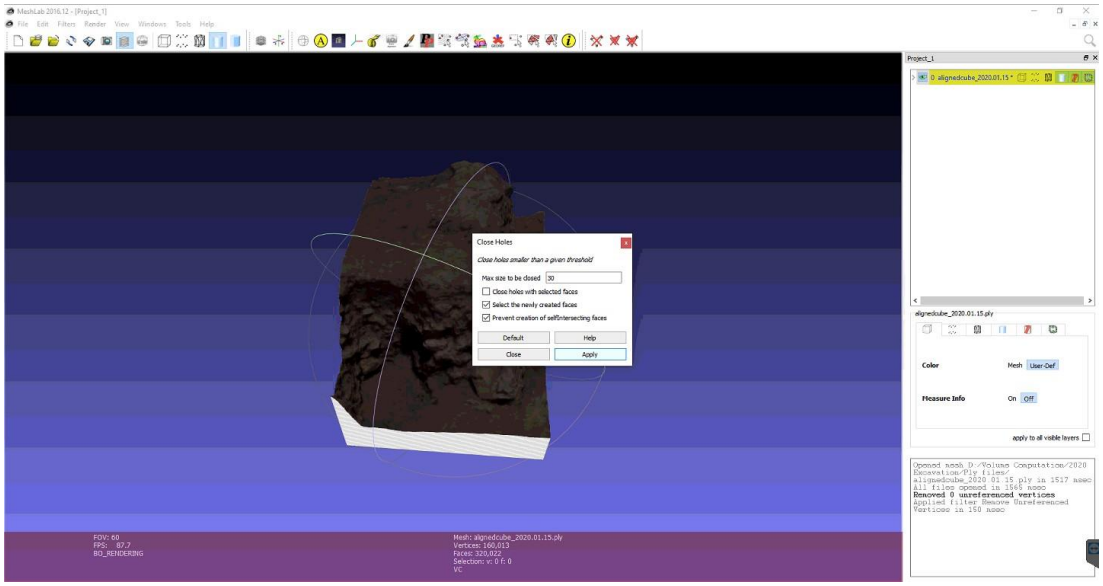

- Save > Export mesh as (ply object) > Save > OK > Exit MeshLab
- Repeat steps 4 and 5 for 3D model representing after excavation.

Avizo Part 2 – Volume estimation

- Import the merged and aligned cubes and 3D models for before (“2020.01.15”) and after (“2020.01.16”) excavation.
- Select “before” model (2020.01.15)
- Scan Surface to Volume
- Properties panel > adjust dimensions to 400 x 400 x 400 > Apply

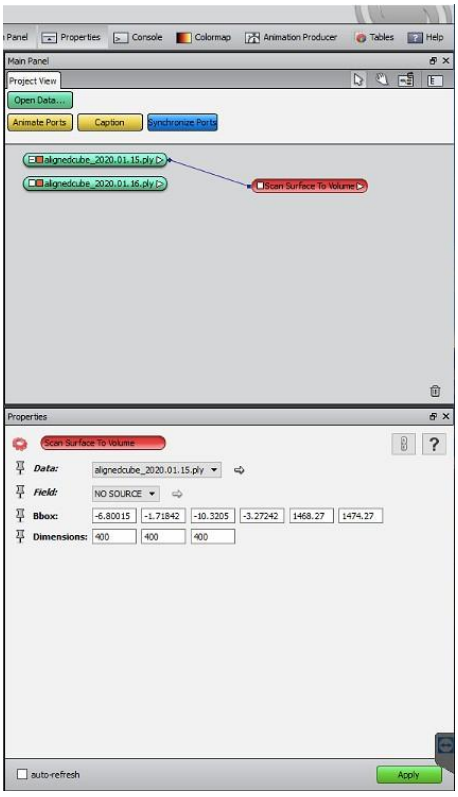

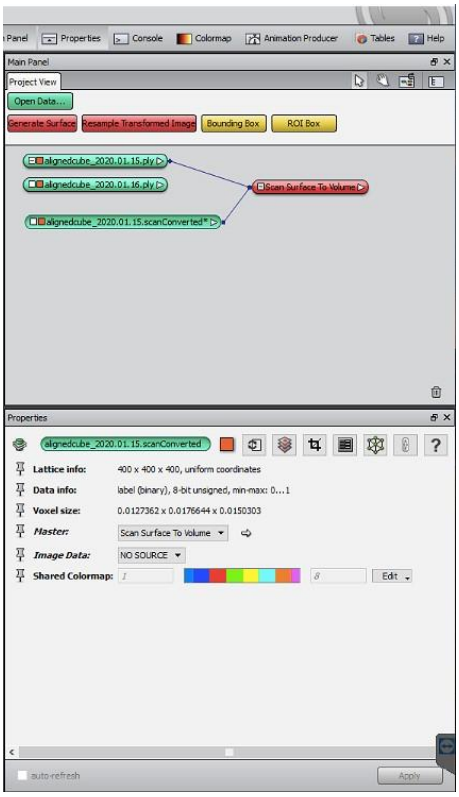

- Select “after” model
- Scan Surface to Volume > connect to “scanConverted” of “before” model (highlighted in red)

- Properties panel > ensure that “data” and “field” are correctly assigned > Apply
- Select “scanConverted” > compute > arithmetic > connect “Input B” to “scanConverted” of “after” model

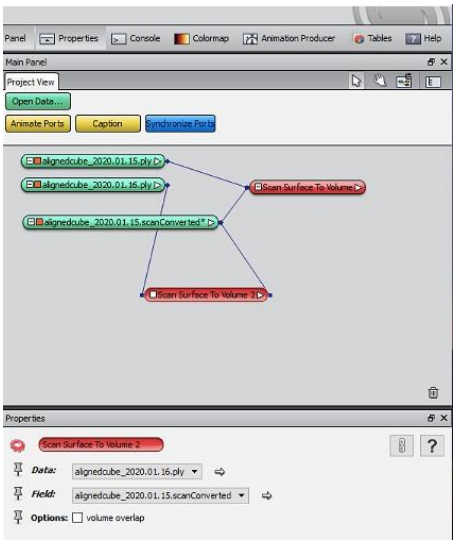

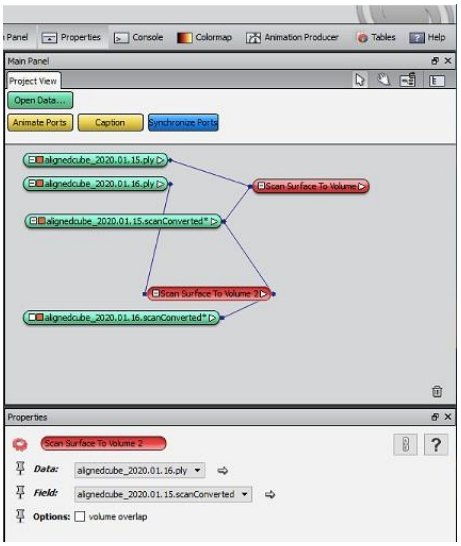

- Properties panel > insert equation “3*A-B” in “Expr” > Apply
- Select result > properties panel > select the segmentation editor

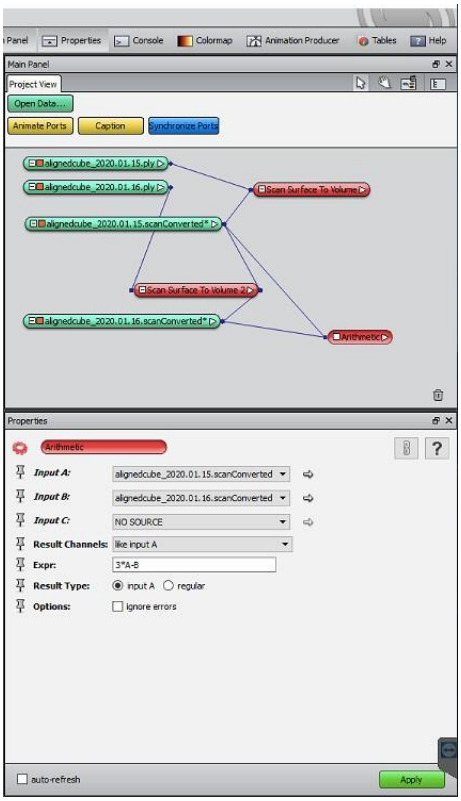

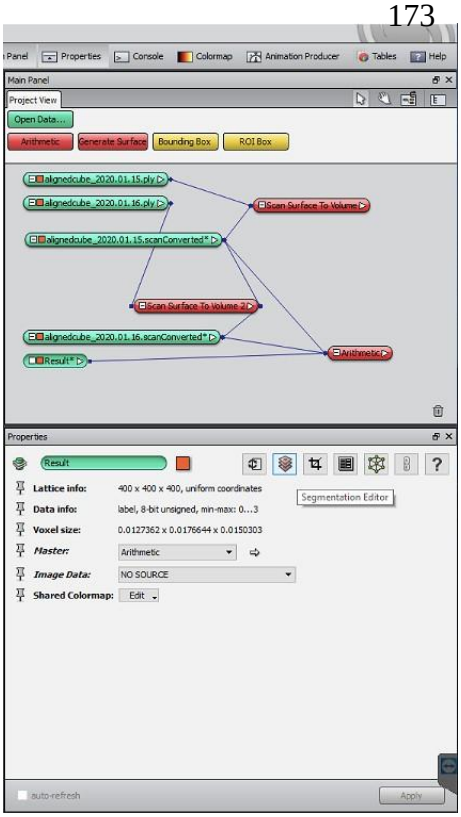

- Results panel > select the pointer tool > using the slider select unshaded areas of the 3D model (hold shift to select multiple)

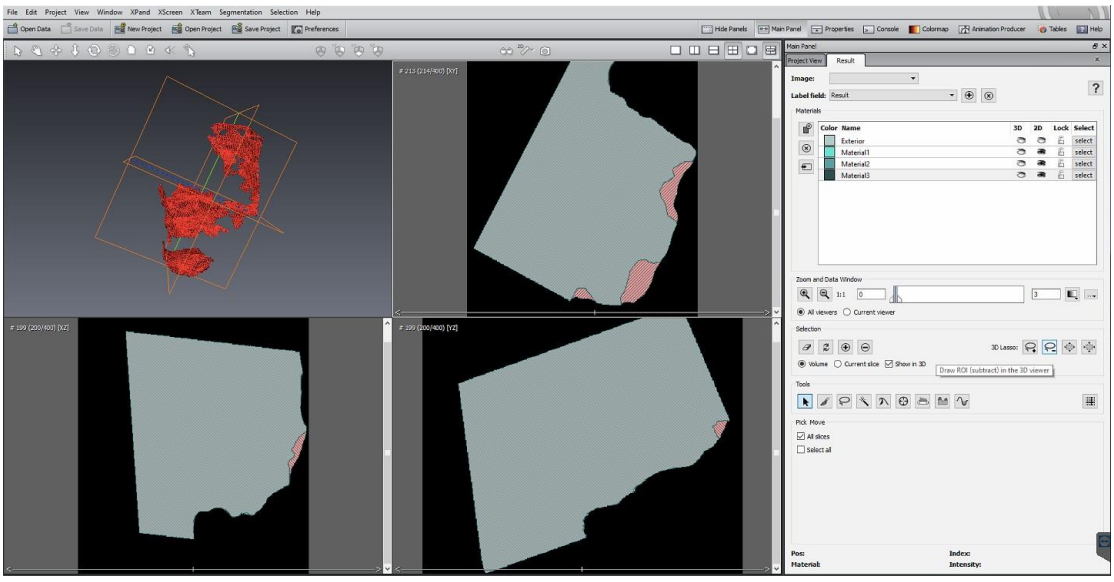

- Results panel > select 3D Lasso (subtract)

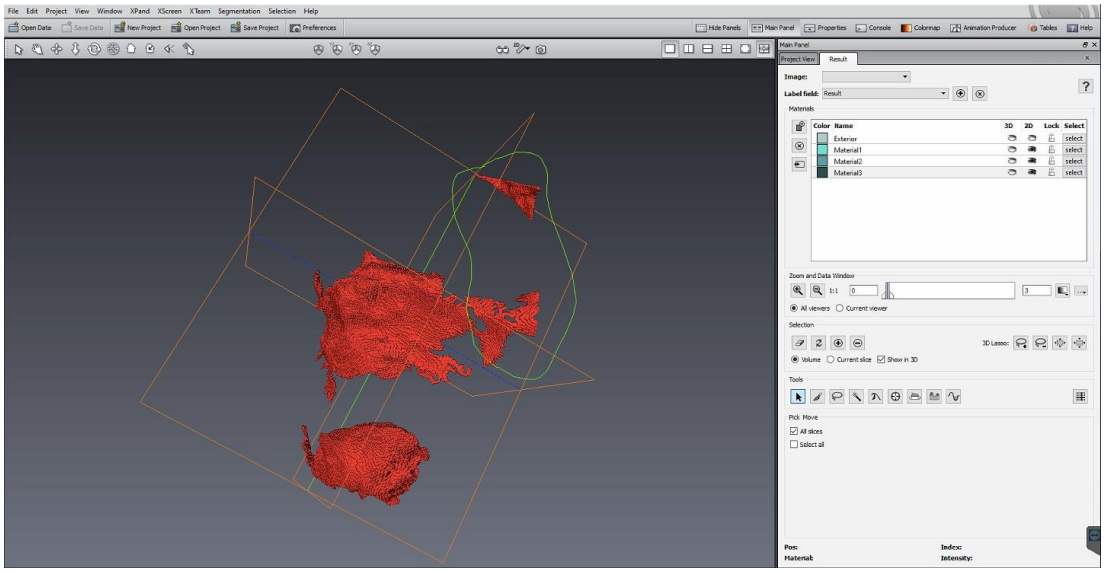

- Rename and assign a colour to the volume materials

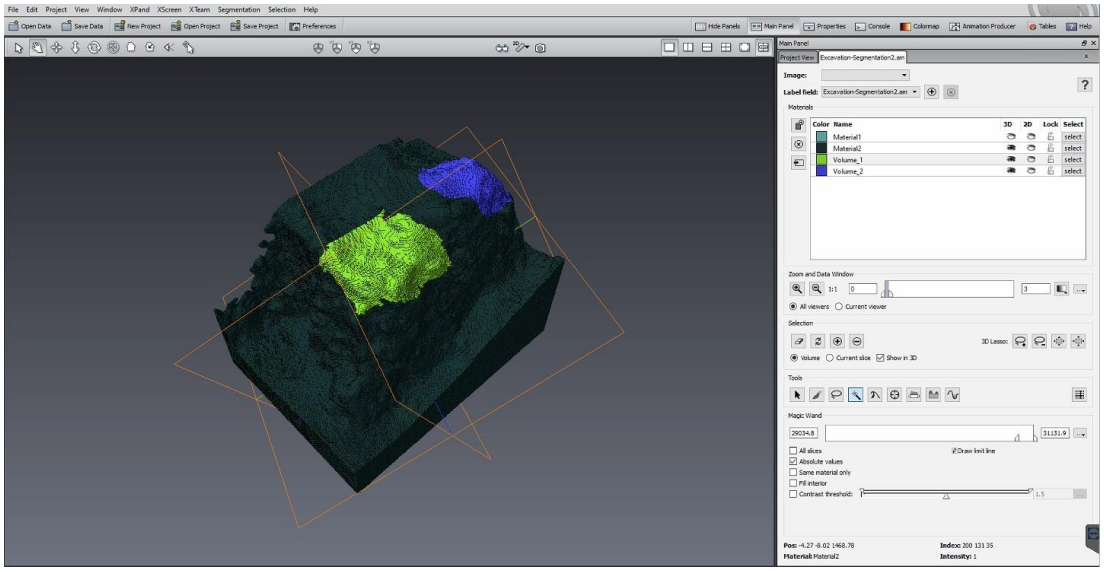

- View isolated volumes

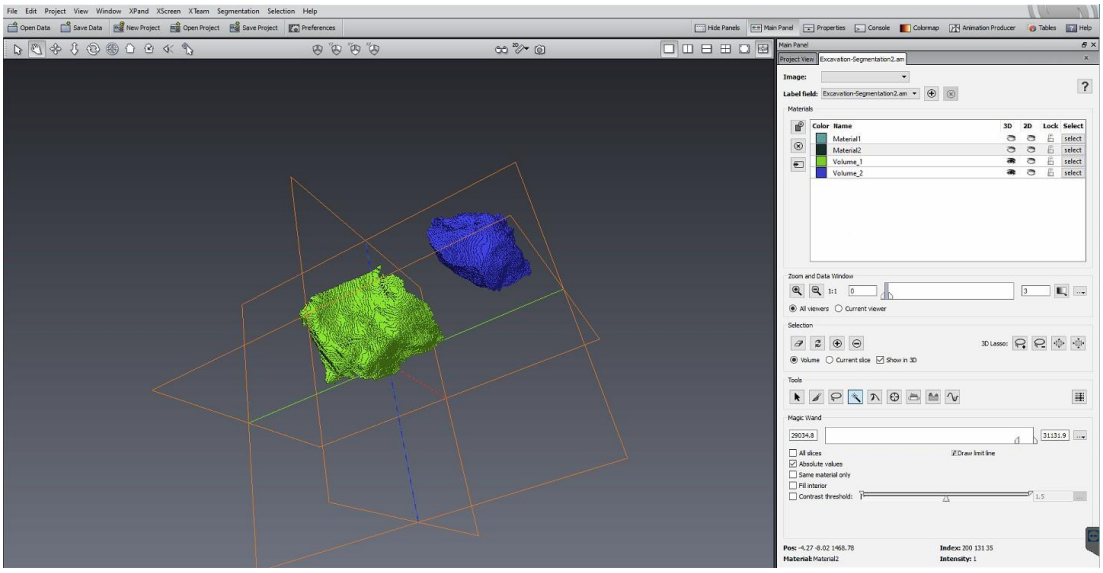

Volume Estimation Measurement

- Select results > measure and analyse > material statistics > apply

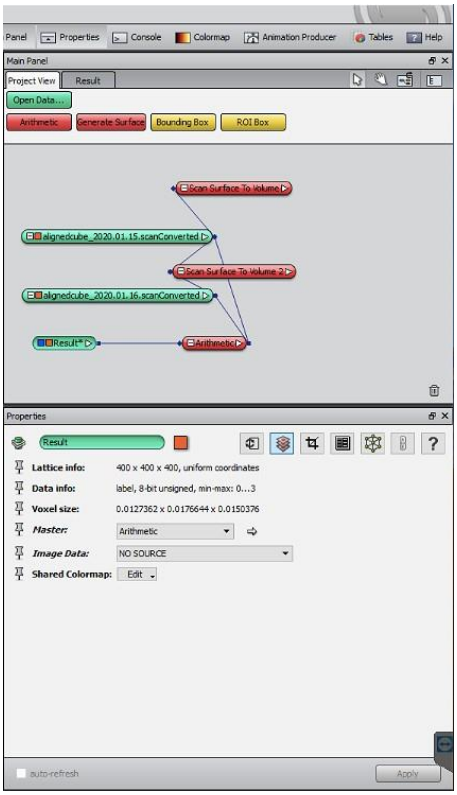

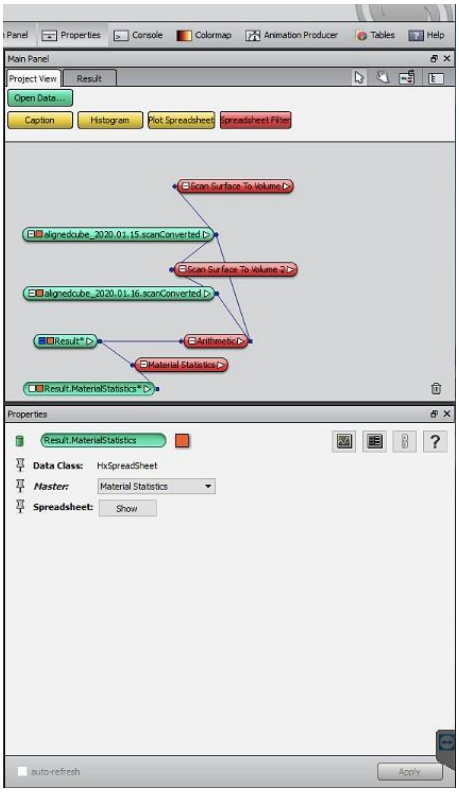

Part 3

3D spatial patterning

Applied in: A new method to evaluate 3D spatial patterns within early hominin-bearing sites. An example from Kromdraai (Gauteng Province, South Africa)".

Software: RStudio

There are several statistical means for spatial patterning analysis. Below we detail methods implemented in Kromdraai namely:

Hopkins Statistic (H) ***for measuring clustering tendency***

K-Means and DBSCAN for clustering

Silhouette coefficient (S_i) for cluster validation

The following R scripts for k-means and DBSCAN clustering were sourced from several websites (specified below). Engineer, Jean Dumoncel assisted in developing the tools such that they were applicable for 3D spatial analysis. Further analysis using these scripts was conducted by me.

Software: RStudio

R Scripts

Functions

Data visualisation function (for scatterplot)

myscatter3d is a modified version of the function scatter3d from the R package car.

checked in 23 December 2009 by J. Fox

```
# 5 January 2010: fixed axis labeling in myscatter3d.formula. J. Fox
# 13 May 2010: changed default id.n to conform to showLabels
# 30 July 2010: checks for rgl
# 23 October 2010: added surface.alpha and ellipsoid.alpha arguments
# 2012-03-02: fixed some argument abbreviations. J. Fox
# 2013-02-20: fixed error message, docs for surface.col argument. J. Fox
# 2013-08-20: changed rgl:::rgl.projection to rgl::rgl.projection; more such fixes to come. J.
Fox
# 2013-08-31: rgl functions used now exported; got rid of ::: and ::. J. Fox
# 2014-08-04: changed name of identify3d() to Identify3d(). J. Fox
# 2014-08-17: added calls to requireNamespace and :: as needed. J. Fox
# 2014-09-04: J. Fox: empty groups produce warning rather than error
# 2015-12-12: Added axis.ticks argument and code contributed by David Winsemius to add
tick labels to axes. J. Fox
# 2016-02-06: Changed call to rgl.clear() to next3d() for compatibility with embedding in
HTML. J. Fox
# 2017-06-27: introduced id argument replacing several arguments. J. Fox
# 2017-11-30: use carPalette(), avoid red and green. J. Fox

myscatter3d <- function(x, ...){
  if (!requireNamespace("rgl")) stop("rgl package missing")
  UseMethod("myscatter3d")
}

myscatter3d.formula <- function(formula, data, subset, radius, xlab, ylab, zlab, id=FALSE,
...){
  na.save <- options(na.action=na.omit)
```

```
 on.exit(options(na.save))
 m <- match.call(expand.dots=FALSE)
 if (is.matrix(eval(m$data, sys.frame(sys.parent()))))
   m$data <- as.data.frame(data)
 m$na.action <- na.pass
 m$id <- m$xlab <- m$ylab <- m$zlab <- m$... <- NULL
 m[[1]] <- as.name("model.frame")
 formula <- as.character(formula)
 formula <- paste(formula[2], formula[1], formula[3])
 formula <- as.formula(sub("\\|", "+", formula))
 m$formula <- formula
 X <- eval(m, parent.frame())
 if ("(radius)" %in% names(X)){
   radius <- X[, "(radius)"]
   X <- X[, names(X) != "(radius)"]
 }
 else radius <- 1
 names <- names(X)

 if (missing(xlab)) xlab <- names[2]
 if (missing(ylab)) ylab <- names[1]
 if (missing(zlab)) zlab <- names[3]
 if (ncol(X) == 3)
   myscatter3d(X[,2], X[,1], X[,3], xlab=xlab, ylab=ylab, zlab=zlab, radius=radius, id=id, ...)
 else if (ncol(X) == 4)
   myscatter3d(X[,2], X[,1], X[,3], groups=X[,4], xlab=xlab, ylab=ylab, zlab=zlab,
radius=radius, id=id, ...)
```

```
  else stop("incorrect myscatter3d formula")
}

myscatter3d.default <- function(x, y, z,
                        xlab=deparse(substitute(x)), ylab=deparse(substitute(y)),
                        zlab=deparse(substitute(z)), axis.scales=TRUE, axis.ticks=FALSE,
                        revolutions=0, bg.col=c("white", "black"),
                        axis.col=if (bg.col == "white") c("darkmagenta", "black", "darkcyan")
                        else c("darkmagenta", "white", "darkcyan"),
                        surface.col=palette()[-1],
                        surface.alpha=0.5,
                        neg.res.col="magenta", pos.res.col="cyan",
                        square.col=if (bg.col == "white") "black" else "gray", point.col="yellow",
                        text.col=axis.col, grid.col=if (bg.col == "white") "black" else "gray",
                        fogtype=c("exp2", "linear", "exp", "none"),
                        residuals=(length(fit) == 1), surface=TRUE, fill=TRUE,  grid=TRUE,
grid.lines=26,
                        df.smooth=NULL, df.additive=NULL,
                        sphere.size=1, radius=1, threshold=0.01, speed=1, fov=60,
                        fit="linear", groups=NULL, parallel=TRUE, ellipsoid=FALSE, level=0.5,
ellipsoid.alpha=0.1,
                        # id.method=c("mahal", "xz", "y", "xyz", "identify", "none"),
                        # id.n=if (id.method == "identify") Inf else 0,
                        # labels=as.character(seq(along=x)), offset = ((100/length(x))^(1/3)) *
0.02,
                        id=FALSE, model.summary=FALSE, ...){
  if (!requireNamespace("rgl")) stop("rgl package missing")
```

```
if (!requireNamespace("mgcv")) stop("mgcv package missing")


#    id.method <- match.arg(id.method)
if (residuals == "squares"){
  residuals <- TRUE
  squares <- TRUE
}
else squares <- FALSE
summaries <- list()
if ((!is.null(groups)) && (nlevels(groups) > length(surface.col)))
  stop(sprintf("Number of groups (%d) exceeds number of colors (%d)",
               nlevels(groups), length(surface.col)))
if ((!is.null(groups)) && (!is.factor(groups))) stop("groups variable must be a factor")
counts <- table(groups)
if (any(counts == 0)){
  levels <- levels(groups)
  warning("the following groups are empty: ", paste(levels[counts == 0], collapse=", "))
  groups <- factor(groups, levels=levels[counts != 0])
}
bg.col <- match.arg(bg.col)
fogtype <- match.arg(fogtype)
if ((length(fit) > 1) && residuals && surface)
stop("cannot plot both multiple surfaces and residuals")
xlab # cause these arguments to be evaluated
ylab
zlab
rgl::next3d()
```

```
rgl::rgl.viewpoint(fov=fov)

rgl::rgl.bg(color=bg.col, fogtype=fogtype)


valid <- if (is.null(groups)) complete.cases(x, y, z)

else complete.cases(x, y, z, groups)

x <- x[valid]

y <- y[valid]

z <- z[valid]

labels <- labels

minx <- min(x)

maxx <- max(x)

miny <- min(y)

maxy <- max(y)

minz <- min(z)

maxz <- max(z)

if (axis.scales){

  lab.min.x <- nice(minx)

  lab.max.x <- nice(maxx)

  lab.min.y <- nice(miny)

  lab.max.y <- nice(maxy)

  lab.min.z <- nice(minz)

  lab.max.z <- nice(maxz)

  minx <- min(lab.min.x, minx)

  maxx <- max(lab.max.x, maxx)

  miny <- min(lab.min.y, miny)

  maxy <- max(lab.max.y, maxy)

  minz <- min(lab.min.z, minz)
```

```
maxz <- max(lab.max.z, maxz)
min.x <- (lab.min.x - minx)/(maxx - minx)
max.x <- (lab.max.x - minx)/(maxx - minx)
min.y <- (lab.min.y - miny)/(maxy - miny)
max.y <- (lab.max.y - miny)/(maxy - miny)
min.z <- (lab.min.z - minz)/(maxz - minz)
max.z <- (lab.max.z - minz)/(maxz - minz)
if (axis.ticks){
  if (axis.scales) {
    x.labels <- seq(lab.min.x, lab.max.x,
                    by=diff(range(lab.min.x, lab.max.x))/4)
    x.at <- seq(min.x, max.x, by=nice(diff(range(min.x, max.x))/4))
    rgl::rgl.texts(x.at, -0.05, 0, x.labels, col = axis.col[1])

    z.labels <- seq(lab.min.z, lab.max.z,
                    by=diff(range(lab.min.z, lab.max.z))/4)
    z.at <- seq(min.z, max.z, by=diff(range(min.z, max.z))/4)
    rgl::rgl.texts(0, -0.1, z.at, z.labels, col = axis.col[3])

    y.labels <- seq(lab.min.y, lab.max.y,
                    by=diff(range(lab.min.y, lab.max.y))/4)
    y.at <- seq(min.y, max.y, by=diff(range(min.y, max.y))/4)
    rgl::rgl.texts(-0.05, y.at, -0.05, y.labels, col = axis.col[2])
  }
}
else {
  rgl::rgl.texts(min.x, -0.05, 0, lab.min.x, col=axis.col[1])
```

```
    rgl::rgl.texts(max.x, -0.05, 0, lab.max.x, col=axis.col[1])
    rgl::rgl.texts(0, -0.1, min.z, lab.min.z, col=axis.col[3])
    rgl::rgl.texts(0, -0.1, max.z, lab.max.z, col=axis.col[3])
    rgl::rgl.texts(-0.05, min.y, -0.05, lab.min.y, col=axis.col[2])
    rgl::rgl.texts(-0.05, max.y, -0.05, lab.max.y, col=axis.col[2])
   }
  }
  if (!is.null(groups)) groups <- groups[valid]
  x <- (x - minx)/(maxx - minx)
  y <- (y - miny)/(maxy - miny)
  z <- (z - minz)/(maxz - minz)
  size <- sphere.size*((100/length(x))^(1/3))*0.015
  radius <- radius/median(radius)
  if (is.null(groups)){
   if (size > threshold) rgl::rgl.spheres(x, y, z, color=point.col, radius=size*radius)
   else rgl::rgl.points(x, y, z, color=point.col)
  }
  else {
   if (size > threshold) rgl::rgl.spheres(x, y, z, color=surface.col[as.numeric(groups)],
radius=size*radius)
   else rgl::rgl.spheres(x, y, z, color=point.col, radius=size*radius, alpha=1)
  }
  if (!axis.scales) axis.col[1] <- axis.col[3] <- axis.col[2]
  rgl::rgl.lines(c(0,1), c(0,0), c(0,0), color=axis.col[1])
  rgl::rgl.lines(c(0,0), c(0,1), c(0,0), color=axis.col[2])
  rgl::rgl.lines(c(0,0), c(0,0), c(0,1), color=axis.col[3])
  rgl::rgl.texts(1, 0, 0, xlab, adj=1, color=axis.col[1])
```

```
rgl::rgl.texts(0, 1.05, 0, ylab, adj=1, color=axis.col[2])
rgl::rgl.texts(0, 0, 1, zlab, adj=1, color=axis.col[3])
# if (axis.scales){
#     rgl::rgl.texts(min.x, -0.05, 0, lab.min.x, col=axis.col[1])
#     rgl::rgl.texts(max.x, -0.05, 0, lab.max.x, col=axis.col[1])
#     rgl::rgl.texts(0, -0.1, min.z, lab.min.z, col=axis.col[3])
#     rgl::rgl.texts(0, -0.1, max.z, lab.max.z, col=axis.col[3])
#     rgl::rgl.texts(-0.05, min.y, -0.05, lab.min.y, col=axis.col[2])
#     rgl::rgl.texts(-0.05, max.y, -0.05, lab.max.y, col=axis.col[2])
# }
if (ellipsoid) {
  dfn <- 3
  if (is.null(groups)){
    dfd <- length(x) - 1
    ell.radius <- sqrt(dfn * qf(level, dfn, dfd))
    ellips <- ellipsoid(center=c(mean(x), mean(y), mean(z)),
                        shape=cov(cbind(x,y,z)), radius=ell.radius)
    if (fill) rgl::shade3d(ellips, col=surface.col[1], alpha=ellipsoid.alpha, lit=FALSE)
    if (grid) rgl::wire3d(ellips, col=surface.col[1], lit=FALSE)
  }
  else{
    levs <- levels(groups)
    for (j in 1:length(levs)){
    group <- levs[j]
      select.obs <- groups == group
      xx <- x[select.obs]
      yy <- y[select.obs]
```

```
    zz <- z[select.obs]
    dfd <- length(xx) - 1
    ell.radius <- sqrt(dfn * qf(level, dfn, dfd))
    ellips <- ellipsoid(center=c(mean(xx), mean(yy), mean(zz)),
                shape=cov(cbind(xx,yy,zz)), radius=ell.radius)
    if (fill) rgl::shade3d(ellips, col=surface.col[j], alpha=ellipsoid.alpha, lit=FALSE)
    if (grid) rgl::wire3d(ellips, col=surface.col[j], lit=FALSE)
    coords <- ellips$vb[, which.max(ellips$vb[1,])]
    if (!surface) rgl::rgl.texts(coords[1] + 0.05, coords[2], coords[3], group,
                        col=surface.col[j])
   }
  }
}
if (surface){
  vals <- seq(0, 1, length.out=grid.lines)
  dat <- expand.grid(x=vals, z=vals)
  for (i in 1:length(fit)){
   f <- match.arg(fit[i], c("linear", "quadratic", "smooth", "additive"))
   if (is.null(groups)){
    mod <- switch(f,
          linear = lm(y ~ x + z),
          quadratic = lm(y ~ (x + z)^2 + I(x^2) + I(z^2)),
          smooth = if (is.null(df.smooth)) mgcv::gam(y ~ s(x, z))
          else mgcv::gam(y ~ s(x, z, fx=TRUE, k=df.smooth)),
          additive = if (is.null(df.additive)) mgcv::gam(y ~ s(x) + s(z))
          else mgcv::gam(y ~ s(x, fx=TRUE, k=df.additive[1]+1) +
                    s(z, fx=TRUE, k=(rev(df.additive+1)[1]+1)))
```

```
      )
      if (model.summary) summaries[[f]] <- summary(mod)
      yhat <- matrix(predict(mod, newdata=dat), grid.lines, grid.lines)
      if (fill) rgl::rgl.surface(vals, vals, yhat, color=surface.col[i], alpha=surface.alpha,
lit=FALSE)
      if(grid) rgl::rgl.surface(vals, vals, yhat, color=if (fill) grid.col
                          else surface.col[i], alpha=surface.alpha, lit=FALSE, front="lines",
back="lines")
      if (residuals){
        n <- length(y)
        fitted <- fitted(mod)
        colors <- ifelse(residuals(mod) > 0, pos.res.col, neg.res.col)
        rgl::rgl.lines(as.vector(rbind(x,x)), as.vector(rbind(y,fitted)), as.vector(rbind(z,z)),
                  color=as.vector(rbind(colors,colors)))
        if (squares){
          res <- y - fitted
          xx <- as.vector(rbind(x, x, x + res, x + res))
          yy <- as.vector(rbind(y, fitted, fitted, y))
          zz <- as.vector(rbind(z, z, z, z))
          rgl::rgl.quads(xx, yy, zz, color=square.col, alpha=surface.alpha, lit=FALSE)
          rgl::rgl.lines(xx, yy, zz, color=square.col)
        }
      }
    }
    else{
      if (parallel){
        mod <- switch(f,
```

```
            linear = lm(y ~ x + z + groups),
            quadratic = lm(y ~ (x + z)^2 + I(x^2) + I(z^2) + groups),
            smooth = if (is.null(df.smooth)) mgcv::gam(y ~ s(x, z) + groups)
            else mgcv::gam(y ~ s(x, z, fx=TRUE, k=df.smooth) + groups),
            additive = if (is.null(df.additive)) mgcv::gam(y ~ s(x) + s(z) + groups)
            else mgcv::gam(y ~ s(x, fx=TRUE, k=df.additive[1]+1) +
                    s(z, fx=TRUE, k=(rev(df.additive+1)[1]+1)) + groups)
        )
        if (model.summary) summaries[[f]] <- summary(mod)
        levs <- levels(groups)
        for (j in 1:length(levs)){
          group <- levs[j]
          select.obs <- groups == group
          yhat <- matrix(predict(mod, newdata=cbind(dat, groups=group)), grid.lines,
grid.lines)
          if (fill) rgl::rgl.surface(vals, vals, yhat, color=surface.col[j], alpha=surface.alpha,
lit=FALSE)
          if (grid) rgl::rgl.surface(vals, vals, yhat, color=if (fill) grid.col
                    else surface.col[j], alpha=surface.alpha, lit=FALSE, front="lines",
back="lines")
          rgl::rgl.texts(1, predict(mod, newdata=data.frame(x=1, z=1, groups=group)), 1,
              paste(group, " "), adj=1, color=surface.col[j])
          if (residuals){
            yy <- y[select.obs]
            xx <- x[select.obs]
            zz <- z[select.obs]
            fitted <- fitted(mod)[select.obs]
```

```
            res <- yy - fitted
            rgl::rgl.lines(as.vector(rbind(xx,xx)),                    as.vector(rbind(yy,fitted)),
as.vector(rbind(zz,zz)),
                    col=surface.col[j])
            if (squares) {
              xxx <- as.vector(rbind(xx, xx, xx + res, xx + res))
              yyy <- as.vector(rbind(yy, fitted, fitted, yy))
              zzz <- as.vector(rbind(zz, zz, zz, zz))
              rgl::rgl.quads(xxx, yyy, zzz, color=surface.col[j], alpha=surface.alpha, lit=FALSE)
              rgl::rgl.lines(xxx, yyy, zzz, color=surface.col[j])
            }
          }
        }
       else {
        levs <- levels(groups)
        for (j in 1:length(levs)){
        group <- levs[j]
          select.obs <- groups == group
          mod <- switch(f,
                    linear = lm(y ~ x + z, subset=select.obs),
                    quadratic = lm(y ~ (x + z)^2 + I(x^2) + I(z^2), subset=select.obs),
                    smooth = if (is.null(df.smooth)) mgcv::gam(y ~ s(x, z), subset=select.obs)
                    else mgcv::gam(y ~ s(x, z, fx=TRUE, k=df.smooth), subset=select.obs),
                    additive = if (is.null(df.additive)) mgcv::gam(y ~ s(x) + s(z),
subset=select.obs)
                    else mgcv::gam(y ~ s(x, fx=TRUE, k=df.additive[1]+1) +
```

```
                    s(z, fx=TRUE, k=(rev(df.additive+1)[1]+1)), subset=select.obs)
    )
    if (model.summary) summaries[[paste(f, ".", group, sep="")]] <- summary(mod)
    yhat <- matrix(predict(mod, newdata=dat), grid.lines, grid.lines)
    if (fill) rgl::rgl.surface(vals, vals, yhat, color=surface.col[j], alpha=surface.alpha,
lit=FALSE)
    if (grid) rgl::rgl.surface(vals, vals, yhat, color=if (fill) grid.col
                    else surface.col[j], alpha=surface.alpha, lit=FALSE, front="lines",
back="lines")
    rgl::rgl.texts(1, predict(mod, newdata=data.frame(x=1, z=1, groups=group)), 1,
            paste(group, " "), adj=1, color=surface.col[j])
    if (residuals){
      yy <- y[select.obs]
      xx <- x[select.obs]
      zz <- z[select.obs]
      fitted <- fitted(mod)
      res <- yy - fitted
      rgl::rgl.lines(as.vector(rbind(xx,xx)),                    as.vector(rbind(yy,fitted)),
as.vector(rbind(zz,zz)),
            col=surface.col[j])
      if (squares) {
        xxx <- as.vector(rbind(xx, xx, xx + res, xx + res))
        yyy <- as.vector(rbind(yy, fitted, fitted, yy))
        zzz <- as.vector(rbind(zz, zz, zz, zz))
        rgl::rgl.quads(xxx, yyy, zzz, color=surface.col[j], alpha=surface.alpha, lit=FALSE)
        rgl::rgl.lines(xxx, yyy, zzz, color=surface.col[j])
      }
```

```
          }
        }
      }
    }
  }
 }
 else levs <- levels(groups)
 if (revolutions > 0) {
   for (i in 1:revolutions){
     for (angle in seq(1, 360, length.out=360/speed)) rgl::rgl.viewpoint(-angle, fov=fov)
   }
 }
 if (model.summary) return(summaries) else return(invisible(NULL))
}

# the following function is a slight modification of rgl.select3d() in the rgl package,
# altered to pass through arguments (via ...) to rgl.select()

car.select3d <- function (...) {
 if (!requireNamespace("rgl")) stop("rgl package is missing")
 rgl::.check3d()
 rect <- rgl::rgl.select(...)
 llx <- rect[1]
 lly <- rect[2]
 urx <- rect[3]
 ury <- rect[4]
 if (llx > urx) {
```

```
  temp <- llx
  llx <- urx
  urx <- temp
 }
 if (lly > ury) {
  temp <- lly
  lly <- ury
  ury <- temp
 }
 proj <- rgl::rgl.projection()
 function(x, y, z) {
  pixel <- rgl::rgl.user2window(x, y, z, projection = proj)
  apply(pixel, 1, function(p) (llx <= p[1]) && (p[1] <=
                                urx) && (lly <= p[2]) && (p[2] <= ury) && (0 <= p[3]) &&
      (p[3] <= 1))
 }
}



showLabels3d <- function(x, y, z, labels,
                  id.method = "identify", id.n=length(x), col=c("blue"),
                  res=y - mean(y), range.x=range(x), range.z=range(z),
                  offset = ((100/length(x))^(1/3)) * 0.02) {
 if (!requireNamespace("rgl")) stop("rgl package is missing")
 if (id.method == "none") return(NULL)
 if(id.n > 0L) {
  if (missing(labels))
```

```
    labels <- as.character(seq(along=x))
  getPoints <- function(w) {
    names(w) <- labels
    iid <- seq(length=id.n)
    ws <- w[order(-w)[iid]]
    match(names(ws), labels)
  }
  ind <- switch(id.method,
              xz = getPoints(rowSums(qr.Q(qr(cbind(1, x, z))) ^ 2)),
              y = getPoints(abs(res)),
              xyz = union(getPoints(abs(x - mean(x))), union(abs(z - mean(z)),
                                          getPoints(abs(res)))),
              mahal= getPoints(rowSums(qr.Q(qr(cbind(1, x, y, z))) ^ 2)))
  rgl::rgl.texts(x[ind], y[ind] + offset, z[ind], labels[ind],
              color = col)
  return(labels[ind])
 }
}

ellipsoid <- function(center=c(0, 0, 0), radius=1, shape=diag(3), n=30){
 if (!requireNamespace("rgl")) "rgl package is missing"
 # adapted from the shapes3d demo in the rgl package
 degvec <- seq(0, 2*pi, length.out=n)
 ecoord2 <- function(p) c(cos(p[1])*sin(p[2]), sin(p[1])*sin(p[2]), cos(p[2]))
 v <- t(apply(expand.grid(degvec,degvec), 1, ecoord2))
 v <- center + radius * t(v %*% chol(shape))
 v <- rbind(v, rep(1,ncol(v)))
```

```
 e <- expand.grid(1:(n-1), 1:n)
 i1 <- apply(e, 1, function(z) z[1] + n*(z[2] - 1))
 i2 <- i1 + 1
 i3 <- (i1 + n - 1) %% n^2 + 1
 i4 <- (i2 + n - 1) %% n^2 + 1
 i <- rbind(i1, i2, i4, i3)
 rgl::qmesh3d(v, i)
}
```

K-Means clustering function

This function has been copied and pasted from the following website: http://www.semspirit.com/artificial-intelligence/machine-learning/clustering/k-means-clustering/k-means-clustering-in-r/

```
success_ratio <- function(cm) {
 total_success = 0
 total = 0
 for(irow in 1:length(cm[,1])) {
  for(icol in 1:length(cm[irow,])) {
  if (irow == icol) {
     total_success = total_success + cm[irow, icol]
   }
   total = total + cm[irow, icol]
  }
 }
 return( (100*total_success)/total )
```

```
}

getElbowPoint <- function(x_values, y_values) {

  # Max values to create line
  max_x_x <- max(x_values)
  max_x_y <- y_values[which.max(x_values)]
  max_y_y <- max(y_values)
  max_y_x <- x_values[which.max(y_values)]
  max_df <- data.frame(x = c(max_y_x, max_x_x), y = c(max_y_y, max_x_y))

  # Creating straight line between the max values
  fit <- lm(max_df$y ~ max_df$x)

  # Distance from point to line
  distances <- c()
  for(i in 1:length(x_values)) {
    distances <- c(distances, abs(coef(fit)[2]*x_values[i] - y_values[i] + coef(fit)[1]) /
sqrt(coef(fit)[2]^2 + 1^2))
  }

  # Max distance point
  x_max_dist <- x_values[which.max(distances)]
  y_max_dist <- y_values[which.max(distances)]

  return(c(x_max_dist, y_max_dist, max(distances)))
}
```

```
getWCSSData <- function(X) {
  wcss_values <- vector()
  max_wcss_steps = sqrt(length(X[,1]))
  for(i in 1:max_wcss_steps) {
    wcss_values[i] <- sum(kmeans(X, i, iter.max = 1000)$withinss)
  }
  return(wcss_values)
}

showElbowGraph <- function(x_clusters, y_wcss) {
  nb_wcss_values = length(y_wcss)
  extremes_line_coef = (x_clusters[nb_wcss_values] - x_clusters[1]) /
(y_wcss[nb_wcss_values] - wcss_values[1])
  extremes_orth_line_coef = -1 / extremes_line_coef
  elbowPoint_orth_proj = c(elbowPoint_info[1] + elbowPoint_info[3]/2, elbowPoint_info[2]
+ extremes_orth_line_coef * (elbowPoint_info[3]/2))

  plot(x_clusters, y_wcss, type="b", main = 'WCSS value according to the number of clusters',
xlab = 'Number of clusters', ylab = 'WCSS value')
  lines(x=c(x_clusters[1], x_clusters[nb_wcss_values]), y=c(y_wcss[1],
y_wcss[nb_wcss_values]), type="b", col='green')
  lines(x=c(elbowPoint_info[1], elbowPoint_orth_proj[1]), y=c(elbowPoint_info[2],
elbowPoint_orth_proj[2]), type="b", col='red')
}

library(plotly)
```

```
init3DGraph <- function() {
  p<-plot_ly(evaluate = FALSE)
  return(p)
}

setTrace <- function(p, x, y, z, n, c) {
  p<-add_trace(p, x=as.vector(x),y=as.vector(y),z=as.vector(z), type="scatter3d",
mode="markers", name = n, marker = list(size = 4, color = c), evaluate = FALSE)
  return(p)
}

show3DGraph <- function(p, x_name, y_name, z_name) {
  layout(p, scene = list(xaxis = list(title = x_name), yaxis = list(title = y_name), zaxis =
list(title = z_name)))
}
```

K-Means 3D clustering

Script to recreate 3D k-means clustering and visualisation in rgl.

These codes are readily available online but have been adapted for this dataset.

More info:

http://www.semspirit.com/artificial-intelligence/machine-learning/clustering/k-means-clustering/k-means-clustering-in-r/

http://www.sthda.com/english/wiki/factoextra-r-package-easy-multivariate-data-analyses-and-elegant-visualization

https://stat.ethz.ch/R-manual/R-devel/library/stats/html/kmeans.html

https://www.rdocumentation.org/packages/car/versions/2.0-0/topics/scatter3d

Packages

```
#install.packages("clustertend")

#install.packages("rgl")

#install.packages("plotly")

#install.packages("factoextra")

#install.packages("car")


library(car)

library(rgl)

library(plotly)

library(clustertend)

library(factoextra)
```

Calculate K-means for the complete dataset

1. Apply Function

```
source("Kmeans Function.R")
```

2. Load Dataset and define matrix

```
dataset =read.table("dataset_unitp.txt",header=TRUE,sep="\t",row.names=1)
X = dataset[1:3]
y = dataset[,1:1]
```

3. Generate the WCSS curve data in order to find the elbow point (nearly-optimal clustering point)

```
set.seed(124)

wcss_values = getWCSSData(X)
nb_clusters = seq(1, length(wcss_values), 1)
elbowPoint_info = getElbowPoint(x_values = nb_clusters, y_values = wcss_values)
showElbowGraph(nb_clusters, wcss_values)
```

4. Insert optimal k shown on graph e.g. kmeans(X, k,...)

```
kmeans <- kmeans(X, 4, iter.max = 300, nstart = 10)
clus = kmeans$cluster
```

Hopkins Statistic (H)

More info: https://www.datanovia.com/en/lessons/assessing-clustering-tendency/

1. Calculate the Hopkins statistic

```
hopkins(X,n = nrow(X)-1)
```

Calculate the true Hopkins statistic as 1-H, see: https://stats.stackexchange.com/questions/332651/validating-cluster-tendency-using-hopkins-statistic

```
#Test IRIS dataset to verify
```

2. Test H for a random dataset

```
random_df <- data.frame(
  x = runif(nrow(X), min(X$X), max(X$X)),
  y = runif(nrow(X), min(X$Y), max(X$Y)),
  z = runif(nrow(X), min(X$Z), max(X$Z))
)

set.seed(123)
hopkins(random_df, n = nrow(random_df)-1)
```

3. Plot H for random dataset

```
open3d()
plot3d(x = random_df$x, y = random_df$y, z = random_df$z)
```

K-mean clustering: visualisation of dataset

1. Apply Function

```
source("myscatter3d.R")
```

2. Create a 2D visualisation of clusters

```
fviz_cluster(kmeans, data = X, stand = FALSE, show.clust.cent = FALSE, geom =
"point",palette = "set2", ggtheme = theme_classic())
```

3. Create a 3D visualisation of clusters

```
x <- X$X
y <- X$Y
z <- X$Z
t = dataset$Taxa
colors = palette(rainbow(length(levels(t))))[t]

colors = palette(rainbow(length(levels(dataset$Taxa))))[dataset$Taxa]
```

4. Plot Legend and colour according to Taxa

```
open3d()
legend3d("center", levels(dataset$Taxa), pch = rep(16,
length(levels(dataset$Taxa))),col=palette(rainbow(length(levels(dataset$Taxa)))))
```

5. Create an interactive 3D Plot

```
open3d()
myscatter3d(x = x, y = y, z = z,groups = as.factor(clus),axis.scales=FALSE, ellipsoid=T,
        surface=FALSE,point.col = colors, ellipsoid.alpha = 0, level=0.7,add=TRUE,labels =
dataset$Taxa, xlab = "Easting", ylab = "Northing", zlab = "Elevation")
```

Silhouette analysis

More info: http://www.sthda.com/english/wiki/print.php?id=241

*Silhouette analysis results may rearrange the clusters, be sure to interpret the corresponding clusters correctly.

1. Calculate silhouette statistic

```
library (factoextra)
km.res <- eclust(X, "kmeans", k = 4, nstart = 10, graph = FALSE) #compute kmeans
fviz_silhouette(km.res, palette = "rainbow") #silouhette analysis
```

K-means for individual Taxa/Skeletal Regions

1. Specify the new dataset by isolating the taxa/skeletal region from the complete dataset

1.1. To Isolate Specific Taxa

```
carn=subset(dataset, Taxa=="Carnivore")
```

1.2. Set Dataset

```
X = carn[1:3]

y = carn[,1:1]
```

2. Repeat the same procedure as above applied for the complete dataset.

2.2. WCSS curve data to find the elbow point:

```
set.seed(124)

wcss_values = getWCSSData(X)

nb_clusters = seq(1, length(wcss_values), 1)

elbowPoint_info = getElbowPoint(x_values = nb_clusters, y_values = wcss_values)

showElbowGraph(nb_clusters, wcss_values)

set.seed(124)

kmeans <- kmeans(X, 3, iter.max = 300, nstart = 10)

clus = kmeans$cluster
```

2.3. Hopkins Statistic - repeat steps as described above.

3. Create a 3D visualisation of clusters for carnivores

```
x <- X$X

y <- X$Y

z <- X$Z
```

3.1. K-Means Scatter Plot

```
scatter3d(x = x, y = y, z = z,groups = as.factor(clus),axis.scales=FALSE,
        surface=FALSE,point.col = colors, ellipsoid.alpha = 0.0, level=0.7,add=TRUE,labels =
row.names(carn), xlab = "Easting", ylab = "Northing", zlab = "Elevation")
```

Repeat steps above applied to complete dataset.

4. Silhouette Analysis - repeat steps as described above.

DBSCAN 3D clustering

Script to recreate 3D DBSCAN clustering and visualisation in rgl.

These codes are readily available online but have been adapted for this dataset.

More info: https://www.datanovia.com/en/lessons/dbscan-density-based-clustering-essentials/

https://www.geeksforgeeks.org/dbscan-clustering-in-ml-density-based-clustering/

Packages

```
#install.packages("fpc")
#install.packages("dbscan")
#install.packages("factoextra")
#install.packages("car")
#install.packages("rgl")
#install.packages("plotly")

library(fpc)
library(dbscan)
library(factoextra)
library(car)
library(rgl)
library(plotly)
```

Calculate DBSCAN for the complete dataset

1. Apply Function

```
source("DBScan Function.R")
```

2. Load Dataset and define matrix

```
dataset = read.table("dataset_unitp.txt",header=TRUE,sep="\t",row.names=1)
df = dataset[1:3]
dist_matrix = dist(dataset[,1:3])
```

3. Find eps value

```
dbscan::kNNdistplot(df, k = 3)
abline(h = 0.8, lty = 2)
```

3.1 compute

```
set.seed(123)
db <- fpc::dbscan(df, eps = 0.8, MinPts = 3, scale=FALSE) #elbow is around 1 (showm by
previous graph) method = c("hybrid", "raw", "dist")
```

DBSCAN clustering: visualisation of dataset

1. Create a 2D visualisation of clusters

```
#Version 1 (used in article)
```

```
fviz_cluster(db, data = df, stand = FALSE, show.clust.cent = FALSE, geom = "point",palette = "rainbow", ggtheme = theme_classic())

#Version 2
plot(db, df, main = "DBSCAN", frame = FALSE)
```

2. Create a 3D visualisation of clusters

```
####
```

2.1. Create an interactive 3D Plot

```
open3d()
myscatter3d(x = dataset$X, y = dataset$Y, z = dataset$Z, groups = as.factor(toto), point.col = colors, labels = dataset$Taxa, surface=FALSE, ellipsoid.alpha = 0, level=0.7,add=TRUE, axis.scales=FALSE, ellipsoid=T, xlab = "Easting", ylab = "Northing", zlab = "Elevation")
```

2.2. Plot Legend and colour according to Taxa

```
open3d()
legend3d("center", levels(dataset$Taxa), pch = rep(16, length(levels(dataset$Taxa))),col=palette(rainbow(length(levels(dataset$Taxa)))))
```